Role of Chronic Shear Stress in Endothelial Form and Function

A thesis submitted to Imperial College London for the degree of Doctor of Philosophy

Claire Marie Frances Potter

February 2013

Imperial College London

Faculty of Medicine

National Heart & Lung Institute

Declaration

I, Claire Potter declare that this thesis and the research to which it refers is a product of my own work.

Information derived from other sources, including my own previous work and work carried out with the assistance of others, has been appropriately cited and acknowledged.

Abstract

Endothelial cells *in vivo* exist in a dynamic environment, subject to the physical forces of blood flow as it is regulated through the cardiac cycle. Arguably, the most important force endothelial cells are subject to is shear stress, the frictional force of blood flow across the cell surface. Areas of the vasculature that experience laminar shear stress appear resistant to the development of atherosclerotic plaques, whereas those that experience low shear stress, due to complex patterns of blood flow, appear susceptible. *In vitro* study of the effects of chronic shear stress on the endothelium has been somewhat limited, due to the methods of modelling shear stress available, which are for the most part only suitable for culture for up to 24 hours.

I have validated an orbital shaker method of modelling two flow environments seen in the vasculature, unidirectional flow and non-directional flow, with associated shear stress profiles, for chronic time periods of up to 7 days. I have shown clear differences between the two environments in terms of endothelial cell morphology and protein expression and identified many ways in which sheared cells differ from their static counterparts, in terms of morphology, protein expression, vascular mediator release and transcriptional profile.

Shear stress appears to be a protective force, inhibiting expression of inflammatory mediators and significantly altering response to inflammatory stimulus. The orbital shaker may prove a useful model for *in vitro* study of the endothelium in a situation similar to that of physiological conditions.

Contents

List of Figures

Chapter 1: Introduction

Chapter 2: General Methods

Chapter 3*:* Analysis of the effect of complex *in vitro* shear stress on morphology of endothelial cells: correlation with shear directionality

Chapter 4: Morphology of the Native Endothelium in Porcine Aorta

Chapter 5: Effect of Shear on PAEC NFκB

Chapter 6: Understanding the relation between complex shear stress, endothelial cell mediator release and morphological response to shear

List of Tables

Acknowledgements

I have been lucky enough to have been supervised by Professor Jane Mitchell, Professor Peter Weinberg and Dr Julia Gorelik and am grateful for the valuable advice and encouragement they have provided.

I appreciate the kind assistance I have been given colleagues working in the 3 labs I have spent time in. I am particularly grateful for the support and inspiration I received from Dr Martina Lundberg. Special thanks also extend to Dr Christina Warboys for training in cell isolation, Dr Alexey Moshkov for technical assistance with SICM, Dr Louise Harrington and Mr Stephen Rothery for direction in imaging and immunohistochemistry, Ms Hime Gashaw for her exceptional lab management and Sarah Mazi and Dr Mark Paul-Clark for their patient explanations and help with transcriptomic analysis. Thanks also go to collaborator Dr R. Eric Berson at the University of Louisville for providing mathematical solutions.

This PhD was funded through the British Heart Foundation centre of Research Excellence at Imperial College and I am grateful for their support and that of other members of the centre.

Finally, thanks to my parents, Elaine and Jeff, and to Dave for their patience and for always believing that I could do it.

Publications associated with work in this thesis

Journal Articles

Kirkby NS; Lundberg MH; Harrington LS; Leadbeater PD; Milne GL; **Potter CMF**; Al-Yamani M; Adeyemi O; Warner TD; Mitchell JA (2012) Cyclo-oxygenase-1 and Not Cyclo-oygenase-2 is Responsible for Physiological Production of Prostacyclin in the Cardiovascular System. *Proceedings of the National Academy of Sciences of the United States of America* 109(43) 17597-17602

Potter CMF; Schobesberger S; Lundberg MH; Weinberg PD; Mitchell JA; Gorelik J (2012) Shape and Compliance of Endothelial Cells After Shear Stress *in vitro* or from Different Aortic Regions: Scanning Ion Conductance Microscopy Study. *PLoS ONE* 7(2): e31228

Miragoli M; Moshkov A; Novak P; Shevchuk A; Nikolaev S; El-Hamamsy I; **Potter CMF**; Wright P; Abdul Kadir, SSH; Lyon AR; Mitchell JA; Chester AH; Klenerman D; Lab MJ; Korchev YE; Harding SE; Gorelik J (2011) Scanning Ion Conductance Microscopy: A Convergent High-Resolution Technology for Multi-Parametric Analysis of Living Cardiovascular Cells. *Journal of the Royal Society Interface 8(60):913-925*

Potter CMF; Lundberg MH; Harrington LS; Warboys CM; Warner TD; Berson RE; Moshkov AV; Gorelik J; Weinberg PD; Mitchell JA (2011) Role of Shear Stress in Endothelial Cell Morphology and Expression of Cyclooxygenase Isoforms. *Arteriosclerosis, Thrombosis and Vascular Biology 31:384-391*

Abstracts

Potter CMF; Lundberg MH; Gashaw HH; Harrington LS; Warner TD; Weinberg PD; Mitchell JA. (2010) Cyclo-oxygenase Immunoreactivity in Human Aortic Endothelial Cells Cultured under Static and Shear Stress Conditions. *Proceedings of the British Pharmacological Society* Volume 8, issue 1, abstract 142P from the BPS Winter Meeting 2010, London, UK.
http://www.pa2online.org/abstracts/1vol8issue1abst142.pdf

Potter CMF; Lundberg MH; Gashaw HH; Gorelik J; Moshkov AV; Harrington LS; Weinberg PD; Mitchell JA. (2010) Effect of Chronic Shear Stress on Endothelial Cell Morphology In Vitro and In Vivo: Relevance to Areas at Risk of Atherosclerosis in the aorta. *Basic & Clinical Pharmacology & Toxicology* 107 s1: 530, paper number 2801

Reed DM; Wright WR; **Potter CMF**; Gashaw HH; Bailey LK; Paul-Clark M; Mitchell JA. (2010) TLR3 and TLR4 Ligands Induce Intracellular IL-1β Immunoreactivity in Human Aortic Endothelial Cells (HAECs) and Lung Microvascular Endothelial Cells (HLMVECs). *Basic & Clinical Pharmacology & Toxicology* 107 s1: 540-541, paper number 1520

Potter CMF; Lundberg MH; Gashaw HH; Harrington LS; Warner TD; Weinberg PD; Mitchell JA (2009) Relative expression of cyclo-oxygenase (COX)-1 and COX-2 in porcine endothelium subjected to chronic shear stress. *Proceedings of the British Pharmacological Society* Volume 7, Issue 4, abstract 043P from the BPS Winter Meeting 2009, London, UK
http://www.pA2online.org/abstracts/Vol7Issue4abst043P.pdf

Abbreviations Used in this Thesis

6-keto $PGF_{1\alpha}$ 6-keto Prostaglandin $F_{1\alpha}$

AA Arachidonic Acid

ACE Angiotensin Converting Enzyme

APS Ammonium persulfate

BH_4 Tetrahydrobiopterin

BOEC Blood Outgrowth Endothelial Cells

BSA Bovine serum albumin

cAMP Cyclic Adenosine Monophosphate

cGMP Cyclic Guanosine Monophosphate

CFD Computational Fluid Dynamics

COX-1/2 Cyclo-oxygenase isoform 1/2

CXCL8/IL-8 CXC family Chemokine ligand 8/Interleukin-8

DAPI 4', 6-diamidino-2-phenylindole

DMEM Dulbecco's Modified Eagle Medium

DMSO Dimethyl Sulfoxide

DNA Deoxyribonucleic acid

Dyn/cm^2 Dynes per centimetre squared

ECE Endothelin Converting Enzyme

ECGS Endothelial Cell Growth Supplement

ECM Extracellular Matrix

EDTA Ethylenediaminetetraacetic Acid

EGM-2 Endothelial Growth Medium-2

ELISA Enzyme Linked Immunosorbent Assay

ET-1 Endothelin-1

ETA Endothelin receptor A

ETB Endothelin receptor B

FCS Foetal Calf Serum

HAEC Human Aortic Endothelial Cells

HBSS Hank's Balanced Salt Solution

HEPES-BSS 4-(2-hydroxyethyl)-1-piperazineethanesulfonic acid buffered saline solution

HRP Horse Radish Peroxidase

HUVEC Human Umbilical Vein Endothelial Cells

IL-1β Interleukin-1β

LDL Low Density Lipoprotein

MyD88 Myeloid Differentiation Primary Response Protein 88

NFκB Nuclear Factor Kappa B

NGS Normal Goat Serum

NO Nitric Oxide

NOS Nitric Oxide Synthase

PAEC Porcine Aortic Endothelial Cells

PBS Phosphate Buffered Saline

PECAM-1 Platelet-Endothelial Cell Adhesion Molecule

PGI_2 Prostacyclin

PRR Pattern recognition receptor

RNA Riboxynucleic acid

SICM Scanning Ion Conductance Microscopy

TEMED N,N,N',N'-tetramethyl-ethane-1,2-diamine

TLR Toll-like receptor

TMB Tetramethyl benzadine

vWF von Willebrand Factor

Chapter 1

Introduction

1.1 Overview

The vasculature is the life line of the body, ensuring all organs are supplied with oxygen and nutrients. The luminal surface of every blood vessel in this vast network is lined with endothelial cells, of which there are an estimated 1-6 $x10^{13}$ in an adult human (Cines *et al.*, 1998). In spite of its abundance, the early scientific view was that the endothelium was merely, a 'nucleated cellophane wrapper'(Florey, 1966), comparable to the 'inner tube of a bicycle tyre'(Nachman *et al.*, 2004) and that there was little merit in investigating it further. Fortunately not all scientists took this view and in recent decades an increasing body of evidence has identified the critical role the endothelium plays in homeostatic vascular function, through release of key vasoactive hormones, in pathogen sensing and as a site for leukocyte recruitment.

The fact that the endothelium has such a crucial role in vascular homeostasis and its presence throughout the body means that loss of endothelial function has severe health implications. Endothelial dysfunction is associated with a number of diseases, not limited to atherosclerosis, diabetes, hypertension, heart disease and thrombosis. Endothelial biology, physiology and pharmacology are therefore active areas of research. Due to the inaccessibility of the endothelium *in situ* much of this work has required the use of endothelial cells in *in vitro* culture. This approach has contributed to landmark observations in the field, including isolation, purification and sequencing of endothelial nitric oxide synthase (eNOS/NOS III) and on the therapeutic side, generation of endothelial cells from stem cells to act as treatments in vessel regeneration (Leeper *et al.*, 2010).

Importantly, as endothelial cells in native vessels are continually exposed to the dynamic forces of blood flow, they have a high degree of mechanosensitivity to physical forces. One key force is that of shear stress, the frictional action of blood flow across the endothelial cell surface. Shear stress is known to be a regulator of endothelial cell morphology, function and enzyme expression but despite this, the majority of *in vitro* experiments are performed under static conditions. Where shear stress has been considered experiments have tended to be acute, on a time scale of hours, which may simply be perceived as an inflammatory insult to the cell, rather than the physiological stimulus to which it has been exposed for its entire life span. There is a need in the field for techniques to study endothelial cells under

chronic shear stress, in environments which represent the complex shear patterns seen throughout the body. A major limitation of models described so far has been that they are not conducive for sustained endothelial culture. Addressing this need is a key feature in the aims of my PhD, in which I have sought to investigate endothelial cell morphology, protein expression and gene induction under conditions of both acute and chronic shear stress. In order to do this I have utilised an orbital shaker model, as described in further detail below.

1.2 Form and function of the native endothelial cell

The first reported observation of the endothelium comes from pathologist Rudolf Virchow, who in 1858 described it as 'as simple a membrane as any that is ever met within the body' (Aird, 2007; Laubichler, 2007). It was termed the endothelium by Wilhelm His in 1865, who identified it as the layer of cells lining the blood and lymph vessels (Aird, 2007). A great deal of research has been carried out since this time, establishing the endothelium as not merely a 'simple' liner but a layer of dynamic and multifunctional cells, vital in the maintenance of haemostasis through roles as a barrier and anti-thrombotic surface, in metabolism, in hormone release and in inflammatory sensing.

Barrier function

The endothelium plays a key role as the interface between the blood and underlying tissues and facilitates regulation of exchange of molecules, ions, blood gasses and water between the two. Permeability of the endothelial barrier is thought to be under control of two major forms of endothelial junctions: tight junctions, which open and close to allow passage of ions and solutes and adherens junctions which principally regulate cell to cell contacts (Bazzoni *et al.*, 2004). Tight junctions are composed of proteins such as occludin, Junctional adhesion molecule (JAM) and members of the claudin family (Bazzoni, 2006) (see Figure 1.1). These proteins form strands within cell plasma membranes that work to occlude intercellular space.

Adherens junctions are formed of cadherins which bind to catenins, regulating actin distribution and co-ordinating cell movement in angiogenesis (Lampugnani *et al.*, 2007) (see Figure 1.1). These two forms of junctions act together and their regulation of cell permeability can be influenced by a number of stimuli, including inflammatory mediators, which can cause cell contraction resulting in increased permeability. Junctional changes are thought to initiate a signalling cascade throughout the cell, which may play a role in vessel response to physical stimulus (discussed in section 1.2).

Also thought to be important, though less well studied are gap junctions. The endothelium forms homocellular gap junctions with neighbouring endothelial cells and heterocellular gap junctions with underlying smooth muscle (Evans *et al.*, 2002). These junctions are thought to allow the passage of small molecules and charge, and are formed by the association of channel forming proteins known as connexins. 6 connexins associate to form a connexon and 1 connexon from each cell forms a channel. There are a number of known connexins, an estimated 20 in humans (Willecke *et al.*, 2002), but endothelial cells express 3, predominantly Cx37, alongside Cx40 and Cx43 (Yeh *et al.*, 1998). Homocellular gap junctions are thought to play a role in angiogenesis and co-ordinated cell response. Heterocellular junctions between endothelial cells and smooth muscle are thought to be one means by which endothelium dependent hyperpolarisation of smooth muscle and the resultant vasorelaxation may be communicated (Chaytor *et al.*, 2003).

Acting as a physical barrier to transport through the endothelium is the glycocalyx. This layer, formed of lipid anchored proteoglycans with glycosaminoglycan side-chains, is thought to extend up to 4.5 µm from the endothelial membrane surface (Megens *et al.*, 2007). Typical side-chains include heparin sulphate, chondroitin sulphate, and hyaluronic acid, which confer a negative charge. This charge may prevent binding of some molecules to the surface for subsequent entry, as well as prevent adhesion of circulating cells in the initiation of inflammatory signalling events.

The range of junctional proteins employed illustrates that effective barrier capabilities are vital for maintenance of endothelial integrity. A classical indicator of vascular pathologies is endothelial dysfunction, which is characterised in part by loss of effective barrier function (Deanfield *et al.*, 2005). Lack of an effective barrier is associated with a number of

conditions including oedema and stroke (Stamatovic *et al.*, 2008), where increased water uptake leads to rising interstitial pressure which compromises tissue perfusion, and may be related to lipid uptake and the inflammatory events of atherosclerosis (Hennig *et al.*, 1985).

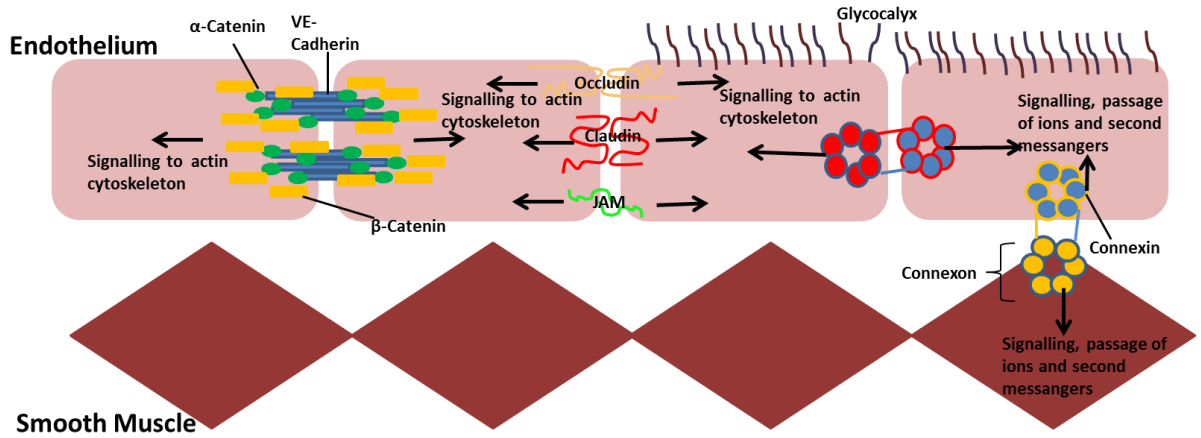

Figure 1.1 Representation of endothelial junctional signalling molecules

Between endothelial cells several major junctions exist; i) Adherens junctions, ii) Tight junctions, iii) Gap junctions.

i) Adherens junctions are formed through interaction of cadherins and catenins. Vascular endothelial cadherin (VE-cadherin) is a transmembrane protein. It binds to the accessory proteins α and β-catenin which serve to anchor it to the cytoskeleton. Regulation of these junctions controls leukocyte extravasation.

ii) Tight junctions are comprised of a number of proteins including occludin, claudin and junctional adhesive molecule (JAM). Complexes of these proteins form between neighbouring cells and work to physically occlude the space between them.

iii) Gap junctions are channels made from the interaction between two hemi-channels on adjacent cells known as connexons. Connexons are groups of 6 proteins known as connexins. 3 types of these proteins are found in vascular cells Cx37, Cx43 and Cx45. These proteins can be grouped together in different arrangements to form different types of channels. In homotypic gap junctions all 12 connexins making up the 2 connexons are the same, whereas in heterotypic gap junctions each connexion is formed from a different connexin. It is also possible for heteromeric gap junctions to form where each connexon is made up of a number of different connexins. These junctions are responsible for the movement of ion flow between cells and, as such are important in the transfer of calcium ions between endothelial cells and smooth muscle cells to regulate smooth muscle contraction. Gap junctions can also form between the endothelium and adherent cells such as leukocytes. Adhesion of circulating cells such as leukocytes can be prevented by the physical barrier that is the glycocalyx, a series of proteins extending from the endothelial surface. The glycocalyx is thought to be pressure sensitive and may communicate mechanical stimulus through the endothelium to the underlying smooth muscle.

Release of vasoactive hormones

Enzymes present in the endothelium are involved in the synthesis of a number of hormones, which are essential in the control of vascular tone and homeostasis, and create an anti-thrombotic environment. Disruption of the balance of these hormones leads to cardiovascular disease, hypertension, atherosclerosis and thrombosis. Examples of these hormones are described below:

a) Nitric Oxide

Nitric oxide (NO) is a free radical gas molecule. A physiological role for NO in the vasculature was first identified when it was confirmed to be the unknown substance previously termed endothelium derived relaxing factor, that had been implicated in the relaxation of rabbit thoracic aorta in 1980 (Furchgott *et al.*, 1980; Ignarro *et al.*, 1987; Palmer *et al.*, 1987). A potent vasodilatory agent, it is produced in the endothelium through the actions of nitric oxide synthase (NOS). NO diffuses to underlying smooth muscle cells, where it acts to stimulate soluble guanylate cyclase (sGC) enhancing cyclic guanosine monophosphate (cGMP) synthesis from guanosine triphosphate (GTP). cGMP mediates smooth muscle relaxation through lowering of intercellular calcium levels and activation of myosin phosphatase(Waldman, 1988) . A schematic of this process is shown in Figure 1.2.

Nitric oxide synthases (NOS) exist in 3 isoforms: NOS-I/nNOS first isolated from the brain and found to have a role in neuronal signalling and in relaxation of skeletal muscle, NOS-II/iNOS a form of the enzyme inducible in response to inflammatory stimuli and NOS-III/eNOS the constitutive form found in endothelial cells. NOS acts through catalysis of the oxidation of the amino acid L-arginine to L-citrulline producing NO (Palmer *et al.*, 1988). L-arginine bioavailability is thus also of importance in the regulation of vascular tone. Key enzymes involved in its synthesis are arginosuccinate synthetase-1 (ASS-1) which catalyses the condensation of L-citrulline and aspartic acid to form L-arginosuccinate, and arginosuccinate lyase (ASL) which catalyses the reaction generating L-arginine from L-arginosuccinate as well as stabilising the NOS multi-protein complex (Erez *et al.*, 2011).

NO has been found to have a role not only in vessel vasodilation but also in inhibition of platelet adhesion to the endothelium (Radomski *et al.*, 1987), inhibition of platelet aggregation (Radomski *et al.*, 1990) and control of smooth muscle migration and proliferation (Jeremy *et al.*, 1999). NO is a short-lived molecule, as it is a radical species, and its availability can be limited due to removal, through reaction with superoxide ions, another reactive oxygen species. Superoxide can be produced through uncoupling of the mitochondrial electron transport chain or by NOS in the absence of its co-factor tetrahydrobiopterin (Cosentino *et al.*, 1995). The effects of superoxide can be mitigated by the endothelial enzyme, superoxide dismutase (SOD) though this is found to be reduced in patients with endothelial dysfunction (Landmesser *et al.*, 2000).

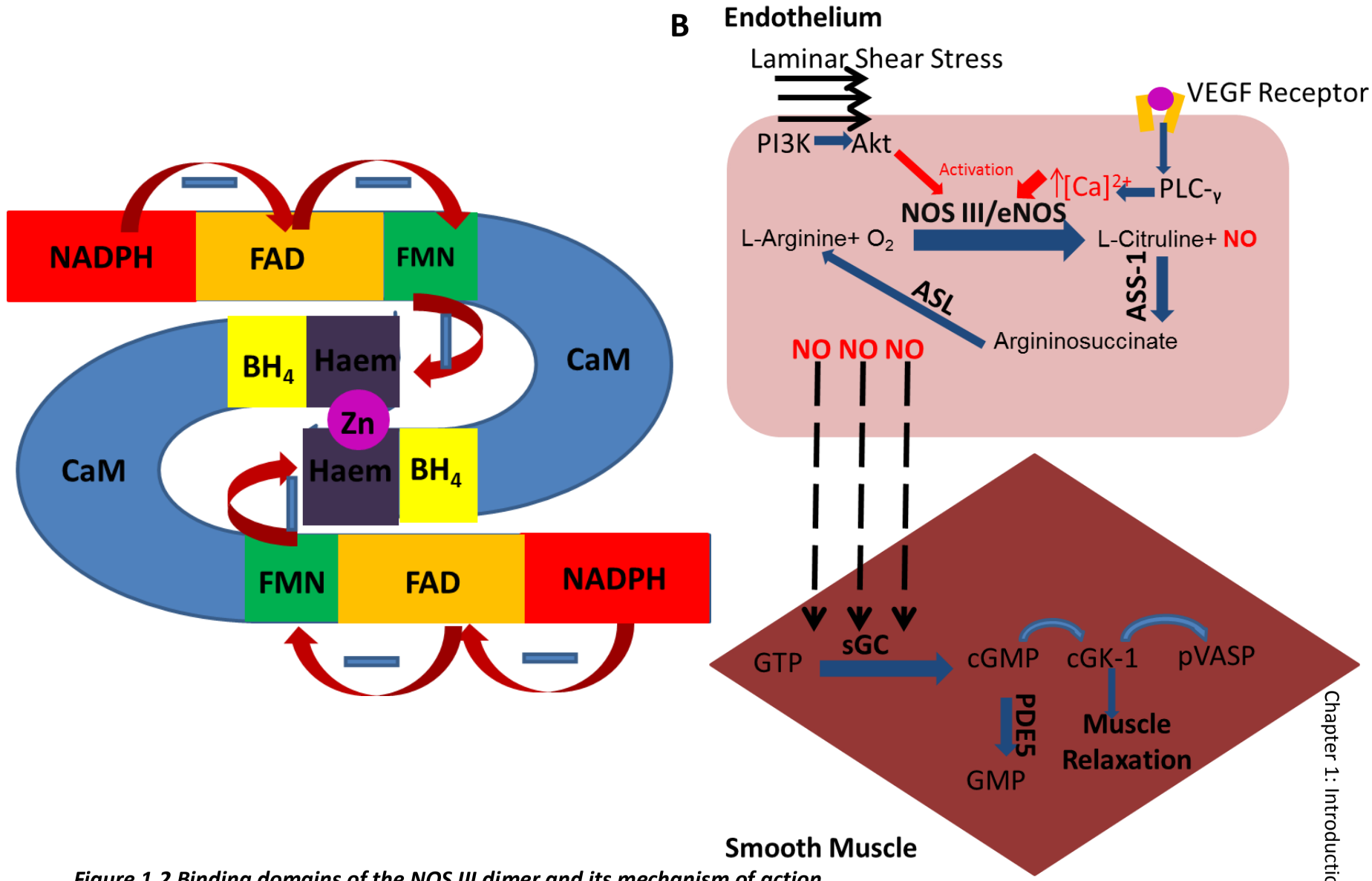

Figure 1.2 Binding domains of the NOS III dimer and its mechanism of action

(Legend continues on next page)

Figure 1.2 Structural domains of NOSIII dimer and mechanism of action <u>(Legend continued from previous page)</u>

A. Adapted from(Fleming et al., 1999). When activated NOS III/eNOS forms a dimer. The two subunits are made up of a reductase domain and an oxygenase domain and a central haem prosthetic group. The reductase domain is found at the C-terminus. Here nicotinamide adenine dinucleotide phosphate (NADPH) binds, where it is dehydrogenated leading to a flow of electrons first to flavin adenine dinucleotide (FAD) and then flavin mononucleotide (FMN), where the electrons are transferred to the haem group of the oxygenase domain at the N-terminus. A zinc tetrathiolate cluster, needed to stabilise the dimer, is also found at the N-terminus and this is also where essential co-factor in nitric oxide (NO) synthesis tetrahydrobiopterin (BH4) binds. In the absence of BH4 the radical species superoxide can be produced. In order for electron transfer to be initiated calcium binding to calmodullin (CaM) is necessary. The sensitivity of CaM can be regulated by Akt dependent phosphorylation and the level of calcium in the cytoplasm increased through the action of phospholipaseC^{-}_{γ}.

B. NOS III/eNOS can be activated by a number of mechanisms, including the examples provided here; of laminar shear stress and vascular endothelial growth factor (VEGF) binding to its receptor on the endothelial surface. When active, NOSIII/eNOS catalyses the conversion of L-arginine and O_2 to L-citrulline and NO. The L-citrulline can be recycled back to arginine through the activity of the enzymes arginosuccinate lyase (ASL) and arginosuccinate synthetase-1 (ASS-1).

NO diffuses through the endothelial membrane to the smooth muscle where it activates soluble guanylate cyclase (sGC) which converts guanosine trisphosphate (GTP) to cyclic guanosine monophosphate (cGMP) . cGMP may be converted to guanosine monophosphate (GMP) through the actions of phosphodiesterase 5 (PDE5) or go on to activate guanylate cyclase kinase-1 (GCK-1) which results in the relaxation of smooth muscle.

b) *Prostacyclin*

Prostacyclin (PGI_2) is a vasodilatory anti-thrombotic lipid mediator discovered in the lab of John Vane in 1976 (Moncada *et al.*, 1976). It is generated through the metabolism of arachidonic acid, liberated from lipids in the endothelial cell membrane by the enzyme phospholipase A_2 (Flower, 1976), to the unstable intermediate prostaglandin H_2 which can be further metabolised to PGI_2 by the enzyme prostacyclin synthetase (Needleman *et al.*, 1979). After arachidonic acid liberation, the rate limiting step of this reaction is the conversion of arachidonic acid to Prostaglandin H_2 which is catalysed (in endothelial cells) by the endothelial enzyme cyclo-oxygenase (COX) (see Figure 1.3). COX exists in two isoforms COX-1, often thought of as the constitutive isoform and the inducible isoform COX-2. Prostacyclin is not the only product of PGH_2 from the catalytic action of COX and endothelial cells are not the only tissues that express it. In platelets the main product of the reaction and further processing enzymes (thromboxane synthase (Hammarström *et al.*, 1977)) is thromboxane (TXA_2) (Samuelsson *et al.*, 1978).

The commonly prescribed class of anti-inflammatory drugs non-steroidal anti-inflammatory drugs (NSAIDs) work to reduce pain and inflammation through inhibition of the actions of COX. NSAIDs are effective treatments; but traditional drugs, such as Ibuprofen, Naproxen and Diclofenac, which inhibit both COX-1 and COX-2, are associated with serious gastrointestinal side effects, which limit their use in some patients (Wolfe *et al.*, 1999). With the discovery of COX-2 and the idea that this isoform, rather than COX-1, is the therapeutic target for NSAIDs, COX-2 selective drugs were introduced as agents with a safer profile for gastro-intestinal side effects (Flower, 2003; Vane *et al.*, 2000). However, with the introduction of COX-2 selective NSAIDs, such as the now infamous Vioxx, came the idea that inhibition of COX could predispose patients to cardiovascular side effects (Bombardier *et al.*, 2000). These side effects are thought to be much rarer than gastro-intestinal side effects (Rahme *et al.*, 2007), but the publicity surrounding them has very much placed COX-2 and cardiovascular health in the spotlight (Topol, 2004). Some have attributed the increased risk of adverse cardiovascular events, such as stroke and myocardial infarction, associated with long-term NSAID use to suppression of COX-2, and subsequent PGI_2 generation, in the

endothelium and the inevitable disruption in the balance with prothrombotic events of COX-1 in the platelet (Funk *et al.*, 2007; Yu *et al.*, 2012) .

Which isoform of COX dominates in the endothelium is a topic which has inspired controversy. Research carried out in our group (Mitchell *et al.*, 2006) and others (Kawka *et al.*, 2007) has failed to show evidence of COX-2 in the native vasculature or in static cultured cells however, others have suggested that this absence is due to a lack of physical forces in culture (FitzGerald, 2002) that drive expression *in vivo* as well as the enzyme being short-lived in endothelial cells post mortem or in static culture. This idea, that lack of physical force causes COX-1 to dominate and COX-2 to be lost in cultured cells has inspired a significant component of this PhD thesis. It is important to understand how shear stress regulates endothelial cell hormones, and the ability to use appropriate models of shear stress to do this features in Chapters 3, 5, 6 and 7 of this thesis. Figure 1.3 shows in detail the synthesis and sensing pathways for prostacyclin within the vasculature.

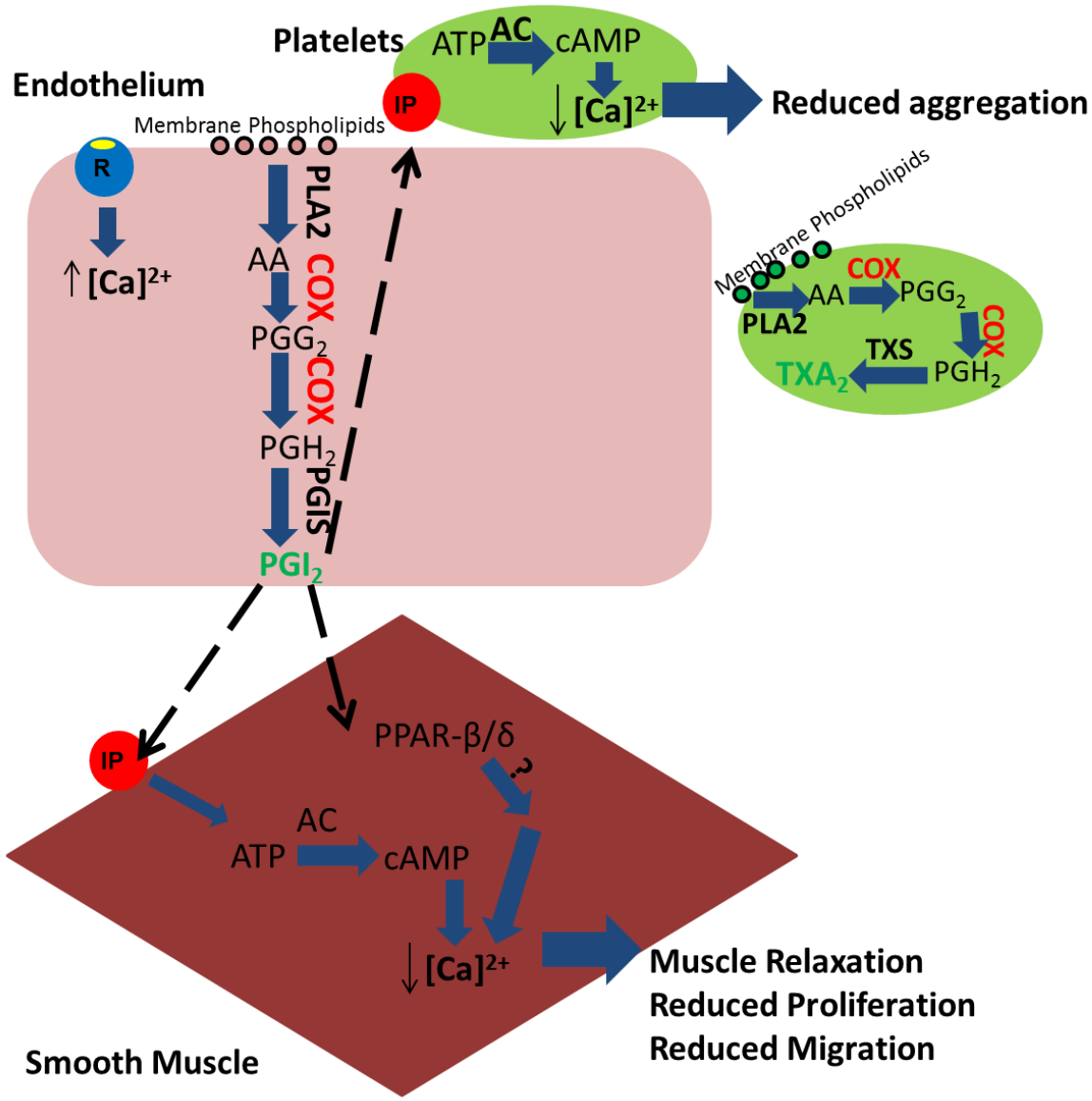

Figure 1.3 Prostacyclin Synthesis and Signalling in the Vasculature ***(Legend continues on next page)***

Figure 1.3 Prostacyclin Synthesis and Signalling in the Vasculature (Legend continued from previous page)

Image adapted from (Mitchell et al., 2008)

Prostacyclin (PGI_2) production in the endothelium is initiated by an increase in intracellular calcium, normally triggered by a ligand binding to receptor. An example of one such ligand receptor interaction is that of acetyl choline and the acetyl choline receptor. An increase in intracellular calcium can activate the conversion of membrane phospholipids to free arachidonic acid (AA) catalysed by the enzyme phospholipase A_2 (PLA_2). The oxidase activity of COX in either of its two isoforms then catalyses the synthesis of prostaglandin G_2 from this AA before the peroxidase activity of COX rapidly catalyses the formation of PGH_2. Prostacyclin synthetase (PGIS) is the final enzyme to act in this chain to produce PGI_2. COX activity is the rate limiting step in this process. In platelets due to the greater abundance of thromboxane synthetase (TXS) over PGIS the pro-aggregatory protein thromboxane A_2 (TXA_2) is produced through a similar chain of events.

PGI_2 acts on platelets and underlying smooth muscle through binding to the prostanoid receptor (IP). Once bound PGI_2 activates the adenylate cyclase (AC) catalysed transformation of adenosine-trisphosphate (ATP) to cyclic adenosine monophosphate (cAMP) which leads to a fall in intracellular calcium levels. In platelets this leads to a reduced tendency for platelet aggregation and in smooth muscle reduced proliferation, reduced motility and increased relaxation. PGI_2 is also known to act on peroxisome proliferator Receptor β/δ (PPAR-β/δ) which has similarly protective effects though the events precipitating these are not well understood.

c) *Endothelin (ET)-1*

ET-1 is a vasoconstrictor agent that was first discovered in porcine aortic endothelial cells (PAEC) in culture in the 1980s (Yanagisawa *et al.*, 1988). 3 isoforms of ET were identified, but ET-1 is the only form released from vascular endothelial cells. ET-1 release is triggered by angiogenic and inflammatory stimuli (Hexum *et al.*, 1990; Ohta *et al.*, 1990) and its synthesis is known to be inhibited by the vasodilatory agents NO (Boulanger *et al.*, 1990) and PGI_2 (Prins *et al.*, 1994) discussed above. It is synthesised as a precursor molecule known as preproET-1, which is processed to a molecule known as BigET-1, before cleavage to ET-1. Both these steps are catalysed by the enzyme Endothelin Converting Enzyme (ECE). ET-1 acts on 1 of 2 known receptors: ETA or ETB, though it is a more potent activator of ETA receptors (see Figure 1.4). Pathological release of ET-1 is associated with disease, including pulmonary hypertension (Giaid *et al.*, 1993). As such ET-1 is an important therapeutic target in the treatment of pulmonary hypertension where antagonists of ETA receptors (ETRAs), such as Bosentan, are first line therapies (Opitz *et al.*, 2008).

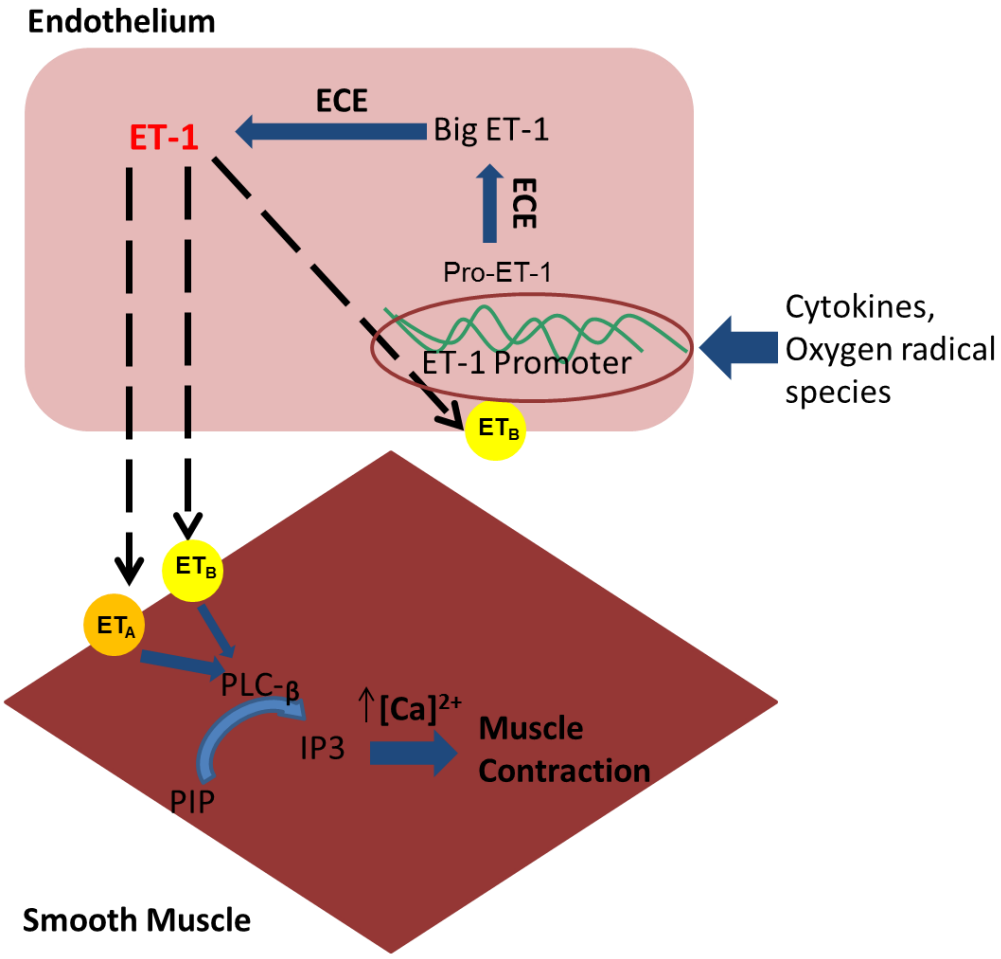

Figure 1.4 ET-1 synthesis and signalling (<u>Legend continues on next page)</u>

Figure 1.4 ET-1 synthesis and signalling <u>(Legend continued from previous page)</u>

Inflammatory signalling leads to transcription factor binding to the ET-1 promoter sequence and the subsequent production of the protein Pro-ET-1. In the presence of endothelin converting enzyme (ECE) the protein is further cleaved to Big-ET-1 and finally the active form ET-1. ET-1 is active on the receptors ETA and ETB though it is a more potent activator of ETA. ETA and ETB receptors are found on smooth muscle cells and their activation leads to increased activity of phospholipase C-β. PLC-β facilitates the cleavage of membrane phospholipid phosphatidylinositol 4,5-bisphosphate to inositol trisphosphate. This initiates the release of calcium from the endoplasmic reticulum leading to the eventual increase in intracellular calcium levels, that results in muscle contraction.

There are additional ETB receptors found on endothelial cells themselves and it is thought that action of ET-1 on these receptors leads to the clearance of ET-1 from the vasculature.

D) *Angiotensin-Converting Enzyme*

Angiotensin is a vasoconstrictive hormone synthesised by the liver in the form of its inactive precursor angiotensinogen. Angiotensinogen is subsequently cleaved to angiotensin I through the actions of renin, a substance produced in the kidney. Angiotensin converting enzyme (ACE) catalyses the cleavage of angiotensin I, a decapeptide to angiotensin II an octapeptide (Yang *et al.*, 1971). Angiotensin II acts on the angiotensin receptor to produce vasodilation. ACE also acts to inactivate the vasodilator bradykinin produced by the kidney (Yang *et al.*, 1967).

Endothelium in innate immunity

Being at the interface of blood flow and prominent in the lungs the endothelium is highly likely to come into contact with any blood born or inhaled pathogens and as such must act on the frontline of the body's defence system. As well as providing a physical barrier to pathogen entry the endothelium also has a role in pathogen sensing and leukocyte recruitment. The endothelium expresses highly specialised pattern recognition receptors (PRRs) of pathogen associated molecular patterns (PAMPs). Receptors expressed include those of the Toll-like receptor (TLR) family, including TLR-4 the receptor responsible for the detection of Gram-negative bacterial coat protein, lipopolysaccharide and the NOD family of receptors (Janeway *et al.*, 2002). Upon activation these receptors can trigger a signalling cascade, leading to subsequent release of inflammatory cytokines such as CXCL8 and IL-1β, common readouts of inflammatory disease (Takeda *et al.*, 2005). Expression of adhesive surface molecules such as intercellular adhesion molecule-1 (ICAM-1) can also be increased leading to recruitment of leukocytes and initiation of the complement pathway.

TLR-4 is of particular interest in this study. After activation TLR-4 can trigger inflammatory signalling through one of two pathways, a pathway dependent on interaction with protein Myd88 (Fitzgerald *et al.*, 2001) through adaptor protein TIRAP or a Myd88 independent pathway (Kawai *et al.*, 2001). Both pathways activate a TRAF6 associated signalling cascade which activates transcription factor NFkB, which is associated with upregulation of inflammatory gene expression. The Myd88 independent pathway additionally activates Interferon regulator 3 which induces interferon regulated inflammatory gene activation (Kawai *et al.*, 2001). Whilst TLRs and other PRRs are essential for endothelial cells to function as immune cells, their activation by host molecules and/or subclinical levels of pathogens is thought to initiate and drive vascular inflammation leading to pathology such as atherosclerosis (Morré *et al.*, 2000) (see Figure 1.5).

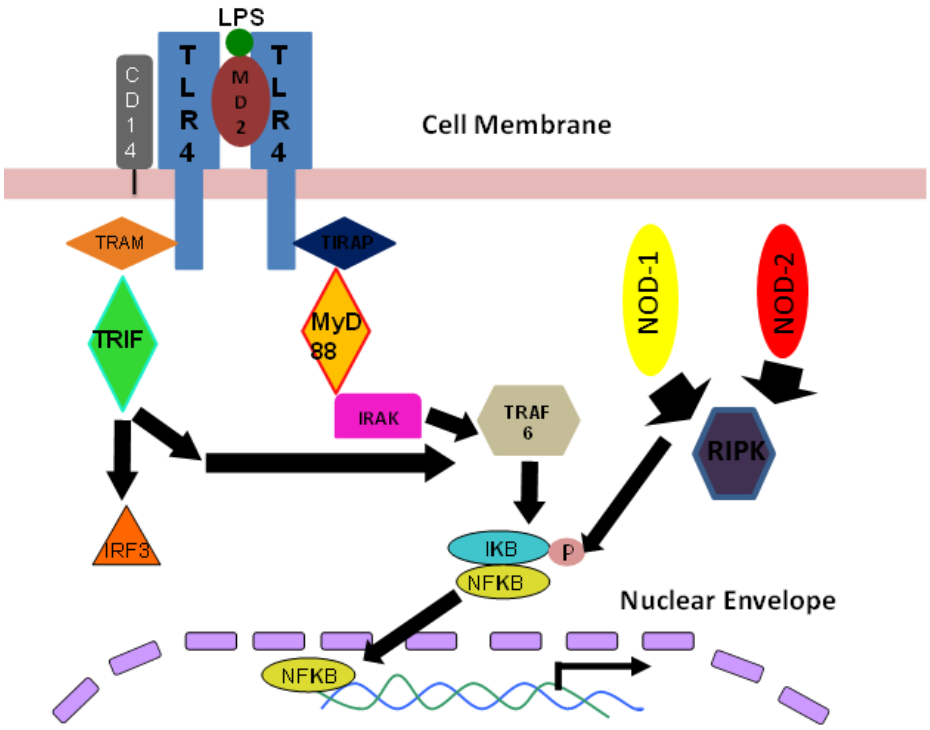

Figure 1.5 Innate Immune Response in the Endothelium ***(Legend continues on next page)***

As a front line in defence against infectious particles passing from the blood stream into underlying tissues the endothelium is equipped with a number of tools for the sensing of foreign particles. First amongst these defence mechanisms is the expression of pattern recognition receptors (PRRs) which are able to sense pathogen associated molecular patterns (PAMPs). Several classes of such receptors exist. One major class is that of Toll-like receptors (TLRs) of which 11 are commonly expressed in humans.

Figure 1.5 Innate Immunity Activation in the Endothelium <u>(Legend continued from previous page)</u>

When activated through binding of ligand LPS, TLR-4 can activate expression of inflammatory mediators either through a myeloid differentiation primary response protein 88 MyD88) dependent or independent pathway. In the MyD88 dependent pathway the toll/interleukin receptor domain (TIR) on the TLR interacts with death domains (DDs) on Toll/IL-1 domain related Adaptor Protein (TIRAP) which associate with MyD88. MyD88 recruits Interleukin receptor associated kinases (IRAKs) 1 and 4. IRAK 1 is phosphorylated by IRAK 4 leading to the association of tumour necrosis factor associated receptor 6 (TRAF 6). TRAF 6 and IRAK 1 dissociate from the receptor and undergo a sequence of events leading to TRAF ubiquitylation and triggering transforming growth factor β activated kinase (TAK 1). TAK 1 activates Inhibitor of nuclear factor kappa B Kinase kinase (IKK). This kinase phosphorylates Inhibitor of nuclear factor kappa B (IκB). Nuclear Factor κ B (NFκB) then translocates into the nucleus where it binds to transcriptional activation sites leading to inflammatory gene expression.

The MyD88 independent pathway is able to initiate the TRAF 6 signalling cascade and also activates Interferon Regulator 3, allowing interferon mediated transcription of inflammation promoting genes.

The internal PRRs NOD-1 and NOD-2 are also able to initiate NFkB activation. NOD-1 is the most prevalent isoform in endothelial cells and recognises a peptide of the bacterial peptidoglycan wall known as iE-DAP to initiate NFκB activation through kinase RIP-K2.

1.3 Endothelial Cells in Culture

Development of isolation protocols

Discovery of the role the endothelium has to play in health has increased the desire for researchers to engage in its comprehensive characterisation. The study of cell types in isolation, to determine information about their specific roles and signalling pathways, independently of confounding influences from nearby tissues has long been used as a tool for this kind of study. The comparatively inaccessible nature of the endothelium compared to other cell types, due to the fact it exists inside vessels, makes it a logical target for *in vitro* study. Despite numerous attempts documented as far back as the 1920s (Nachman *et al.*, 2004) it took a number of decades for the successful isolation of the first endothelial cells. Some early efforts at attaining credibility in the 1960s (Fryer *et al.*, 1966; Pomerat *et al.*, 1963) showed signs of success but were hampered by the lack of a suitable marker to distinguish endothelial cells from contaminating fibroblasts and smooth muscle cells, as had been identified in the cultures of other groups (Nachman *et al.*, 2004). The advent of electron microscopy and the discovery of Weibel-Pallade bodies (Weibel *et al.*, 1964), rod shaped organelles specific to the endothelium, and the later identification of von Willebrand factor (Hoyer *et al.*, 1973; Jaffe *et al.*, 1973a), a protein enriched in endothelial cells and known for its role in attachment of platelets to sites of injury, meant for the first time scientists could confirm the purity of a population of isolated endothelial cells and Jaffe and colleagues (Jaffe *et al.*, 1973b), shortly followed by Gimbrone and associates (Gimbrone *et al.*, 1974) were able to publish methods for the preparation of high yield, stable cultures of human umbilical vein endothelial cells (HUVEC) through collagenase digestion. These cells proved to be a popular choice as umbilical cords were in plentiful supply and as the groups were both based at hospitals minimum transit time was required between obtaining the cord and isolation to flask. The early methods of Jaffe and Gimbrone were subsequently adapted for to the isolation of cells of the major vessels of large mammals, principally the aortas of cows and pigs (see Table 1.1 for key references). Methods have since been developed for successful isolation and culture of endothelial cells from a full range of human vessels including aorta, pulmonary artery and coronary artery. Indeed, as discussed below, these cells are now commercially available and supplied with highly specialised media.

Endothelial Cell Type	Publication Author and Date
Umbilical Vein	(Jaffe *et al.*, 1973a)
Aortic	(Gimbrone *et al.*, 1974)
Coronary Artery	(Gimbrone *et al.*, 1974)
Aortic Valve	(Johnson *et al.*, 1987)
Microvasculature	(Folkman *et al.*, 1979)

Table 1.1 Summary of landmark cell isolation protocols

Endothelial heterogeneity

Despite appearing to share a common line of development, from mesodermal angioblasts in the early stages of embryogenesis, endothelial cells are heavily influenced by the environment of their development and show a surprising heterogeneity based on location of isolation (Aird, 2012). Cells of the microvascular circulation appear to be particularly specialised compared to those of the larger vessels, likely due to their reduced contact with underlying smooth muscle cells. A key difference is their increased level of caveolae compared to large vessels (Simionescu *et al.*, 2002). Caveolae are vesicles at the endothelial cell surface which allow transport across the endothelium through the process of transcytosis. Though caveolae are more common in the microcirculation this is not the case in the blood-brain barrier, at the interface of transport of nutrients to the brain. Here caveolae are reduced compared to all other regions of the vasculature, likely because of the importance of maintaining brain cell integrity. Differences between populations of endothelium from discrete regions of the vasculature are apparent when looking at the binding of specific antibodies (Garlanda *et al.*, 1997). Antibody screening revealed that specific markers exist for endothelium of different organs, for example lymphatic endothelium and HUVEC express desmoplakin (Valiron *et al.*, 1996), where it has a role in cell junction formation, but it is not expressed in most adult vascular endothelial cells. Glucose transporter Glut-1 is highly expressed in the blood-brain barrier though not other adult endothelial tissues (Pardridge *et al.*, 1990).Though this heterogeneity has been well known by scientists for decades it is only in more recent years that the commercial provision of endothelial cells from specific vascular beds has become widespread.

Cell culture requirements

Having successfully isolated cells it is important that they can be maintained and expanded in culture until such point as a significant number is available for experimental activity. To do this cells require nutrition. Early cell cultures were grown in blood or plasma but in 1950 the first cell culture medium termed Mixture 199 (M199) was developed (Morgan *et al.*, 1950). This medium contained an optimum concentration of trace elements, essential amino acids and sugars for cell growth and agents to ensure a balanced pH and was the result of trials of 199 solutions of different nutrient compositions and concentrations. The

first endothelial cell culture isolation procedures were into Dulbecco's Modified Eagle Medium (DMEM), a formulation which contains similar components to M199 but at different concentrations. DMEM contains a higher glucose, pyruvate and glutamine content than M199 but a reduced number of amino acids. M199 contains adenine and adenosine unlike other mediums (Bidarra *et al.*, 2011). In seeking to further optimise the application of these mediums to different cell types manufacturers also offer variations on these classic formulas with options for modified glucose concentrations and altered pH.

Though classic culture mediums are still widely used the increasing commercial interest in providing endothelial cells through isolation and culture or the differentiation of stem cells for medical or pharmaceutical use has driven research into more sophisticated media varieties. New formulations for medium are designed to eradicate the need for biological agents, particularly serum to ensure preparation homogeneity, maximum patient compatibility, reduced possibility of contamination, to ensure cells stay differentiated down an endothelial path after multiple passages and to optimise growth times (Grosvenor, 2012). Examples of such mediums include Clonetics EGM-2 which is available with a selection of additives that can be customised depending on the outcomes desired by the end user.

1.4 Endothelial cells *in vivo* and the role of physical forces

Endothelial cells exist in the dynamic environment of the vessel and as such are subjected to a number of physical forces including cyclic strain, due to the change in pressure across the cardiac cycle and the resultant expansion and relaxation of the vessels and shear stress, the frictional force per unit area of the blood flow acting across the endothelial surface. Shear stress is thought to be the force with the foremost importance but a role for cyclic strain in endothelial health is increasingly being explored (Collins *et al.*, 2006; Sung *et al.*, 2007; von Offenberg Sweeney *et al.*, 2004).

Calculating shear stress

Shear stress is expressed as force over unit area acting parallel to the vessel surface. SI units for this would be reported in Newtons per metre^2 (N/m^2) or Pascals (Pa) but for historical reasons in vascular research they are often presented as dynes per centimetre^2 (dyn/cm^2) (Slager *et al.*, 2005). 10dyn/cm^2 is equivalent to 1 Pa or 1 N/m^2. Shear stress was initially calculated experimentally through determination of a solution through equations, largely reliant on accurate determination of flow velocity. Shear stress is a product of the velocity gradient, also known as the shear rate, near the vessel wall and viscosity. Therefore in order to calculate shear stress flow must be measured near a wall or a velocity profile assumed. Shear stress levels and how they vary throughout the vasculature is now more commonly mapped using sophisticated computer software based on imaging data collected through angiography, ultrasound or MRI which provides accurate geometries and information regarding the flow entering each arterial segment (Katritsis *et al.*, 2007). In straight segments of arteries flow is often laminar, this means it is streamlined, typically with velocity highest at the centre of the vessel and lowest immediately adjacent to the vessel wall. These streamlines can be disturbed by changes in the blood vessel geometry. Turbulence occurs where there are vortices leading to disorder. In this case inertial forces have a dominant effect over viscosity (Malek *et al.*, 1999)

Determining a solution for the level of shear stress requires a number of assumptions on the part of the investigator. Often, to simplify the calculation, a steady flow of blood is assumed, rather than the pulsatile situation seen *in vivo,* so that velocity changes that occur with the cardiac cycle are ignored. It is also assumed that blood has the properties of a Newtonian fluid, meaning it has a constant viscosity, when this is not the case. As blood is a suspension of cells in liquid it is non-Newtonian, meaning viscosity varies depending on the velocity which varies depending upon the interactions between blood cells. At high levels of shear stress blood viscosity is thought to be similar to a Newtonian fluid, but at low levels of shear stress this assumption does not hold true. Rigidity of vessels is assumed and boundary conditions at the edge of the vessel are imposed (Katritsis *et al.*, 2007). Early measurements of shear stress required velocity measurements, calculated based on flow of

a dye through curved pipes, but with advancements in imaging techniques patient specific data can now often be obtained.

Computational shear stress modelling involves constructing an accurate representation of vessel geometry, at times these geometries are based on individual data samples or they may be an amalgamation of geometric data compiled from a number of specimens. The representation of the vessel is then split into discrete elements, in a process known as meshing, and shear stress calculated in each discrete area to give an overall representation in the model vessel. For each element a series of equations termed the Navier-Stokes equations are solved. These partial differential equations allow calculation of fluid velocity in each area. Key equations solved describe conservation of mass, momentum and energy.

Shear stress has been modelled in many of the major arteries of key species for experimental study including mouse (Suo *et al.*, 2007; Van Doormaal *et al.*, 2012), rabbit (Barakat *et al.*, 1997; Vincent *et al.*, 2011) and human (Ku *et al.*, 1985; Moore Jr *et al.*, 1994; Zhang *et al.*, 2012). Often assumptions are made that there will be similarities between species, but there are pronounced differences in shear stress magnitude, principally due to scaling laws (Weinberg *et al.*, 2007). It is important to note that due to the different parameters investigators input into their programmes, different assumptions and the different software used there is some disagreement in the solutions obtained. It is generally reported that shear stress in straight regions of the human arterial tree is on average between 12-15 dyn/cm^2 and at curvatures and branch points 2-5dyn/cm^2.(Malek *et al.*, 1999). However, the validity of these measurements has been called into question by some, as they are based on old measurements and more recent calculations suggest these values may be 10 fold lower with a normal range of 1-2 dyn/cm^2 (Cheng *et al.*, 2003; Tang *et al.*, 2006).

The most commonly modelled arteries are the aortic arch, the coronary artery and the carotid arteries. These arteries are large enough to dissect out for assessment without causing too much damage to their structure and clearly display areas with different geometries. Ultrasound measurements can readily be obtained from these arteries and their patency in health and disease is thought to be clinically relevant. The arch has regions of streamlined shear stress where it is straight, but flow in these streamlines is thought to

become disturbed as the artery curves. Flow in the coronary artery is laminar in straight sections, but is thought to become complex as the artery branches particularly when vessel movement occurs as the heart beats.

As well as modelling shear stress in the native vasculature researchers have sought to modify shear stress in vessels by artificial means such as a surgically applied flow limiting cuff. This cuff can be placed around a straight section of a mouse carotid artery and tightened to alter flow velocity in order to assess how the vessel responds to changes in shear stress. Shear stress is lowered upstream of the cuff, raised within the cuff and oscillatory downstream of the cuff. This is because positioning of the cuff disrupts flow into the artery. Flow is reduced at the opening of the cuff due to the reduced size of the lumen where the cuff tightens over the artery, then on entering the cuffed region flow is accelerated and then vortices occur as the arterial lumen once again widens downstream of the cuff. Low level shear stress appears to have the greatest effect in increasing formation of vulnerable plaque (Cheng *et al.*, 2006). Such methods can help to ensure that shear stress levels in regions of the vasculature compared between animals are truly consistent.

Shear stress in endothelial cell function

The role of shear stress in endothelial homeostasis first became an area of focus for researchers looking at the underlying causes of atherosclerosis. Atherosclerosis is a disease characterised by the formation of cholesterol rich plaques in the walls of vessels and concomitant arterial remodelling. Fatty streaks, early stage indicators of the formation of such plaques have been found in cadavers of children as young as 3 (Holman, 1958) but the full mechanism behind the initiation of these plaques remains unclear. Autopsy data has long suggested that atherosclerosis is a disease that is non-uniformly distributed, occurring only at discrete patches of the vasculature (Roberts *et al.*, 1959). In the 1960s a number of researchers suggested that this patchy distribution of lesions may be due to damage by high levels of shear stress. Experiments by Fry et al applying shear stress through jet injection of fluid over *ex vivo* endothelial tissue appeared to confirm high shear stress as damaging as shear stress levels above 380 dyn/cm^2 stripped the endothelial layer (Fry, 1969). To confirm these findings, attempts were made to assess physiological shear stress by creating an artificial vessel system, a model of pipes produced to have similar geometries to human

vessels, it was found that the regions where vessels were prone to atherosclerotic plaques and fatty streaks would in fact be predicted to experience low shear stress and further studies carried out on *ex vivo* human specimens and on resin casts made from human tissue confirmed this (Caro, 1969). There was a surprising reluctance in recognition of this theory throughout the scientific community but in the present decade it has largely been accepted. With advanced molecular imaging techniques allowing assessment of flow through the major blood vessels in living subjects and the advent of modelling, software models of flow and geometries can now be developed which are more accurate than ever before. However, the underlying reasons for the protective nature of shear stress have not yet been elucidated. Early studies showed that cell permeability differed between cells of atheroprone and atheroprotected regions. Vessel uptake of Evan's blue dye has been used in a number of species, including rat, pig and dog, to show distinct patterns of increased permeability at certain sites in the vessel walls which may correlate with cholesterol uptake and lesion initiation (Gerrity, 1977; Somer *et al.*, 1972). It has also been shown that shear stress has an effect of shear on cell lipid synthesis (Qin *et al.*, 2007) and handling (Murase *et al.*, 1998; Sun *et al.*, 2007) and this could be another area of interest. It has been suggested that cells in areas of low shear stress are 'primed' for activation of the inflammation associated transcription factor NFkB (Hajra *et al.*, 2000).

The mechanism by which cells sense and respond to shear stress is also not fully understood. A number of sensors have been put forward. A leading theory is that signalling is reliant on a CD31/PECAM-1-VE-cadherin-VEGF2R complex (Tzima *et al.*, 2005). The hypothesis is that CD31/PECAM-1 directly senses shear stress and that VE-cadherin acts as an adaptor to bring CD31/PECAM-1 into contact with VEGFR2. Once in contact with CD31/PECAM-1 VEGFR2 is phosphorylated by a src family kinase and once activated triggers a cascade of activation through PI3K. Though there is a lot of evidence for the involvement of PECAM-1/CD31 in shear sensing (Bagi *et al.*, 2005; Fleming *et al.*, 2005; Osawa *et al.*, 2002) precisely how it is mechanosensitive has not been determined. Further work is being carried out to clearly establish the interactions between the proteins of the complex and the cell cytoskeleton as well as the interactions between components of the complex itself. Other alternative theories have been proposed which may or may not act in concert with this mechanosensory complex. One such theory is the tensegrity model which suggests that

the actin cytoskeleton is deformed in response to flow and this mechanical deformation is communicated through a network of filaments in the cell leading to mechanical deformation of the nucleus, activating events leading to transcription factor recruitment (Ingber, 2003; Pourati *et al.*, 1998). A network of filaments in the cytoskeleton activated y mechanosensing by myocardial microcilia has been proposed to play a role in flow mediated development of the heart and endothelial endocardium in embryogenesis (Garita *et al.*, 2011). The glycocalyx has also been suggested as a mechanosensor and it is proposed that the pattern of fluid flow disrupting the protruding glycoprotein strands may lead to dissipation of shear stress which can then in some way be communicated through the cell to initiate signalling cascades(Pahakis *et al.*, 2007). Flow responsive ion channels are an additionally proposed means of shear responsiveness (Barakat *et al.*, 2003).

Shear stress and endothelial cell enzyme expression

The protective nature of shear stress has, by some, been attributed to increased expression of beneficial vascular enzymes such as NOS and COX and suppression of release of hormones such as ET-1. Studying hormone release by the vessel *in situ* has proved to be difficult for a number of reasons. Such reasons include the inaccessibility of the tissue, the close proximity of endothelial cells which have experienced very different patterns of shear and the short-lived nature of many vascular mediators. There are inconsistencies in the literature about shear and these hormones and this may well be down to the lack of standardisation in the way that shear stress is applied and studied in vitro, this notion is discussed in detail below.

1.5 Modelling Shear Stress *in vitro*

Since the suggestion that shear stress plays an important role in endothelial function scientists have sought to model it in cell culture and this may be useful in determining the unconfirmed mechanisms by which cells sense shear stress. With advancements in technology our ability to predict complex patterns of *in vitro* shear stress and translate these predictions to cell culture systems has improved. However, a number of assumptions must still be made in the preparation of these model systems, which can cast doubt on their

accuracy. A number of models have been described in the literature. In this section I discuss in detail the utility and limitations of each model available.

Cone and Plate

One of the first developed means of applying shear flow *in vitro* was a modification of the cone and plate viscometer conventionally used for measuring liquid viscosity (Bussolari *et al.*, 1982; C. F. Dewey *et al.*, 1981). The instrument originally consisted of a rotating, stainless steel cone and a static, stainless steel plate into which indentations had been drilled in which sat glass coverslips. Later modifications allowed for positioning of the cone over a plastic culture dish (Ohno *et al.*, 1993). Movement of the cone generates a flow of medium over the surface of the plate and level of shear stress and condition of flow can be adjusted through manipulation of cone angle and fluid height (Figure 1.8 A). Velocity of medium increases from the centre to the edge of the plate as does cone height, which means shear stress across the plate remains constant. This will only be true at certain cone angles and velocities so careful consideration of these is carried out. This technique has been applied successfully to cells over a number of days (See Table 1.2) however it is difficult to ensure that uniform flow is maintained across all areas of the plate and the technique is limited to only looking at one sample condition at a time.

Disc and Plate

Closely related to the cone and plate system is the disc and plate, where a stainless steel rotating disc, rather than a cone, is lowered towards a stationary plate (Figure 1.8B). Rotation of this disc causes medium to flow in concentric circles, generating a laminar flow profile with shear lowest at the centre of the dish and highest at the edge (Ando *et al.*, 1987).

Parallel Plate Flow Chamber

The parallel plate flow chamber system was developed in 1985 (Levesque *et al.*, 1985), (Figure1.8C). In this system cells are grown to confluence on a glass coverslip, on top of this a rectangular plastic chamber is placed. A stainless steel plate with a hole in the centre is

positioned beneath the coverslip and a border between this steel plate and the chamber secured with silicon glue to form an enclosed chamber. Flow is maintained through a continuous loop with flow entering at one side of the chamber and exiting from the other before repeating this circuit. Flow remains continuous, ensuring all cells experience the same level of shear stress. Shear stress levels are adjusted through increases or decreases in the flow rate. This system has been adapted by many groups resulting in a wide range of possible flow rates and levels of shear stress. In order that cells experience disturbed flow a modification was later developed in which a step disrupts the inflow culture medium affecting its distribution (Truskey *et al.*, 1995). To try and make conditions more physiologically relevant others have used motors to power medium inflow so that it has pulsatility much like flowing blood (Yee *et al.*, 2006).

Fibre and cartridge

To prepare a model system with a more realistic geometry and flow environment to the native blood vessel a fibre and cartridge system has been used (Ott *et al.*, 1995) (Figure1.8D). In this system permeable propylene fibres are mounted into a plastic support and contained in a hollow cartridge through which media flows in and out. Cells are gradually injected into the fibres and the cartridge rotated to ensure even distribution. The permeability of this system and the increased surface area the use of multiple fibres per cartridge brings have been suggested to be advantages of this technique and cells can be maintained in this system for long time periods. However, the lack of a glass viewing component for assessment of cell viability across the duration of the experimental time course is a clear disadvantage and extraction of the cells from the system for subsequent analysis can prove challenging. It is however possible to cut through the fibres for imaging by scanning electron microscopy.

Glass beads

Another means of increasing the surface area available for cell culture is to use glass microcarrier beads. These can be positioned in a column and perfused with medium applying a level of shear stress which should vary with flow rate (Buga *et al.*, 1991), however

as the path of flow the fluid will take is influenced by bead positioning measuring an accurate level of shear stress cells experience in this kind of setting is difficult.

Capillary tube

Another system which attempts architecture more similar to that of the native vessel is the glass or distensible capillary tube. Medium is pushed through these tubes from a reservoir using a flow control pump regulated by computer. Specialist capillary tubes have been developed that are manufactured from deformable silicon have been developed which allow modelling of cyclic stretch on the endothelial as well as shear stress. The capillary tubes can easily be mounted on a microscope stage for live imaging, however their small size makes it difficult to extract a significant number of cells for immunohistochemical analysis (Peng *et al.*, 2000).

Orbital shaker

Orbital shakers, rotating platforms typically used in stirring or mixing solutions have been used to induce shear stress for a number of reasons, firstly they allow shear stress to be applied to cells in multiwall plastic culture dishes that conventional static culture experiments would be carried out in, secondly they allow for higher throughput experiments as plates can be stacked on the shaker, and lastly the fact that the cells are in individual wells means that multiple treatments can be carried out on the same plate Though shear stress has been known to be non-uniform across the wells (Dardik *et al.*, 2005) sophisticated computer modelling can now be applied to the swirling motion of medium in the well to give an accurate reflection of the shear applied to the wells throughout the orbit of the shaker (see Chapter 2 and 3 for further details).

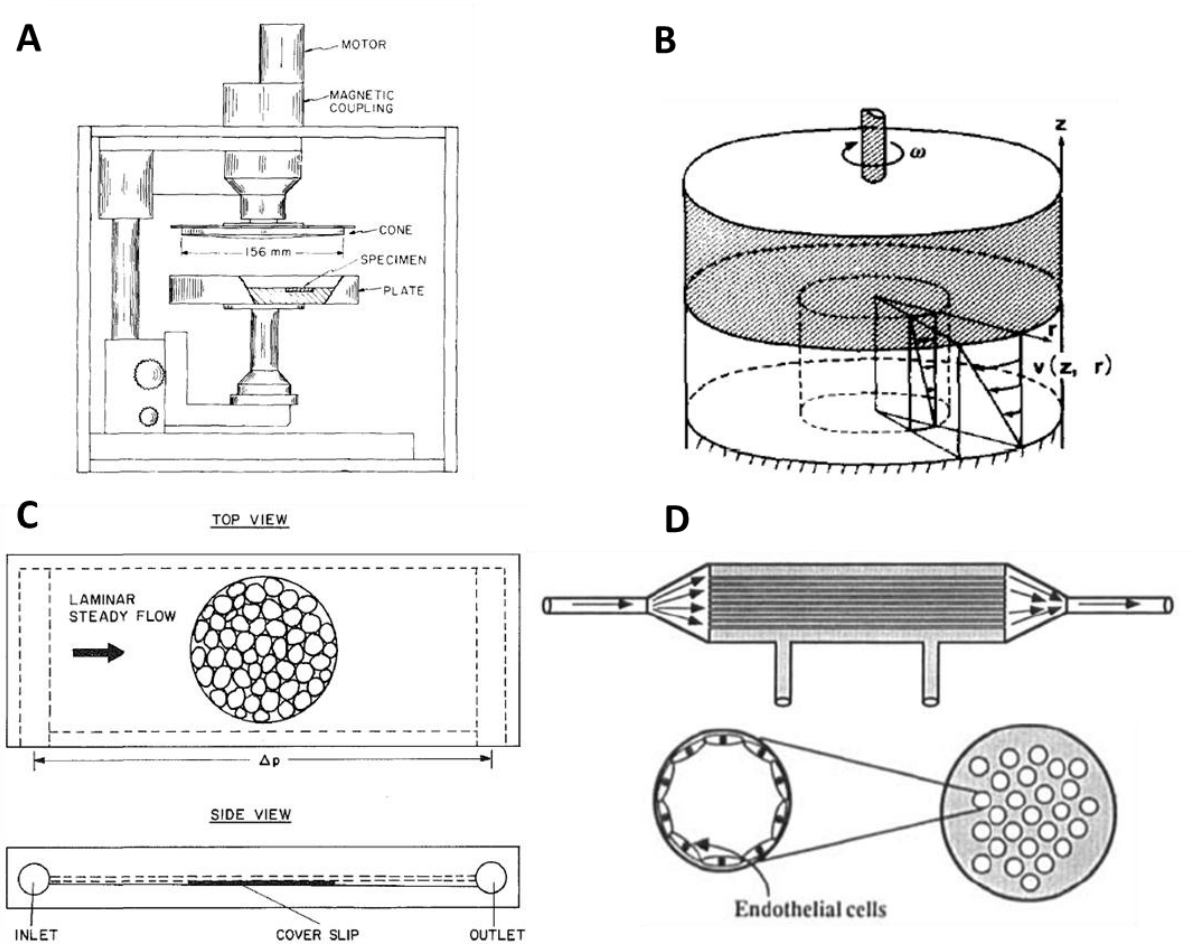

Figure 1.6 Commonly used systems to administer shear stress

A. Cone and plate viscometer ((Dewey et al., 1981)

B. Disk and plate viscometer (Ando et al., 1987)

C. Flow Chamber (Levesque et al., 1985)

D. Fibre and Cartridge(Ott et al., 1995)

1.6 What have we learned from shear stress models? : 'All models are wrong but some are useful'

The advent of *in vitro* shear stress application technologies coincided with the advancement of technology for analysing gene expression of multiple targets. Scientists were quick to consider assessment of mRNA levels, first through differential display (Topper *et al.*, 1996) and then, as technology advanced, microarray (de Waard *et al.*, 1999) as a possible means of determining the proteins behind the atheroprotective and atheroprone phenotypes of endothelial cells. Initial research was focused on finding a protective protein that would be upregulated in response to shear stress. Early experiments typically involved shearing cells for 1 to 6 hours and looking at selected potential target molecules to see if their mRNA levels had increased (see Table 1.2). Such short term applications are unlikely to be physiological when endothelial cells *in vivo* have been exposed to physical forces for the duration of their lifespan and research from others suggests that cell morphological changes may still be occurring over the duration of these experiments (Mott *et al.*, 2007). As a result of this early work it was initially believed that there was a shear stress responsive element (SSRE) in the promoters of certain genes including PDGF-B, HO-1 and COX-1 which would be activated by shear stress application (Resnick *et al.*, 1993) . It has since been confirmed that this sequence is a homologue of the NFkB binding sequence (Khachigian *et al.*, 1995) which suggests that early application of flow may be perceived as an inflammatory stimulus. In spite of this knowledge the majority of publications relating to experiments where shear stress has been applied are still carried out at these early time points. Any experiments performed for a period over 24 hours in length are considered to be representative of chronic shear stress application but in very few instances are such experiments performed (Table 1.2). No data is evident which addresses the question of the length of time it takes an endothelial cell to adjust to a new flow environment at both a morphological and a transcriptional level but it would seem that keeping cells under flow for as long a duration as practical would create the environment most physiologically relevant.

More recent research has looked to identify genes that are downregulated with shear stress compared to static conditions and this has principally focused on genes relating to inflammatory cytokine signalling.

It is a subject of debate as to whether it is appropriate to model a single force on the endothelial cell layer rather than the number of forces known to operate in the native vessel but modelling is a process of continual refinement. No model is going to be able to accurately represent all elements of the vasculature, but by studying individual influences on cells we can get an idea of the important factors that come into play. All models are wrong but through comparison to the *in vivo* system we can establish how they are wrong which increases our understanding.

1.7 Shear stress and the transcriptome

Earlier sections of this work have introduced the need to study changes in endothelial cells as they experience different flow environments and to compare their expression of certain proteins, in order to establish whether a target protein can be modified, to prevent a vessel from becoming susceptible to atherosclerotic plaque development. The easiest way to identify subtle, yet rapidly occurring changes in protein synthesis is to study changes in the messenger riboxynucleic acid (RNA) transcriptome. The transcriptome consists of all RNA in a particular organism, regardless of whether it is coding or non-coding. As RNA expression is the first step in the process of gene expression, study of the transcriptome highlights genes that are being actively expressed. Most commonly, in order to assess the transcriptome, RNA is gathered from a target sample before it is incubated with DNA nucleotides to form complementary strands of cDNA. This cDNA is then hybridised to a chip loaded with reference DNA of the organism under study. Fluorescent markers are used to quantify how many copies of a particular gene have hybridised to the chip and comparisons can show whether or not gene expression is above average or below average identifying changes under the conditions of study. There has been some controversy over the technique, not least the fact that gene expression does not necessarily translate to active protein. mRNA fluctuations can be transient and the vast amount of data produced can be difficult to

analyse. These problems aside, transcriptomics can be a useful tool for assessment of cell response to environmental changes, when used in conjunction with other analytical techniques. Transcriptomics seems well suited for the screening of differences between atheroprone and atheroprotective cells.

A study of transcript profiles in the inner curvature of the porcine aortic arch and the descending aorta (areas predicted to experience low shear stress characteristic of disturbed flow and laminar high shear stress respectively) has indicated that in regions of disturbed flow a pro-inflammatory profile of cytokines is active, as are some elements of the NFkB pathway but protective anti-oxidant pathways are also upregulated and NFkB protein appears to be confined, inactive, to the cytoplasm. Researchers inferred from this that a balance of pro and anti-inflammatory genes exists in the endothelium. The cell collection process in this study leaves room for error, with the regions of proposed high shear stress and low shear stress not clearly defined in a way reproducible in all tissue sampling.

Cell models such as those outlined in 1.5 could prove a valuable means of investigating the effects of shear in a more clearly reproducible way. A number of transcriptomic studies have been carried out in endothelial cells, key examples are highlighted in Table 1.2. Whilst the majority are in agreement that the key changes induced by shear stress are to cytoskeletal genes, genes related to angiogenesis and the nitric oxide synthase pathway there is some variation in results when it comes to looking at inflammatory pathways. Chu et al (Chu *et al.*, 2008) found an increase in genes associated with inflammation and leukocyte adhesion others found an increase in antioxidants and anti-inflammatory markers (Conway et al 2010). This discrepancy is surprising considering the similarity in the two studies but may relate to the way data was analysed in each case. Standardisation of technique and repeats with cells from multiple donors would help to alleviate such problems.

Species and Endothelial Cell Type	Model of Shear	Duration of Shear	Publication Author and Date
Human Umbilical Vein	Parallel Plate Flow Chamber	6 hours or 24 hours 25 dyn/cm^2	(McCormick *et al.*, 2001)
Human Umbilical Vein	Parallel Plate Flow Chamber	24 hours 1 dyn/cm^2 15 dyn/cm^2	(Conway *et al.*, 2010)
Human Coronary Artery	Parallel Plate Flow Chamber	24 hours 15 dyn/cm^2	(Chu *et al.*, 2008)
Human Aortic	Parallel Plate Flow Chamber	24 hours 12 dyn/cm^2	(Chen *et al.*, 2001)
Human Aortic	Cone and Plate	5 or 24 hours 1 dyn/ cm^2 or 10 dyn/ cm^2	(Brooks *et al.*, 2002)
Human Aortic	Parallel Plate Flow Chamber	4 or 24 hours 12 dyn/cm^2	(Heydarkhan-Hagvall *et al.*, 2006)
Human Umbilical Vein	Parallel Plate And Cone and Plate	3, 6, 12, 24, 48 hours 12 dyn/cm^2 15 dyn/cm^2 1.5 dyn/cm^2	(Ohura *et al.*, 2003)
Porcine Aortic Endothelial	Perfusion Pump	24 hours 15 dyn/cm^2	Zhang et al 2012

Table 1.2: Summary of shear stress transcriptomics papers

1.8 Hypothesis and aims

In summary, scientists and engineers throughout the field of endothelial cell biology have now fully embraced the need to understand how shear stress influences endothelial function. As discussed above, there are numerous controversies and unanswered questions that require focused research and understanding. A key limitation of previous research has been the absence of simple protocols where cells can be exposed to shear stress in perpetuity in a system reflecting the polarised patterns of shear stress in the *in vivo* situation, hence, the hypothesis and aims of my PhD.

Hypothesis:

The natural environment of endothelial cells is continuous shear stress; modelling this is critical to our continued understanding of vascular biology.

My overall aim was

To use and validate the orbital shaker model of chronic, complex shear stress on endothelial cells.

My specific aims were:

- To establish how complex shear stress affects endothelial cell morphology. My key consideration was to be able to study these effects over prolonged periods of time. As mentioned above, others have performed similar experiments, but for much shorter periods of time. I was able to shear cells for up to 7 days without loss of viability. To meet this aim I imaged cell morphology and calculated cell 'alignment' and nuclear density. I also investigated how morphology of endothelial cells under shear patterns was influenced by the gross inflammatory insult of lipopolysaccharide (LPS).

- To establish how results obtained using endothelial cells in isolation exposed to different types of shear stress represented what we seen in endothelial cells on native tissue. Again, to meet this aim, morphology, alignment and compliance of cells was measured.

- To investigate how complex shear stress affects the expression of key endothelial protective proteins, namely COX and NOS III/eNOS over chronic time periods.

- To investigate how complex shear stress *in vitro* affects LPS driven NFκB responses

- To determine how prolonged shear stress affects the entire transcriptome of human endothelial cells exposed to control conditions and after activation with LPS

Chapter 2
General Methods

All reagents were obtained from Sigma Aldrich UK, Ltd unless otherwise specified.

2.1 Cells Used

2.1.1 Porcine Aortic Endothelial Cells (PAEC)

Cell Isolation

Thoracic aortas of 6-month old White Landrace Cross pigs were obtained from an abattoir and supplied by Fresh tissue Supplies (Henfield, East Sussex). Cells from more than 30 pig aortas were successfully grown and used for studies throughout this PhD. Unless otherwise stated, protocols were conducted with cells from 3 separate pigs.

The vessels were collected in Hank's balanced salt solution (HBSS) supplemented with 100U.ml^{-1} penicillin, 100µg.ml^{-1} streptomycin, 2.5µg.ml^{-1} amphotericin B and 50µg.ml^{-1} gentamycin and stored at 4^{o}C for up to 24 hours prior to delivery. On arrival aortas were washed with Millipore water to remove any residual blood clots and stored at 4^{o}C, for up to 3 hours in phosphate buffered saline (PBS) supplemented with 100U.ml^{-1} penicillin, 100µg.ml^{-1} streptomycin, 2.5µg.ml^{-1} amphotericin B and 50µg.ml^{-1} gentamycin.

Isolation was based on the method of Bogle et al (Bogle *et al.*, 1996). Each vessel was stripped of adventitia, taking care not to damage the intercostal arteries, which were individually ligated. The vessel was flushed through with PBS supplemented with antibiotics before a 3 way tap was secured with a bag tie at the proximal end of the aorta and clamped at the distal end. 10ml of 0.2mg.ml^{-1} type II collagenase solution was then injected through the 3-way tap and the vessel incubated at 37^{o}C for 10 minutes. Following the incubation the aorta was lightly massaged before collection of the collagenase solution into a 50ml falcon tube through release of the clamp. 10ml of PBS, containing antibiotics, was also flushed through the vessel. This was collected in the same 50ml falcon tube, which was then spun at 190 relative centrifugal force (RCF) in a Hettich Rotina 420R centrifuge for 5 minutes, to obtain a pellet of cells. The supernatant was discarded and the pellet carefully resuspended in 5ml of Dulbecco's modified Eagle medium (DMEM) supplemented with 20% heat-

inactivated foetal-calf serum, 200mM L-glutamine, 100U.ml^{-1} penicillin, 100µg.ml^{-1} streptomycin, 2.5µg.ml^{-1} amphotericin B, 50µg.ml^{-1} gentamycin, non-essential amino acids (L-alanine, L-asparagine, L-aspartic acid, L-glutamic acid, L-proline and L-serine at manufacturers recommended concentrations, Invitrogen Life Sciences, UK), 90µg.ml^{-1} heparin and 5µg.ml^{-1} endothelial cell growth supplement (ECGS) obtained from bovine neural tissue. The cell suspension was placed in a 25cm^2 tissue culture flask, which had been pre-coated with a solution of 1% gelatin at room temperature for 1 hour. PAEC were grown at 37^{o}C in an atmosphere of 95% air and 5% CO_2. 24 hours after isolation the medium was changed to remove non-adherent cells or contaminating cell types such as monocytes. From this point on cell medium was replaced every 2-3 days.

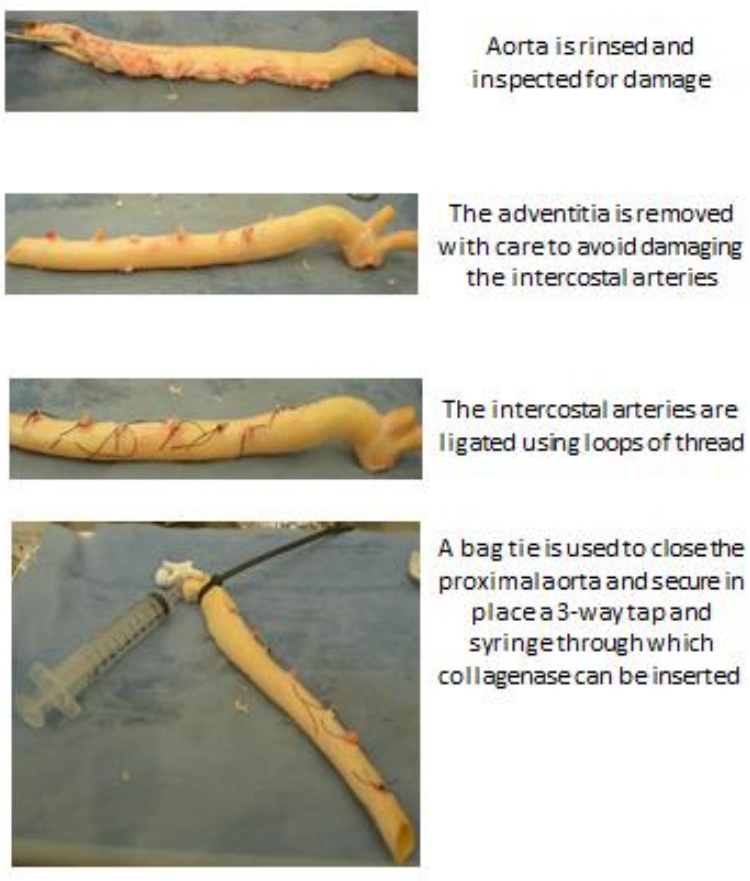

Figure 2.1 ***An overview of the aorta preparation process prior to cell isolation; C. Potter, original images.***

Assessment of cell purity

As is extensively shown throughout the Results chapters, endothelial cells had cobblestone morphology, which is typical of endothelial cells when grown under static conditions. Immunohistochemistry protocols showed that all PAEC stained positive for CD31/PECAM-1, a marker of endothelial cells. Dr. Christina Abbott, another member of our group, tested that the cells were negative for smooth muscle actin and positive for uptake of acetyl LDL.

Cell maintenance and passage

On reaching confluence cells were passaged. The medium from the confluent flask of cells was removed and the cells rinsed twice with PBS at room temperature. The cells were then treated with a 1% solution of trypsin and ethylenediaminetetraacetic acid (EDTA) for 5 minutes at 37^{o}C. After cells became rounded and non-adherent the trypsin solution was neutralised with an equal volume of medium, before the solution was transferred to a sterile falcon tube. The falcon tube was spun at room temperature, 190 RCF for 5 minutes to produce a pellet of cells. The supernatant was discarded and the pellet resuspended in DMEM with additives described above, but 10% rather than 20% FCS. PAEC were used in experiments at passage 2.

2.1.2 Human Aortic Endothelial Cells (HAEC)

Cell Isolation

Cells isolated from deceased donors were purchased from Lonza (New Jersey, USA) in cryovials at passage 3. Details of the donors are given in Table 2.1. Unless otherwise stated, protocols were conducted with cells from 3 separate donors as defined in the Methods section of the relevant Results chapters.

Donor Code	Age of Donor	Sex of Donor
4F1523	40	Female
6F4193	51	Female
6F4009	41	Male
6F3303	54	Female
00000243221	40	Male

Table 2.1 Details of HAEC donor age and sex

Assessment of isolation purity

Results of tests performed by the supplier indicate that HAEC are positive for the endothelial cell marker von Willebrand Factor VIII (vWF) and acetylated low density lipoprotein (LDL) uptake and negative for α smooth muscle actin. As shown throughout the relevant Results chapters, HAEC had cobblestone morphology, which is typical of endothelial cells when grown under static conditions.

Cell maintenance and passage

Cells in cryovials were resuscitated as recommended by Lonza. The cryovial was removed from liquid nitrogen and allowed to thaw in a waterbath at 37^{o}C. Immediately on thawing the contents of the vial were distributed between 4 25cm^{2} culture flasks, each containing 5ml of warmed EGM-2 complete medium (Lonza) and placed in an incubator at 37^{o}C and 5% CO_2. After 24 hours medium was aspirated to remove the cryopreservant. Following this, medium was changed every 48 hours. As the cells became increasingly confluent a greater volume of EGM-2 medium was added; when cells were under 25% confluent media volume was 1 ml per 5 cm^{2}, at 25-45% confluence volume was 1.5 ml per cm^{2} and at over 45% confluence media volume was 2 ml per 5 cm^{2}.

Cell passage was carried out when cells reached 80% confluence using Clonetics reagents (Lonza) (see 2.1.2). Where HAEC were to be used in immunohistochemistry experiments medium was replaced 3 days prior to the experiment taking place with EGM-2 without

hydrocortisone. In transcriptomics studies cell media contained hydrocortisone. HAEC were used in experiments between passage 5 and 7.

As supply of these cells was limited, frozen stocks were made at each passage. $1x10^6$ cells were resuspended in a 2ml solution of 80% complete EGM-2, 10% FCS and 10% Dimethyl sulfoxide (DMSO) and frozen in a -80^oC freezer with a cooling of 1^oC per minute in a Nalgene Mr. Frosty cooling container. After 24 hours frozen cell stocks were immediately transferred to a liquid nitrogen store.

2.1.4 Human Blood Outgrowth Endothelial Cells

Cell Isolation

Cells were isolated by Richard Starke and Koralia Paschalaki at Hammersmith Hospital and were a gift of Dr. Anna Randi (obtained under the ethics code 08/H0708/69). The isolation method was based on that of Ingram et al (Ingram *et al.*, 2004). Mononuclear cells were obtained from the blood of healthy donors and resuspended in EGM-2 medium supplemented with the bullet kit and 10% FCS (Hyclone, Thermofisher). These mononuclear cells were seeded onto 6-well plates which had been pre-coated with type I rat tail collagen for 1 hour at 37^oC. After 24 hours non-adherent cells were aspirated and fresh medium added. Medium was replaced daily for 7 days and following this every second day until the plates were confluent. In the case of successful isolation endothelial cell colonies were identified by day 22.

Donor characteristics are identified below:

Donor Code	Age of Donor	Sex of Donor
A	22	Female

Table 2.2 Details of BOEC donor

Assessment of isolation purity

Isolation purity was assessed at passage 3. BOEC were positive for endothelial surface marker CD31/PECAM-1 and endothelial marker vWF and negative for hematopoietic marker CD45. Immunohistochemistry in this thesis showed cells to be CD31 positive.

Cell maintenance and passage

At confluence the colonies were passaged into 25cm^2 flasks pre-coated with type I rat tail collagen. BOEC were used at passage 5-6.

2.1.2 Human Umbilical Vein Endothelial Cells (HUVEC)

Cell Isolation

HUVEC were isolated from freshly collected human umbilical cords (obtained under the ethics code 04/Q0604/4 approved by the East London and the City Local Research Ethics Committee) by Elaine Shervill of Royal Veterinary College, College Road, London, UK and were a kind gift of Professor Caroline Wheeler-Jones also of Royal Veterinary College. Cell isolations were performed using the method of Jaffe et al (Jaffe *et al.*, 1973b) into M119 medium supplemented with 20% FCS, L-glutamine (2mM), 20µg.ml^{-1} l ECGS and 45µg.ml^{-1} heparin.

Assessment of isolation purity

HUVEC had the typical endothelial-cell cobble stone morphology when grown under static conditions. In immunohistochemistry cells tested positive for expression of CD31/PECAM-1, a marker of endothelial cells.

Cell maintenance and passage

75cm^2 culture flasks at ~60-70% confluence were delivered filled with excess M199. On arrival the M199 was aspirated and cells washed twice with PBS. The M199 was replaced with Lonza Endothelial Growth Medium-2 supplemented with the full bullet kit (EGM-2 complete: contains 2% FCS and human insulin like growth factor, human vascular endothelial cell growth factor, human epithelial cell growth factor, human fibroblast growth factor, ascorbic acid, hydrocortisone, gentamicin and amphotericin at undisclosed concentrations). When cells reached ~80% confluence they were passaged. Cells were first washed twice with 4-(2-hydroxyethyl)-1-piperazineethanesulfonic acid buffered saline solution (HEPES- BSS) before they were treated with trypsin-EDTA (2ml per 5cm^2 culture area) for 5 minutes at room temperature. When all cells were rounded and non-adherent

the trypsin was neutralised using trypsin neutralising solution (4ml per 5cm^2 culture area). Cell suspensions were centrifuged at 190 RCF for 5 minutes at room temperature and the supernatant discarded. The pellet was resuspended in EGM-2 complete. All cells used in experiments were between passages 2-3. Cells in flasks were maintained at a minimum density of 4000 cells per cm^2.

2.2 Modelling Shear Stress

2.2.1 Use of an orbital shaker and Transwell™ System

Numerous methods for applying fluid dynamic shear stress across a layer of cultured endothelial cells exist (see Introduction). However, the protocols used to study shear stress in the literature are invariably limited to relatively short durations of study. It was a key aim of my PhD thesis to study how longer periods of shear stress affect endothelial cell behaviour. In order to address this question I had to identify a model that would allow long term shear to be applied, in a system that would also allow for cell imaging and sample collections. With this in mind, and based on past experiences of one of my supervisors, Professor Peter Weinberg (Warboys *et al.*, 2010), we chose to use an orbital shaker method. This provided an environment where a large number of cells could be subjected to chronic shear stress (up to 7 days), cells could be imaged and media could be sampled. Importantly, this method is not reliant on media recirculation, thus reducing the possibility of infection and cell death. This choice was particularly important since study of cell morphology and correlation of this with mathematical models generated by our collaborator formed a substantial part of my PhD thesis.

A POS-300 Orbital shaker (Grant Instruments) was used at a speed of 150 revolutions per minute, to generate the motion to produce a swirl of medium over the cell surface, introducing non-homogenous shear stress. Cells were initially cultured in 6-well plates containing Transwell™ inserts (Corning). Plates could be stacked on the shaker to increase throughput of the system (see Figure 2.2.1). Inserts were coated with a layer of extra cellular matrix protein (ECM) depending on the cell line used (see Table 2.2.1). Cells were seeded on the polyester filter of the upper chamber of the Transwell™ at appropriate

seeding densities (see Table 2.2.1). Cells were seeded in 3 lots of 0.5ml suspensions, applied to the filter 5 minutes apart to ensure the cells did not become trapped in the filter. 2.6mls of medium was added to the lower chamber (see Figure 2.2.1). Cells were seeded and left for 24 hours to reach confluence before they were placed on the orbital shaker. For all cells exposed to shear stress appropriate control cells from the same animal were monitored, which were grown under static conditions for the same duration of time. In later experiments the orbital shaker was used at the same speed setting, though cells were cultured on the base of wells of conventional 6-well plates with a media volume of 3ml.

Cell counts were carried out to ensure the correct seeding density in a Neubauer Haemocytometer using the 10X objective of a Nikon Eclipse TS100 microscope. 20µl of cell suspension was added to 20µl of trypan blue and 10µl of this suspension was pipetted into the haemocytometer. Non-viable cells were stained blue and not counted. Cells were counted in each $1mm^2$ corner and the total averaged. Medium was added to the original cell suspension to bring the total cells per ml to a number suitable for plating.

A

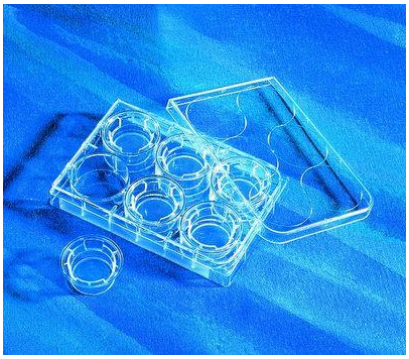

B

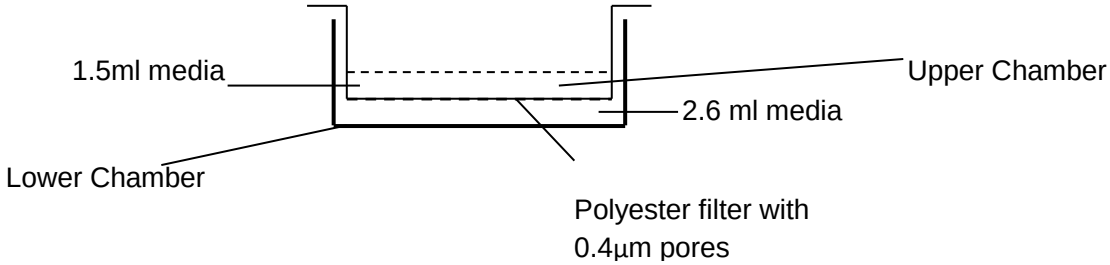

C

Figure 2.2 Transwell™ supports and their use in an orbital shaker model of shear stress

A. 6-well Transwell™ plate. Image shows that an insert with a flexible membrane support can be used for cell culture and can be removed.

B. Illustration of the media distribution at the beginning of an experiment on the orbital shaker. Dashed line indicates fluid meniscus (Potter et al., 2011)

C. The POS-300 orbital shaker

Cell Type/study	Seeding Density	ECM seeded onto	6-well plate used
PAEC	400,000 per well	Bovine Fibronectin	6-well Transwell™ or standard 6-well
HUVEC	150,000 per well	Human Fibronectin	6-well Transwell™
HAEC-Immunohistochemistry	150,000 per well	Bovine Fibronectin	6-well Transwell™
HAEC-Transcriptomics	80,000 per well	None	Standard 6-well
BOEC	150,000 per well	Gelatin	6-well Transwell™

Table 2.3 Seeding densities and matrices each endothelial cell population was seeded onto.

2.2.2 Computational Modelling

In order to understand the full shear stress profile across the cells in a Transwell™ over the orbital period of the shaker, computational fluid dynamics (CFD) analysis was required. Our collaborator Dr. R. Eric Berson, University of Louisville had previously modelled the movement of medium in Transwell™ culture plates on an orbital shaker by solving the three-dimensional (3-D) Navier-Stokes equations using commercial CFD software (Fluent 6.2) (Warboys *et al.*, 2010). Shear stress at the base of the well was derived from the computed fluid motion. As explained in detail in the first Results chapter (Chapter 3), this analysis was expanded for this study and additional data obtained about the shear stress directly at the centre of the well. Though the mean shear across the well was approximately the same in all regions, it was clear from initial experiments that cells at the edge of the well and cells in the centre were not experiencing the same conditions, as their morphologies were quite different. Cells at the edge of the well were elongated and seemed aligned in the direction of flow whereas those in the centre had a phenotype more similar to cells cultured under static conditions. Further post-processing of this solution additionally

identified the temporal pattern of the radial and tangential components of the shear at various radial positions in the well during one orbital period (see Chapter 3).

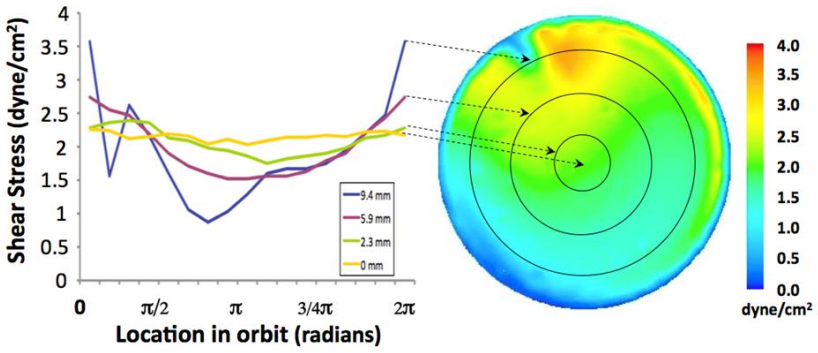

Figure 2.3 The computational fluid dynamics solution over the area of a single well of a 6 well Transwell™ plate.

Shear stress was modelled at various locations on the Transwell™ surface throughout a single orbit of the orbital shaker platform. See (Potter et al., 2011)

2.3 Immunohistochemistry

2.3.1 Immunostaining of cells

Transwell™ polyester filters are easy to cut out and mount on glass microslides for viewing with an immunofluorescence or confocal microscope. Immunofluorescent staining of cells was carried out on the filters attached to their supports. Though the antibodies used differed between experiments, the general method remained the same and is detailed below.

Cells were fixed using a formalin solution. 10% formalin which contains 4% formaldehyde was diluted with PBS to give a formaldehyde concentration of 2%. The cells were then briefly washed twice with PBS. Filters were then stored at 4^{o}C in PBS for up to 7 days or permeabilised immediately. Permeabilisation was with 0.2% Triton X-100 in PBS for 15 mins. Post-permeabilisation cells were briefly rinsed twice with PBS. Cells were then blocked using a solution of 3% BSA in PBS for 1 hour at room temperature. A volume of 1ml per filter was used.

After removal of the blocking solution filters were either treated with 500µl of primary antibody solution or in the case of staining control wells, which contained secondary antibody only, with 500µl of 1% BSA-PBS. A volume of 500µl was used as this is the minimum amount required to cover the complete filter surface. The antibody solution was a 1:250 dilution of primary antibody in 1% BSA-PBS solution. Primary antibody incubation was carried out over 2 hours at room temperature. After the 2 hour incubation cells were washed 3 times, each wash was for 5 minutes with 1ml of PBS per well.

After washing cells were treated with 500µl of secondary antibody solution. The secondary antibody solution was a 1:500 dilution of secondary antibody in PBS. Secondary antibody incubation was 1 hour at room temperature in darkness. After the incubation time cells were washed 3 times, each time for 5 minutes, with 1ml of PBS per well.

A 1:50 dilution of CD31-FITC conjugate in PBS was added to the cells and left overnight at 4^{O}C in darkness. In the morning cells were warmed to room temperature and 4',6-diamidino-2-phenylindole (DAPI) added at a concentration of 1:100 in PBS for 5 minutes. Cells were then washed 3 times, each time for 5 minutes, with 1ml of PBS per well. A scalpel was then used to remove the filter from its plastic support. This was carried out directly over a glass microslide (Santa Cruz Biotechnology, Ca., USA). A single drop of aqueous mounting medium (Vectashield, Vector labs, Cambridgeshire, UK) was positioned on the centre of the filter and coverglass (Santa Cruz Biotechnology) gently lowered over it with forceps. The coverslip was pressed to ensure air bubble removal and flatness of the filter before the slide edges were sealed with nail varnish. Slides were stored in darkness until imaging, the same day, using confocal microscopy.

An identical staining protocol was followed for immunohistochemistry on cells in 6 well plates in terms of incubation times and antibody concentrations. A volume of 700µl was deemed sufficient to cover the well surface for antibody application. No mounting was necessary in imaging of 6 well plates.

The primary antibodies used in this thesis (Table 2.1) are well validated within the literature and within the group. For COX and NOS III/eNOS, primary antibody specificity for cells used in this thesis was confirmed by western blotting (see Results chapters) and, where possible internal controls were used within protocols (e.g. LPS treatment of cells to show increased COX-2 expression in Chapter 6 or NFκB mobilisation in Chapter 5.) Secondary antibody specificity was confirmed in each experiment through the use of secondary controls, to which specific primary antibody had not been added. Any non-specific staining was subtracted from fluorescence values before data was captured for analysis (see below) as described by others (Zakkar *et al.*, 2011).

Primary Antibody	Species	Supplier	Order Code	Concentration	Corresponding Secondary
Anti-COX-1	Rabbit polyclonal anti-serum raised against ovine COX-1	Cayman Chemical	160108	1:250	Invitrogen AlexaFluor568 Goat-anti rabbit 1:500 Code: A11011
Anti-COX-2	Rabbit polyclonal raised against murine COX-2	Cayman Chemical	160126	1:250	Invitrogen AlexaFluor568 Goat-anti rabbit 1:500 Code: A11011
Anti-NOS III	Rabbit polyclonal raised against human	Thermo Scientific (Pierce Antibodies)	PA1-037	1:100	Invitrogen AlexaFluor594 Goat-anti rabbit 1:500 Code: A11012
Anti-NFkB	Rabbit polyclonal raised against human NFkB p65 (C-20)	Santa Cruz Biotechnology (Insight Biotechnology)	sc-372	1:250	Invitrogen AlexaFluor568 Goat-anti rabbit 1:500 Code: A11011
Anti-VE-cadherin	Raised in goat against human VE-Cadherin (C19)	Santa Cruz Biotechnology (Insight Biotechnology)	sc-6458	1:250	Invitrogen AlexaFluor568 Donkey-anti goat 1:500 Code: A11057
Anti-CD31 Human	Raised in mouse against human	AbD Serotec	MCA 1738F	1:50	Direct FITC conjugate
Anti-CD31 Porcine	Raised in mouse against porcine	AbD Serotec	MCA 1746F	1:50	Direct FITC conjugate

Table 2.4 Antibodies used in immunohistochemistry procedures

2.3.2 Immunostaining of Tissue

Porcine hearts with intact aortas were delivered from the abattoir (Cheale Meats, Essex, UK) within 4 hours of slaughter in HBSS supplemented with 100U.ml^{-1} Penicillin, 100µg.ml^{-1} Streptomycin, 5µg.ml^{-1} Amphotericin B and 50µg.ml^{-1} Gentamycin. Aortas were removed and areas of the aortic arch and brachiocephalic artery dissected out, first using surgical scissors and then into smaller sections for immunohistochemistry using a cork borer and cutting board.

Fixation was for 15 minutes in a formalin solution containing 2% formaldehyde. Post fixation, tissue was rinsed with PBS and a combined permeabilising and blocking step was carried out through a 4 hour, room temperature incubation in PBS with 0.5% Triton X-100 and 5% normal goat serum (NGS). After this time, tissue was washed 3 times for 5 minutes with PBS. CD31 in PBS with 1% goat serum was then added and the tissue left at room temperature overnight. The next morning, after 3 x 5 minute washings with PBS, cells were incubated with DAPI for 15 minutes. All staining was carried out in the cavities of single cavity slides (Agar Scientific, Essex, UK) which had been carefully drawn around with a PAP pen to prevent liquid release. Post-staining the cavity of each slide was filled with hard-set mounting medium (Vectashield) and a coverslip coated with clear nail polish carefully lowered into place over the tissue.

2.4 Western Blotting

For these experiments, cells were grown in 6 well plates at an appropriate density under static conditions for 24 hours, prior to 24 hour treatment with LPS or a vehicle control. At this time point cells were rinsed twice with PBS and plates transferred to a box of ice. Cells were homogenised using a lysis buffer comprised of 8.4mls of T-wash buffer, 100µl of 100mM protease inhibitor PMSF (phenylmethylsulphonyl fluoride) in DMSO and a Roche protease inhibitor cocktail prepared in 1.5mls of distilled water. T-wash buffer is 500ml PBS, 1.86g EDTA and 5ml Triton X-100.

50µl of homogenising buffer was applied to one well and the well scraped vigorously with a cell scraper for 2 minutes. The 50µl homogenising buffer and cell suspension was then applied to a second well which was scraped vigorously for a further 2 minutes. Cell suspensions were snap frozen in liquid nitrogen and transferred to a -80^{o}C freezer for storage until use.

Prior to use, protein concentration in the homogenates was determined using the Bradford assay. Homogenates were compared against a standard of known concentrations of BSA. Samples were diluted with PBS to ensure that 10µg of protein was run in each lane of a 10 well gel. Protein samples were heated to 90^{o}C for 10 minutes in Lamelli loading buffer (Bio-Rad, Hertfordshire, UK) at equal volume to that of the protein solution. 7.5% polyacrylamide gels were used. The resolving gel was prepared from 3ml of ProtoGel (National Diagnostics, GA., USA), 3ml of resolving buffer, 6 ml of water, 150µl ammonium persulfate (APS) and 15µl of N,N,N',N'-tetramethyl- ethane-1,2-diamine (TEMED). This was left to set for 30 minutes before the stacking gel was applied. The stacking gel was prepared using 700µl ProtoGel, 1.3 ml stacking buffer, 3ml water, 75µl of APS and 35µl TEMED. This was left for 10 minutes before the gel was loaded. Gels were run for 1 hour at 100V. Bands were transferred onto blotting paper by wet transfer at 20V. Bands were exposed by blocking for 1 hour with 10% milk buffer at room temperature, incubation of primary antibody at the appropriate concentration overnight at 4^{o}C and incubation with secondary antibody for 1 hour at 4^{o}C before treatment with developing agent and exposure at 2 minute intervals for up to 10 minutes.

2.5 Confocal Microscopy

2.5.1 Imaging

Immunofluorescently stained cells and tissues were imaged using confocal microscopy. In conventional immunofluorescent wide field microscopy a light source excites fluorescence from all parts of a specimen. This leads to detection of secondary fluorescence outside the region of focus, which can interfere with the signal of interest which can lead to poor resolution. This problem can be avoided in laser scanning confocal microscopy. Laser light

travels through a pinhole and is focused through an objective onto a single focal plane of the sample known as an optical section. Reflected light and fluorescence are separated by a dichromatic mirror and fluorescent light at the specific wavelength of interest is directed to a photomultiplier. The photomultiplier converts the fluorescent light into a digital signal. As the laser scans across the sample a digital image builds up pixel by pixel. The brightness of each pixel corresponds to the intensity of the fluorescent light emitted by the sample. Multiple photomultipliers can be used to detect fluorescence of more than one wavelength.

All confocal microscopy was carried out using a Leica SP5 inverted microscope equipped with a diode laser, an argon laser and a helium neon laser and Leica LAS AF software. The microscope is the property of the Facility for Imaging and Light Microscopy, South Kensington Campus, Imperial College London.

Details of laser settings used in each experiment can be found in Table 2.5. Settings were determined at the start of each experiment and maintained throughout experimental runs to ensure the measurements were comparable. Gain settings and averaging of signal were determined by looking at the microscope limits of detection of signal from a positive control sample, likely to have the highest level of immunofluorescence, and a negative control sample, likely to have a low level of signal compared to most samples viewed.

Experiment	**Diode Laser (Blue)**		**Argon Laser (Green)**		**HeNe Laser (Red)**	
	Wavelength (nm)	**Gain**	**Wavelength (nm)**	**Gain**	**Wavelength (nm)**	**Gain**
PAEC COX-1, COX-2	406-458	750	493-544	1000	585-680	850
HAEC COX-1, COX-2	406-458	700	493-544	1000	585-680	850
BOEC NOS III	420-480	630	500-550	1000	585-680	850
PAEC NFkB	420-480	650	500-550	950	585-680	780
PAEC NOS III	420-480	650	500-550	1000	590-700	900
Tissue	420-480	660	500-550	730	N/A	N/A

Table 2.5 Confocal Microscope settings

When looking at cells, two regions of interest in each Transwell™ were studied; the area directly at the centre of the well, which was known to have experience shear of a constant magnitude with no preferred direction, and an area 3.4mm from the edge of the well thought to experience unidirectional, pulsatile flow. Positioning was determined by marking the centre of the well and the two outside edges and counting 7 fields of vision from the edge to the centre. Images were taken from the left and right edge and left and right of the centre point.

When examining native tissues one image was taken per tissue section of interest. Up to 5 sections were obtained from each region. To ensure visibility of whole fields it was necessary to create maximum projection, composite images from a stack of images generated in the z plane of the tissue. This was necessary as the tissue was not of uniform thickness. For this reason CD31 immunofluorescence in tissue was not quantified.

2.5.2 Quantification and Analysis

Cell Counts

In order to assess the validity of comparisons in immunoreactivity between different regions of the Transwell™ inserts and between different regions of the tissue, cell counts were carried out on each confocal image generated. Initially these cell counts were carried out manually, with a 175µm by 175µm region of the 387.5 by 387.5µm image counted in each case. Only whole cells were counted and any DAPI staining that was thought to be non-specific as it had been taken up by the Transwell™ filter excluded. In later studies a nuclear focused image which could be used for automated cell counting was taken. The method of counting used for each protocol is indicated in the text of the relevant chapters.

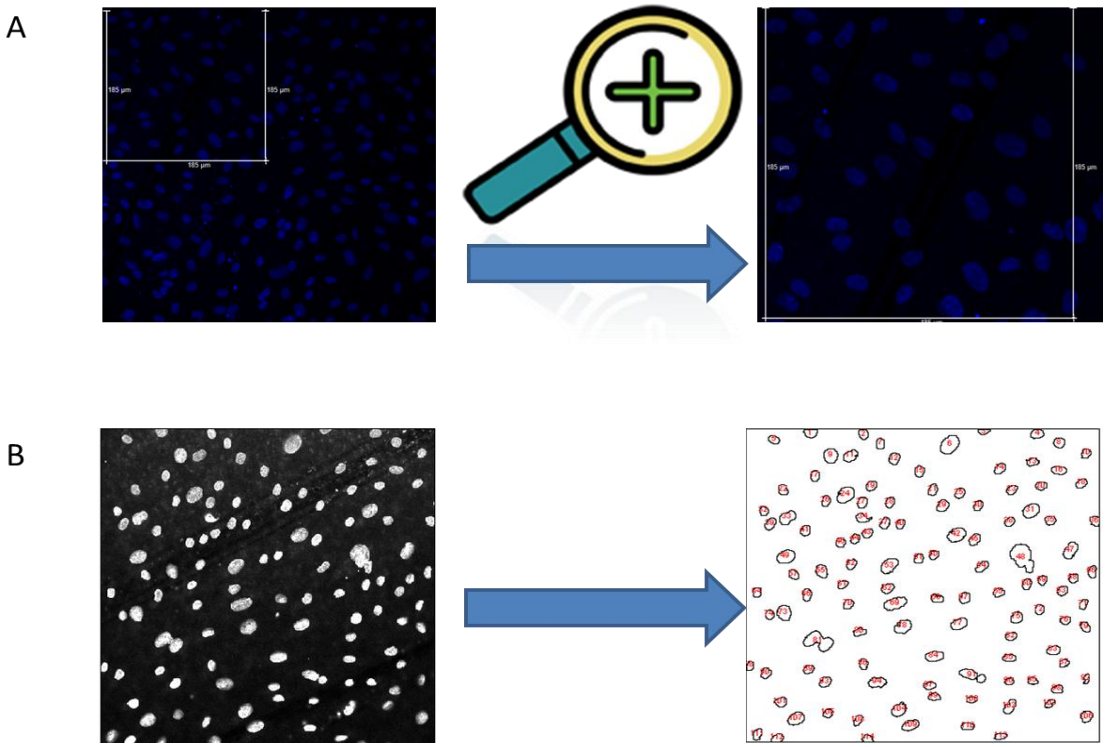

Figure 2.4 The two methods of cell counting used in assessing cell number in confocal fields

A: Manual counts-A 175µm^2 region in the top corner of the frame is selected and zoomed in on and nuclei counted manually

B: Automated counts- Fiji software is used to threshold a full field image of the nuclei. Objects deemed to be of appropriate size are outlined and counted.

Assessment of endothelial elongation and alignment

Assessment of cell alignment in confocal images was carried out by a method of blind scoring. Images of the CD31 staining of the two regions of interest were randomised. The images were then rated by 2 to 3 independent observers on a scale of 0-3 on the basis of their alignment. 0 represented no degree of alignment whereas 3 represented unidirectional alignment in a complete field of view (Figure 2.5). This process was then repeated for cells which had been sheared for 24 hours.

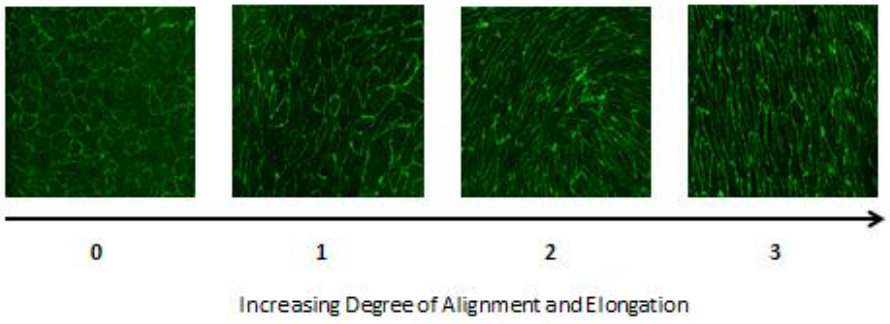

Figure 2.5 Examples of Cell Alignment Scores

Cells were rated from 0-3 with 0 being all cells appear to be cobblestone in nature and randomly orientated and aligned and 3 being all cells in view are elongated and unidirectional in alignment.

Methods for more detailed analysis of NFκB mobilisation (Chapter 5) and nuclear alignment (Chapter 4) are described in detail in the relevant chapters.

2.6 Scanning Ion Conductance Microscopy (SICM)

Scanning ion conductance microscopy (SICM) is a modified form of scanning probe microscopy, developed by Paul Hansma in the 1980s (Hansma *et al.*, 1989) and further adapted, to be compatible with the imaging of live cells and tissues without direct contact (Korchev *et al.*, 1997). There are two defined means of SICM: the classical scanning mode and the recently-developed hopping probe ion conductance microscopy (HPICM). In scanning mode the probe, which is a glass tip filled with an electrolyte solution, is connected to a feedback control system. This control is reliant on the fact that the position of the tip of the probe relative to the sample dictates the ion flow through the pipette. As the probe approaches the sample ion flow into the pipette is impeded. Feedback ensures that the probe is maintained at a set distance from the surface of the sample as the sample is scanned in the x and y directions and recordings of the ion flow allow for generation of a 3-dimensional map of the sample surface. Though effective, this technique is limited in detecting fine surface structures protruding from the cell, which the probe can easily collide with, leading to damage to the sample and/or the probe. To address this limitation HPICM

was developed(Novak *et al.*, 2009). In HPICM rather than relying on the continuous feedback of the conventional system the probe approaches the sample and at a distance from the sample a reference current is set, when this reference current declines by 5% the probe is withdrawn and the sample moved laterally. As the probe always approaches the sample from above there is little chance of surface feature collision.

An additional feature of SICM that has been developed is a function for measuring compliance of individual cells. In this mode an area is scanned and a controlled pressure, administered through a jet of liquid, is applied to a defined point on a cell (Sánchez *et al.*, 2008). This allows for measurement of membrane compliance through monitoring the degree of deformation of each cell and its subsequent recovery.

In studies in this thesis cell or tissue samples were scanned for up to 2 hours in Leibovitz's L-15 medium (Invitrogen).

The pipettes used in scanning/hopping and for deformation have different associated diameters and resistances. In order to generate a high resolution image in HPICM a fine pipette is used with a tip diameter of approximately 100nm and resistance of approximately 100 MΩ. Images generated in compliance mode have a lower resolution as in order to administer a liquid jet the diameter of the pipette tip must be greater. These pipettes are typically 500nm in diameter with a resistance of approximately 20 MΩ.

A

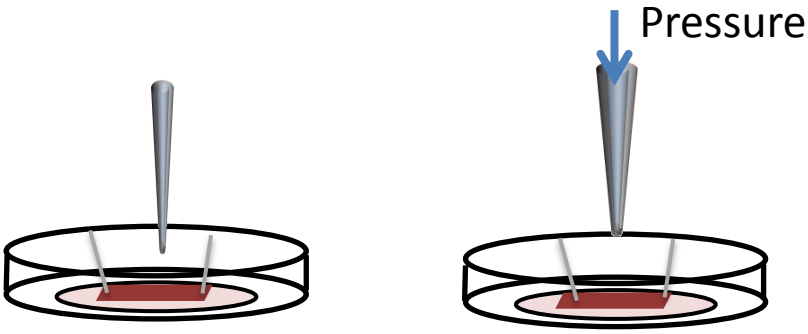

Cells on gel support or tissue pinned to wax

B

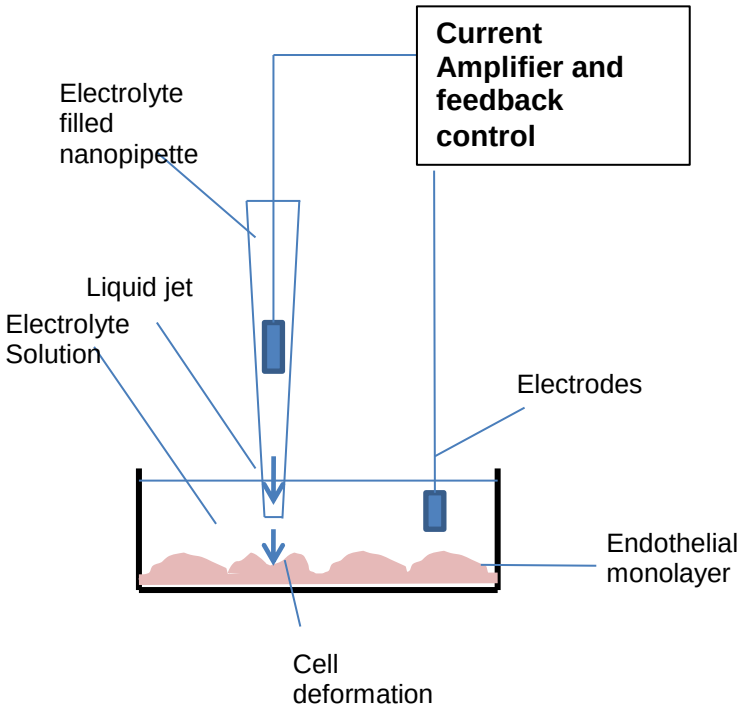

C

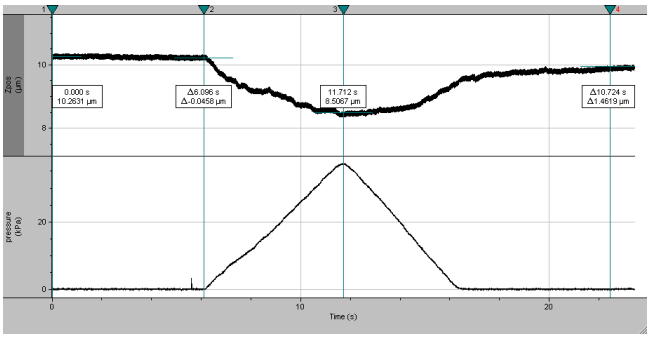

Figure 2.6 Schematic of SICM ***<u>(Legend continues on next page)</u>***

A. Tissue samples are pinned to wax or Transwell™ filters placed on gel supports in dishes filled with Leibovitz's L-15 Medium. In HPICM movement of the stage allows a fine pipette to scan across the surface of the cells.

Figure 2.6 Schematic of SICM ***(Legend continues on next page)***

In SICM for compliance measurements a larger pipette is used and a jet of liquid applied through it to cause deformation at the high point of the underlying cell.

B. Schematic of the microscope showing feedback control as the pipette tip approaches the surface and how application of a jet of liquid leads to localised cell deformation.

C. An example readout showing how an increase in pressure (lower trace) corresponds with cell deformation (upper trace) showing cell recovery as pressure is reduced.

2.6.1 Image analysis

Assessment of cell alignment was also carried out on images generated by SICM. ScanIC software was used to draw a line down the longest axis of the cell. A line was drawn bisecting this at the widest point of the cell at a 90^{o} angle. Cell length to width ratio was calculated and the resulting values referred to as an index of elongation. This means of analysis was used to assess elongation of both cultured cells and those in the native tissue.

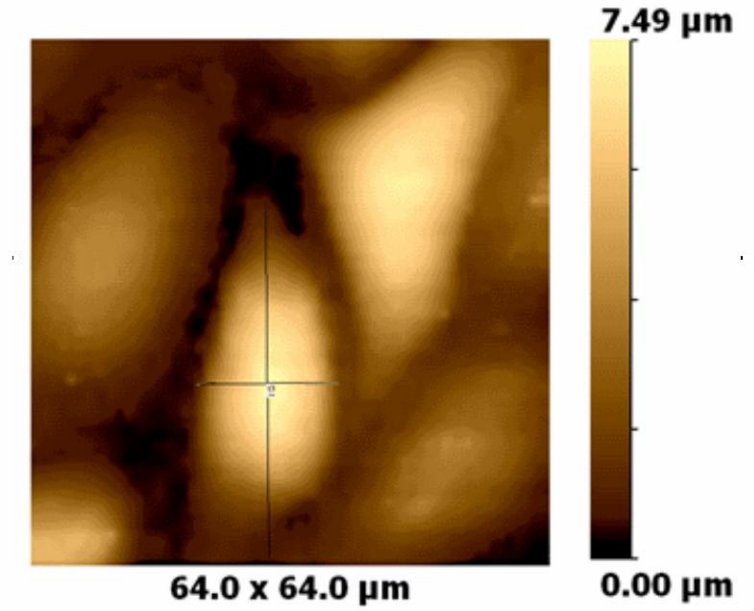

Figure 2.7 ***Example of Calculation of Endothelial Cell Length to Width Ratio***

A 2-dimensional view of cell surface topography is generated based on topography data captured by SICM. Cells with complete outlines in the field of view are assessed. One line is drawn along the longest axis of the cell and another, which bisected the first at 90^{o}. The software (ScanIC) calculates the lengths of the two lines and from this length to width ratios are prepared.

As the topographical information obtained by SICM shows cell structure in 3-dimensions the data can also be used to calculate cell volume. Provided that the image has a gap between cells that can be designated as the base line from which cell height can be measured volume can be calculated in the ScanIC software by highlighting the cell of interest as described in (Korchev *et al.*, 2000).

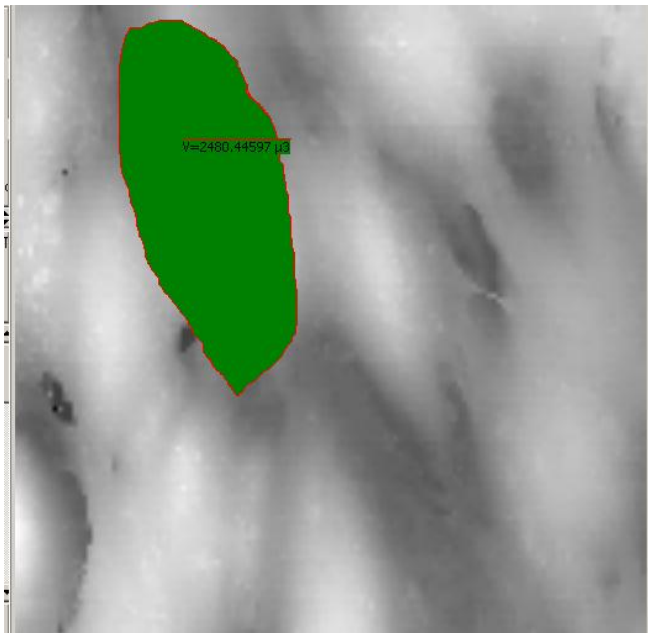

Figure 2.8 Example of measurement of cell volume

Having set the baseline figure from which cell height can be recorded an individual cell is highlighted and its volume calculated by ScanIC software

2.7 Enzyme Linked Immunosorbent Assays (ELISAs)

In order to reliably measure endothelial cell function it is necessary to measure release of soluble physiological mediators which play a role in vascular homeostasis. In this thesis I looked at the inflammatory cytokine CXCL8/IL-8, the vasoconstrictive agent ET-1 and the stable breakdown product of the vasoactive hormone prostacyclin 6-ketoPGF$_{1\alpha}$. These mediators are all released at basal levels in the healthy endothelium and levels are altered when the endothelium is dysfunctional or in the presence of inflammatory stimuli.

To analyse levels of the inflammatory mediators CXCL8/IL-8 (Figure 2.7A) and ET-1 (Figure 2.7B) produced by endothelial cells sandwich ELISA kits designed for the purpose were used, following the manufacturer's instructions, to measure mediator release into the cell medium (R&D Systems human CXCL8/IL-8 Duoset and R&D Systems human/porcine ET-1 quantikine) . Both of these ELISA kits rely on the same principle, which is briefly described below. Firstly a 96 well-plate was coated with an antibody against the agent it is designed to detect e.g. anti-CXCL8/IL-8 in the case of the CXCL8/IL-8 ELISA. Samples were pipetted onto this plate and incubated for a length of time, as were a range of standards of known concentration of the agent of interest. These standards were then used for comparison. If the agent of interest was present in the sample it bound to the plate. Plates were then washed and incubated with a second antibody. This second antibody used is raised against the agent of interest and will bind to any bound to the plate. This detection antibody is conjugated to HRP (horseradish peroxidase) or streptavidin. Plates were washed to remove non-specifically bound antibody before treatment with a hydrogen peroxide and tetramethyl benzidine (TMB) mixture. In the presence of HRP or streptavidin TMB is oxidised in a reaction with hydrogen peroxide to form a blue, free radical cation, with absorbance at 653nm. Treatment of this blue compound with acid leads to further oxidation of TMB and production of a yellow compound, tetramethyl benzidinediine which absorbs light at 450nm. How much of this yellow compound is present can be quantified based on the solutions absorption of light at a yellow wavelength. Absorption values are then compared to absorption values of known quantities of the agent of interest. How yellow the solution is in each well is directly proportional to the amount of agent of interest that was present in the initial sample as per the Beer-Lambert Law $A=\varepsilon cl$ where A is absorbance, ε the molar absorption coefficient, c the molar concentration and l the pathlength of the light .

To quantify the amount of 6-ketoPGF$_{1\alpha}$ in a sample a competitive ELISA was used (Cayman Chemical 6-ketoPGF$_{1\alpha}$). A competitive ELISA works by slightly different principles to a sandwich ELISA. As with the sandwich ELISA a 96 well plate was coated with an antibody against the agent of interest. The plate was then incubated with sample. The plate was then incubated with a tracer of 6-ketoPGF-1α conjugated to acetylcholineesterase. If limited 6-ketoPGF1α was present in the sample this tracer would be able to bind to the initial coating antibody. The plate was then washed and treated with Ellman's reagent the substrate for acetylcholinesterase. If a reaction between acetylcholineesterase and Ellman's reagent occurs the solution turns yellow, therefore how yellow the sample is is inversely proportional to the amount of the agent of interest in the initial sample.

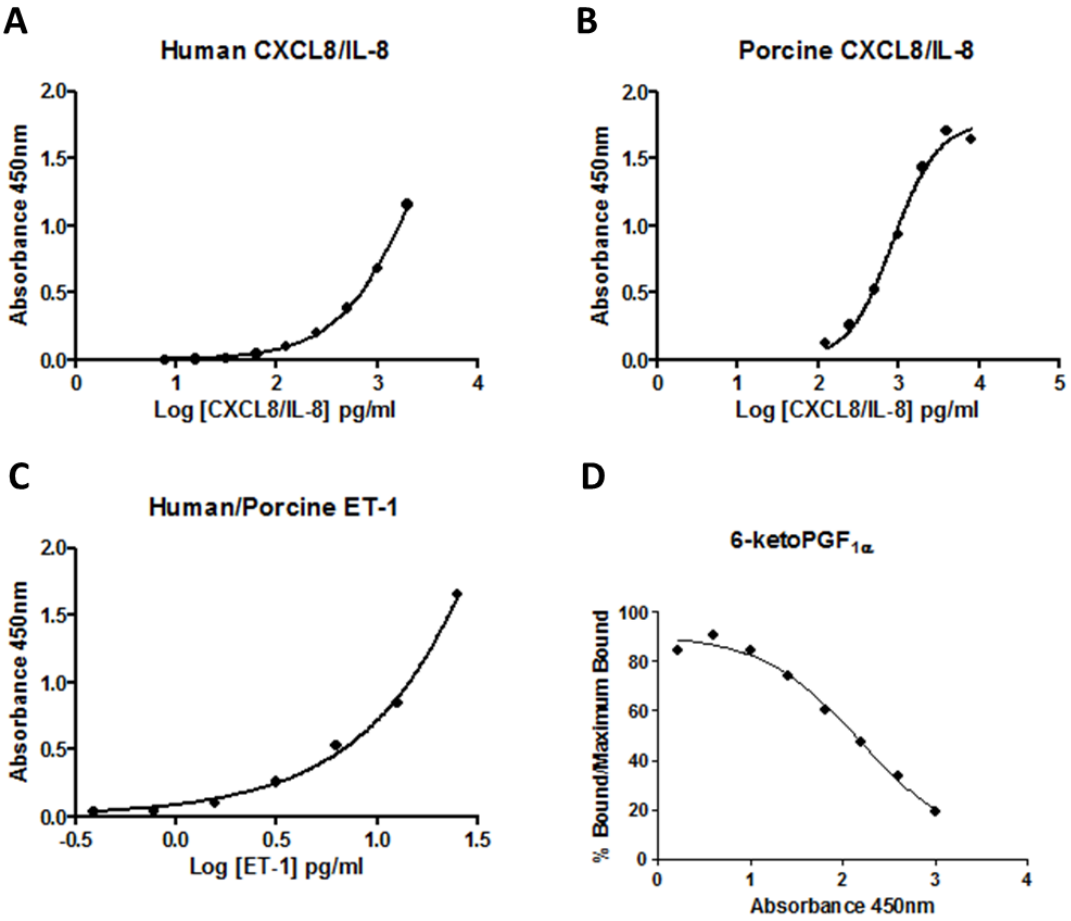

Figure 2.9 Example Standard Curves for each ELISA used

A log scale is typically used to ensure linearity in the range in which most samples fall.

2.8 Transcriptomics Analysis

2.8.1 RNA Extraction

RNA extraction was performed using Qiagen RNeasy mini spin-column kits as per the manufacturer's instructions. Briefly, cell medium was collected and cells washed with sterile PBS before they were treated with a lysis buffer containing guanidine-thiocyanate and β-mercaptoethanol. The lysate was then homogenised through a 2 minute spin in a QIAShredder spin-column at 18,000 G. The homogenised lysate went through a series of further washes in different spin columns with high-salt buffers, which allow binding of RNA to the silica column before the purified RNA was eluted into DNAse/RNAse free water. RNA concentration and purity was confirmed through UV absorption at 260/280nm.

2.8.2 Gene Array

Gene array was performed by staff at St. Bartholomew and The London Genome Centre (BLGC), Queen Mary University.

Total RNA was converted to labelled cDNA via reverse transcription and then hybridised to Illumina Human Ref.8v3 Bead Chip Arrays (Illumina, UK) and quality control performed before data sets were received for further analysis.

Analysis was carried out with the assistance of students Sarah Mazzi and William Wright and Dr. Mark Paul-Clark at Imperial College London. All analysis was performed using GeneSpring GX12.1 (Agilent Technologies). Data sets were $\log_2$ transformed and quantile normalised through a baseline, set to the median intensity of all samples. Significantly differentially expressed genes were identified based on a 1.5 fold cut off. These genes were identified using unpaired t-tests ($p<0.05$) with Benjamini-Hochberg False Discovery Rate (FDR) correction.

2.9 Data and statistical analysis

Data are presented as mean ± S.E.M. for n= separate determinations stated in each case. For experiments on porcine or human endothelial cells, unless otherwise stated, all

protocols were performed on cells from at least 3 separate pigs or separate donors respectively. Where data were blind scored the nature of the image was not known to the scorer. All images were scored by at least 2 independent scorers and the mean of their scores recorded. Data were analysed using GraphPad Prism v5, as described in individual figure legends. Statistical significance was assumed where $p<0.05$.

Chapter 3
Analysis of the effect of complex *in vitro* shear stress on morphology of endothelial cells: correlation with shear directionality

Rationale

Endothelial cells line the luminal surfaces of blood vessels. In this dynamic environment they experience a number of mechanical stimuli tied to the cardiac cycle. These stimuli include cyclic strain, generated as vessels expand and relax with the pulsatility of blood flow, and shear stress, the friction caused by the flow of blood over the cell surface. These forces are not all uniformly experienced by the endothelium, as distribution can vary with changes in local vessel geometries.

Since development of isolation and subculture methods in the early 1970s (Gimbrone *et al.*, 1974; Jaffe *et al.*, 1973b) *in vitro* use of endothelial cells has become standard practice in the study of vascular biology. Culture of endothelial cells is routinely carried out under static conditions and these cultured cells have a cobblestone or polygonal morphology and appear randomly oriented toward one another. Cells of similar cobblestone morphology are seen *in vivo* and are found in regions of blood vessels which are thought to experience complex patterns of blood flow such as those on the outer wall of bifurcations and at the inner curvature of bends. Complex flow patterns result in lowered levels of wall shear stress. The majority of atherosclerotic plaques have been found to occur at regions predicted to experience low shear stress patterns, leading to the hypothesis that shear stress may confer a level of protection from the initiation of inflammation (Caro *et al.*, 1971). Though static culture may provide a viable model for disease prone endothelial cells the cobblestone morphology contrasts with the well characterised elongation and alignment of cells seen in straight regions of blood vessels, which experience laminar flow and seem to be protected from the onset of inflammation.

In order to better model the environment of cells experiencing laminar flow a number of culture methods, in which there is continuous flow of medium have been developed. Often these rely on the recirculation of medium which puts the cells at risk of contamination. Difficulties with sustaining cultures in these set ups for long time periods have led to many investigators carrying out studies with flow for acute time periods often with durations of only 2-6 hours (see Table 1.2). Over a short time frame the physiological relevance of such studies can be called into question.

In this chapter the overall aim was to validate a recently developed orbital shaker model (Warboys *et al.*, 2010) in which cells are exposed to chronic shear stress (for up to 7 days) through investigation into how different flow environments influence cell morphology, size and contact formation.

The main research questions addressed in this chapter are as follows:

- How does porcine endothelial cell morphology compare between cells cultured under static conditions and cells cultured under chronic (7 days) shear stress?
- How does porcine endothelial cell morphology compare between cells cultured under static conditions and cells cultured under acute (24 hours) shear stress?
- How does inflammation influence porcine endothelial cell morphology under static conditions and conditions of acute and chronic shear stress?
- How does shear stress influence cell size and turnover?

Declaration

N=4 images of PAEC stained with CD31 after 7 days of shear stress were obtained as part of an MRes project I submitted to Imperial College in September 2009. Additional data sets are present in this thesis increasing the N and a different form of analysis has been carried out. No figures or text has been reproduced from the MRes.

Methods

Cell culture

Endothelial cells from 2 year old Landrace Cross pigs were isolated by collagenase digestion as described in Chapter 2, section 2.1.1. For each study, cells from 3 separate pigs, all at passage 2, were used.

Cells were plated onto Transwell™ plates at a density of 400,000 per well and reached confluence over the 24 hours prior to commencement of each experiment. To study the impact of inflammatory stimuli on cell response, a number of cells were treated with 0.1µg *E.coli* LPS serotype 0111:B4 per well. Cell culture medium was changed every other day with fresh LPS added where appropriate. Cells were cultured under experimental conditions for between 24 hours and 7 days.

Immunohistochemistry

Cells were fixed with a formalin solution containing 2% formaldehyde before permeabilisation with triton-x 100 as detailed in Chapter 2.3.1. Cells were stained for either CD31/PECAM-1 or VE-cadherin using the protocols outlined in Chapter 2, section 2.3.1.

All visualisation of immunostaining was carried out using a Leica SP5 microscope with a 40x oil objective, as detailed in Chapter 2 section 2.4. The same settings were maintained throughout each experiment.

Immunoreactivity was quantified using LAS AF Lite software and is expressed as mean fluorescence intensity per pixel.

SICM

SICM was carried out on live cells as detailed in Chapter 2.5. Individual wells of cells were brought out of the incubator and scanned for no more than 1 hour. 80 x 80µm areas at the regions of interest were scanned.

Data and statistical analysis

Where representative images are shown, the number taken in the entire set is provided in the figure legend. For pooled observations, data are presented as mean ± S.E.M. for n= separate determinations. Where data were blind scored the nature of the image was not known to the scorer and all images were scored by at least 2 independent scorers and the mean of their scores recorded. Data were analysed using GraphPad Prism as described in individual figure legends. Statistical significance was assumed where $p<0.05$.

Results

Computational fluid dynamics profile of media in Transwell 6-well plates

A key objective of this PhD thesis was to study cells cultured under shear stress for prolonged periods of time. As described in the Introduction, the vast majority of papers describing effects of shear stress on endothelial cells use acute protocols, often for durations of less than 24 hours. This may be because in many shear stress models endothelial cells do not survive well. In order to overcome this problem a simple orbital shaker method, where cells can be cultured under shear stress for prolonged periods on Transwell™ 6-well plates without negatively effecting viability (Warboys *et al.*, 2010) has been used.

Initial studies described in this chapter and in Chapters 4 and 5 were performed using 6-well Transwell™ plates with a diameter of 240 mm and pore size of 0.4µm. Our collaborator, Professor R. Eric Berson modelled the shear stress profile across the well of this specific 6-well plate on an orbital shaker (POS-300, Grant Instruments) set at 150 RPM with 1.5ml of media in the upper chamber above the cells. Under these conditions, Professor Berson's simulation revealed co-ordinates of the well where cells experienced a pulsatile shear gradient (towards the edge of the well) and where cells experienced relatively constant levels of shear (towards the centre of the well) (Figure 3.1). However, in his initial modelling experiments Professor Berson did not map the very centre of the well; this was done later and is explained below. Using the shear map constructed by Professor Berson, a means of

imaging was developed to allow capture of images at the critical regions of the well. Imaging was towards the edge of the well, which was consistent with a gradient of shear reaching the peak in our model (9.4mm from the centre of the well) and at the centre of the well, which experienced a low peak and relatively constant shear (Figure 3.2).

In experiments described below, it became clear that cells at the edge of the well, where peak shear was highest, became aligned with the direction of the shear and that cells at the centre of the well, where peak shear is lower, were less aligned, displaying a morphology more similar to cells cultured under static conditions. These findings were in some ways difficult to explain in the view of Professor Berson at the time; although peak shear varied across the well, his maps showed that the ***average level of shear*** in the well was very similar for all regions (approximately 2 dynes/cm^2). Prompted by the findings, described below, Professor Berson went back to his model and re-interrogated his data to calculate directionality of the shear stress generated in the well. He also took his calculation to the very centre of the well in line with where images were gathered. In doing this, Professor Berson found that the shear at the edge of the well (9.4 mm from the centre) showed a preference in direction which is illustrated in Figure 3.3 by the blue which appears as an ellipse skewed towards the bottom right quadrant and top left quadrant (Figure 3.3). By contrast the shear at the centre of the well has no preferred direction because the wave formation is such that directional movement is equal. Shear at the centre of the well is shown on Figure 3 as a yellow line forming a circle with no preference for any quadrant (Figure 3.3).

It should be stressed that the modelling of the shear profile is precise and only valid for the exact conditions used; this point is illustrated nicely in the final Results Chapter where conventional 6-well culture plates with levels and directionality of shear defined by specific modelling, again provided by Dr Berson have been used (See Chapter 7).

CHRONIC SHEAR STRESS STUDIES (7 days)

Morphology of PAEC cultured under static versus prolonged (7 days) shear stress conditions

As expected PAEC cultured under static conditions over 7 days showed classic cobblestone morphology and expressed the endothelial cell markers CD31 (Figure 3.4 A) and VE-cadherin (Figure 3.4 B). The morphology of PAEC cultured under shear stress for 7 days was somewhat different to that of static cells: PAEC experiencing directional shear (edge of well) appeared elongated and aligned (Figure 3.5) whilst those experiencing non-directional shear appeared to show a mixture of morphologies, dominated by cobblestone like cells, but with some cells appearing to be aligned (Figure 3. 5). When data were collected from multiple experiments cells grown at the edge of the well, experiencing directional shear, were more aligned than those at the centre or those grown under static conditions (Table 3.1). The morphology of cells did not appear to be affected by the process of fixation, as live cells imaged using 'hopping probe' scanning ion conductance microscopy displayed similar morphology to those observed using confocal microscopy (Figures 3.4 and 3.5). Using hopping mode scanning ion conductance microscopy allowed measurement of the volume of PAEC grown under directional (edge) shear, non-directional (centre) shear or static conditions (Figures 3.4C and 3.5C). Cell volume measurements seemed to conform with morphology data, as differences were seen between cells exposed to the two extremes of shear stress (directional versus non-directional) (Figure 3.6).

Endothelial cells cultured under laminar shear stress align within 1-2 days (Dewey *et al.*, 1981; Eskin *et al.*, 1984; Levesque *et al.*, 1985), however, less is known about the kinetics of dealignment. In these studies alignment of PAEC grown under shear stress for 7 days had totally reversed 24 hours after the cessation of shear (Figure 3.7). Using hopping mode SICM morphological changes, consistent with the beginnings of dealignment, in cells grown under shear for 7 days, were detectable as early as 1 hour after stopping shear (Figure 3.8). These observations suggest that time out of shear stress should be considered in any morphological studies performed in cells or tissue and becomes relevant to my interpretation of data presented in Chapter 4.

Effect of gross inflammatory insult, using bacterial LPS, on morphology of PAEC cultured under static versus prolonged (7 days) shear stress

Endothelial cells in their native environment encounter inflammatory insults in the form of circulating pathogens and host inflammatory molecules. Numerous pathogens have been found in atherosclerotic tissue (Koren *et al.*, 2010; Ott *et al.*, 2006) and it is thought that they may play a role in arterial stiffening and initiation of atherosclerosis, though mechanisms behind this are unclear. In order to see whether cell ability to respond to shear stress is impeded in the presence of a gross inflammatory insult experiments were performed where cells were stimulated for 7 days with bacterial lipopolysaccharide (LPS) at 0.1µg/well. In images from cells cultured without LPS, CD31 clearly defined cell borders (Figures 3.4 and 3.5). However, in cells cultured under static conditions, LPS treatment appeared to affect morphology and border visualisation (Figure 3.9A). Specifically CD31 staining appeared 'blurred' having moved from the cell border and redistributed throughout the cytoplasm of the cell. However, 'alignment' scoring was still possible in the majority of images (see Table 3.1). The image selected in Figure 3.9A illustrates a particularly clear example of the CD31 blurring phenomenon and was not used for scoring. By contrast, in PAEC cultured under shear for 7 days the effects of LPS on CD31 patterning and cell morphology appeared reduced (Figure 3.9B). When total CD31 staining was calculated in cells grown at the edge of the wells, there was no effect of shear stress or of LPS (Figure 3.10A). Interestingly, although not statistically significant, and difficult to quantify in real terms, when cells at the centre of the wells were imaged, LPS treatment tended to reduce CD31 staining in static cells; an effect that seemed to be reduced by shear stress in cells grown in this region of the well (Figure 3.10A). However, when the number of cells was calculated (based on the number of nuclei, obtained using FIJI open source software), it was clear that LPS reduced the number of cells at both the centre and the edge of the well, an effect that was prevented by shear stress at the edge of the well (directional shear), but not at the centre of the well (non-directional shear), (Figure 3.10B). As LPS reduced the number of cells, an effect that appeared negated by shear stress, it was important to determine if reduced cell number impacted on cell size, which may relate to morphology. In order to establish whether a reduced cell number provided space for cells to spread out and cover a

larger surface area the area of the image field occupied by nuclei (again using FIJI, by capturing the area of 'blue' DAPI staining) was calculated. In doing this it was found that, whilst cell number was reduced by LPS, the area their nuclei covered was not (Figure 3.10C). This suggested that cells in these regions had larger nuclei. In order to determine if this reflected increased cell size a way of measuring cell area was developed. To do this, the images of the cells stained with CD31 were blinded and from each image 10 clearly defined cells selected. Next the perimeter tool in FIJI was used to define the border of each of the 10 selected cells and calculate the area. In doing this it was found that PAEC in regions where cell nuclei numbers were reduced were indeed larger – again this feature of cells exposed to LPS was prevented in cells exposed to shear stress (Figure 3.11). The finding that cell area had increased in regions of the well where cell number had decreased may explain why no reduction in CD31 levels was seen in regions where cell number had been reduced.

In the presence of LPS, as in its absence, PAEC at the edge of sheared wells, experiencing a gradient of directional shear, were detectably aligned, whereas those in the centre of the well exposed to non-directional shear or in static wells were less aligned (Table 3.1). However, there seemed to be a tendency for PAEC in the LPS treated wells to be more aligned when grown under either static or shear stress conditions (Table 3.1). The concentration of LPS used in these experiments was 0.1µg/well (1.5ml), which is submaximal in terms of cell activation (measured by NFκB translocation in PAEC; data not shown). It has long been known that the immunoregulatory cytokine TNFα causes endothelial cells to elongate (Stolpen, 1986). This may be relevant to the above observations, since LPS induces TNFα release from many cell types (Dumitru *et al.*, 2000; Hoareau, 2010). Unfortunately this was not something I was able to pursue in great detail in my PhD. It was possible to carry out some pilot experiments and image cells more simply using conventional light microscopy to show that the elongation phenomenon, suggested in my experiments above with relatively low levels of LPS, could easily be demonstrated in PAEC using higher concentrations of LPS. In these experiments 7 days exposure to LPS (1µg/ml) induced very obvious elongation of cells (Figure 3.12). The functional consequence of this phenomenon is not clear and warrants further investigation, but the observation that shear stress limits the effects of LPS on morphology may indicate a 'protective' function of shear stress. This question has been explored in greater detail in experiments in Results

Chapter 7 where outcomes of a full transcriptomic analysis of all human genes in endothelial cells exposed to shear stress and LPS are shown.

Acute Shear Stress Studies (24 hours)

The studies above show that endothelial cells survive well for prolonged periods and display morphological changes in response to shear stress using a simple system consisting of a 6-well plate on an orbital shaker. However, in order to compare our model with others in the literature, that generally are used for much shorter periods of time (≤24 hours), additional experiments were performed where cells were sheared for 24 hours. By contrast to observations in cells sheared for 7 days, PAEC did not appear consistently aligned when sheared for 24 hours at either region of the well (Figure 3.13B). However, it was interesting to note that, in the presence of LPS, PAEC at the centre or the edge of sheared wells appeared the most aligned (Figure 3.13C and D). These observations suggest that shear stress and LPS may synergise to cause alignment/elongation of cells. As was seen with cells sheared for 7 days, none of the conditions affected CD31 staining in cells sheared for 24 hours (Figure 3.14A). LPS was found to lead to a significant reduction in cell number (Figure 3.14B) and nuclear area (Figure 3.14C) in all regions of the well suggesting that the protective impact of this level of shear stress is not seen until a later time-point.

Morphology of other endothelial cells studied using the 6-well plate and orbital shaker method

During the course of this research the opportunity arose to investigate how shear stress applied to a number of other endothelial cell types affected alignment. Specifically, in addition to PAEC, porcine pulmonary artery endothelial cells, human aortic endothelial cells (see Chapter 5), human pulmonary artery endothelial cells, human blood out growth endothelial cells (BOEC), human umbilical vein endothelial cells (HUVEC) and human embryonic stem cell derived endothelial cells (hESC) (Figure 3.15) were assessed. In each case the results were consistent with those for PAEC, showing a clear alignment of cells at the edge of sheared wells, where the shear profile had directionality, and less alignment at the centre of the well where shear had low or no directionality.

It is important to point out that the morphological characteristics, consistently seen in endothelial cells grown at the centre versus the edge of the well, exposed to directional versus non-directional shear stress, bear a striking resemblance to endothelial cells in the aortic arch proposed by some to be exposed to high versus low shear stress (Suo *et al.*, 2007).

Figures

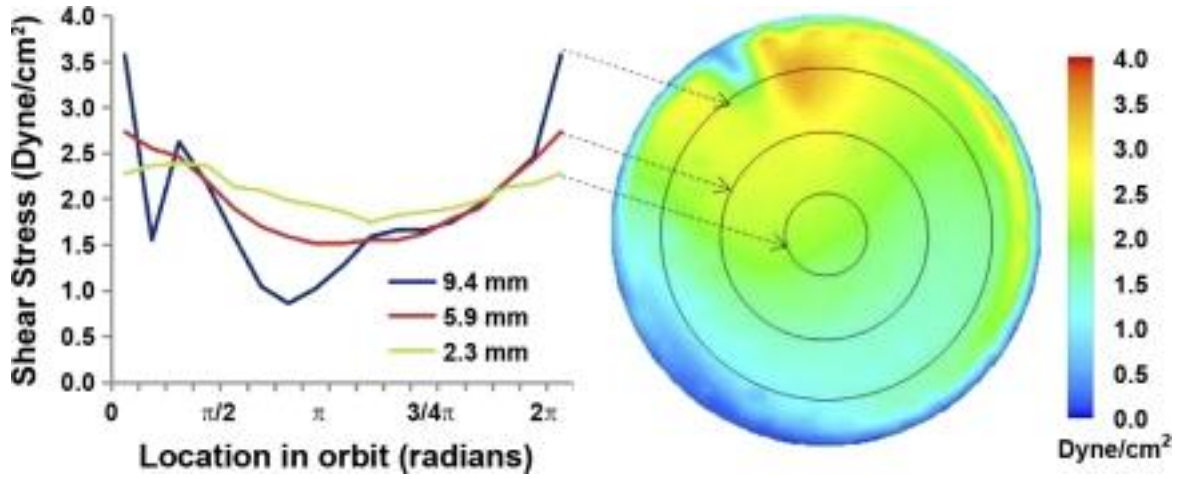

Figure 3.1 Initial computational solution for shear stress profile of one well in a Corning 6-well plate with Transwell™ insert

The graph on the left shows the predicted shear stress (dynes/cm^2) profile experienced by cells 9.4mm, 5.9mm and 2.3mm from the centre of a 24mm diameter Transwell™ respectively. There appears to be an increasing temporal gradient of shear stress moving from the centre to the edge of the well. The map on the right illustrates predicted levels of time-averaged shear stress across the well at a single point in the wells orbit. Reproduced from (Warboys et al., 2010).

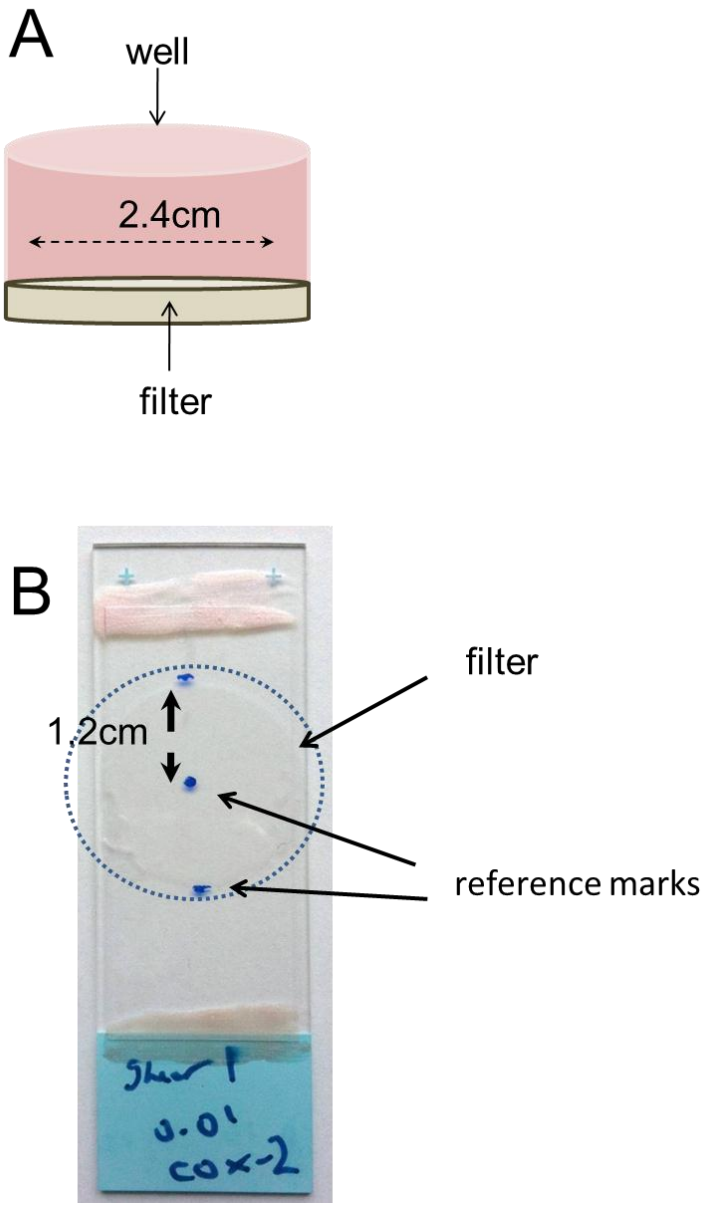

Figure 3.2 Mounting of Transwell™ filter for viewing by confocal microscopy

(A) *Schematic showing how the Transwell™ filter sits in solid support with medium both above and below its surface before it is cut out of this support, mounted on a slide and marked so regions of interest at the edge and the centre respectively can be readily detected as shown in* ***(B)****. Reproduced from (Potter et al., 2011).*

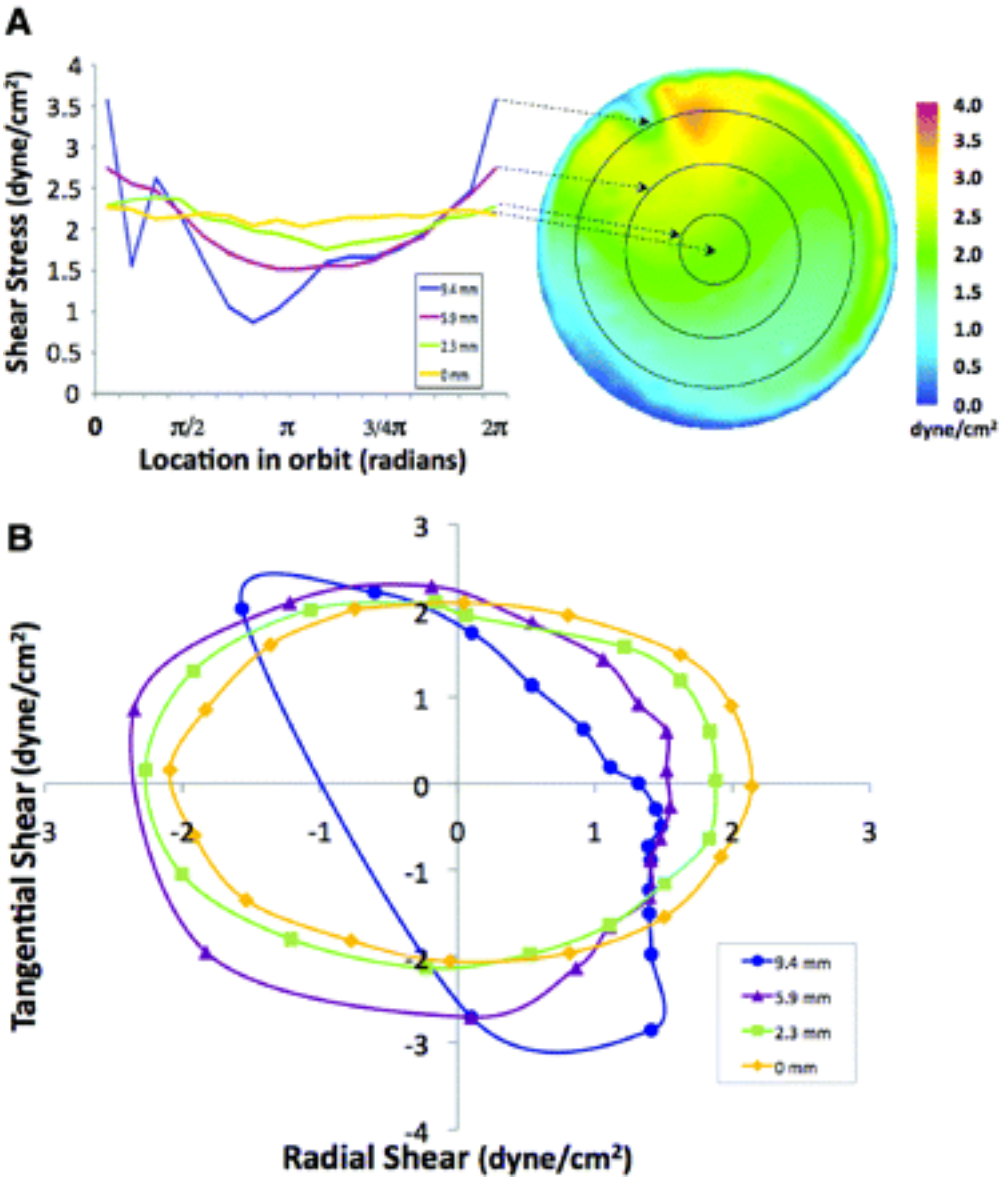

Figure 3.3 Revised computational solution for shear stress profile of one well of a Corning Transwell™ 6-well plate (<u>Legend continues on next page)</u>

Figure 3.3 Revised computational solution for shear stress profile of one well of a Corning Transwell™ 6-well plate (<u>Legend continued from previous page)</u>

Panel A shows the shear stress at the base of the well at one moment in time. The right hand panel shows a shear stress map, whilst the left hand panel shows quantitatively the shear stress magnitude at various distances from the centre of the well, as a function of time during the orbit. The mean shear during the orbit is approximately independent of radial position, but the temporal pattern varies: shear is approximately constant in magnitude at the centre of the well, but is more variable nearer the edge – the difference between the maximum and minimum increases with increasing distance from the centre.

The lower panel shows how the direction of shear varies with distance from the centre and with time through the orbit. The tangential (or circumferential) component of shear is plotted against the radial component. Dots on the lines indicate equal time intervals. Flow that was in a purely tangential (or circumferential) direction, but oscillated backwards and forwards along a circumference, would give a vertical line. Flow that oscillated along a radius (i.e. from the centre towards the edge and back again) would show as a horizontal line. Flow at the centre (and consequently shear) goes in all directions during the cycle. Near the edge, the flow has much less radial component, and is approaching the situation of oscillating backwards and forwards around the circumference.

Data are shown at 4 discrete regions of the well (9.4mm, 5.9mm, 3.4mm and 0mm from the centre). Reproduced from (Potter et al., 2011).

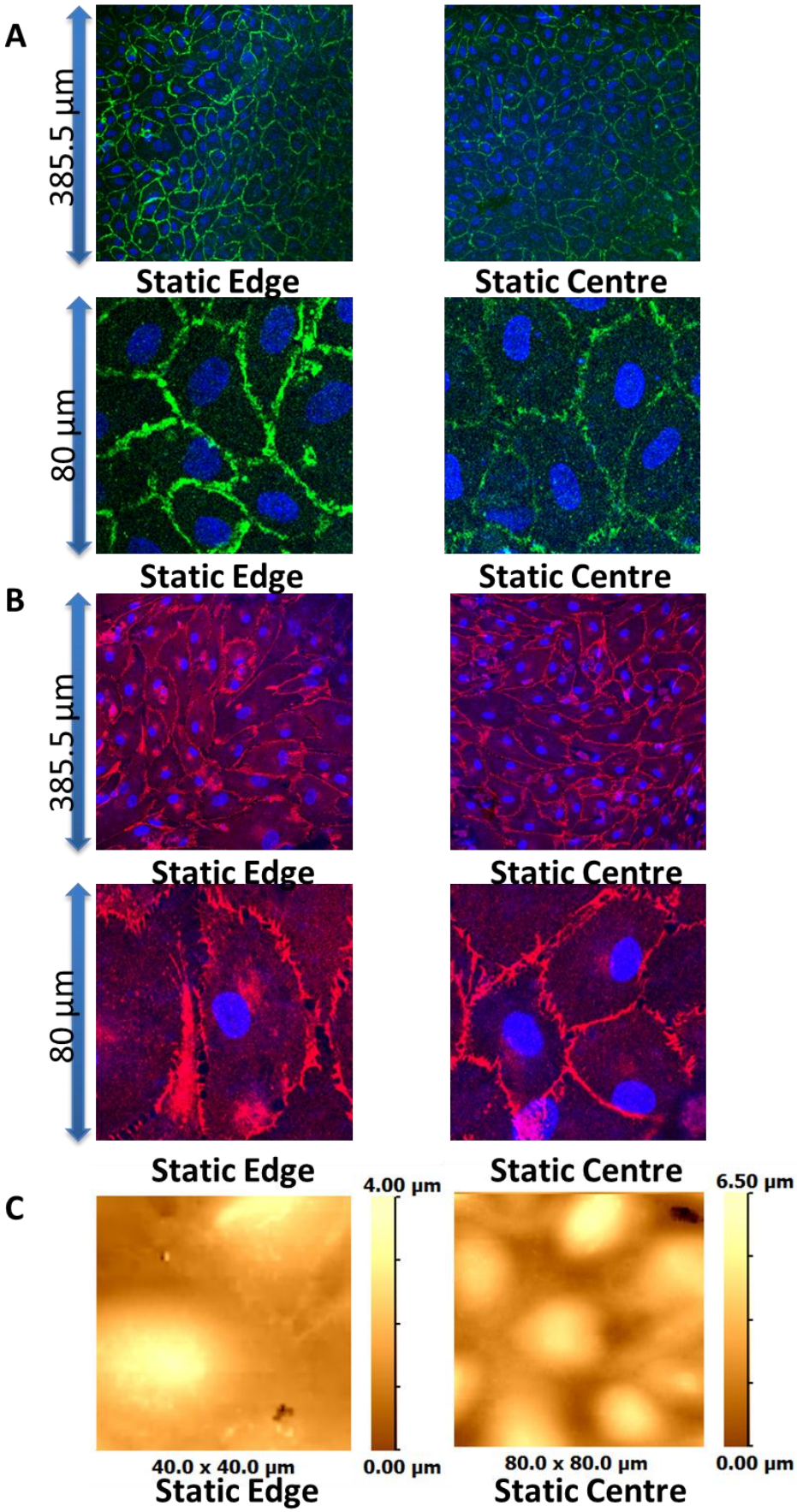

Figure 3.4
Morphology of PAEC after culture on Transwells™ for chronic time periods (4-7 days) under static conditions ***(Legend continues on next page)***

Figure 3.4 Morphology of PAEC after culture on Transwells™ for chronic time periods (4-7 days) under static conditions <u>(Legend continued from previous page)</u>

A and B: *Representative confocal images of a full microscopic field of endothelial cells (385.5µm X 385.5µm) and below 80 X 80 µm enlargements of the same images. Cells were cultured for 7 days under static conditions. Images show DAPI nuclear staining* ***(blue) (A and B)****, CD31 immunoreactivity* ***(green) (A)*** *and VE-cadherin immunoreactivity* ***(red) (B).*** *Images are representative of at least 12 wells; data represent cells of 3 animals with 6 separate isolations/wells imaged per animal and 2 images taken at each region of interest for CD31 and for VE-cadherin. Left side: Edge-9.4mm from the centre of the Transwell™ filter. Right side: Centre-images taken directly at the centre of the Transwell™ filter.*

C: *Representative live cell SICM images of cells after 4 days of static culture at the edge and centre of Transwells™.*

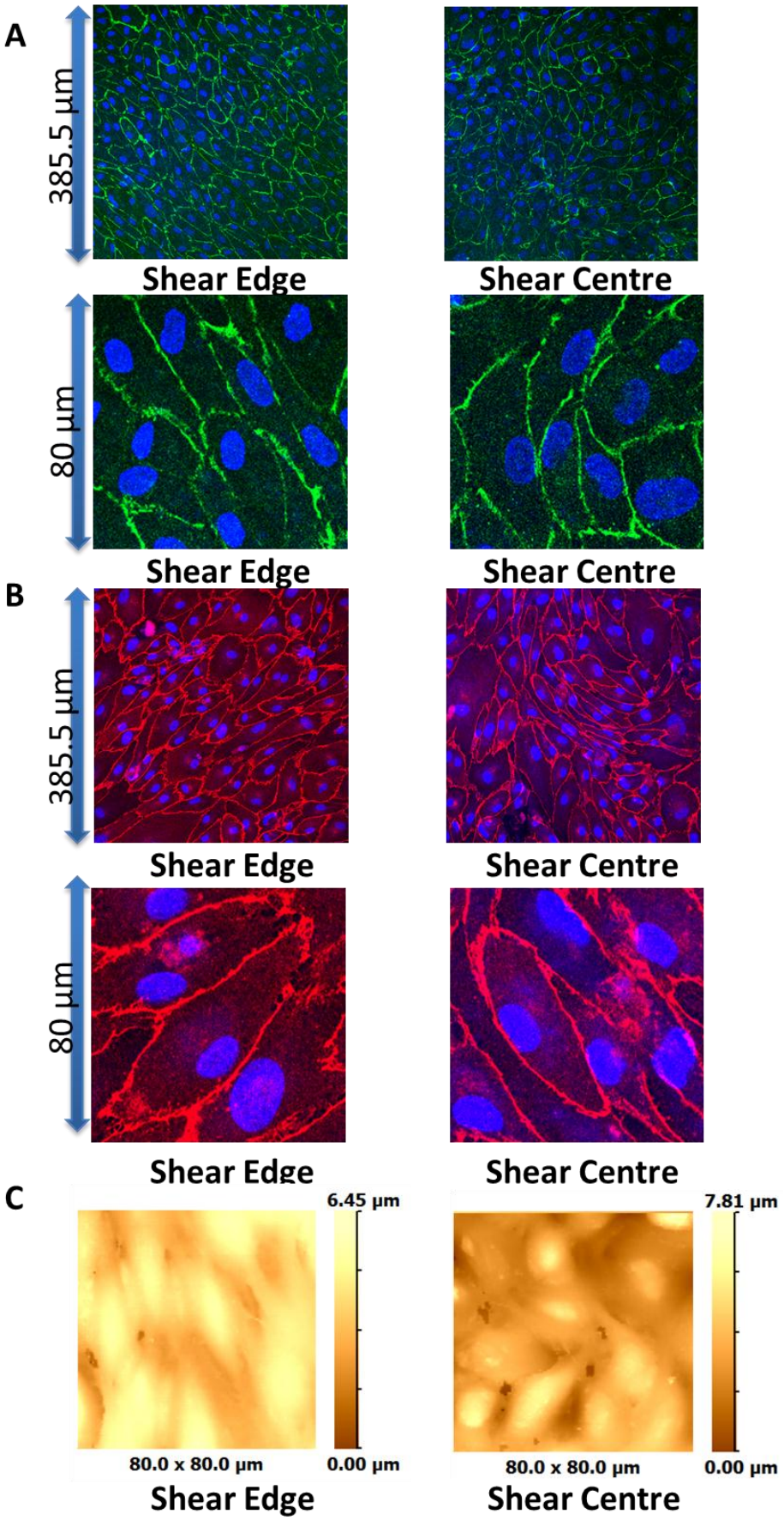

Figure 3.5 Morphology of PAEC after culture on Transwells™ for chronic time periods (4-7 days) under shear stress ***(Legend continued on next page)***

Figure 3.5 Morphology of PAEC after culture on Transwells™ for chronic time periods (4-7 days) under shear stress <u>(Legend continued from previous page)</u>

A and B: *Representative confocal images of a full microscopic field of endothelial cells (385.5µm X 385.5µm) and, below, 80 X 80 µm enlargements of regions of the same images. Cells were cultured for 7 days under shear conditions. Images show DAPI nuclear staining* ***(blue) (A and B)****, CD31 immunoreactivity* ***(green) (A)*** *and VE-cadherin immunoreactivity* ***(red) (B).*** *Images are representative of at least 12; data represent cells of 3 animals with 6 separate isolations/wells imaged per animal and 2 images taken at each region of interest. Left side: Edge-9.4mm from the centre of the Transwell™ filter, a region of oriented shear stress; Right side: Centre-images taken directly at the centre of the Transwell™ filter, a region of non-oriented shear stress.*

C: *Representative live cell SICM images of cells after 4 days of static culture at the edge and centre of Transwells™.*

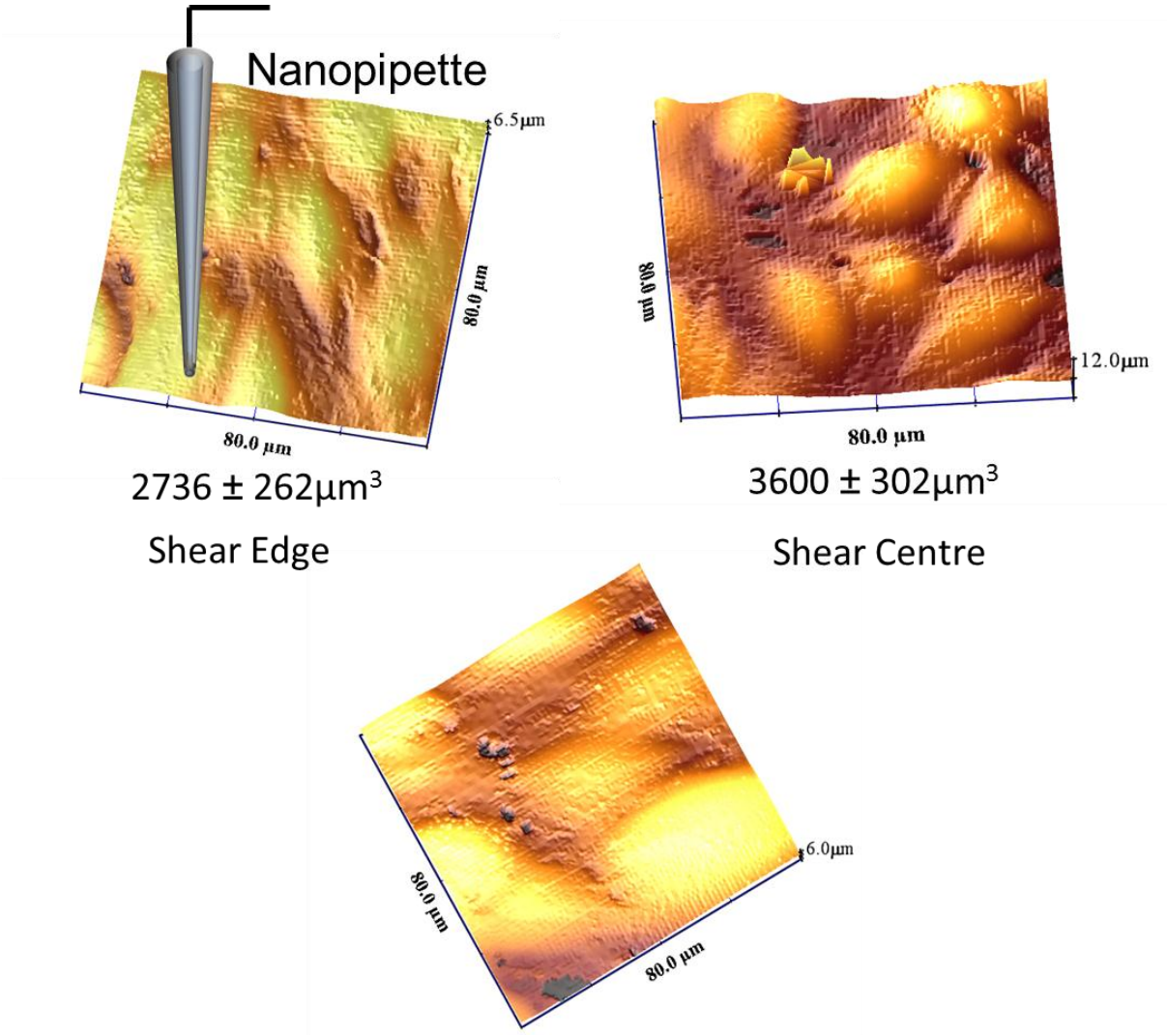

Figure 3.6 Comparison of PAEC volumes under different conditions of shear stress

SICM was used to image cells after 4 days of culture under static or shear stress conditions. Images are representative of at least 6 images across 4 wells. Representative images and mean ±S.E.M (n=20-25 cells per region) are presented here.

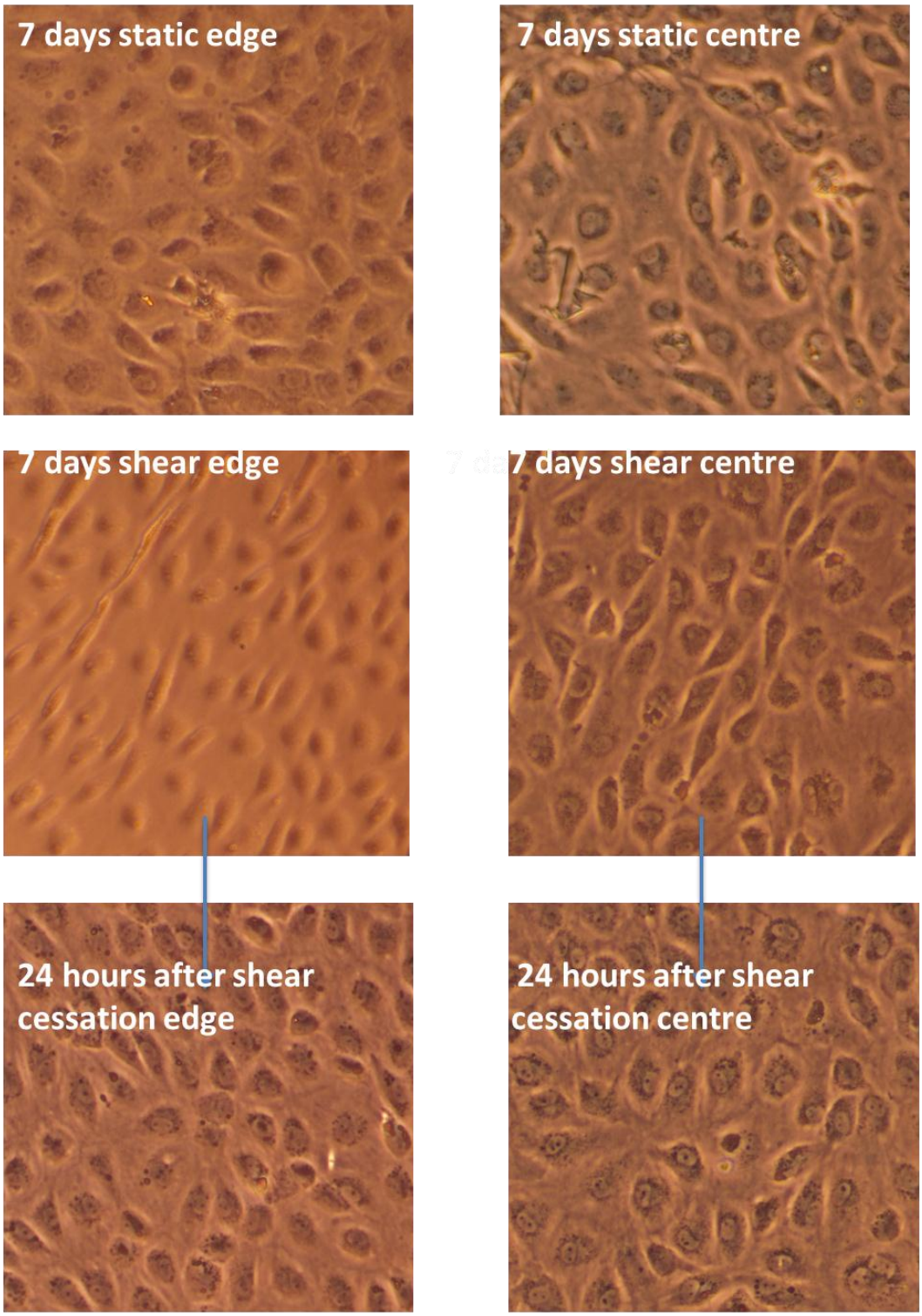

Figure 3.7 Morphological changes observed 24 hours after shear cessation

Representative photographs of at least 2 images of cells from 1 pig at 10X magnification after 7 days under either static or shear stress conditions. Cells that had previously been cultured under shear were then incubated under static conditions for a further 24 hours.

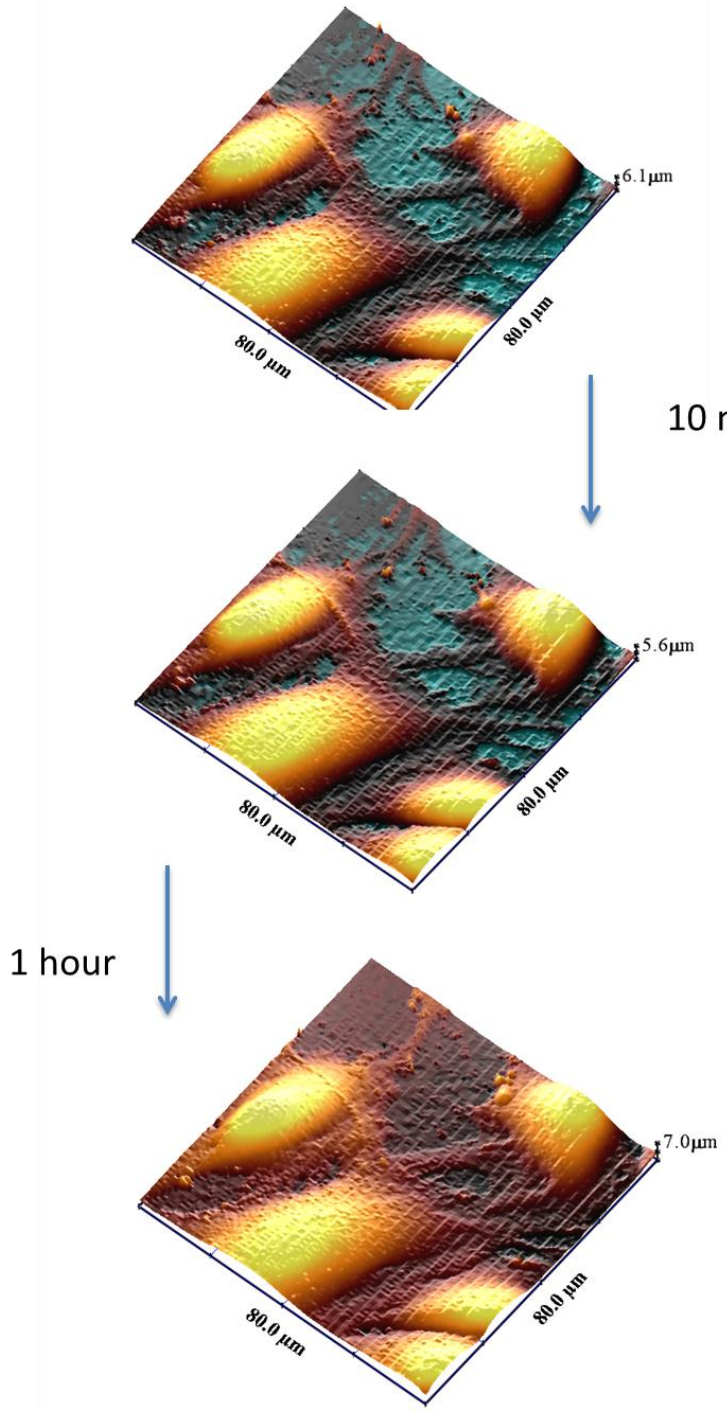

Figure 3.8 Morphological changes observed immediately following shear cessation

PAEC were imaged repeatedly over the course of one hour using SICM during which time slight morphological changes were observed as contacts between cells altered.

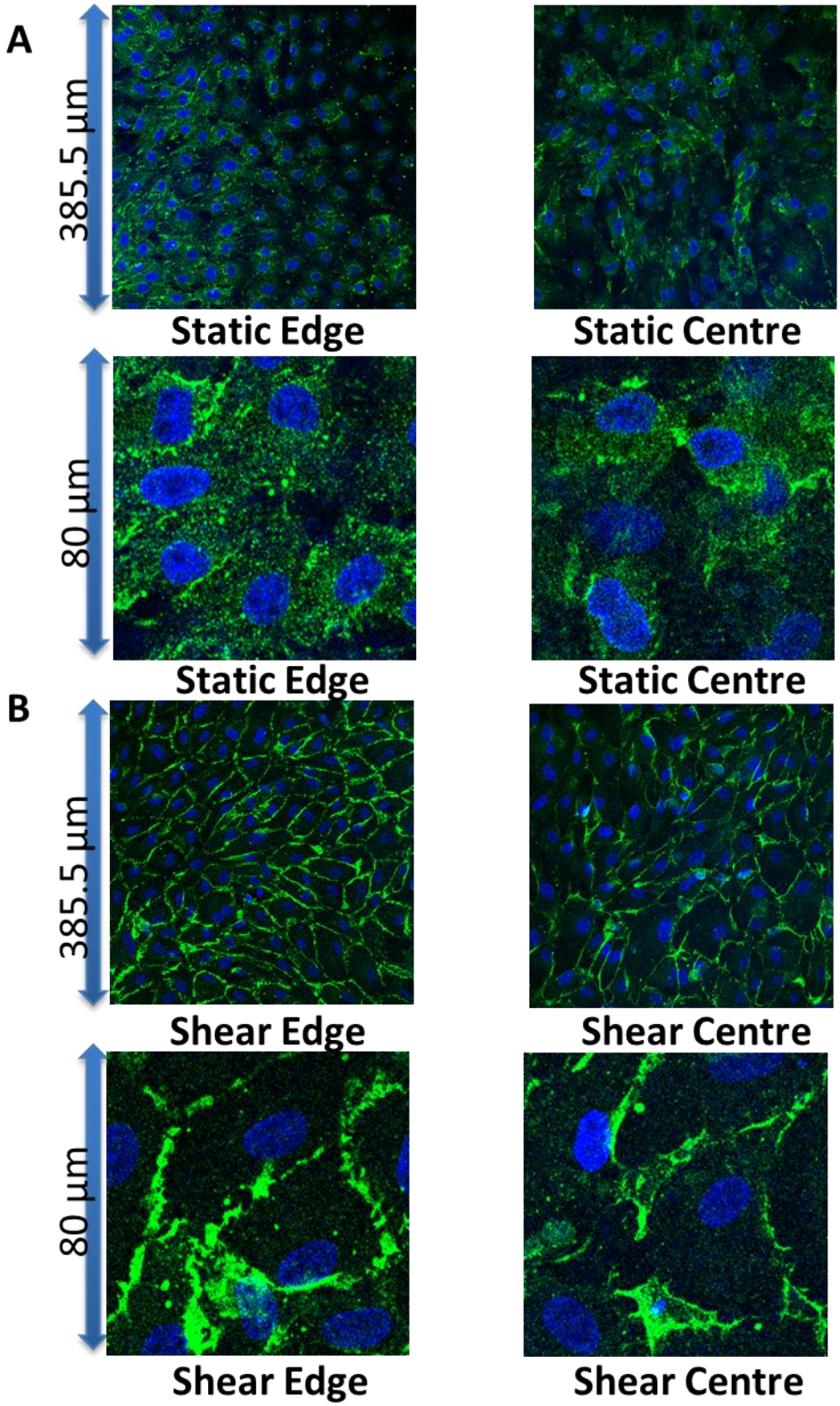

Figure 3.9 Morphology of PAEC after chronic culture (7days) with 0.1µg LPS ***(Legend continues on next page)***

Figure 3.9 Morphology of PAEC after chronic culture (7days) with 0.1µg LPS <u>(continued from previous page)</u>

(A) *Representative confocal images of a full microscopic field of endothelial cells (385.5µm X 385.5µm) and, below, 80 X 80µm enlargements of regions of the same images. Cells were cultured under static conditions for 7 days. Images show DAPI nuclear staining* ***(blue)*** *and CD31 immunoreactivity* ***(green)*** *and represent cells of 3 animals with 4 wells imaged per animal and 2 images taken at each region of interest (n=12). Left side: Edge- 9.4mm from the centre of the Transwell™ filter; Right side: Centre-images taken directly at the centre of the Transwell™ filter.*

(B) *Representative confocal images of a full microscopic field of endothelial cells (385.5 X 385.5µm) and, below, 80 X 80µm enlargements of regions of the same images. Cells were cultured under shear stress for 7 days. Images show DAPI nuclear staining* ***(blue)*** *and CD31 immunoreactivity* ***(green)****. Images are representative of at least 12; data represent cells of 3 animals with 6 separate isolations/wells imaged per animal and 2 images taken at each region of interest. Left side: Edge- 9.4mm from the centre of the Transwell™ filter, a region of oriented shear stress; Right side: Centre-images taken directly at the centre of the Transwell™ filter, a region of non-oriented shear stress.*

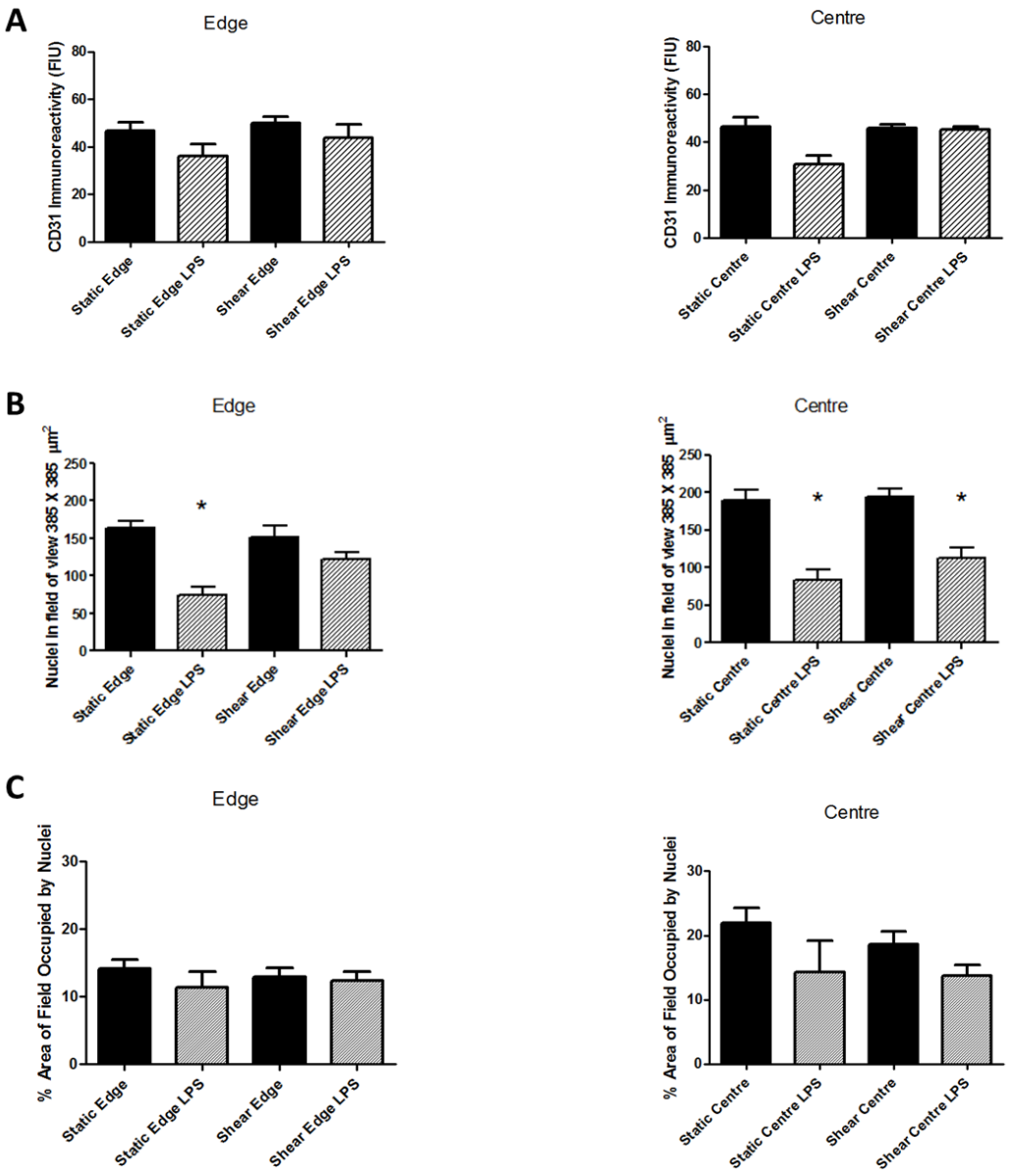

Figure 3.10 Graphical representations of characteristics of PAEC after 7 days culture

A: *CD31 immunoreactivity quantified and expressed as mean fluorescence per pixel in each 385.5 X 385.5µm image using LAS AF Lite version 2.4.1.*

B: *Nuclei counts performed using FIJI open source software. Values are an estimate as in some cases the software is unable to separate nuclei which are very close together.*

C: *Percentage of 385.5µm X 385.5µm image occupied by cell nuclei.*

*All data are mean ±S.E.M for n=12 images gathered from 4 separate isolations/wells repeated with cells of 3 different animals. Data were analysed by One-way ANOVA with Bonferroni post-test. P=<0.05 was deemed significant and is represented by *.*

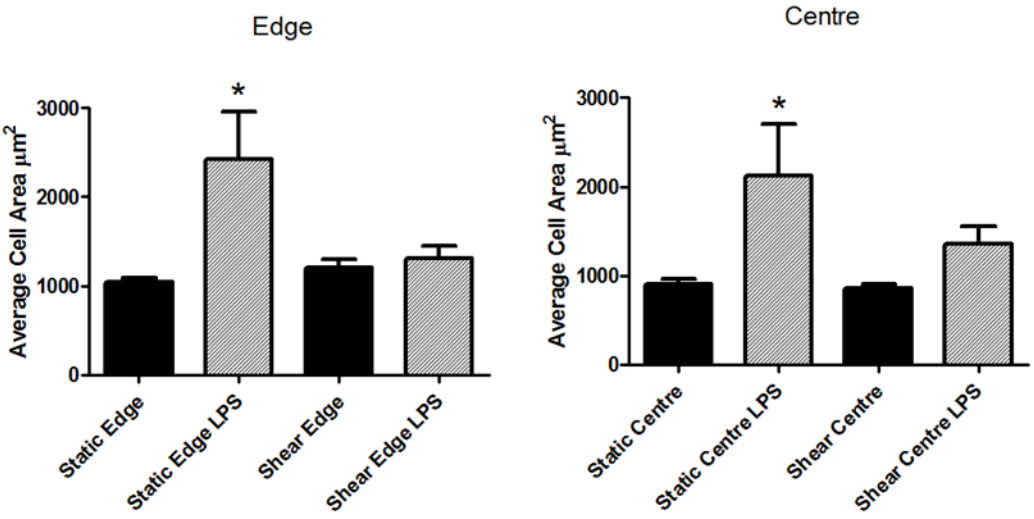

Figure 3.11 Average PAEC areas

*PAEC images were blinded and 10 cells with borders clearly defined by CD31 were selected using the draw tool of FIJI open source software and their area determined. The average cell area in each image was calculated and plotted. Data are shown as mean ±S.E.M for n=9-12 images gathered from 3-4 separate isolations/wells repeated with cells of 3 different animals. Data were analysed by One-way ANOVA with Bonferroni post-test. P=<0.05 was deemed significant and is represented by *.*

Condition	Alignment Score (0-3)
Static Edge	0.17±0.06
Static Edge LPS	0.31±0.12
Shear Edge	1.46±0.14
Shear Edge LPS	2.10±0.15
Static Centre	0.19±0.06
Static Centre LPS	0.13±0.06
Shear Centre	0.69±0.11
Shear Centre LPS	1.12±0.13

Table 3.1 Alignment ratings of PAEC cultured for 7 days

PAEC images with clearly visible CD31 staining were blinded and randomly ordered. PAEC alignment was assessed on a scale of 0-3 with 0 indicative of rounded cells with no clear sense of orientation and 3 indicative of all cells elongated and displaying unidirectional alignment. Data are mean± S.E.M for n=6-12 images gathered from 2-4 separate isolations/wells repeated with cells of 3 different animals separate. Data was averaged from 3 independent scorers.

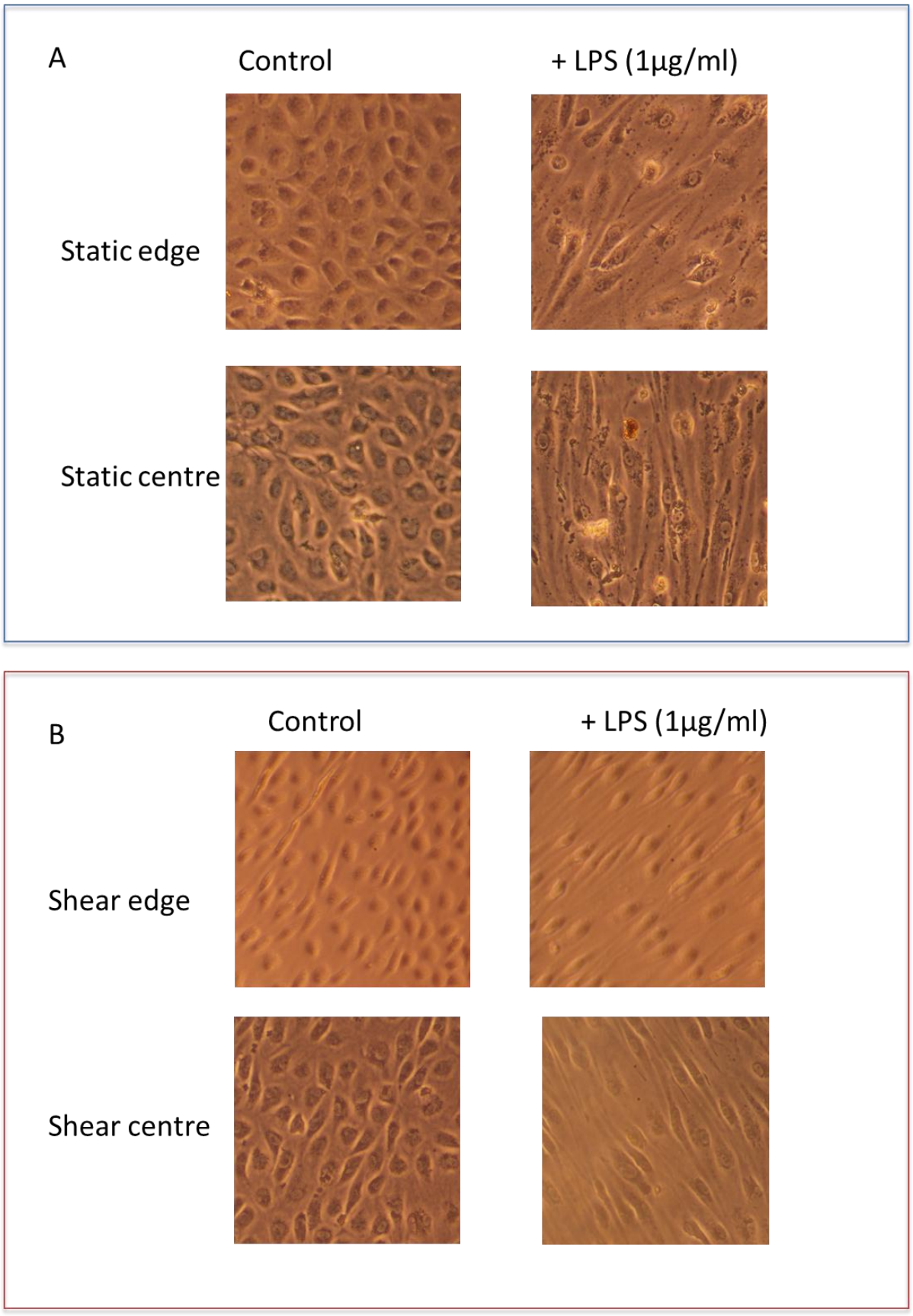

Figure 3.12 PAEC alignment with chronic shear (7 days) in the presence or absence of 1µg/ml LPS ***(Legend continued on next page)***

Figure 3.12 PAEC alignment with chronic shear (7 days) in the presence or absence of 1µg/ml LPS <u>(Legend continued from previous page)</u>

PAEC cultured under static conditions for 7 days displayed the expected cobblestone morphology unless incubated with LPS. Where incubated with LPS, PAEC became increasingly elongated. Some rounded cells are visible which appear to be dead cells which have detached from the culture plate ***(A)****. PAEC cultured under chronic shear stress appeared strongly aligned at the edge of the well and to have a lesser degree of alignment at the centre. In the presence of LPS, cells from both sheared regions appeared consistently elongated and aligned* ***(B)****. Interestingly there seemed to be less damage to the cell membrane of theses sheared cells than to their static counterparts. Images are representative of at least 2 taken from cells cultured from 1 pig.*

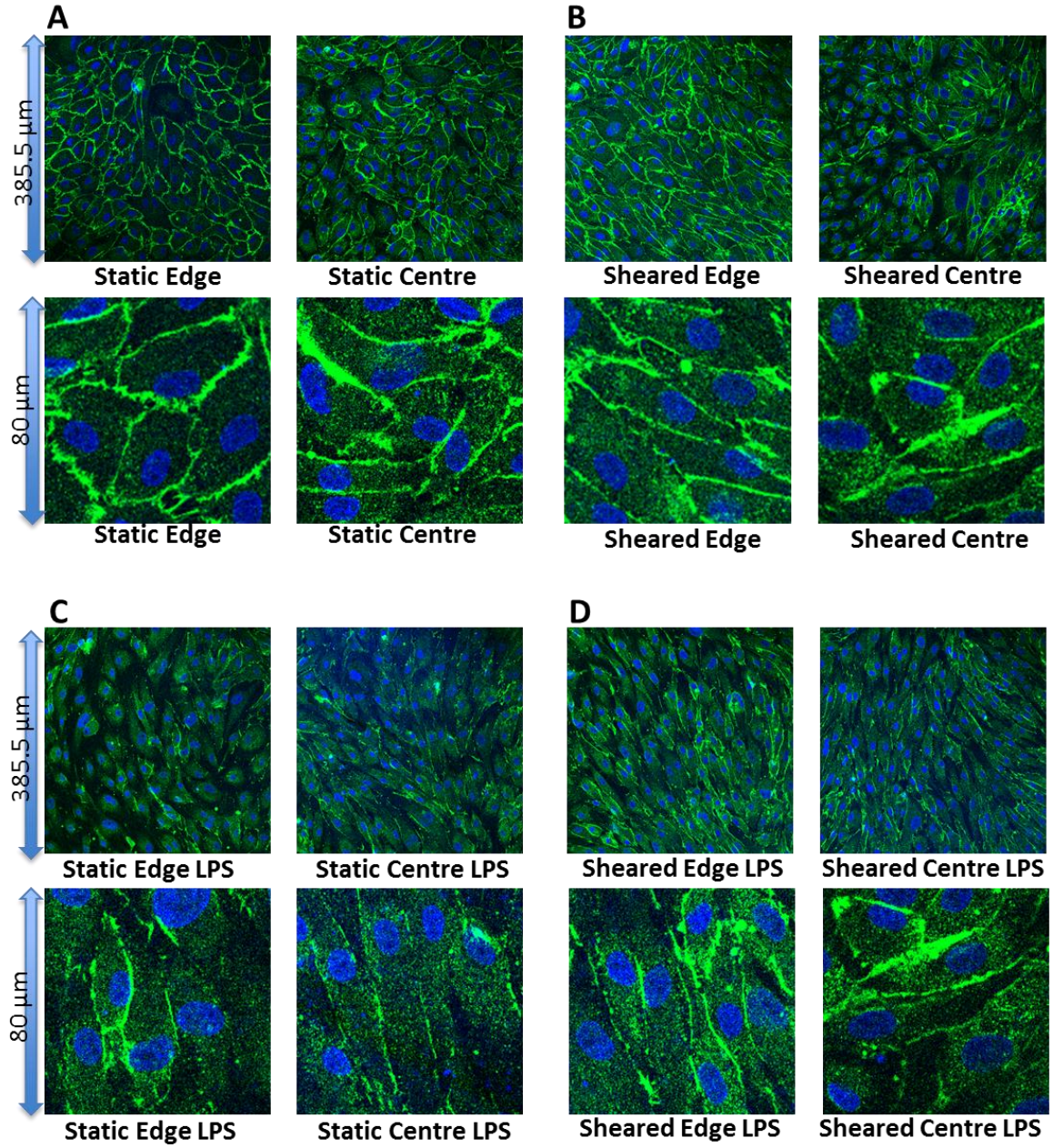

Figure 3.13 PAEC morphology after 24 hours of culture ***(Legend continued on next page)***

(A) Representative confocal images of a full microscopic field of endothelial cells (385.5µm X 385.5µm) and, below, 80 X 80µm enlargements of regions of the same images. Cells were cultured under static conditions for 24 hours. Images show DAPI nuclear staining **(blue)** and CD31 immunoreactivity **(green)** and are representative of at least 12 wells; data represent cells of 3 animals with 4 separate isolations/wells imaged per animal and 2 images taken at each region of interest. Left side: Edge- 9.4mm from the centre of the Transwell™ filter; Right side: Centre-images taken directly at the centre of the Transwell™ filter.

Figure 3.13 PAEC morphology after 24 hours of culture <u>(Legend continued from previous page)</u>

(B) *Representative confocal images of a full microscopic field of endothelial cells (385.5 X 385.5µm) and, below, 80 X 80µm enlargements of regions of the same images. Cells were cultured under shear stress for 7 days. Images show DAPI nuclear staining* ***(blue)*** *and CD31 immunoreactivity* ***(green)****. Images are representative of at least 12; data represent cells of 3 animals with 6 separate isolations/wells imaged per animal and 2 images taken at each region of interest. Left side: Edge- 9.4mm from the centre of the Transwell™ filter, a region of oriented shear stress; Right side: Centre-images taken directly at the centre of the Transwell™ filter, a region of non-oriented shear stress.*

(C) *Representative confocal images of a full microscopic field of endothelial cells (385.5µm X 385.5µm) and, below, 80 X 80µm enlargements of regions of the same images. Cells were cultured under static conditions for24 hours with 0.1µg/well LPS. Images show DAPI nuclear staining* ***(blue)*** *and CD31 immunoreactivity* ***(green).*** *Images are representative of at least 12 wells; data represent cells of 3 animals with 6 separate isolations/wells imaged per animal and 2 images taken at each region of interest.. Left side: Edge- 9.4mm from the centre of the Transwell™ filter; Right side: Centre-images taken directly at the centre of the Transwell™ filter.*

(D) *Representative confocal images of a full microscopic field of endothelial cells (385.5 X 385.5µm) and, below, 80 X 80µm enlargements of regions of the same images. Cells were cultured under shear stress for 7 days with 0.1µg/well LPS. Images show DAPI nuclear staining* ***(blue)*** *and CD31 immunoreactivity* ***(green)****. Images are representative of at least 12; data represent cells of 3 animals with 6 separate isolations/wells imaged per animal and 2 images taken at each region of interest. Left side: Edge- 9.4µm from the centre of the Transwell™ filter, a region of oriented shear stress; Right side: Centre-images taken directly at the centre of the Transwell™ filter, a region of non-oriented shear stress.*

Condition	Alignment Score (0-3)
Static Edge	0.41±0.13
Static Edge LPS	0.57±0.20
Shear Edge	0.89±0.18
Shear Edge LPS	1.81±0.26
Static Centre	0.29±0.11
Static Centre LPS	0.75±0.25
Shear Centre	0.32±0.56
Shear Centre LPS	1.83±0.30

Table 3.2 Alignment ratings of PAEC cultured for 24 hours

PAEC images with clearly visible CD31 staining were blinded and randomly ordered. PAEC alignment was assessed on a scale of 0-3 with 0 indicative of rounded cells with no clear sense of orientation and 3 indicative of all cells elongated and displaying unidirectional alignment. Data are mean± S.E.M for n=8-12 images gathered from 3-4 separate isolations/wells repeated with cells of 3 different animals. Data was averaged from 3 independent scorers.

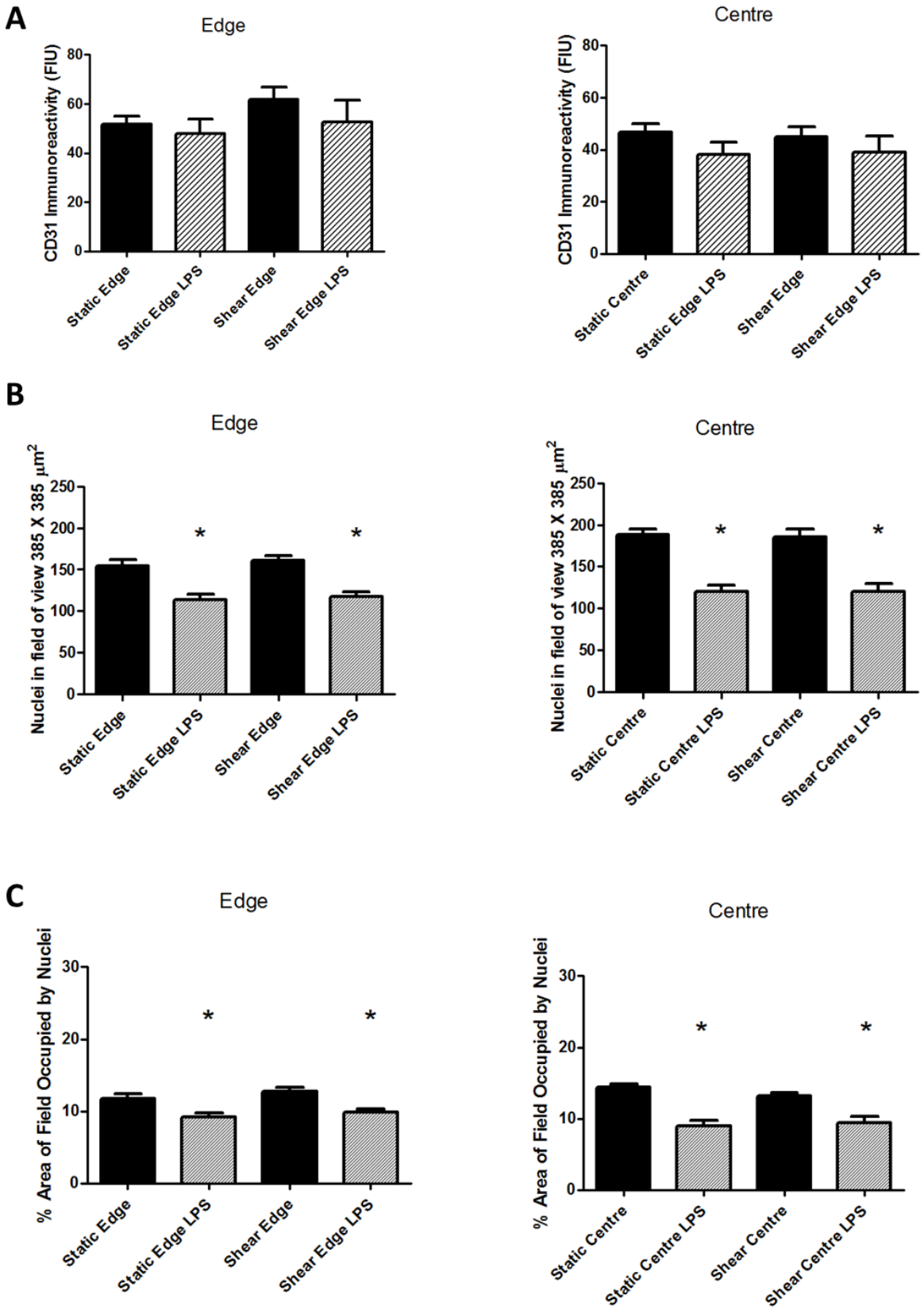

Figure 3.14 Graphical representations of characteristics of PAEC after 24 hours of culture
(Legend continues on next page)

Figure 3.14 Graphical representations of characteristics of PAEC after 24 hours of culture (Legend continued from previous page)

A: *CD31 immunoreactivity quantified and expressed as mean fluorescence per pixel in each 385.5 X 385.5µm image using LAS AF Lite version 2.4.1.*
B: *Nuclei counts performed using FIJI open source software. Values are an estimate as the software is unable to separate nuclei which are very close together.*
C: *Percentage of 385.5µm X 385.5µm image occupied by cell nuclei.*

*All data are mean ±S.E.M for n=12 images gathered from 4 separate isolations/wells repeated with cells of 3 different animals. Data was averaged from 3 independent scorers. Data were analysed by One-way ANOVA with Bonferroni post-test. P=<0.05 was deemed significant and is represented by *.*

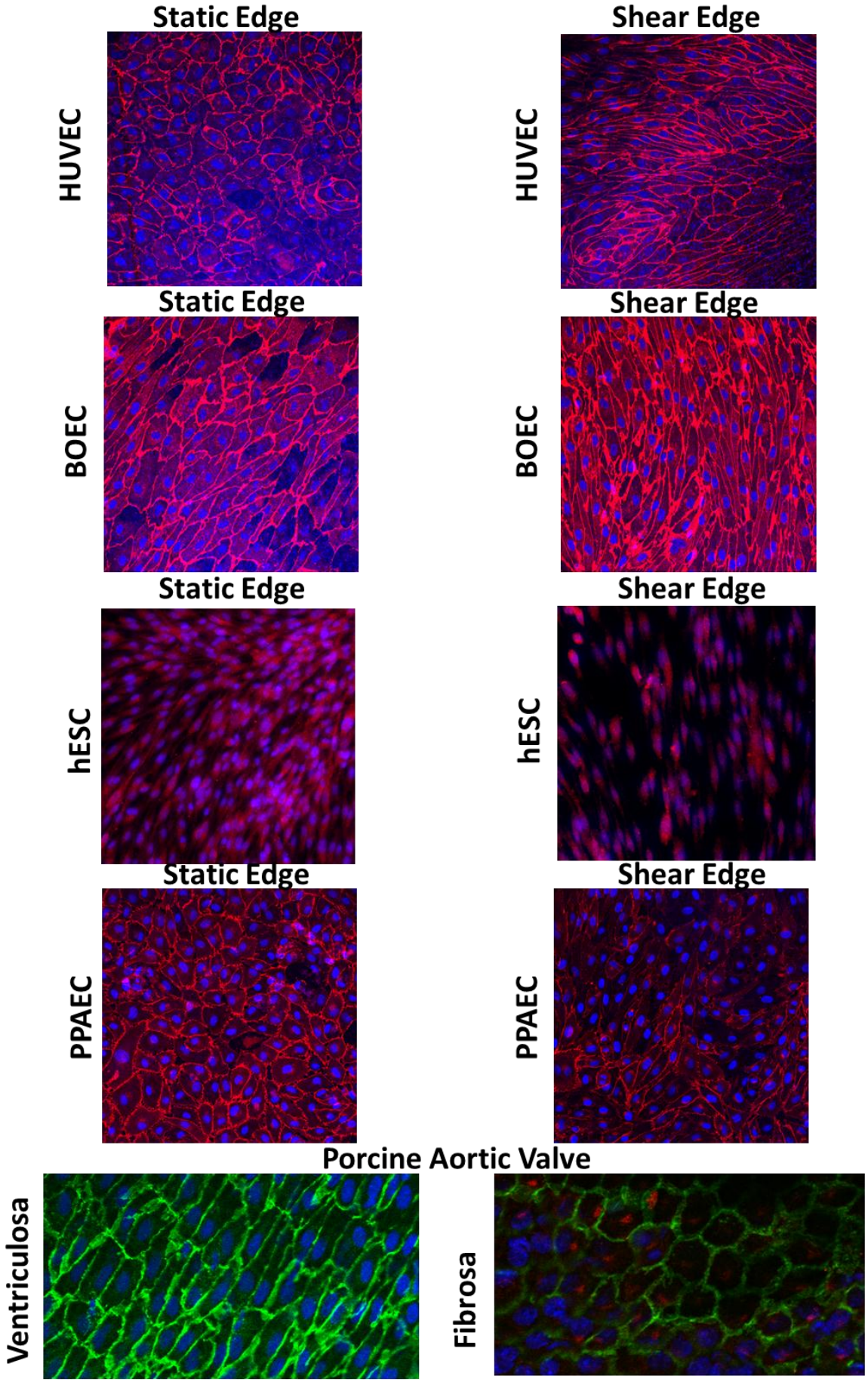

Figure 3.15 Influence of Shear on Morphology of various cell types (Legend continues on next page)

Figure 3.15 Influence of Shear on Morphology of various cell types (Legend continued from previous page)

A. *Human umbilical vein endothelial cells (HUVEC).*
B. *Blood outgrowth endothelial cells (BOEC)*
C. *Human embryonic stem cells (hESC)*
D. *Porcine pulmonary artery endothelial cells (PPAEC)*
E. *Porcine aortic valve endothelial cells (PAVEC): Ventriculosa- Endocardium side of the valve exposed to directional shear stress Fibrosa- Aortic side of the valve, exposed to oscillatory shear stress*

Images shows cell outlines based on vascular endothelial cadherin (red) or CD31 (green) and are representative of 4 to 8 images obtained in pilot studies

Summary

In this chapter the following research questions were addressed:

- *How does porcine endothelial cell morphology compare between cells cultured under static conditions and cells cultured under chronic (7 days) complex shear stress?*

  Data showed that there were distinct morphological differences between PAEC cultured under static conditions, which displayed classic cobblestone morphology, PAEC cultured under a gradient of directional shear stress which appeared to be elongated and aligned in the direction of media flow and conditions of non-directional shear stress with PAEC displaying limited alignment. These differences were confirmed through live imaging using SICM and through fixed cell imaging and immunohistochemistry. These morphological changes were transient, with full reversal seen within 24 hours of cessation of shear stress and with structural changes beginning within 1 hour of stopping shear. There was a striking resemblance between morphology of endothelial cells in the polarised regions of the well and those in areas of predicted high and low shear stress within the aortic arch.

- *How does porcine endothelial cell morphology compare between cells cultured under static conditions and cells cultured under acute (24 hours) shear stress?*

  After 24 hours cells cultured under shear stress appeared to display early signs of alignment whereas static cells appeared to have cobblestone morphology. Evidently due to the low level of peak shear in this model compared to some pre-existing models alignment and elongation take some time to occur.

- *How does inflammation influence porcine endothelial cell morphology under static conditions and conditions of acute and chronic shear stress?*

  An acute inflammatory response was generated through incubation of cells for extended periods with the bacterial antigen LPS. PAEC incubated with LPS appeared

more elongated and aligned, most likely due to a TNFα driven response. LPS also caused CD31 to migrate from cell borders and to be spread throughout the cytoplasm. Cells cultured under directional shear stress appeared protected from this.

- *How does shear stress influence cell size and turnover?*

  Whilst absolute cell numbers did not seem to be influenced by shear stress directional shear stress did appear to prevent the reduction in cell number associated with LPS which was most likely caused by cell death. Where there was a reduction in cell number cells appeared to be larger, presumably spreading out in order to fill additional space.

Chapter 4
Morphology of native endothelium in the porcine aorta

Rationale

Data in Chapter 3 demonstrated that directionality, alongside magnitude of shear may dictate morphology changes in endothelial cells. This chapter describes the use of native tissue from pig aorta to investigate how endothelial cell morphology in regions predicted to experience directional, high shear compares to morphology of cells in regions predicted to experience non-directional, low shear. This type of study has been reported in the literature (Cybulsky *et al.*, 2001) and within our group (see Figure 4.1A) using mouse aortic arches but, to our knowledge, has not been previously attempted in pig tissue. In the mouse aortic arch shear maps have been constructed (Suo *et al.*, 2007). However, detailed analyses of shear patterns in the pig aortic arch are not currently available.

Differences in morphology of the endothelium between the inner and outer curvature of the native aortic arch was less defined than expected based on studies of mouse aorta and cells cultured *in vitro*. In order to increase sensitivity of measurement when gathering morphology data from native tissue nuclear shape co-ordinates have been captured and index of circularity recorded. In order to make direct comparisons in morphology, topography and structural properties SICM has been used to image and measure shape and compliance (referred to as cell 'stiffness') of cells of the aortic arch. Clear differences in native cells of the pig aortic arch led to further studies, using the model of cultured PAEC, again using SICM, to image cells and measure stiffness in order to directly compare the properties of these cells with PAEC grown in vitro exposed to shear stress.

The main research questions discussed in this chapter are:

- How do native endothelial cells of pig aortic arch differ in morphology at regions predicted to experience high (directional) shear versus low (non-directional) shear stress; how does this compare to cells grown in vitro?

- Are cells in predicted regions of laminar (directional) shear stress more aligned than cells of predicted low oscillatory (non-directional) shear stress?

- How do structural properties vary between cells of differing morphologies from tissue *in situ* compared to cells cultured *in vitro*?

Methods

Tissue dissection and handling

Pig hearts with aortas attached were delivered chilled in HBSS within 4 hours of slaughter of the animal. Aortas were carefully dissected from the hearts and excess connective tissue trimmed away. Photographs of each aorta were taken before areas of interest were prepared (Figure 4.1). Once each area had been identified a 3mm cork borer was used to isolate discs of tissue from the aorta and a 2mm cork borer used to isolate 2mm discs of tissue from the brachiocephalic artery. The adventitial layer was sliced away using a fine scalpel blade leaving an intact disc consisting primarily of vessel intima including the endothelium.

Tissue fixation and immunohistochemistry

After dissection, discs of porcine intima were fixed for 15 minutes with a formalin solution containing 2% formaldehyde. Once fixed, tissues were placed on cavity slides. A circle was drawn around each cavity with a PAP hydrophobic barrier pen to ensure solutions would remain on the tissue and all subsequent steps took place on these slides. Incubation steps were carried out in a sealed container lined with damp paper towels to reduce evaporation and possible drying of the tissue. All liquids used in the staining process were in volumes of 200µl.

Permeabilisation and blocking was achieved in a 4 hour step requiring room temperature incubation with triton x-100 and goat serum. CD31 was then added overnight at room temperature. Tissue was then incubated with DAPI for 15 minutes. After washing, cavities were filled with hard set mounting medium and glass coverslides mounted on top. Tissues were imaged immediately.

Tissue imaging

Tissue slides were imaged using a Leica SPF5 inverted confocal microscope. A single image was taken of each disc of tissue. In some cases to achieve a complete view of the endothelium a z stack of images had to be generated and used to form a composite image.

SICM and cell compliance

In order to image live cells in the native tissue a slightly different procedure was applied. Once tissue regions of interest had been identified and dissected, the full thickness area of vessel was pinned to wax sheets, taking care not to stretch the tissue. SICM was used to probe cells at the centre of these pinned regions. As well as in the gathering of morphological data SICM was also used to collect information about the physical properties of cells in situ. A jet of liquid was used to apply pressure to the highest point of cells in each region. Data on the subsequent deformation and recovery of the cell membrane were captured and used to calculate cell compliance as µm change in cell height per kPa pressure applied at the point of maximum deformation (Sánchez *et al.*, 2008).

Data and statistical analysis

Where representative images are shown, the number taken in the entire set is provided in the figure legend. For pooled observations, data are mean ± S.E.M. for n= separate determinations, all protocols were repeated on cells from at least 3 separate pigs. Where data were blind scored the nature of the image was not known to the scorer and all images were scored by at least 2 independent scorers and the mean of their scores recorded. Data were analysed using GraphPad Prism as described in individual figure legends. Statistical significance was assumed where $p<0.05$.

Results:

Endothelial cell morphology in regions of the inner and outer curvature of pig aortic arch.

Pig hearts with aortas attached were delivered to the laboratory and a clear dissection of the arch between the aortic root and the descending aorta was possible in each case (Figure 4.1). Multiple sampling of each region (Figure 4.1) was possible using a 3mm diameter cork borer.

Previous work in the Mitchell group focused on the aortic arch of the mouse suggested that endothelial cells of the inner and outer curvature of the ascending aortic arch display contrasting morphologies with cells of the inner curvature appearing cobblestone and those of the outer curvature appearing elongated (Figure 4.1A). This pattern would appear to fit with observations that shear stress is highest at the outer curvature of bends and lower at the inner curvature (Caro *et al.*, 1971). For this reason tissue was sampled from the inner and outer curvature of the porcine ascending aortic arch to see if the cells displayed similar polarised morphologies to those I had cultured *in vitro* and those imaged from mouse aorta. Cell morphology was evaluated based on the distribution of the endothelial cell marker CD31 **(green)** and the nuclear stain DAPI **(blue).**

Aortas were collected from 3 separate pigs and up to 5 samples per region imaged. Figure 4.2 shows data from Pig 1 and the outer curvature of the arch. From this region of tissue from Pig 1, viable samples and images were obtained from 5 discs of tissue (A-E; Figure 4.2). CD31 was abundantly expressed in endothelium of each sample imaged and, overall, the endothelial layer was relatively intact despite transport, handling, and dissection and mounting. Based on immunohistochemical observations in the mouse and shear plots calculated for the mouse (Suo *et al.*, 2007) we predicted cells of the outer curvature to experience a directional and relatively high level of shear stress. If data presented in Chapter 3 were translated to the intact arch, we would expect cells to be clearly aligned in this region. This was not always the case. Unlike morphology of endothelial cells exposed to directional shear stress in culture (i.e. at the edge of the well shown in Chapter 3); morphology consistent with elongation and alignment was much more difficult to see in

endothelium of the native aortic arch (Figures 4.2, shows all data from 5 samples of 1 pig; Figure 4.3 shows representative samples of tissue from the 3 separate pigs). Moreover, when images of the inner (Figure 4.4) and outer (Figure 4.3) curvature of the porcine aorta were blind scored in the same way as cell data in Chapter 3, no significant differences were seen in cells of the two regions (Table 4.1). In order to extend the sensitivity of cell morphology analysis software was used to capture a circularity index of the endothelial nuclei, which, with these types of images, would be impossible to differentiate by eye and capture by blind scoring. This index was calculated using the equation $4\pi\left(\frac{area}{perimeter^2}\right)$.

A circulatory index of 1 represents a perfect circle and of 0 represents a straight line. Nuclear morphology was imaged using DAPI and is shown in blue. Nuclei circularity index data were gathered from each image by importing the data from the blue channel (Figure 4.2B) into Fiji open source software; the data was then thresholded to exclude artefacts and nuclear dimensions for each cell calculated. Across the 5 samples gathered from the outer curvature of the arch of Pig 1, circularity index was relatively consistent and showed a spread of values in endothelial cells of this region (Figure 4.2). A similar profile of nuclei circulatory index was found in the endothelium of the outer curvature of tissue from 2 other pigs (Pig 2 and Pig 3; Figure 4.3). Using the same thresholded nuclear images it was also possible to carry out measurements to capture 'nuclear angle' of the endothelial cells. This was done in order to try and determine if nuclei in an image were consistently orientated in one direction and thus the cells aligned. This angle is calculated based on an ellipse fitted by the software to the longest length of the nuclei and the longest width bisecting this length. The angle between the length and the x axis of the image is calculated to determine cell angle. A clear peak in the distribution of angles would suggest nuclear alignment using this measure. Representative images from the outer curvature of the arch from the 3 pigs appeared to show a discernible peak, indicating nuclear alignment but it is difficult to assess this objectively.

Similarly good quality sections and images were obtained from samples of the inner curvature of the aortic arch from the 3 pigs (Figure 4.4).

There were no differences in the number of nuclei or the area that nuclei occupy between endothelium of regions from the inner versus the outer curvature of the arch. Taking length to width ratios of endothelial nuclei and averaging them there also appeared to be no difference in nuclear elongation (Figure 4.5) Despite what looked like different patterns of elongation index when plotted against cell count, no difference was seen in endothelial cells of the inner versus outer curvature when this data was averaged (Figure 4.5). In order to better represent this parameter, the data were re-interrogated selecting values (number of cells) displaying an index of 0.9 (i.e. towards circularity) versus 0.2 (i.e. away from circularity and towards linearity). Using this approach, more nuclei of cells in the inner curvature region showed 'circularity' than 'linearity '. The distribution of number of cells between these two extremes was more evenly spread in regions of the outer curvature (Figure 4.6).

Endothelial cell morphology in the brachiocephalic artery

The brachiocephalic artery leaves the aortic arch at the crest of the outer curvature and endothelium lining this artery distal to the orifice is straight and due to the smaller diameter of this artery than the aorta pressure may be predicted to be of a higher magnitude than that seen in adjacent arch endothelium. As a branch point the outer wall is a predicted site for plaque formation but the inner wall higher up the artery is likely to be protected. In contrast to the morphology of the endothelium of the aortic arch, clear visible alignment was noted by visual scoring using CD31 as a guide (Table 4.1). The circularity index of the nuclei in endothelium of the brachiocephalic artery again appeared to be distributed over a broad range but a peak in angle of orientation was very noticeable (Figure 4.7).

Endothelial cell topography and compliance in regions of the inner and outer curvature of pig aortic arch; comparison with sheared cells in culture

Based on the above, it may be concluded that in native tissue, there is no discernible difference in endothelial morphology between regions of the aorta sampled, and although nuclear shape and orientation data were gathered, differences are few. This may be because during the post mortem period endothelial cells have been out of shear and some level of dealigment has occurred or differences observed in the mouse may not translate to

larger animals. In order to better understand endothelial cell morphology at a cellular level and to study physical characteristics of the cells in native arch versus cultured cells, SICM was used (Figure 4.8). SICM has the capability of live cell imaging. This may be advantageous in avoiding potential artefacts of fixation. Using the SICM in hopping mode, endothelial cells of the inner and outer curvature of the pig arch were imaged and seen to display characteristic morphology. Specifically, endothelial cells in the inner curvature appeared cobblestone-like whilst those in the outer curvature appeared flatter, more elongated and aligned. Importantly, the morphology of endothelial cells in the outer curvature of the porcine aortic arch was similar to that seen in cells from the edge of sheared wells of PAEC, whilst morphology of cells in the inner curvature resembled that seen in PAEC grown under static conditions or in the centre of sheared wells (Figure 4.8). Length to width ratios of endothelial cells imaged by SICM were calculated in order to assess cell elongation. The higher the ratio the more elongated the cell. Interestingly in both the outer and inner curvature of the aortic arch there was a distribution of cells including many that were rounded (Figure 4.9). However, the outer curvature of the arch had an increased range of cells at the higher end of the scale. These findings appear to agree with the immunohistochemical findings in that there is an increased preponderance of elongated cells in the outer curvature of the ascending aortic arch, though they are not always in the majority.

Using SICM it is also possible to measure structural properties of live cells (see Methods 2.5). In this way, it was found that endothelial cells in the outer curvature of the porcine aortic arch were less compliant and more resistant to deformation than cells in the inner curvature. In direct corroboration of this, PAEC exposed to directional shear (i.e. the edge of the shear wells) were less compliant than endothelial cells either cultured under static conditions or cultured under shear stress at the centre of the well (Figure 4.10). The degree of similarity between the properties of *in situ* cells and cells in the orbital shaker model was promising; suggesting the conditions of the model may simulate physiological conditions. A direct correlation was seen between elongation and reduced compliance (Figure 4.11). These data, together with the morphology data gathered and calculated using SICM in hopping mode, indicate that endothelial cells exposed to directional shear, be it *in vitro* or *in vivo* are aligned, elongated and resistant to deformation whilst those experiencing no shear

or non-directional shear are non-aligned, rounded and compliant. This difference in physical properties may have some bearing on the integrity of the endothelial wall and its barrier function.

Figures

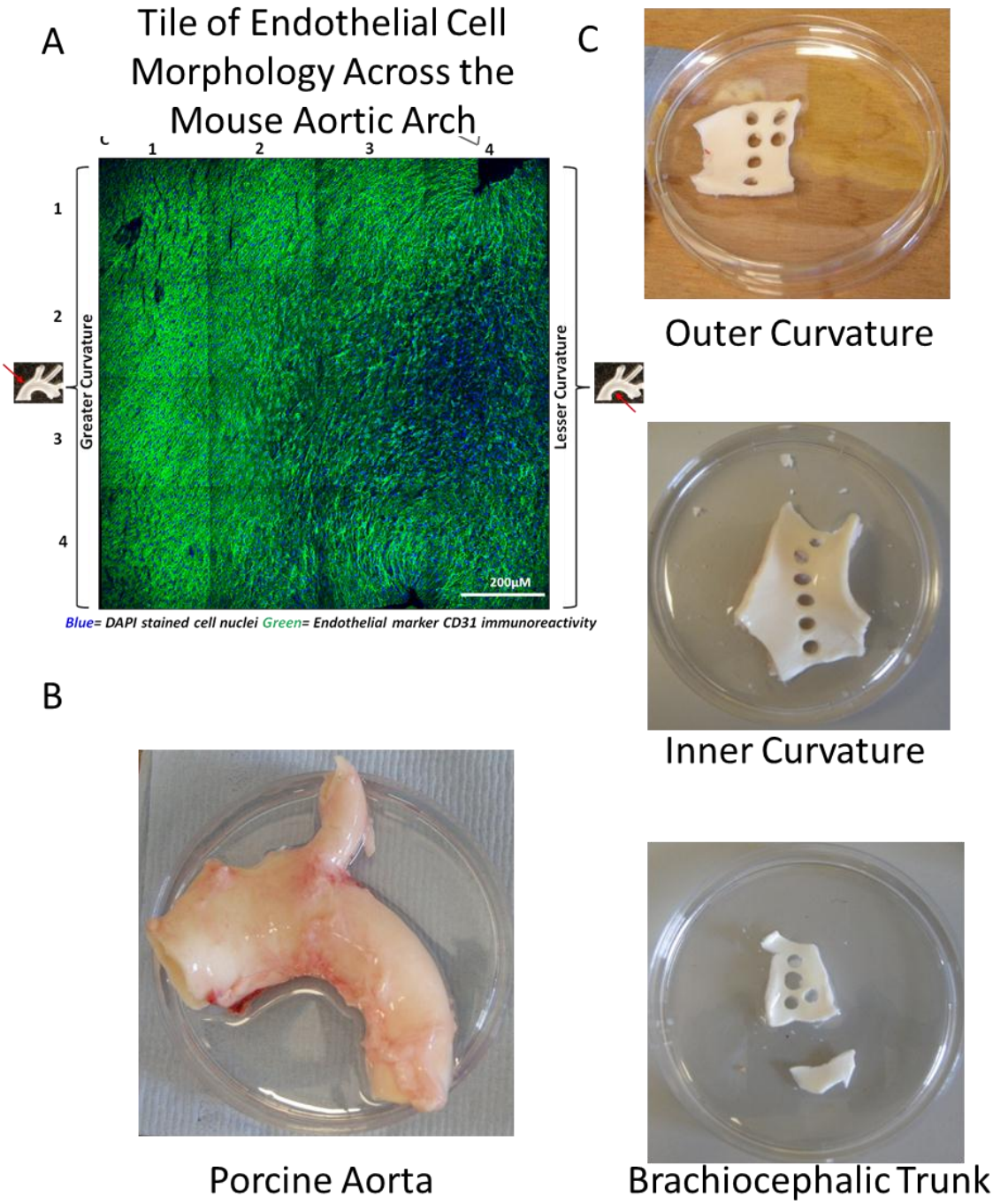

Figure 4.1 Illustration of regions of native porcine tissue dissected for analysis ***(Legend continues on next page)***

Figure 4.1 Illustration of regions of native porcine tissue dissected for analysis <u>(Legend continued from previous page)</u>

A: *The aorta of a 3 month old wild type C57BL/6J mouse was dissected and flattened before imaging with en face confocal microscopy. A tile scan from the outer curvature towards the inner curvature of the aortic arch was performed. Morphology changes, from CD31 rich elongation and alignment at the outer curvature to nuclei rich cobblestone morphology at the inner curvature. (Image courtesy of Martina Lundberg, Imperial College Thesis 2012)*

B: *Porcine hearts with aortas attached were delivered chilled and the aortas carefully dissected at the aortic root and placed in PBS.*

C: *Regions at the inner curvature and outer curvature of the aortic arch were removed and washed in PBS before a 3mm cork borer was used to isolate discs of tissue which could be mounted for imaging. 5 segments were taken from each region. The brachiocephalic artery was also dissected and cleaned before a 2mm cork borer was used to isolate discs of tissue for mounting.*

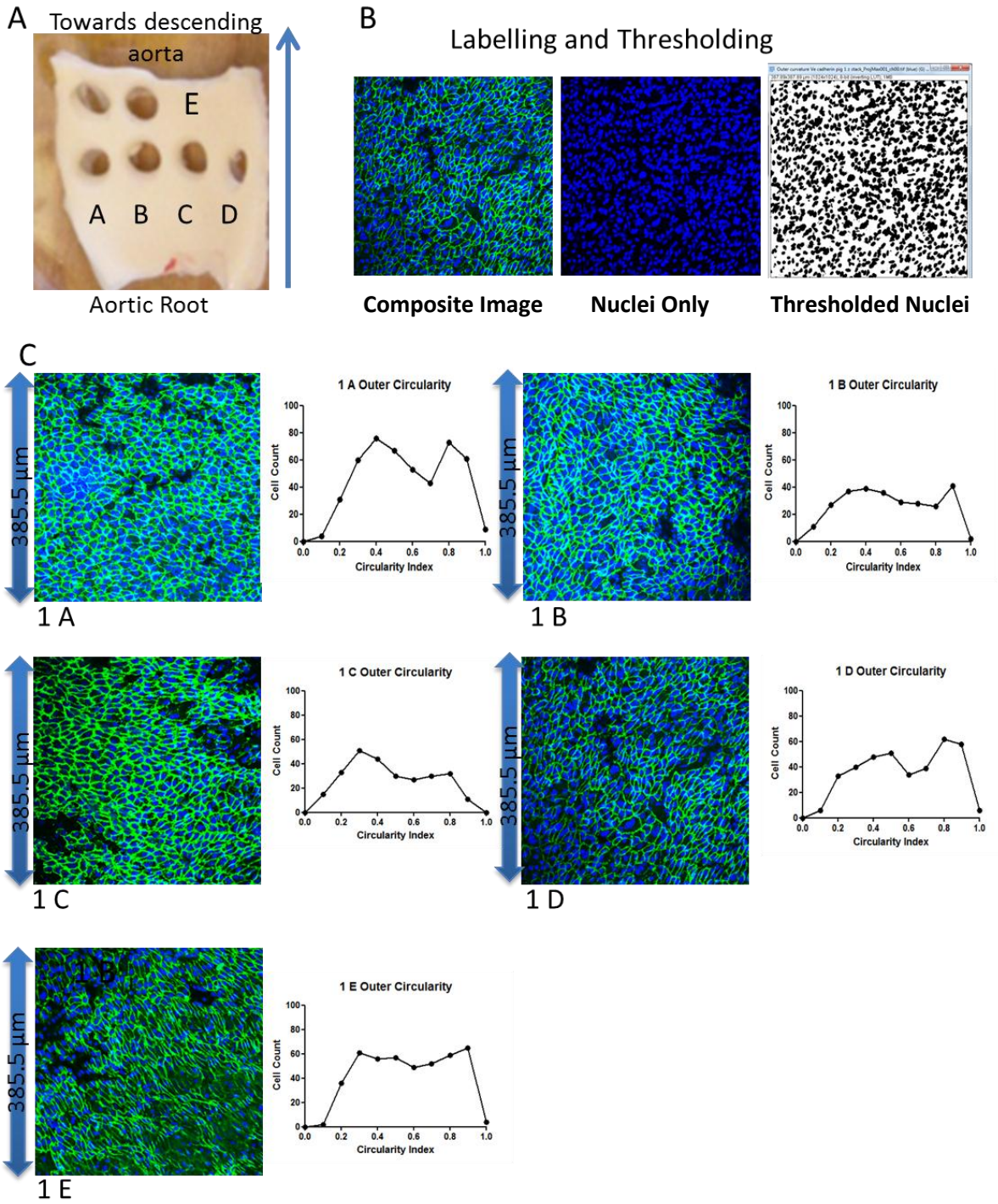

Figure 4.2 Examples of handling, staining and analysis of porcine tissue from the outer curvature of the aortic arch ***(Legend continues on next page)***

A: *5 viable discs of endothelial tissue were isolated from the outer curvature of the aorta of this pig and designated A-E. Discs were removed from regions of tissue that appeared to be relatively flat. Discs of tissue were fixed and stained before mounting on cavity slides for imaging by confocal microscopy.*

Figure 4.2 Examples of handling, staining and analysis of porcine tissue from the outer curvature of the aortic arch <u>(Legend continued from previous page)</u>

B: *Tissue images were processed using FIJI open source software. Images of the nuclei alone were thresholded for subsequent analysis of nuclear profile including area, circularity and angle of orientation.*

C: *The 5 discs of tissue from the outer curvature of the aortic arch of pig 1 are shown. Green shows CD31 an endothelial cell marker largely found at cell borders. In blue are the cell nuclei. Cell circularity was assessed using the equation* $4\pi\left(\frac{area}{perimeter^2}\right)$*. Where 1.0 is a perfectly circular nucleus and values towards 0 tend towards a perfect straight line. A range of values were seen across each tissue sample analysed.*

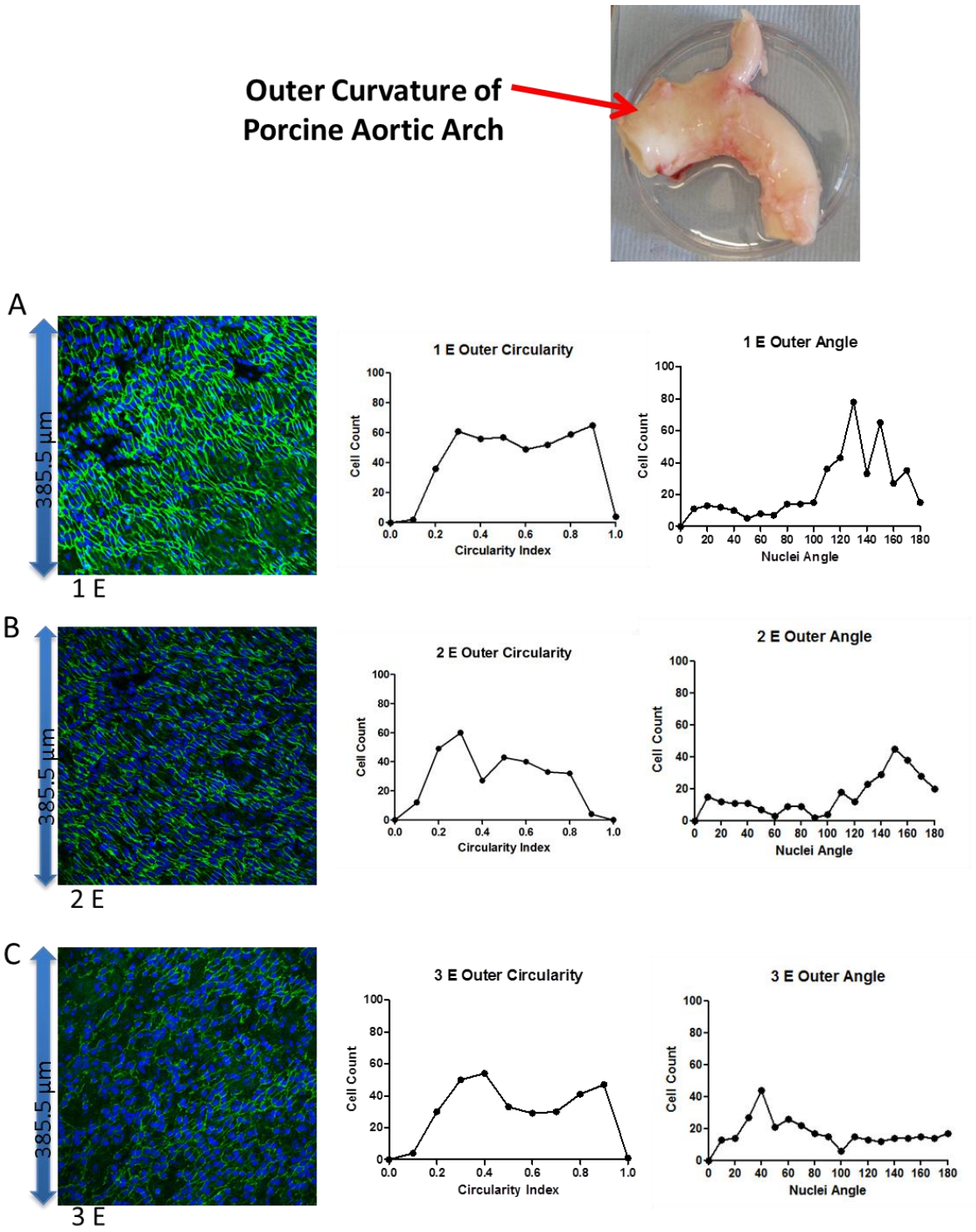

Figure 4.3 Representative images and data from tissue of the outer curvature of the porcine aortic arch

5 tissue samples were taken from a region of the outer curvature of the ascending porcine aortic arch. This was repeated for 3 pigs designated 1 ***(A)****, 2* ***(B)*** *and 3* ***(C)****. A representative image showing CD31, a marker of the endothelial cell border, in green and DAPI stained nuclei in blue is shown for each animal alongside a corresponding plot of nuclear circularity and orientation for each image shown.*

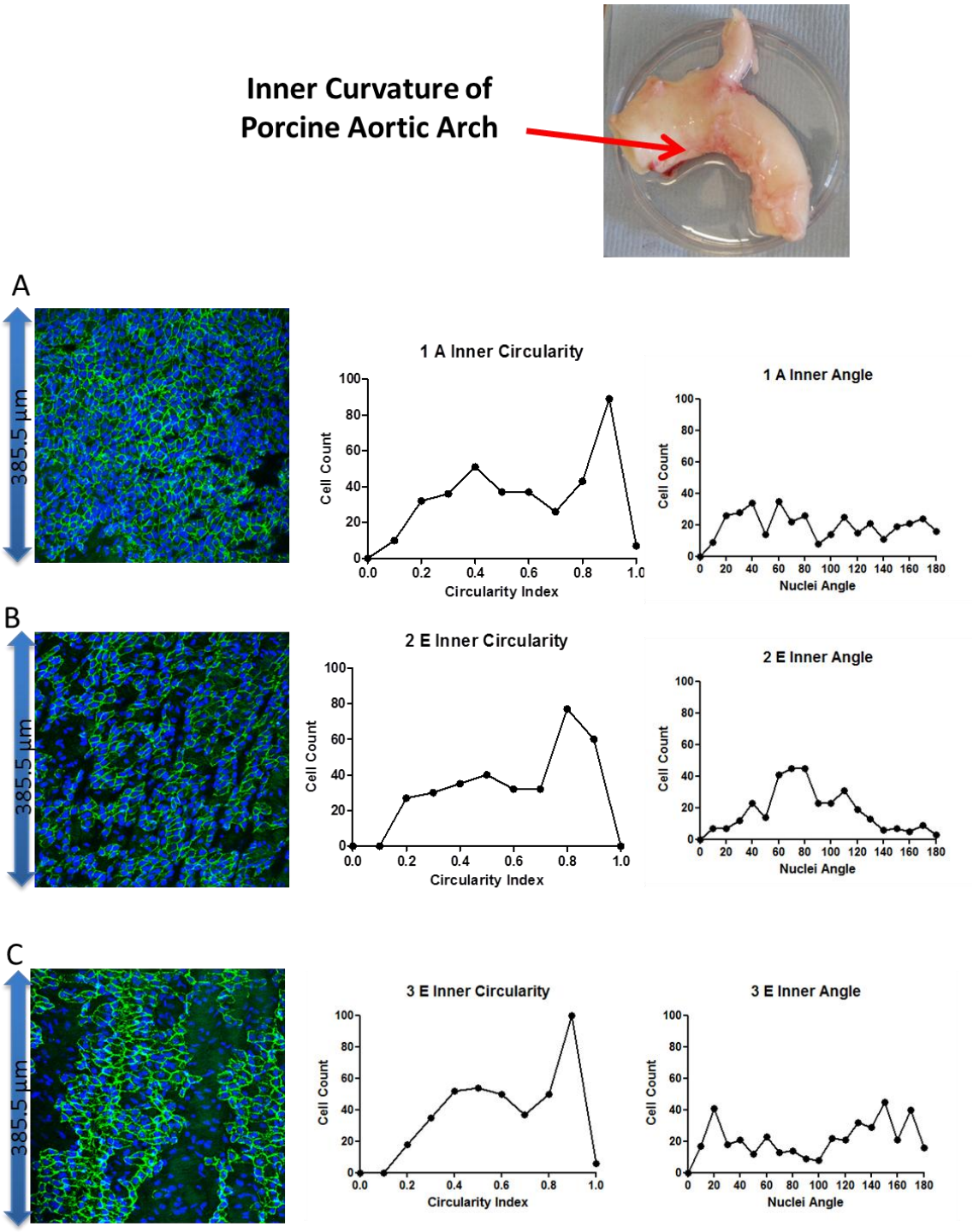

Figure 4.4 Representative images and data from tissue of the inner curvature of the porcine aortic arch

5 tissue samples were taken from a region of the inner curvature of the ascending porcine aortic arch. This was repeated for 3 pigs designated 1 ***(A)****, 2* ***(B)*** *and 3* ***(C)****. A representative image showing CD31, a marker of the endothelial cell border, in green and DAPI-stained nuclei, in blue, is shown for each animal alongside a corresponding plot of nuclear circularity and orientation for each image shown.*

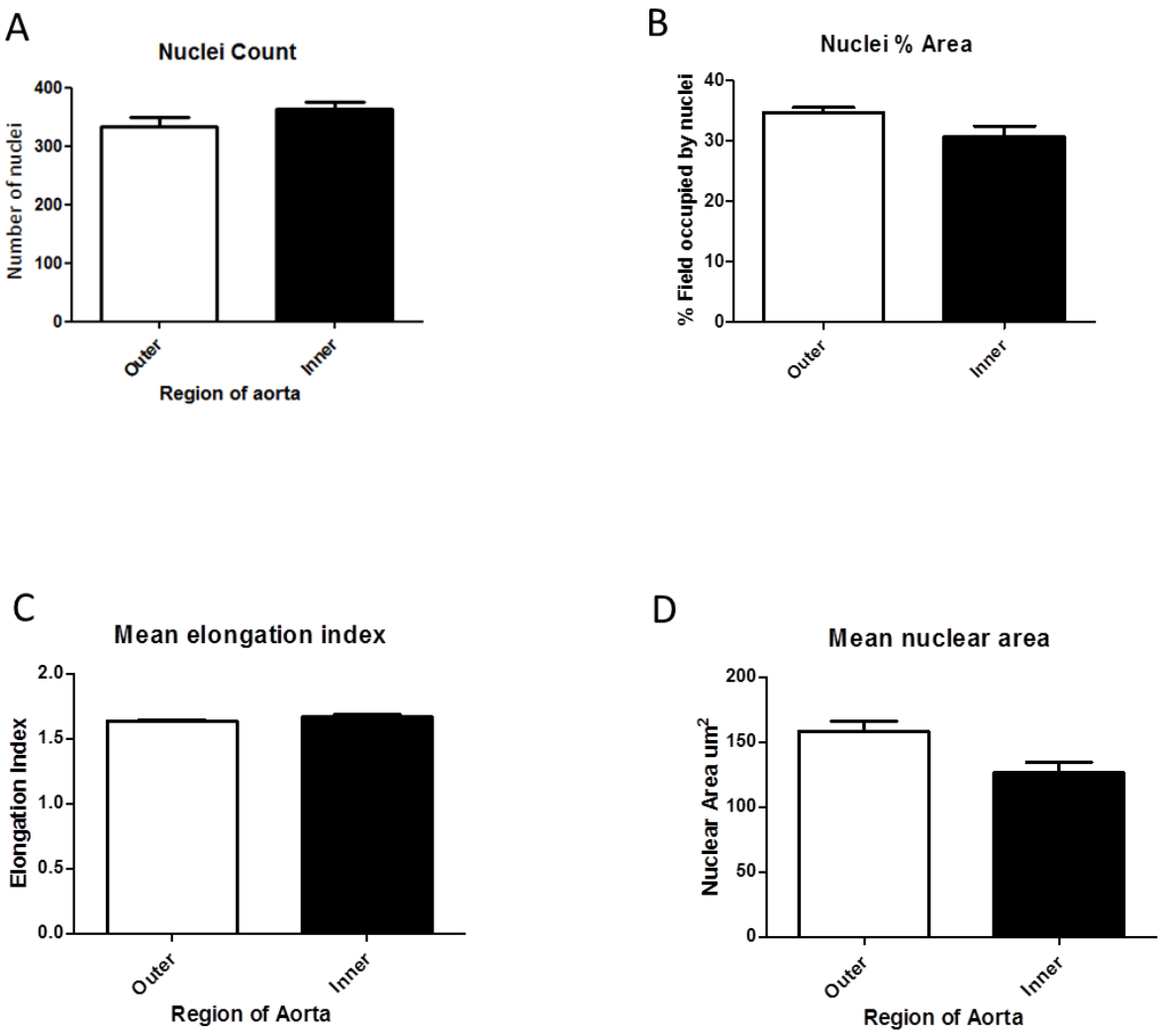

Figure 4.5 Nuclear profile in samples of tissue obtained from the outer and inner curvature of porcine ascending aorta

Nuclei measurements in images gathered from 5 separate sections cut from the inner and outer curvature regions of the aortas of 3 pigs. Images were profiled using FIJI open source software n=13-15. Samples were analysed by Student's t-test and no significant difference was identified between any of the parameters.

A: Estimated nuclear counts in the outer and inner curvature of the porcine ascending aorta

B: Percentage of 385 x 385µm fields occupied by nuclei in the outer an inner ascending curvature of the porcine aorta

C: Mean elongation index (Length to width ratio) of endothelial nuclei from the outer and inner curvature of the porcine ascending aorta

D: Mean nuclear area of endothelial nuclei from the outer and inner curvature of the porcine ascending aorta

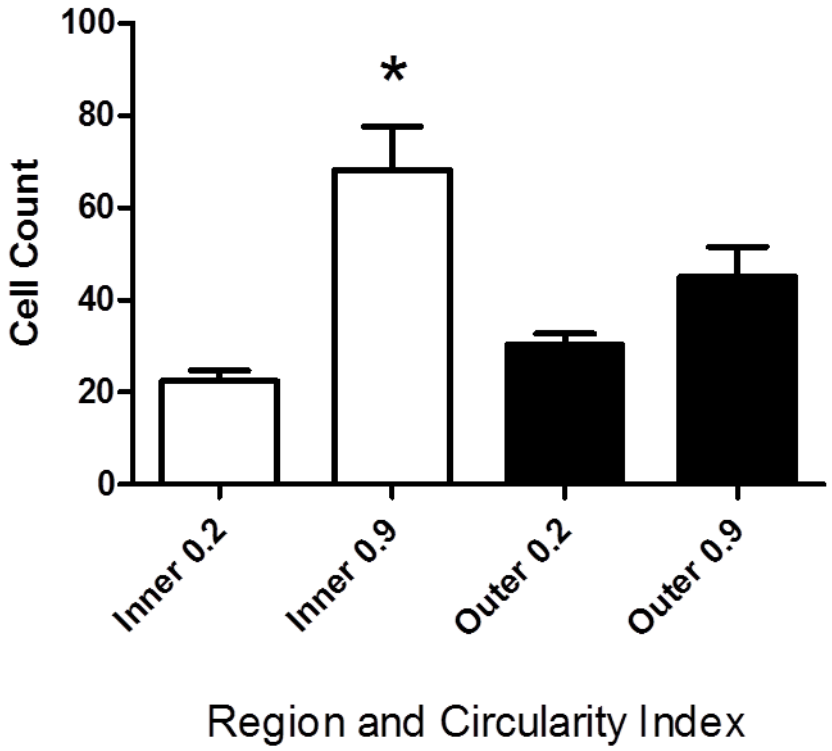

Figure 4.6 Comparison between extremes of circularity and extremes of elongation of nuclei of endothelial cells of the inner and outer curvature of porcine aortic arch tissue

*N=13-15 images of endothelial nuclei from the outer and inner curvature of the porcine aortic arch were profiled for circularity using Fiji open source software. A value of 0 indicates a straight line and a value of 1 a perfect circle. When comparing very circular and very elongated nuclei it was found that there were significantly greater numbers of extremely round nuclei in cells of the inner curvature of the aortic arch. Data were analysed using One-way ANOVA followed by Bonferroni post-test. P=<0.05 was taken as significant and is denoted by *.*

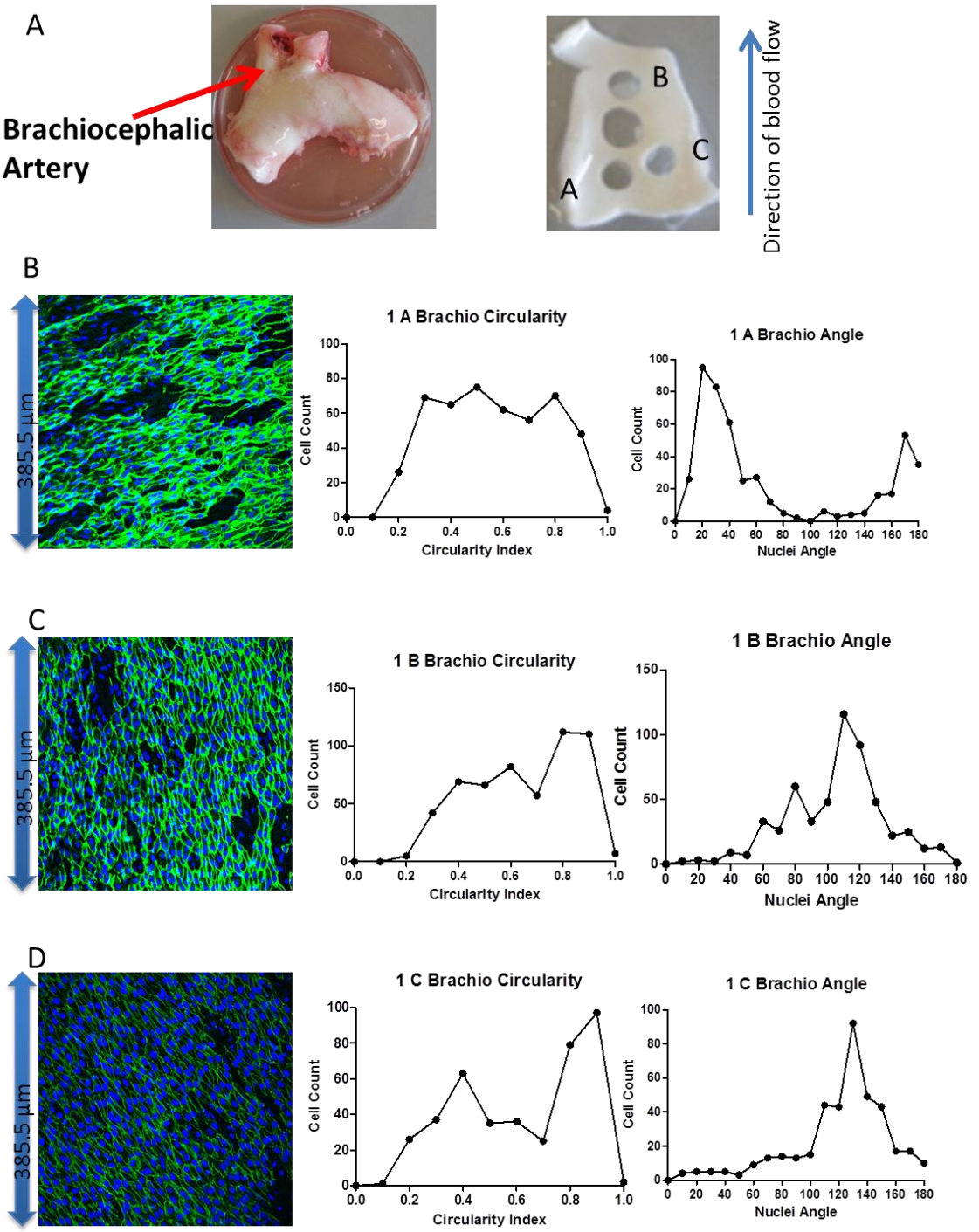

Figure 4.7 Images and nuclear profile of endothelial cells of the porcine brachiocephalic artery

A: *A 2mm cork borer was used to obtain 3 discs of tissue from the brachiocephalic artery of one pig*

B-D: *Images of endothelial cells of the brachiocephalic artery attained with DAPI (blue) to indicate cell nuclei and CD31/PECAM-1 to indicate cell borders. Circularity and angle distributions are provided corresponding to the images shown.*

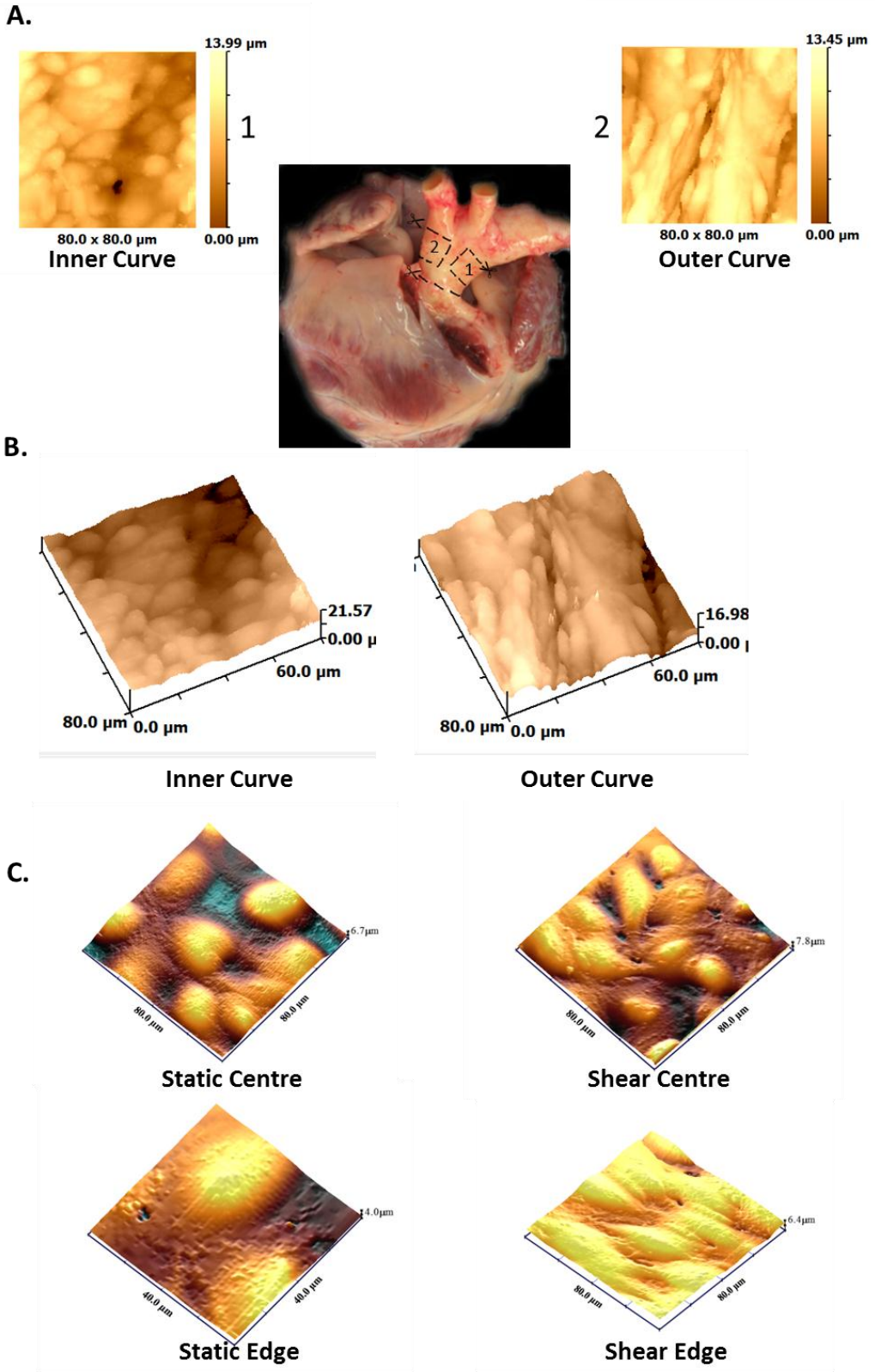

Figure 4.8 Live cell imaging of porcine aortic tissue using SICM <u>(Legend continues on next page)</u>

Figure 4.8 Live cell imaging of porcine aortic tissue using SICM <u>(Legend continued from previous page)</u>

*Porcine aortas attached to hearts were delivered and regions of the inner and outer curvature of the ascending aortic arch carefully dissected out (**A**). Tissue was pinned to wax sheets and 80 x 80µm central areas imaged using SICM. Representative images shown in (**B**) indicate an increased number of elongated cells were seen in tissue of the outer curvature of the aortic arch compared to the inner curvature. This was similar to cells in the regions of directional and non-directional shear respectively **(C)***

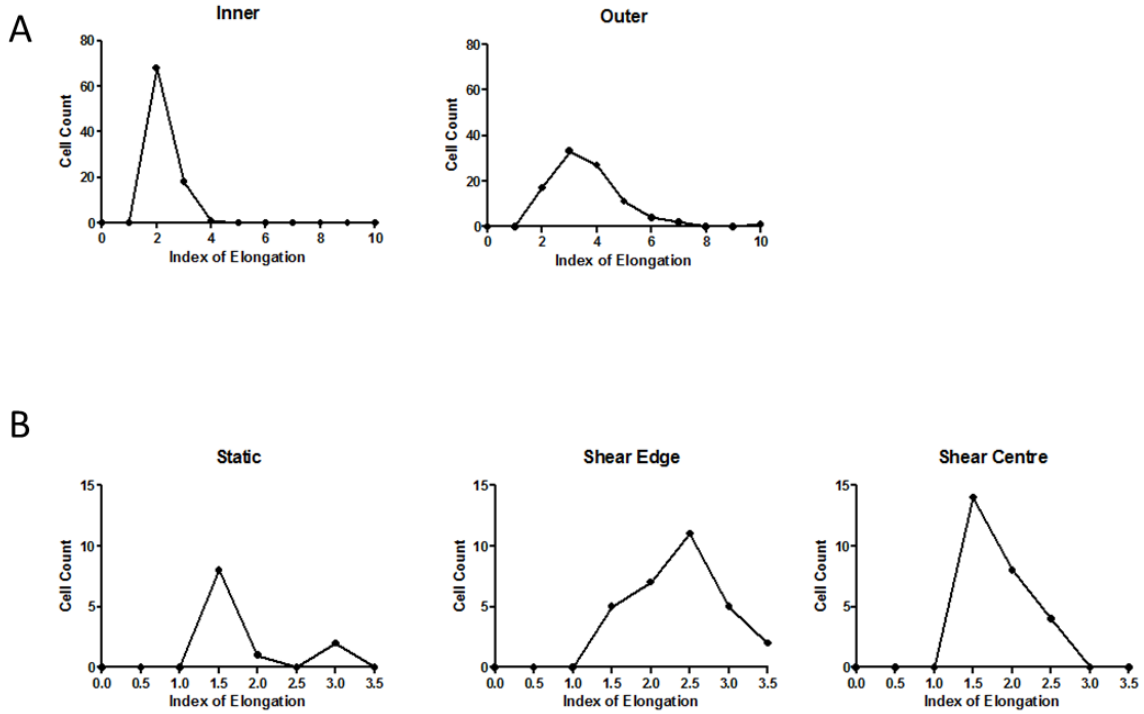

Figure 4.9 Distributions of Index of Elongation values in tissue as compared to in cultured cells

Length to width ratios of all whole cells visible in an 80 x 80µm scan generated by SICM were calculated and the resulting values termed the cell's index of elongation. Though the majority of cells of the inner curvature and outer curvature displayed a low Index of elongation cells of the outer curvature displayed a higher range of values ***(A)****. Cells cultured at the edge under shear stress appeared to have a higher index of elongation compared to those at the shear centre and static cells but the range of values did not reach values as high as those seen in native tissue* ***(B).***

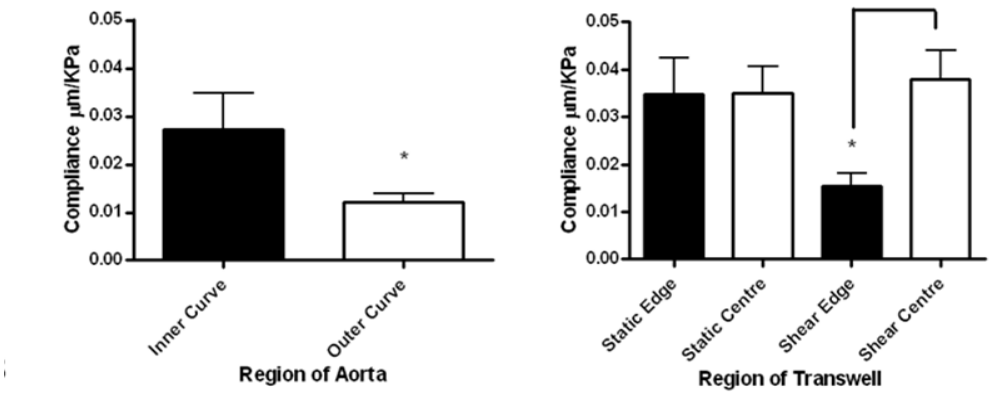

Figure 4.10 Compliance of cells of the ascending porcine aortic arch compared to cultured PAEC

*A jet of liquid was used to apply pressure to the highest point of each cell in order to measure the resulting deformation and recovery. Data represent 15-20 cells of the native tissue from 4 animals and 13-15 cultured cells from 3 animals. Data were analysed using Student's t-test. P>0.05 was deemed significant and is indicated by *. Data reproduced from (Potter et al., 2012)*

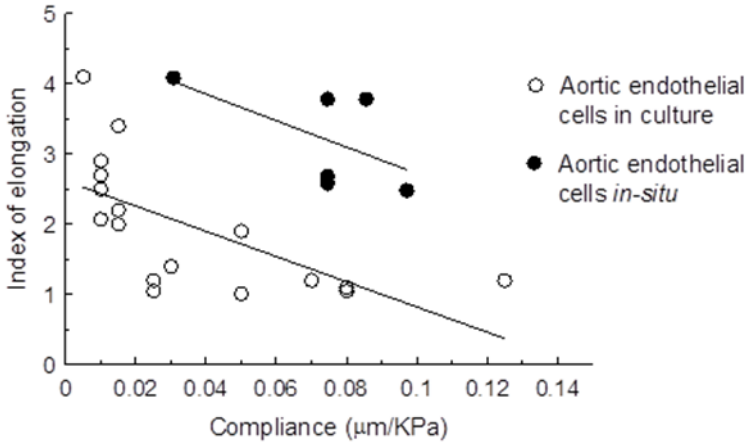

Figure 4.11 Correlation between cell index of elongation and compliance

Cell compliance was plotted against cell elongation index in a pilot study where images were clear enough to distinguish cell borders. Cell compliance appeared inversely proportional to cell index of elongation. Data reproduced from (Potter et al., 2012).

Summary

In this chapter I have explored the following questions

- *How do endothelial cells of the native arch differ in morphology to cells grown in vitro?*

  Endothelial cells from two different regions of the ascending aortic arch showed broadly similar morphologies appearing to be aligned in some cases and to have more cobblestone features in others. This was not as predicted assuming that cells from the outer curvature of the arch would be elongated and aligned and cells of the inner curvature cobblestone in appearance based on findings in the mouse. This shows the importance of noting species differences. The time tissue is out of physiological conditions and the imaging modality are also important factors to take into consideration when analysing these results.

- Are cells in predicted regions of laminar shear stress more aligned than cells of predicted low oscillatory shear stress?

  Limited data were gathered about cells of the brachiocephalic artery, an area which is predicted to experience laminar flow. These data may suggest that shear stress *in vitro* contributes to cell alignment. The lack of elongation and alignment seen in the cells and nuclei of the ascending aorta suggests that the flow patterns and thus shear stress in the pig aorta may be more complex than in the mouse and further modelling would be necessary in order to ascertain this difference.

- How do structural properties vary between cells of differing morphologies?

  Elongated and aligned cells appear to be less compliant than rounded, cobblestone cells both *in vivo* and *in vitro*. This may have a bearing on their permeability and structural integrity and may provide some insight into how cells of certain regions are prone to cholesterol uptake.

Chapter 5

Effect of Shear Stress on PAEC expression of NFκB

Rationale

In earlier chapters it was shown that shear stress plays a clear role in determining endothelial cell morphology. Others have also shown that as well as readily observed physical changes, shear stress also causes changes at a genetic level, regulating transcription pathways, including NFκB (Hajra *et al.*, 2000; Jongstra-Bilen *et al.*, 2006). The transcription factor NFκB is important in endothelial cells where its activation is regulated in response to injury as well as through expression of hormones and activation of adhesion receptors (Hayden *et al.*, 2004). In previous chapters it was shown that shearing endothelial cells in 6-well plates on an orbital shaker generates morphological changes that are consistent with directional and non-directional shear stress. Importantly, these morphological phenotypes of endothelial cells have been implicated in variation in susceptibility to atherosclerosis where NFκB activity is thought to be central to initiation and propagation of disease(Cheng *et al.*, 2006; Collins *et al.*, 2001; Cuhlmann *et al.*, 2011; Kempe *et al.*). Cells in areas of low shear stress which appear rounded and it is these regions which tend to be those at greatest risk of initiation of events triggering atherosclerosis (Caro, 2009). Specifically it has been shown that endothelial cells at the centre of the well, exposed to non-directional shear, are similar in morphology and compliance to cells at the lesser curvature of the aortic arch whilst cells exposed to directional shear stress at the edge of the well are similar in morphology and compliance to elongated cells at the greater curvature of the aortic arch. Using mouse and porcine models, others have shown that endothelial cells in the lesser curvature of the arch that display a cobblestone morphology are primed for NFκB activation and have proposed that this explains why atherosclerotic plaques occur there and not in the greater curvature (Hajra *et al.*, 2000; Passerini *et al.*, 2004). In order to understand how cells in the orbital shaker model may reflect those phenotypes at the level of inflammatory responses, experiments were carried out to measure NFκB activation in cells exposed to directional versus non-directional shear stress for 7 days.

Methods

Cells were cultured on Transwells™ and exposed to shear stress for 7 days through culture on an orbital shaker as described in previous chapters (See Methods Chapter 2). 3 hours before cessation of the experiment a full medium change was carried out on the cells. 1 hour before cessation of the experiment a 100µl volume of either LPS or PBS-vehicle was added to the cell medium to give a final concentration of 1µg/ml LPS. This means of LPS administration ensured that any nuclear translocation of NFκB to its active nuclear state would not be due to the effects of the media change.

PAEC cultured under static and shear stress conditions were imaged using confocal microscopy as described in Chapter 2. However, it is important to note that cells described in this chapter were imaged at 2 planes of focus, a cytosolic based plane centred on CD31 staining and a nuclear plane based on DAPI staining (Figure 5.1). Imaging in two planes was necessary to capture a full measurement of nuclear area, in order that this area could be distinguished from the rest of the cell to give a purely cytosolic read out. Imaging of the nucleus is difficult in the cytosolic plane, as this is focused at the bottom of the cell and here non-specific DAPI staining, where DAPI is caught in the pores of the Transwell™ filter, causes interference. All reported NFκB measurements were based on observations in the cytosolic plane. Measurements were captured for NFκB in the cytosol and nuclear associated NFκB, a single respective value was obtained for each (Figure 5.2).

Data and statistical analysis

Where representative images are shown, the number taken in the entire set is provided in the figure legend. For pooled observations, data are presented as mean ± S.E.M. for n= a given number of separate determinations, all protocols were repeated on cells from at least 3 separate pigs. Data was analysed using GraphPad Prism as described in individual figure legends. Statistical significance was assumed where $p<0.05$.

Results

A strategy to quantify NFκB activation through monitoring of its movement to the nucleus was developed using FIJI opensource software. This involved imaging cells at a nuclear plane and a cytosolic plane (Figure 5.1). Images were then split into the individual channels for green (CD31), blue (DAPI) and red (NFκB). The data from the blue channel, gathered from the nuclear focused image, which defined nuclear area, was then used to produce a mask that could be subtracted from the image of NFkB staining from the red channel, gathered when imaging at the CD31 focused cytosolic plane. This created two images for analysis, the red channel with the mask subtracted, which was used for measuring the cytosolic NFκB and the red channel without the mask subtracted, where the nuclear associated NFκB can be measured (Figure 5.2). Using this method enabled quantification of NFκB immunoreactivity in the cytoplasm and the nucleus. This allowed determination as to whether there was any significant effect of the different types of shear stress on NFκB activation in PAEC after 7 days.

In cells cultured under each condition from either the edge (Figure 5.3 and Figure 5.5) or the centre of the well (Figure 5.4 and Figure 5.6), NFκB immunoreactivity (shown in red) was distributed throughout the cytosol. However, in cells where LPS was added to activate NFκB for 1 hour at the 7 day time point, NFκB immunoreactivity migrated to the nucleus of cells cultured under static or shear stress conditions (Figures 5.3-5.6).

Pooled data showed that basal activation of NFκB, based on immunoreactivity in the nucleus was not significantly altered by shear stress (Figure 5.7). There did appear to be a trend for it to be increased in the nucleus of sheared cells at the centre of the well (that experience non-directional shear stress, Figure 5.7B) which is what would be expected based on the theory that non-directional, low level shear is pro-inflammatory. The most striking observation was that LPS-stimulated NFκB activation was increased in endothelial cells experiencing directional shear stress, cultured at the edge of the well. Though cytoplasmic levels of NFκB were reduced at the static edge clearly providing evidence of translocation to the nucleus this was merely a trend in sheared cells both at the edge and centre of the well (Figure 5.8). There was no decline at the static centre.

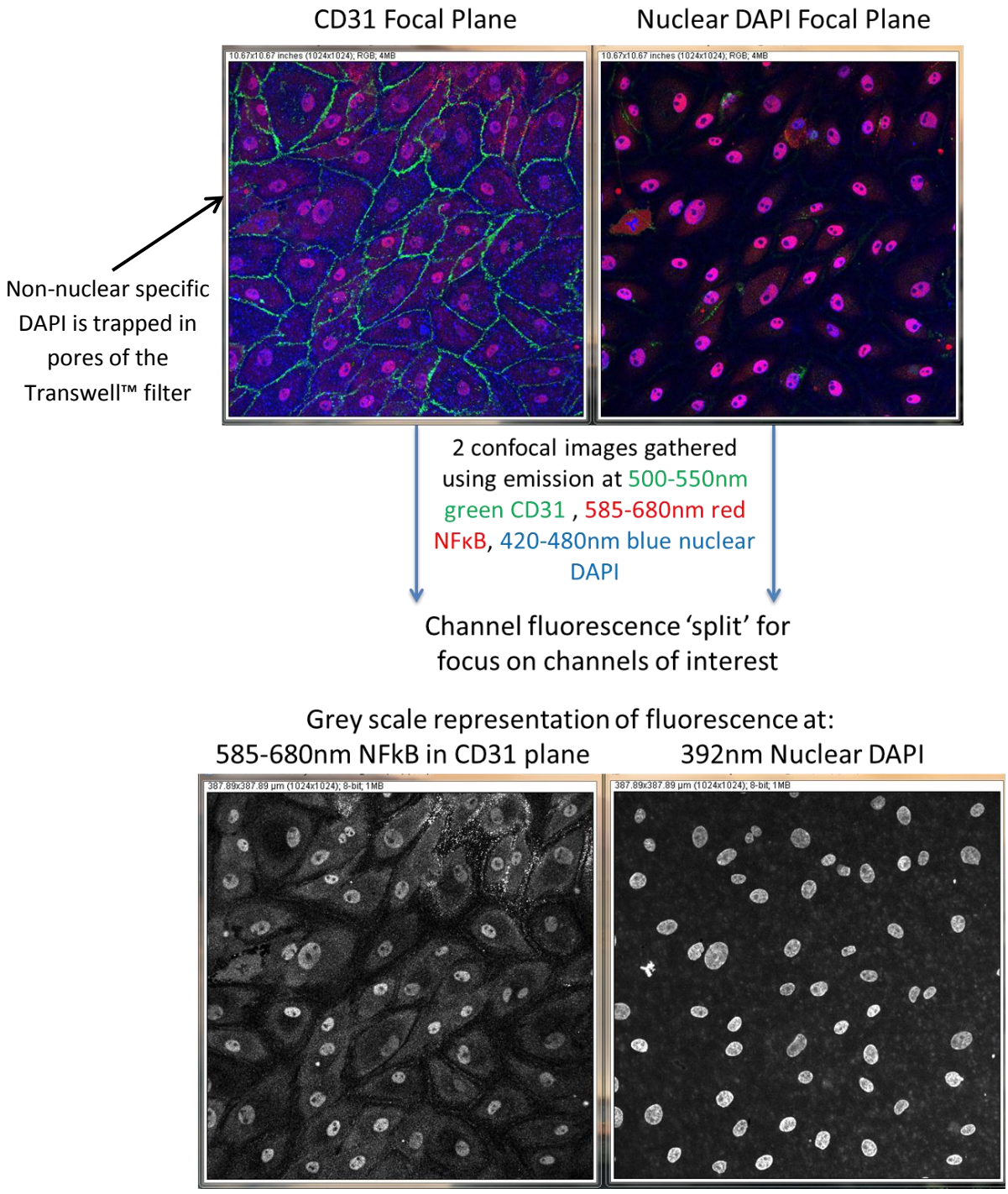

Figure 5.1 Schematic showing how the initial confocal images are prepared for NFκB quantification

385 x 385µm, Images of the same region of cells were gathered at two focal planes. One at the level of the nuclei the other at the level of the CD31 delineated cell membrane. Quantification was carried out based on the NFκB staining of the cell membrane focused channel and the nuclear image captured merely to make a mask determining nuclear outline.

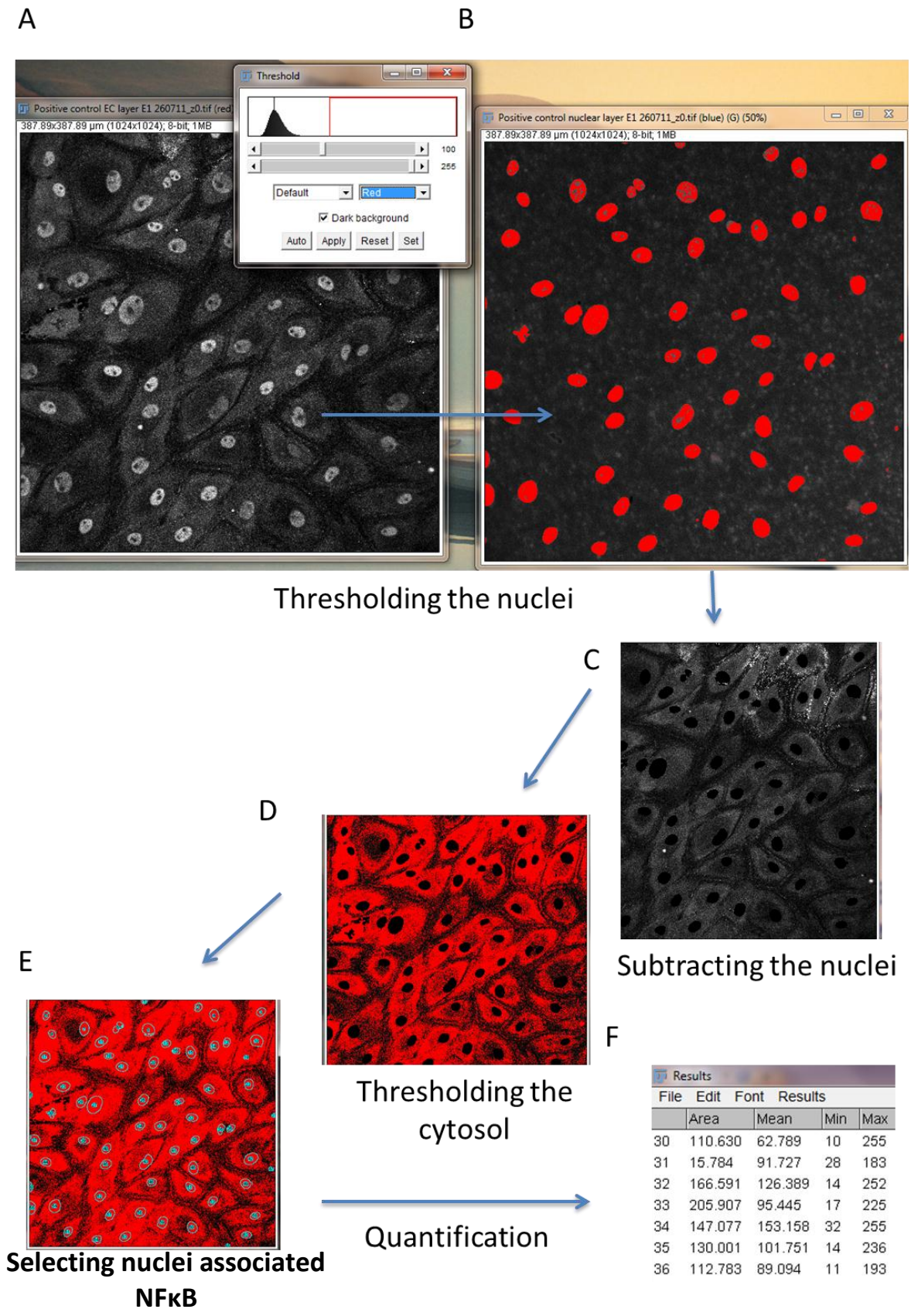

Figure 5.2 Schematic outlining the different stages of the NFκB quantification process
(Legend continues on next page)

Figure 5.2 Schematic outlining the different stages of the NFκB quantification process <u>(Legend continued from previous page)</u>

A: *The images required for analysis are selected: The NFκB staining of the cell membrane focused channel and the nuclear image of the nuclei focused channel*

B: *The nuclei of the nuclear focused channel are thresholded meaning they are selected to ensure no artefacts are picked up as nuclei and are used to create a binary mask.*

C: *The area of the nuclear mask can be subtracted from the image of NFκB staining to produce an image of NFkB that is purely cytosolic in nature*

D: *To ensure no artefacts are measured the image of cytosolic NFκB is thresholded and a single quantified value of mean fluorescence per pixel is generated.*

E: *The original NFκB staining image is re-interrogated and levels of NFκB associated with each nucleus are quantified as individual values of mean fluorescence per pixel*

F: *Quantification values are generated and the mean fluorescence per pixel of NFκB associated with each nucleus is averaged for the number of nuclei in the 385 x 385µm image.*

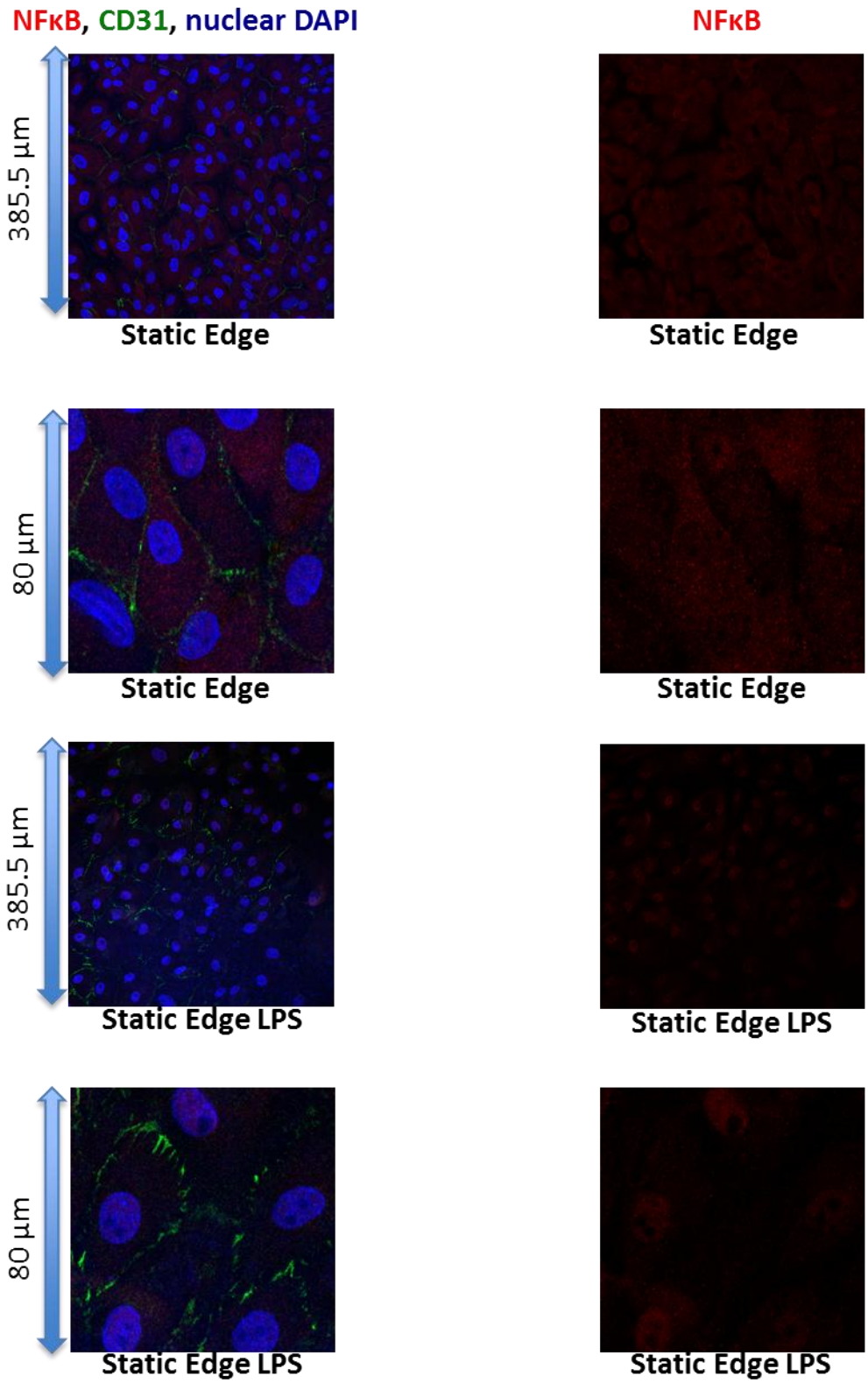

Figure 5.3 NFκB Immunoreactivity in PAEC after 7 days culture at the static edge of a Transwell™ ***(Legend continues on next page)***

Figure 5.3 NFκB Immunoreactivity in PAEC after 7 days culture at the static edge of a Transwell™ <u>(Legend continued from previous page)</u>

Images are representative of n=10-12 images gathered from 4 separate isolations/wells repeated with cells of 3 different animals. A full field 385.5 x 385.5µm image was taken of each cell area. An 80 X 80µm enlargement of a region of each image is shown below for clarity of intracellular localisation. Those on the left are composites formed of the CD31 and NFκB staining observed at the cell membrane focused view and nuclei staining observed at a nuclear focused view. These composites have been produced to aid the reader in identifying the region of the cell in which the NFκB is present. On the right, NFκB staining alone at the cell membrane focus is shown. In untreated cells NFκB was seen largely in the cytosol with clear voids in the pattern of staining where the nucleus occupies the cell. When cells were treated with LPS there was a clear translocation of NFκB into the nucleus. Voids can be seen showing that NFκB is not present in the nucleolus.

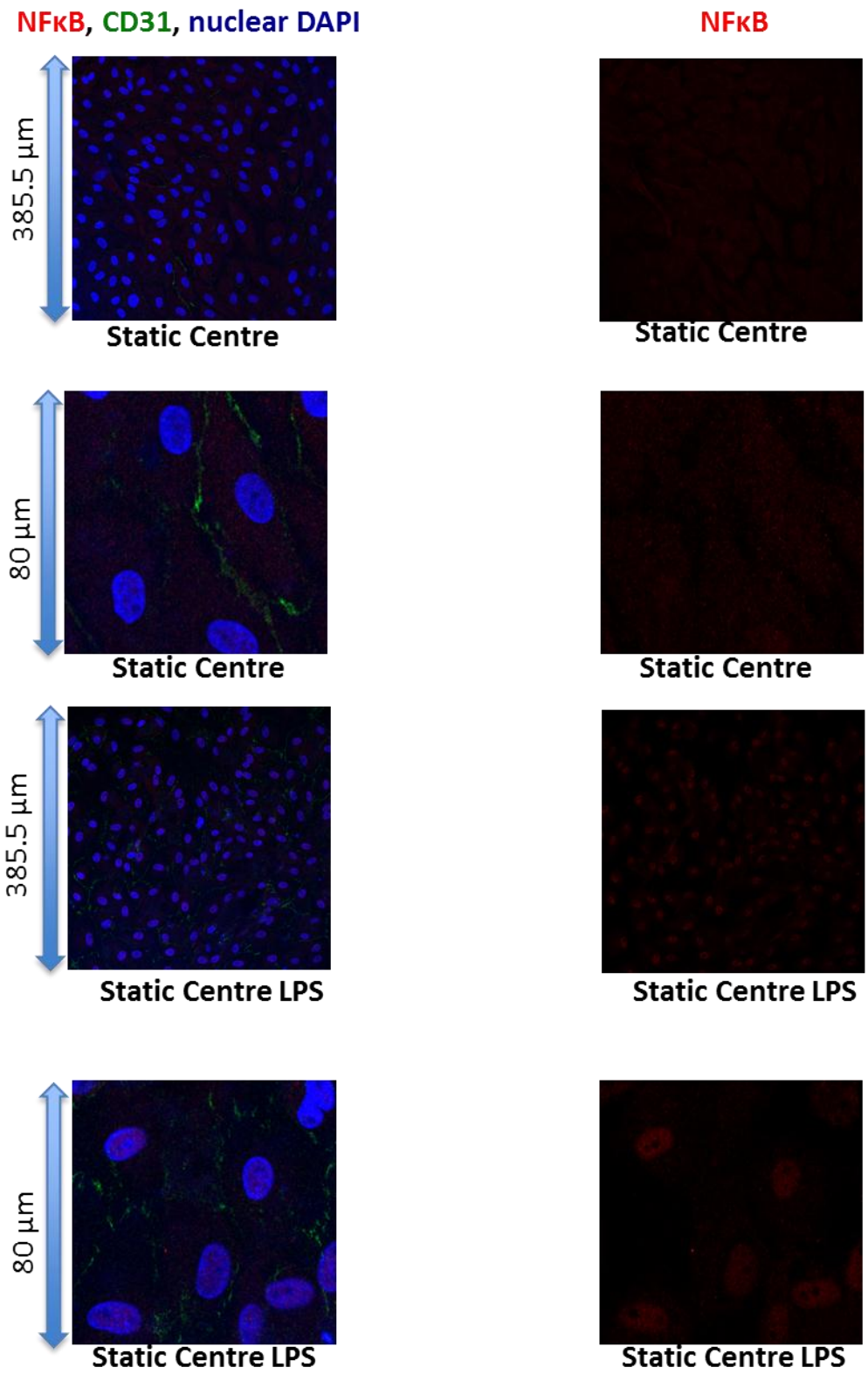

Figure 5.4 NFκB Immunoreactivity in PAEC after 7 days culture at the static centre of a Transwell ***(Legend continued on next page)***

Figure 5.4 NFκB Immunoreactivity in PAEC after 7 days culture at the static centre of a Transwell <u>(Legend continued from previous page)</u>

Images are representative of n=10-12 images gathered from 4 separate isolations/wells repeated with cells of 3 different animals. A full field 385.5 x 385.5µm image was taken of each cell area. An 80 X 80µm enlargement is shown below for clarity of intracellular localisation. Those on the left are composites formed of the CD31 and NFκB staining observed at the cell membrane focused view and nuclei staining observed at a nuclear focused view. These composites have been produced to aid the reader in identifying the region of the cell in which the NFκB is present. On the right NFκB staining alone at the cell membrane focus is shown.

In untreated cells NFκB was seen largely in the cytosol with clear voids in the pattern of staining where the nucleus occupies the cell. When cells were treated with LPS there was a clear translocation of NFκB into the nucleus. Voids can be seen showing that NFκB is not present in the nucleolus.

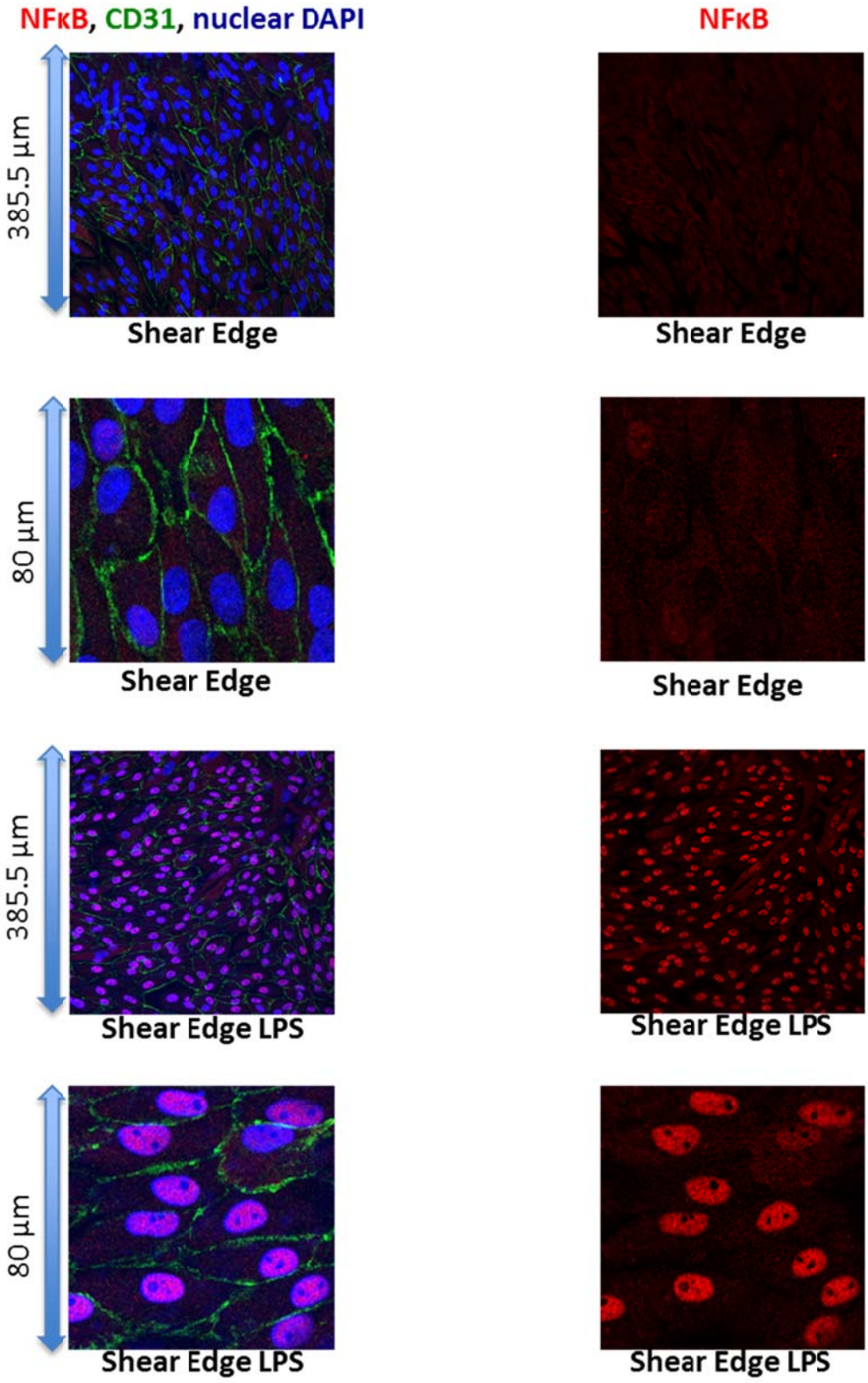

Figure 5.5 NFκB Immunoreactivity in PAEC after 7 days culture under shear stress at the edge of a Transwell™ ***(Legend continued on next page)***

Figure 5.5 NFκB Immunoreactivity in PAEC after 7 days culture under shear stress at the edge of a Transwell™ <u>(Legend continued from previous page)</u>

Images are representative of n=10-12 images gathered from 4 separate isolations/wells repeated with cells of 3 different animals. Those on the left are composites formed of the CD31 and NFκB staining observed at the cell membrane focused view and nuclei staining observed at a nuclear focused view. These composites have been produced to aid the reader in identifying the region of the cell in which the NFκB is present. On the right NFκB staining alone at the cell membrane focus is shown. Images were taken at regions 9.4mm from the centre of the Transwell™ where cells experienced a temporal gradient of directional shear. In untreated cells NFκB was seen largely in the cytosol with clear voids in the pattern of staining where the nucleus occupies the cell. When cells were treated with LPS there was a clear translocation of NFκB into the nucleus and an apparent increase in expression. Voids can be seen showing that NFκB is not present in the nucleolus. A full field 385.5 x 385.5µm image was taken of each cell area. An 80 X 80µm enlargement of a region of each image is shown below for clarity of intracellular localisation.

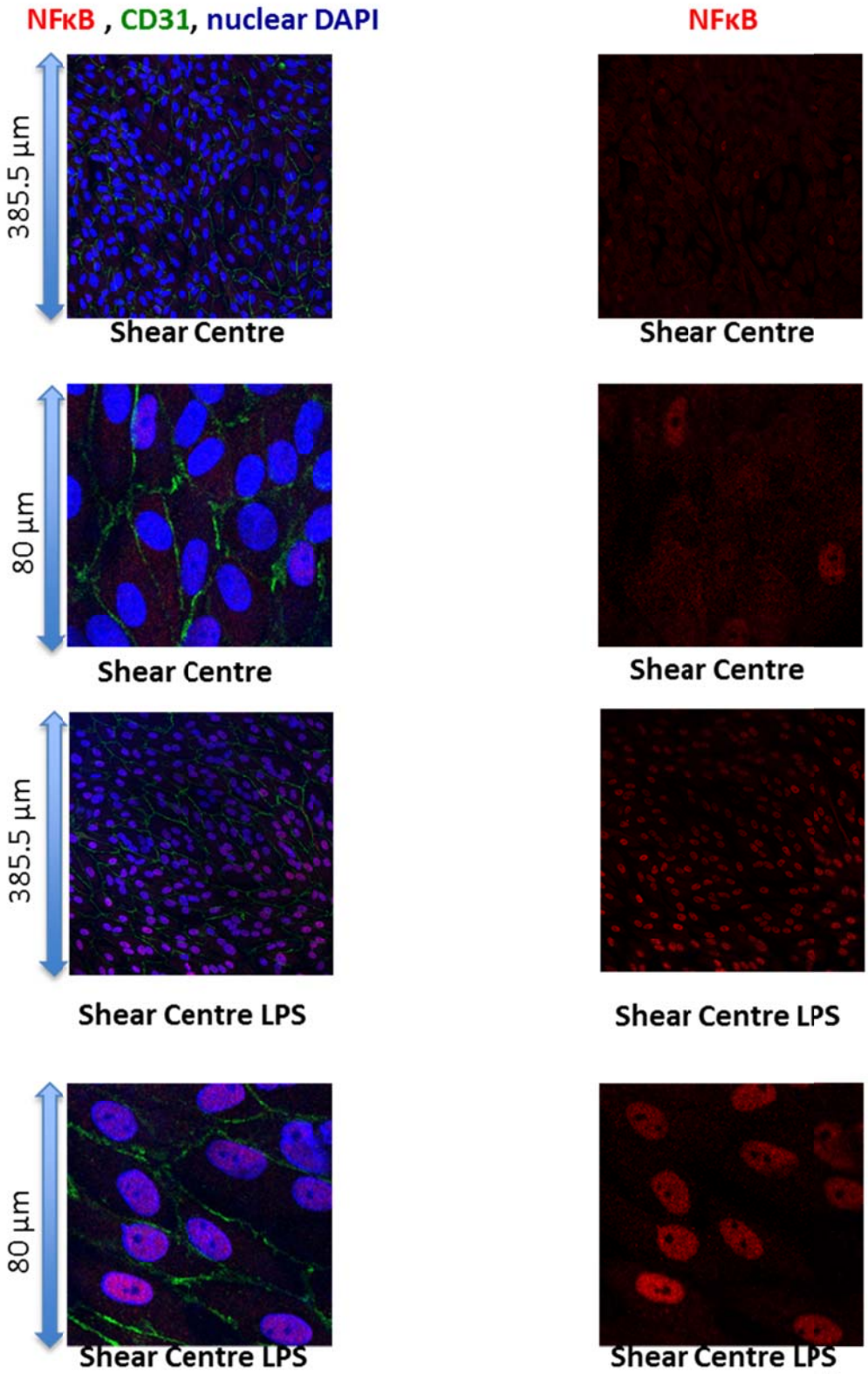

Figure 5.6 NFκB Immunoreactivity in PAEC after 7 days culture under shear stress at the centre of a Transwell™ ***(Legend continues on next page)***

Figure 5.6 NFκB Immunoreactivity in PAEC after 7 days culture under shear stress at the centre of a Transwell™ <u>(Legend continued from previous page)</u>

Images are representative of n=10-12 images n=12 images gathered from 4 separate isolations/wells repeated with cells of 3 different animals. Those on the left are composites formed of the CD31 and NFκB staining observed at the cell membrane focused view and nuclei staining observed at a nuclear focused view. These composites have been produced to aid the reader in identifying the region of the cell in which the NFκB is present. On the right NFκB staining alone at the cell membrane focus is shown. Images were taken at the centre of the Transwell™ where cells experienced consistently low shear of no preferred direction. In untreated cells NFκB was seen largely in the cytosol with clear voids in the pattern of staining where the nucleus occupies the cell. When cells were treated with LPS there was a clear translocation of NFκB into the nucleus and an apparent increase in expression. Voids can be seen showing that NFκB is not present in the nucleolus. A full field 385.5 x 385.5µm image was taken of each cell area. An 80 X 80µm enlargement of a region of each image is shown below for clarity of intracellular localisation.

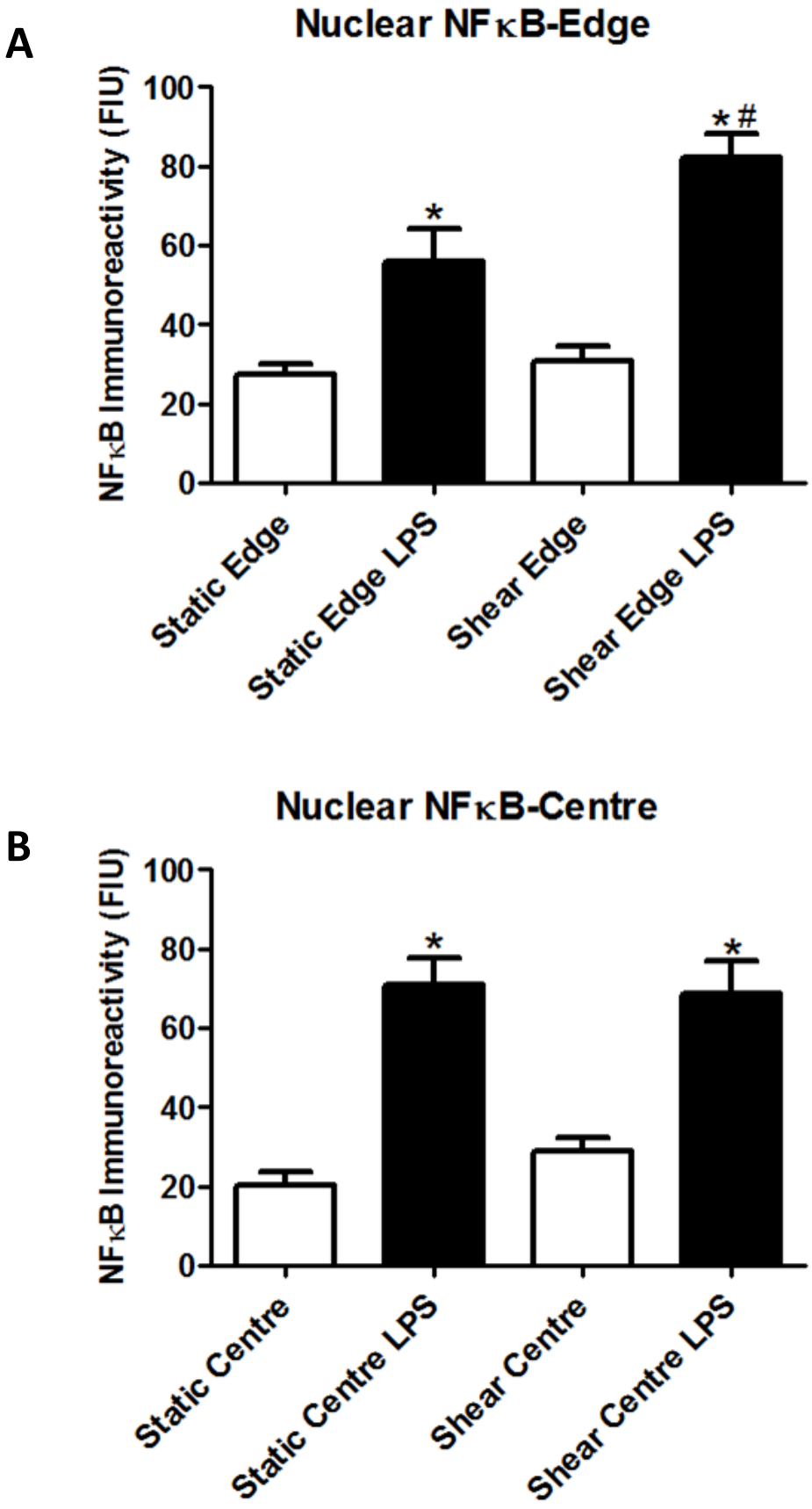

Figure 5.7 Graphical Representation of NFκB quantification at the PAEC nucleus (<u>Legend continued on next page</u>).

Figure 5.7 Graphical Representation of NFκB quantification at the PAEC nucleus <u>(Legend continued on next page).</u>

*NFκB immunoreactivity was quantified as mean fluorescence per pixel associated with each nucleus in 10-12 385.5 X 385.5µm regions of interest imaged of cells from across 4 wells/isolations using cells of 3 different animals. Nuclear NFκB immunoreactivity was averaged to produce a single number per image which is represented graphically. Data are presented as mean ±S.E.M and were analysed by one-way ANOVA followed by Bonferroni post-test. Where LPS treated cells displayed significantly (P=<0.05) greater amounts of NFκB than their untreated counterparts this is indicated by *. # indicates significantly greater NFκB than all other conditions represented.*

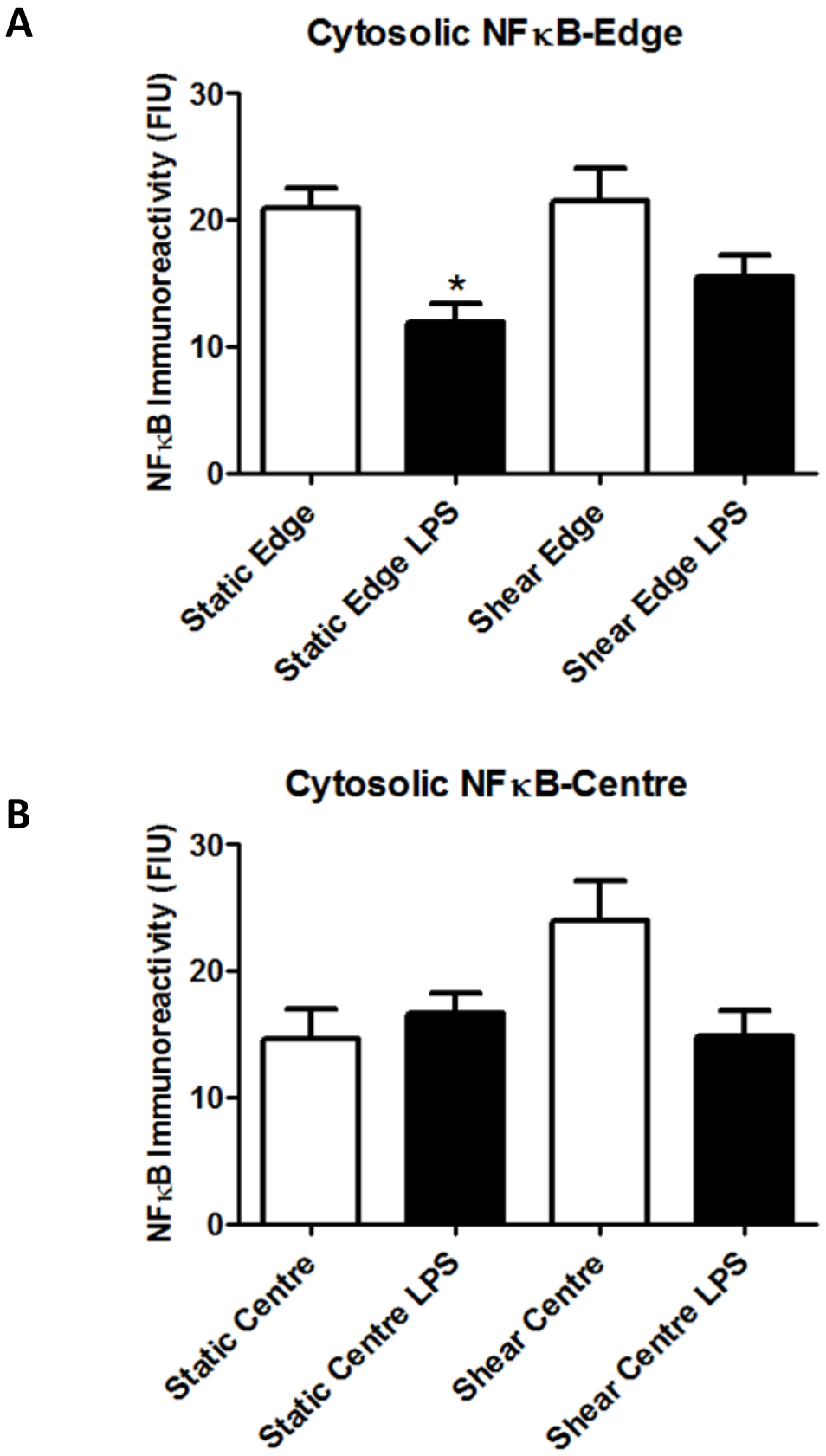

Figure 5.8 Graphical representation of NFκB immunoreactivity in the PAEC cytoplasm after 7 days of culture ***(Legend continued on next page).***

Figure 5.8 Graphical representation of NFκB immunoreactivity in the PAEC cytoplasm after 7 days of culture <u>(Legend continued from previous page).</u>

*NFκB immunoreactivity was quantified as mean fluorescence per pixel in the cytosolic regions of interest imaged of n=12 from 4 separate wells/isolations using cells of 3 separate animals. Data are presented as mean ±S.E.M and were analysed by one-way ANOVA followed by Bonferroni post-test. P=<0.05 was taken as significant and is shown by *.*

Summary

Experiments detailed in this chapter sought to identify the localisation of NFkB in endothelial cells under two different conditions of shear stress and compare this to NFkB levels in static cells. Additionally NFkB localisation changes in response to inflammatory stimulus and how this is influenced by shear stress was also addressed.

It was found that in the absence of LPS challenge NFkB localisation is predominantly cytoplasmic and that this is a trend seen regardless of shear stress conditions. It was only at the static edge that levels of cytosolic NFkB were significantly reduced as NFkB moved to the nucleus which may suggest that in static cells there may be less NFkB protein synthesis than in sheared cells.

The observation that NFκB is increasingly activated at the edge of the sheared well in some ways goes against what has been shown for 'aligned' cells exposed to directional shear stress in the greater curvature of the aortic arch. This is perhaps in keeping with the controversy around the levels of shear stress recorded for the aortic arch.

It has been shown in previous chapters that shear stress appears to be protective against LPS induced cell death, the increased response in activation of NFkB when stimulated with LPS may play a role in protection of the cells. It has been documented that NFkB regulated genes can be involved in prevention of apoptosis initiated by TNFα (Kucharczak *et al.*, 2003) which is one possible explanation.

Chapter 6

Understanding the relation between complex shear stress, endothelial cell mediator release and morphological response to shear

Rationale

Earlier chapters have described how endothelial cells demonstrate profound morphological changes when exposed to directional shear stress for several days. A critical question in the field is related to how shear stress affects endothelial cell hormone release. Often, endothelial cells at regions of the vasculature prone to atherosclerosis development are described as 'dysfunctional'. The classification of a dysfunctional endothelium normally extends to an inability to regulate contractility of the local vascular environment. As described in the Introduction, endothelial cells release a selection of very potent vasoactive hormones including but not limited to, the powerful vasodilators PGI_2 and NO and the potent vasoconstrictor ET-1. Some literature sources suggest that shear stress activates endothelial cells, causing the induction of inflammatory forms of vasoactive genes (e.g. COX-2 and NOSII). However, others suggest that culturing cells under static conditions results in differentiation of cells and loss of endothelial phenotype. The results of previous chapters suggest that the 6-well/orbital-shaker method of shear stress would be useful to investigate the impact of shear stress on endothelial cell hormones. Often endothelial mediator release is assessed only over a short time period of hours. The ability to assess release of such hormones over long time periods is a clear advantage of this method of shear stress administration; however it will not be possible to differentiate release between different cells of the well. For this reason this system was utilised to study how a temporal gradient of directional shear compared to continual, non-directional shear stress affects expression of key enzymes which regulate media release in the same well.

Declaration

N=4 images of PAEC stained with COX-1/2 after 7 days of shear stress were obtained as part of an MRes project I submitted to Imperial College in September 2009. Additional data sets are present in this thesis and a different form of analysis has been carried out. No figures or text has been reproduced from the MRes.

Methods

Treatments

Cells were cultured on 6-well Transwell plates as described in Chapter 2.

Drug treatments were prepared in vehicle of either DMSO or water before serial dilution was carried out in cell culture medium. Vehicle controls of the appropriate dilution of DMSO or water were prepared for comparison. Drugs were present in cell medium throughout the full duration of the experiment with fresh treatments prepared at each medium change.

Immunohistochemistry

Immunohistochemistry was performed using the antibodies described in Chapter 2.3. After staining Transwell™ filters were mounted onto glass slides and immediately imaged by confocal microscopy. Immunofluorescence was calculated for each region of the well having subtracted background fluorescence for the corresponding region

ELISA

ELISAs were carried out according to the manufactures instructions summarised in Chapter 2.7. Samples were frozen and thawed only once before assessment to avoid loss of analyte due to breakdown in the freeze thaw process.

Alignment Scoring

Scoring followed the criteria set out in Chapter 2.5.2 and was rated by 2 independent observers

Data and Statistics

All data was analysed using GraphPad Prism v5 and is reported as mean ±SEM.

Results

Expression of COX-1 and COX-2 in PAEC cultured under static versus shear stress conditions

Under control culture conditions endothelial cells express COX-1 (Caughey *et al.*, 2001; Mitchell *et al.*, 2006). However, some have suggested that COX-2 is the important isoform of the enzyme in endothelial cells (Yu *et al.*, 2012). It is suggested that the reason that cultured endothelial cells are found to express abundant levels of COX-1 but show low levels of COX-2 is that COX-2 is shear regulated and rapidly lost when cells are moved to static conditions. In order to investigate how COX expression may be regulated in cells under shear stress PAEC were used. As our group has previously shown for human cells (Mitchell *et al.*, 2006) COX-1 immunoreactivity was detected as a protein band of approximately 70KDa in PAEC homogenates (Figure 6.1). COX-2 immunoreactivity was absent in control cells, but detected as a band of 70KDa in cells treated for 24 hours with LPS (0.1µg/ml). In line with this, COX-1 immunoreactivity (shown in red) was abundantly expressed in PAEC cultured for 7 days under static or shear stress conditions (Figure 6.2) and can be seen to have a granular appearance throughout the cytosol. By contrast, COX-2 immunoreactivity was very sparsely expressed in PAEC cultured for 7 days under static or shear stress conditions and appears to be at levels only a little above that of non-specific background staining (Figure 6.3). When data were pooled from cells of 3 pigs, it was clear that neither COX-1 nor COX-2 immunoreactivity was increased by shear stress, either by a directional, temporal gradient of shear at the edge of the well or non-directional shear at the centre of the well (Figure 6.4). It is notable that COX-2 immunoreactivity was reduced in cells at the centre of the well exposed to non-directional shear compared to cells cultured under static conditions in the same region of control wells (Figure 6.4).

Others have shown that COX-2 is upregulated by shear stress at acute time points of 24 hours or less (Di Francesco *et al.*, 2009; Okahara *et al.*, 1998; Topper *et al.*, 1996). In order to investigate the possibility that shearing cells for 7 days was too long to see COX-2 induction, experiments were repeated where cells were sheared for only 24 hours. In these experiments, as for those performed for 7 days, COX-1 immunoreactivity was abundantly

expressed throughout the cell with only low levels of COX-2. In these experiments, as with those above, shear stress did not affect COX-1 or COX-2 immunoreactivity at either region of the well studied (Figures 6.5, 6.6 and 6.7).

In order to validate the model and to show that the system would be able to detect COX-2 protein if expressed, additional experiments were performed where cells were treated with LPS. LPS is known to induce COX-2 (Feng *et al.*, 1993), and was used as a positive control for cell extracts used in Western blots shown in Figure 6.1. Cells were cultured for 7 days in the presence or absence of 0.1µg LPS and COX-1 and COX-2 imaged at the edge and centre of sheared and static wells. In these experiments LPS did not induce detectable COX-2 in cells after 7 days culture at either region of the well under static or shear stress conditions (Figure 6.9, images of staining not shown). A cells ability to respond to LPS can become desensitised and tolerance to LPS-induced stimulation has been reported elsewhere (Lush *et al.*, 2000). In order to determine if this had happened in experiments protocols were repeated where cells were treated for 24 hours with or without LPS in wells that were either sheared or kept under static conditions. In these experiments, LPS induced clear COX-2 immunoreactivity in cells at both regions of the well cultured under either shear or static conditions. As others have reported (Parfenova *et al.*, 2001), COX-2 appeared as a bright ring of immunofluorescence in the nuclear envelope of treated cells (Figure 6.8).

Expression of COX-1 and COX-2 in human aortic endothelial cells cultured under static versus shear stress conditions

Our group have previously shown that where cultured under static culture conditions, human aortic endothelial cells express abundant COX-1 with very low levels of COX-2, unless cells are stimulated (Mitchell *et al.*, 2006). In order to translate findings in porcine cells to human equivalent cells experiments were repeated using human aortic endothelial cells (HAEC). As was seen with PAEC, HAEC expressed abundant COX-1 immunoreactivity in cells at the centre or edge of the well cultured under static or shear stress conditions. Again, COX-2 immunoreactivity was sparse (Figure 6.10A). Shearing cells for 7 days did not result in increased COX-2, if anything, there was a tendency for COX-2 levels to be reduced in

sheared cells compared to cells cultured under static conditions. When data from cells of 3 donors were pooled, no effect of shear was seen on COX-1 or COX-2 expression (Figure 6.10C). Again to ensure that my system allowed for COX-2 detection, I treated some cells with LPS (0.1μg/ml) for 24 hours. In HAEC LPS induced significant increases in COX-2 in cells cultured under shear stress conditions.

Experiments described above show that COX-1 is abundant in porcine and human aortic endothelial cells and that the level of shear stress present in the orbital shaker is not associated with increased expression of either COX-1 or COX-2. This is true for cells exposed to directional or non-directional shear stress.

Expression of NOSIII in endothelial cells under static versus shear stress conditions

NOSIII is another important endothelial cell enzyme which has been suggested to decline in cells in culture (Yoon *et al.*, 2010). PAEC expressed NOSIII as a single protein band of approximately 150 KDa (Figure 6.11). Shear stress has been suggested to increase NOSIII and to cause its translocation from the Golgi apparatus to the caveoli. Since the Golgi is part of the nuclear membrane and in order not to under estimate expression or translocation to this region, I imaged endothelial cell NOSIII at the nuclear (guided by blue DAPI staining) and cytosolic (guided by green CD31 staining) planes. NOSIII immunoreactivity (shown in red) was abundantly detected in PAEC in both the nuclear and cytosolic planes (Figure 6.12). Interestingly, when viewed at the cytosolic plane, unlike COX enzymes, NOSIII immunoreactivity was increased by 7 days of shear stress in PAEC exposed to both directional and non-directional shear at the edge and centre of the wells respectively (Figure 6.13). Increases in NOSIII expression viewed at the nuclear plane were only obvious in cells exposed to non-directional shear stress (Figures 6.12-6.13). In order to confirm whether findings were translated to humans experiments were repeated with a human cell type. In this case, the human cells used were derived from blood outgrowth progenitors and were

isolated and cultured as previously described (Ingram *et al.*, 2004). NOSIII expression was similarly increased in regions of shear in these cells in a pilot study (Figures 6.14-6.15).

Release of endothelial cell hormones

Experiments above suggest that whilst shear stress does not affect COX enzyme expression, it does critically regulate NOSIII expression. In line with this, release of the COX product PGI_2 measured through surrogate 6-keto$PGF_{1\alpha}$ was not increased by shear stress over the duration of the 7 day study (Figure 6.18). If NOSIII protein expression data translated to activity, I would expect that NO release from NOSIII may be increased in my cells after shear. Unfortunately, there are two main problems in measuring NO activity and tracking it individual cells. Firstly, levels of NO released by these cells (expected to be in the sub nM range) are undetectable by the commonly used Greiss assay and probe based methods have not always proved reliable. Secondly, measuring simple mediator release would not allow me to correlate relative levels in different regions of the well. NO activity can be bio-assayed by measuring the intracellular second messenger, cGMP. I had hoped to overcome both of these obstacles by using a FRET reporter for cGMP, which had been successfully transfected into HEK cells by other members of my group. However, attempts to transfect primary endothelial cells with this reporter resulted in cell death. Optimizing this in primary endothelial cells was unfortunately beyond the scope of this thesis. However, it was possible to detect two other key endothelial cell hormones released from cells. IL-8, which is an important immune modulator released by endothelial cells, and ET-1, which is a potent vasoconstrictor were both readily detectable in conditioned media from my PAECs. IL-8 release tended to decline over the course of 7 days, this was not affected by shear stress (Figure 6.19). ET-1 release (Figure 6.20), on the other hand, profiled similarly to PGI_2 release, and was detected at relatively high levels for the duration of the 7 day protocol. Again, ET-1 release was not affected by shear stress.

Effect of vasoactive hormones released by endothelial cells on cell alignment after shear stress.

In order to investigate any role vasoactive hormones may play in endothelial cell alignment during shear I performed experiments where cells were treated with inhibitors of the COX

pathway (Diclofenac, 100µM), the NOS pathway (L-NAME, 100µM), ET-1 receptor signalling (ETA antagonist, BQ123 0.01µM; ETB receptor antagonist, BQ788 0.01µM). As expected, cells treated with Diclofenac had reduced levels of PGI_2 release. This was not affected by shear stress. For other inhibitors, neither prostacyclin ET-1 nor IL-8 release was notably affected at any of the time points studied. As was seen in experiments described in Chapter 3, shear stress caused clear alignment of PAEC at the edge of sheared wells, where cells are exposed to directional shear stress. Alignment was not mediated by products of the COX, NOS or ET-1 pathways (Figure 6.21). Similarly, inhibition of NOS, COX or ET-1 pathways did not significantly induce alignment (Figure 6.21).

Figures

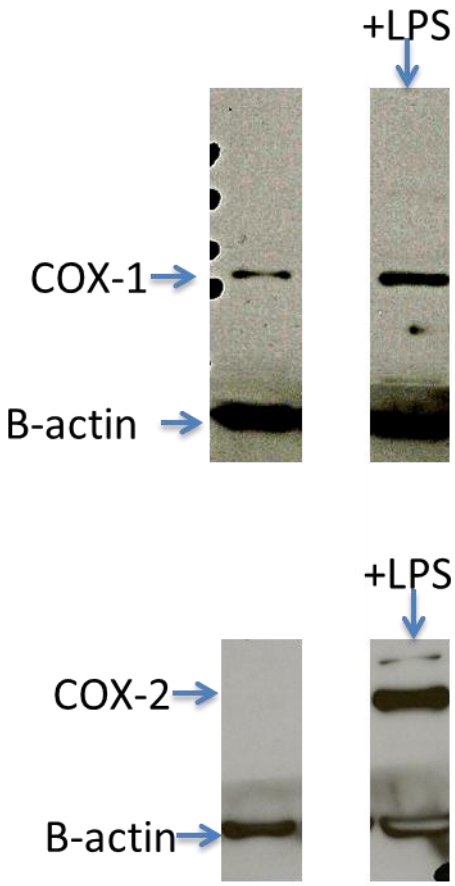

Figure 6.1. Western blots showing COX-1 and COX-2 expression in PAEC

Western blot of COX-1 (upper panel) and COX-2 (lower panel) in porcine aortic endothelial cells cultured under static conditions. Indicated lanes show cells after treatment with 0.1µg/ml LPS for 24 hours. COX-1 and COX-2 appear as a band around 70KDa. COX-2 is only present after treatment with LPS. β-actin was used as a protein loading control.

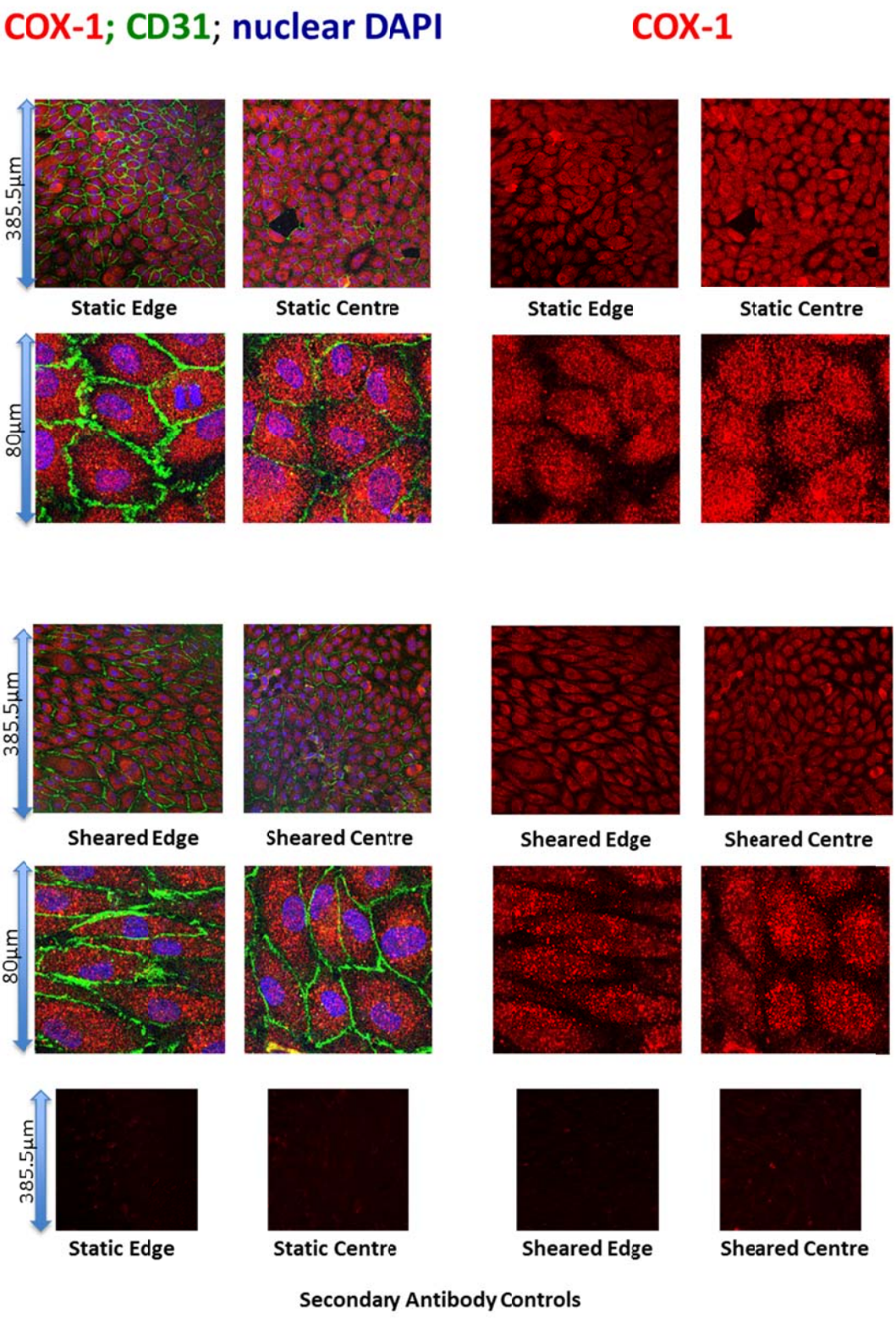

Figure 6.2. COX-1 expression in static and sheared PAEC after 7 days of culture under static and shear stress conditions ***(Legend continued on next page)******.***

Figure 6.2. COX-1 expression in static and sheared PAEC after 7 days of culture under static and shear stress conditions <u>(Legend continued from previous page).</u>

Images representative of n=10-12 images obtained at the edge (9.4mm from the centre of the Transwell™) or either side of the centre point. Full field 385.5 x 385.5µm images are shown and below 80 x 80µm enlargements of the same image to aid the reader in assessing cell localisation of COX-1. Control wells to which no primary anti-COX-1 antibody was added are shown for reference.

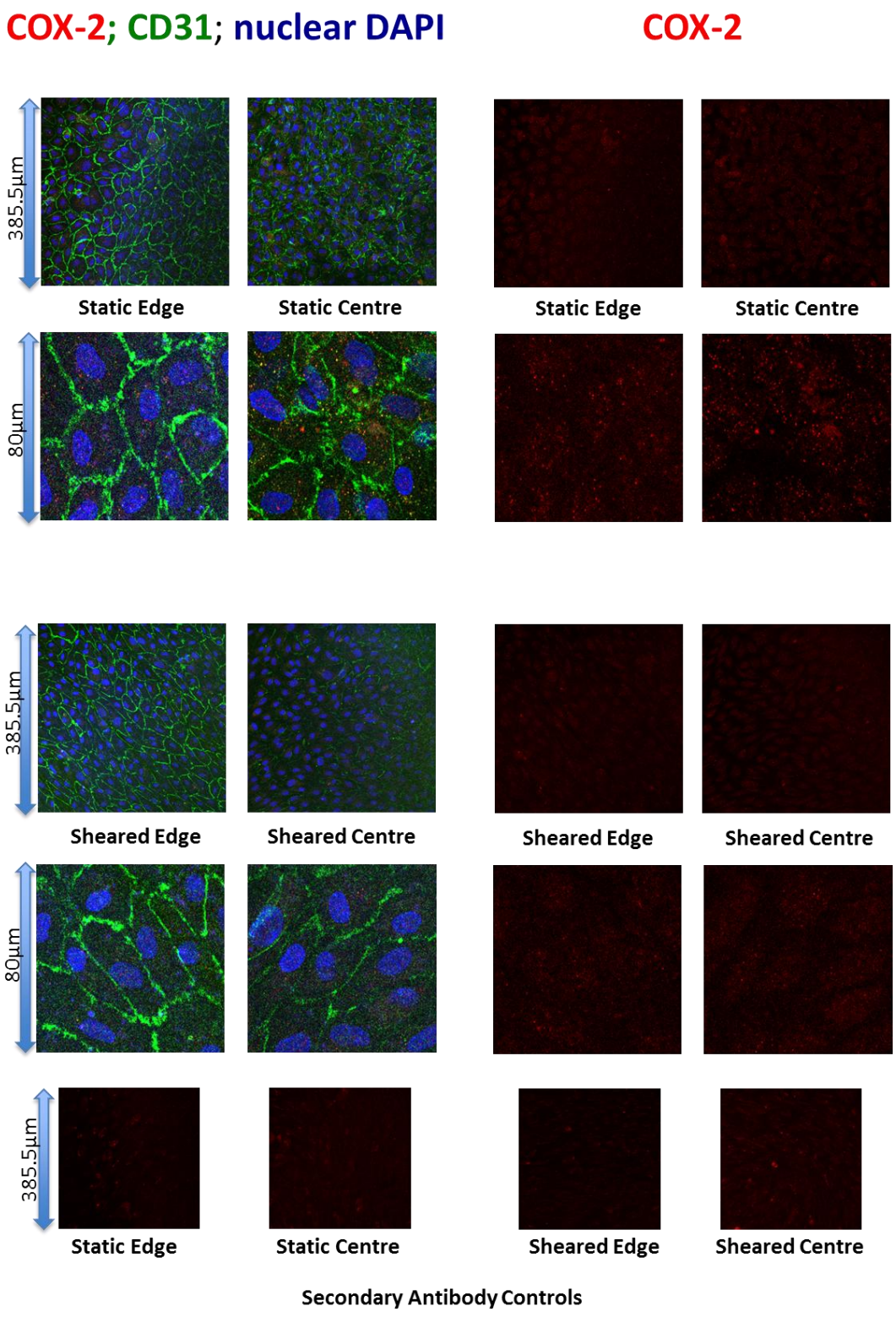

Figure 6.3. COX-2 expression in static and sheared PAEC after 7 days of culture under static and shear stress conditions ***(Legend continued on next page).***

Figure 6.3. COX-2 expression in static and sheared PAEC after 7 days of culture under static and shear stress conditions <u>(Legend continued from previous page).</u>

Images representative of n=10-12 images obtained at the edge (9.4mm from the centre of the Transwell™) or either side of the centre point. Full field 385.5 x 385.5µm images are shown and below 80 x 80µm enlargements of regions of the same image to aid the reader in assessing cell localisation of COX-2. Control wells to which no primary anti-COX-2 antibody was added are shown for reference.

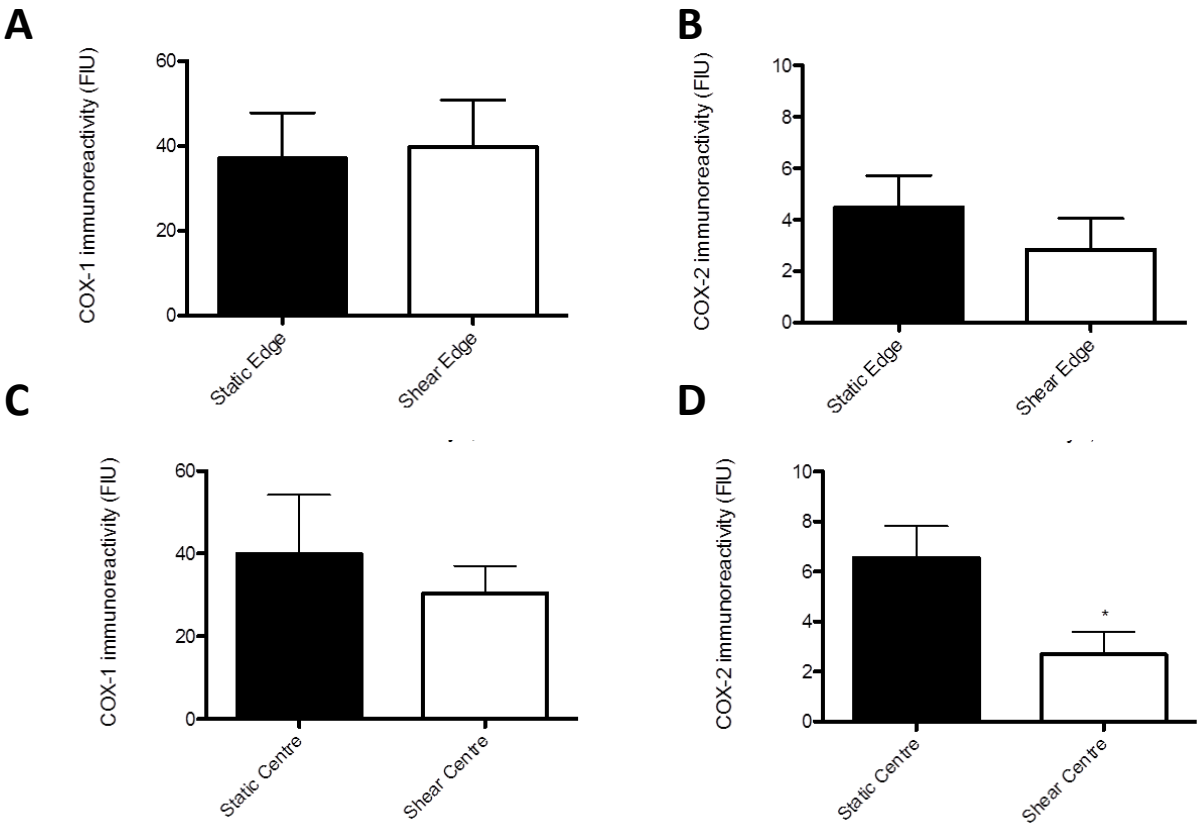

Figure 6.4 Quantification of COX-1 and COX-2 expression in static and sheared PAEC exposed to directional (edge) and non-directional (centre) shear stress for <u>7 days</u>.

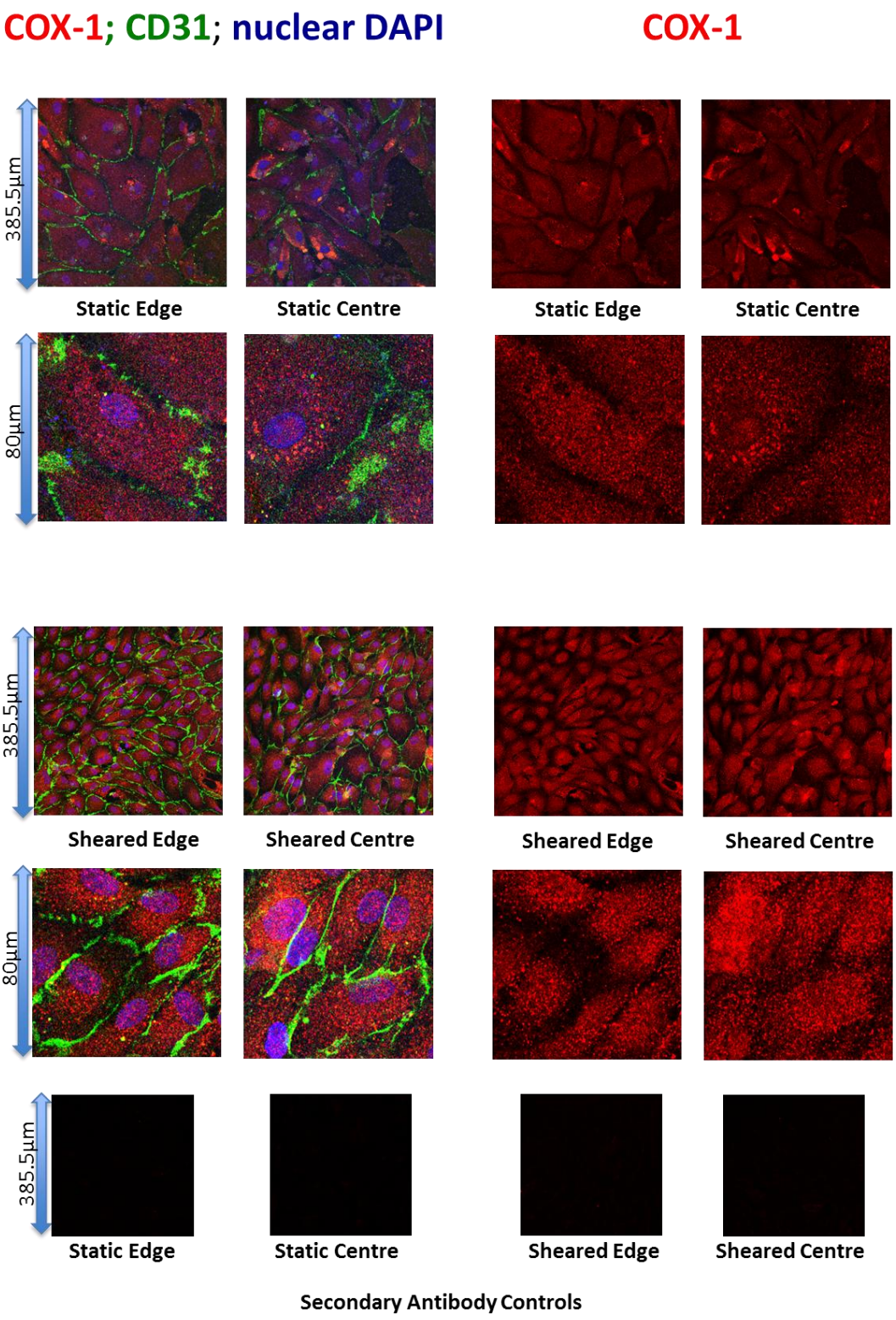

Figure 6.5 COX-1 expression in static and sheared PAEC after 24 hours of culture <u>(Legend continued on next page).</u>

Figure 6.5 COX-1 expression in static and sheared PAEC after 24 hours of culture <u>(Legend continued from previous page).</u>

Images representative of n=10-12 images obtained at the edge (9.4mm from the centre of the Transwell™) or either side of the centre point. Full field 385.5 x 385.5µm images are shown and below 80 x 80µm enlargements of regions of the same image to aid the reader in assessing cell localisation of COX-1. Control wells to which no primary anti-COX-1 antibody was added are shown for reference.

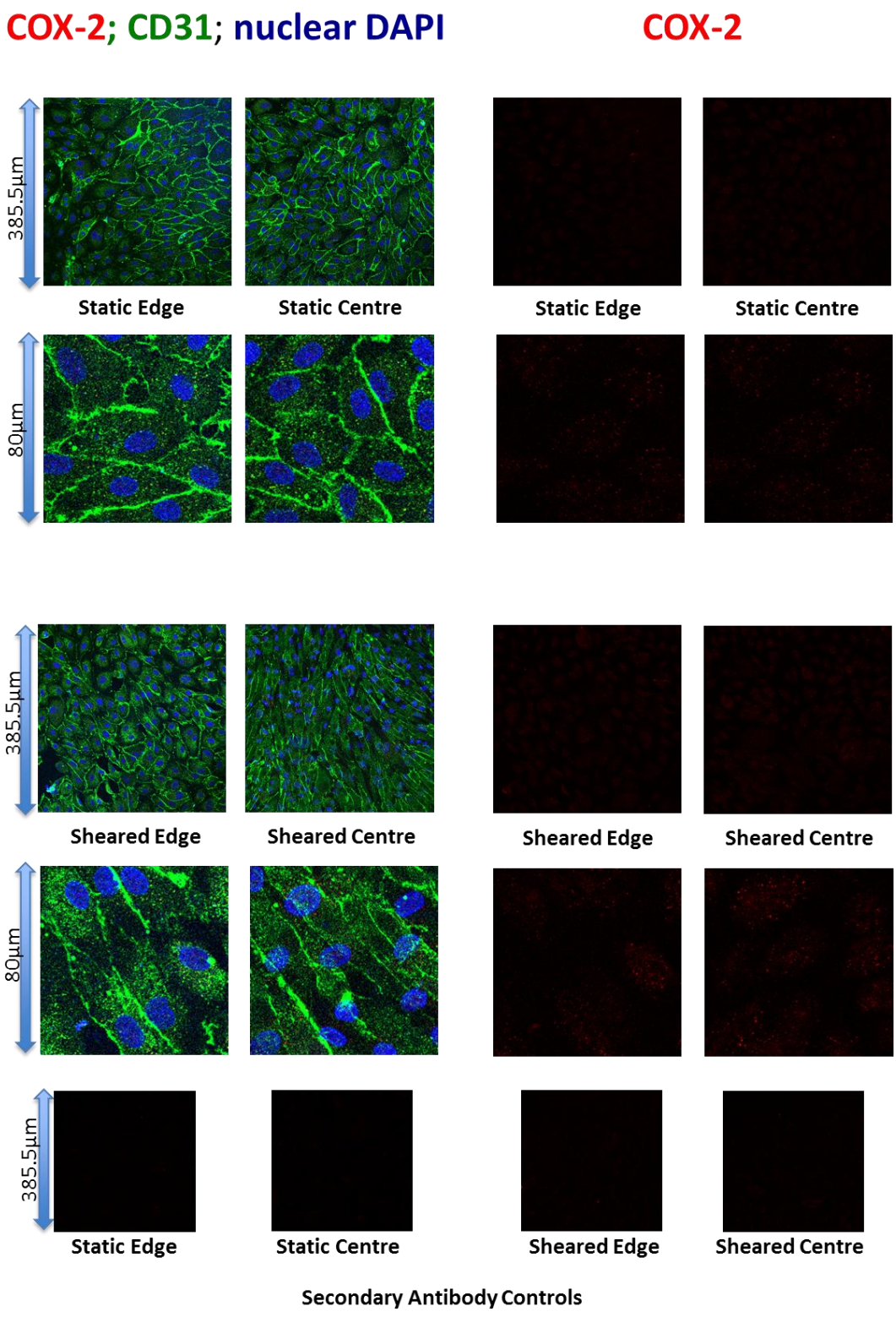

Figure 6.6. COX-2 expression in static and sheared PAEC after 24 hours of culture under static and shear stress conditions <u>(Legend continued on next page).</u>

Figure 6.6. COX-2 expression in static and sheared PAEC after 24 hours of culture <u>(Legend continued from previous page)</u>.

Images representative of n=10-12 images obtained at the edge (9.4mm from the centre of the Transwell™) or either side of the centre point. Full field 385.5 x 385.5µm images are shown and below 80 x 80µm enlargements of regions of the same image to aid the reader in assessing cell localisation of COX-2. Control wells to which no primary anti-COX-2 antibody was added are shown for reference.

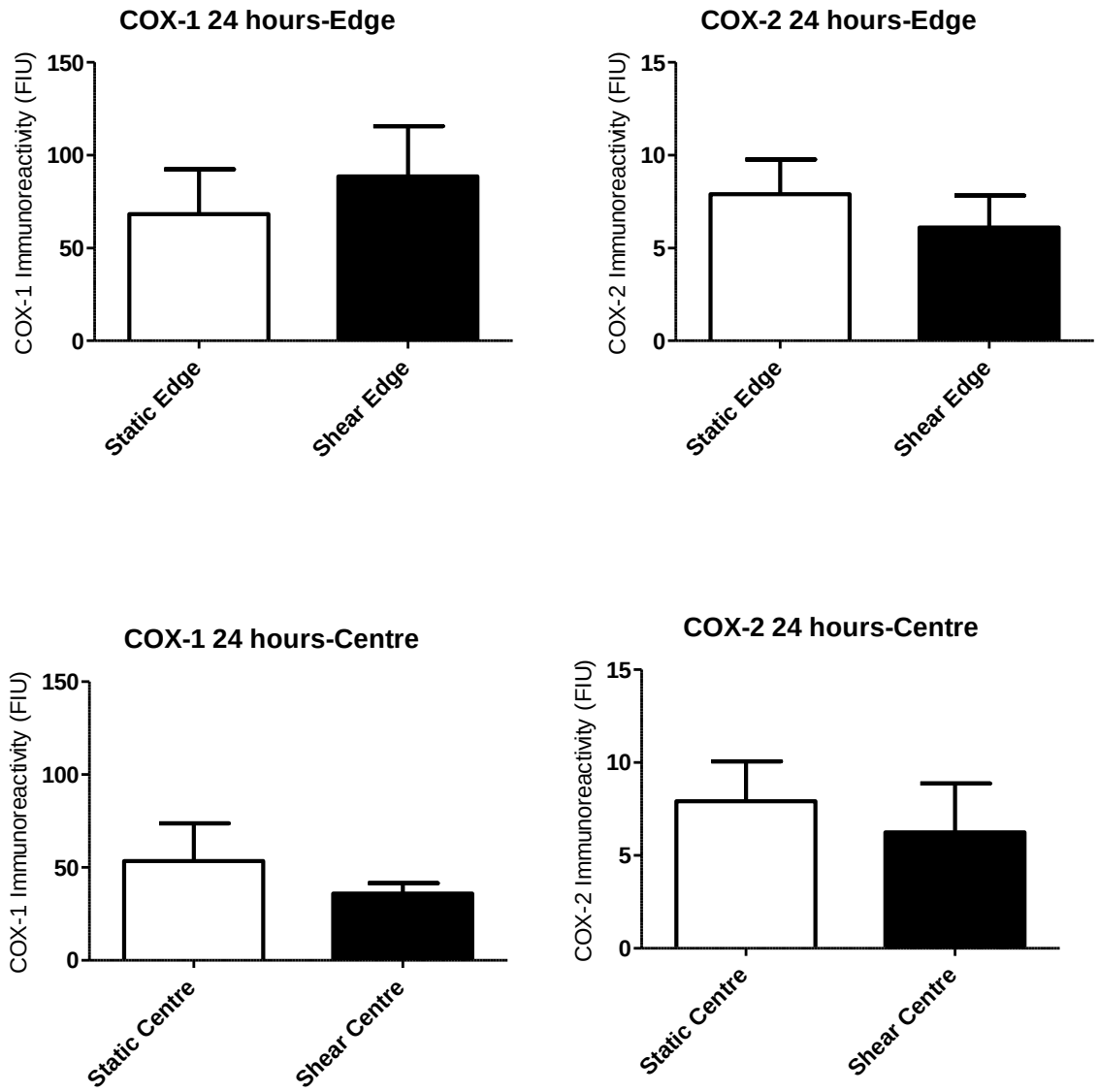

Figure 6.7 Quantification of COX-1 and COX-2 immunoreactivity in static and sheared PAEC exposed to directional (edge) and non-directional (centre) shear stress for <u>24 hours.</u>

*COX immunoreactivity was quantified as mean fluorescence per pixel with background non-specific staining subtracted. N=5-6 from 3 separate wells each using a different cell isolation. Data are presented as mean ±S.E.M and were analysed using Student's t-test P=<0.05 was taken as significant and is shown by *.*

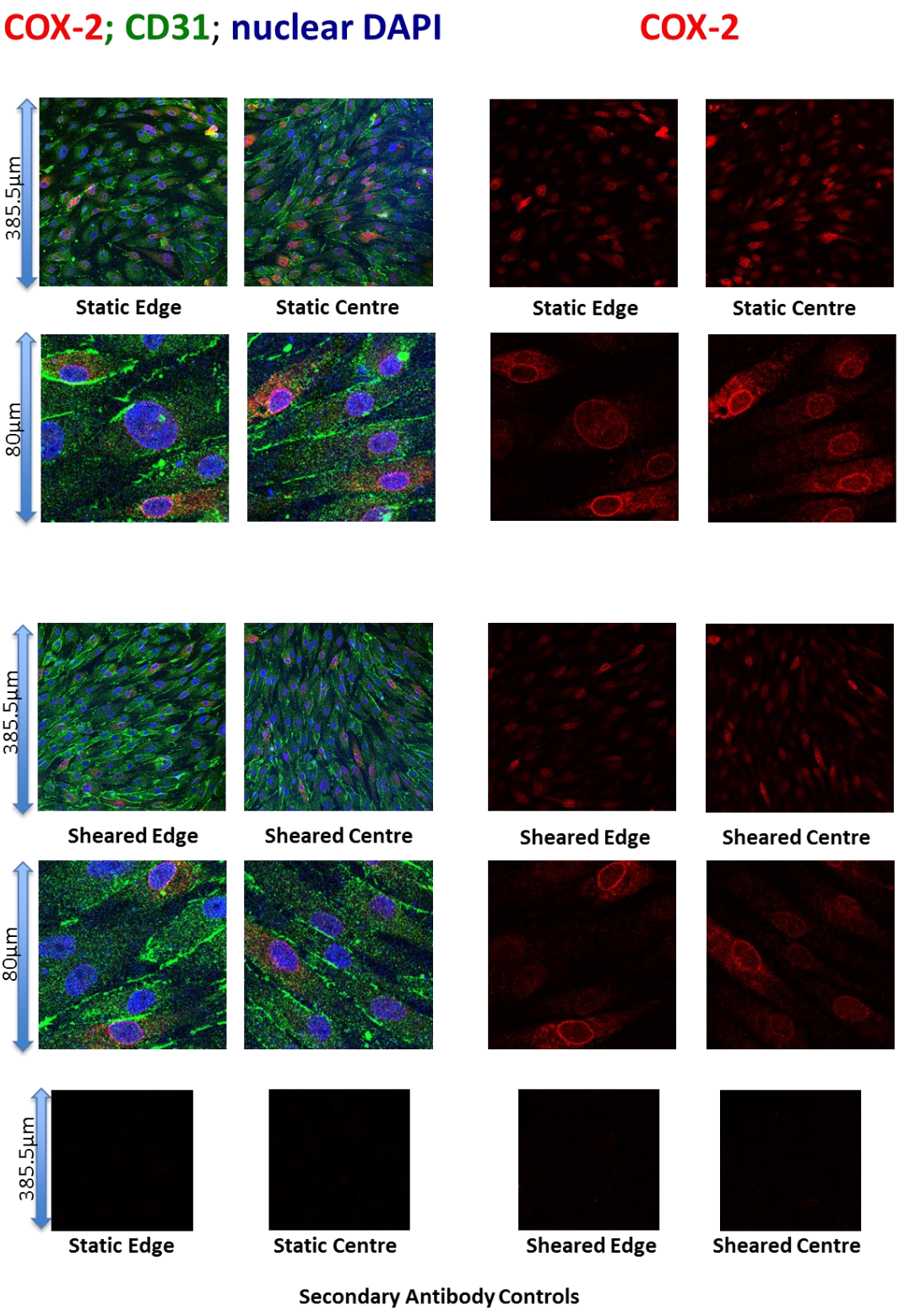

Figure 6.8. COX-2 expression in static and sheared PAEC after 24 hours of culture with 0.1µg LPS ***(Legend continued on next page)***

Figure 6.8. COX-2 expression in static and sheared PAEC after 24 hours of culture with 0.1 µg LPS <u>(Legend continued from previous page).</u>

Images representative of n=10-12 images obtained at the edge (9.4mm from the centre of the Transwell™) or either side of the centre point. Full field 385.5 x 385.5µm images are shown and below 80 x 80µm enlargements of sections of the same image to aid the reader in assessing cell localisation of COX-2. Control wells to which no primary anti-COX-2 antibody was added are shown for reference.

LPS treatment clearly induced expression of COX-2 which can be seen primarily as a red ring in the nuclear envelope.

A

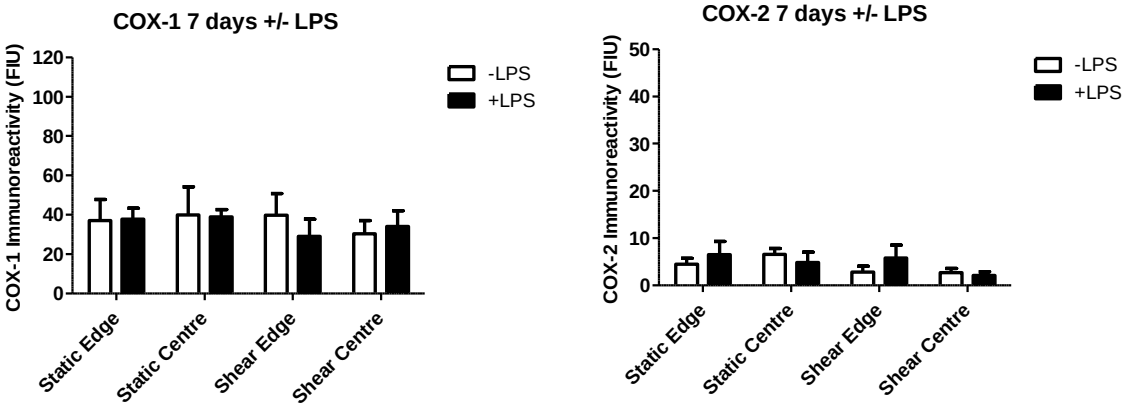

B

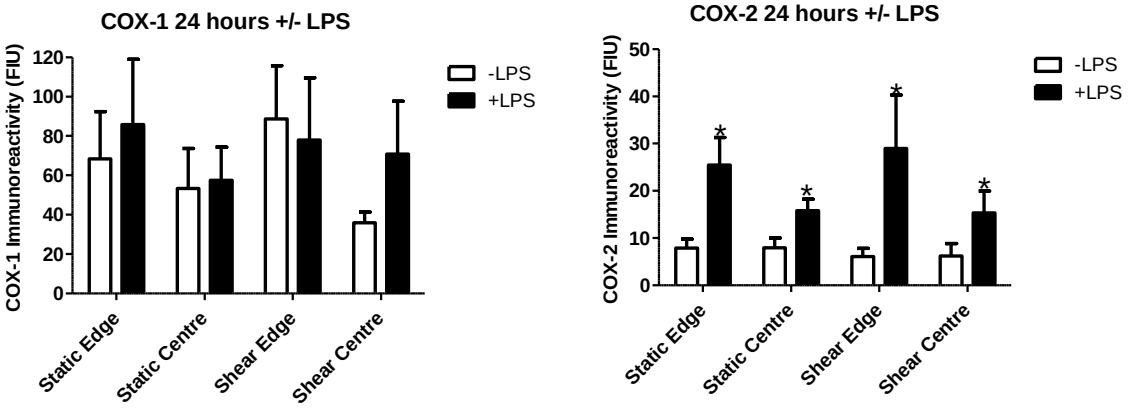

Figure 6.9 COX immunoreactivity in PAEC under static or shear stress conditions in the presence or absence of LPS

A. COX-1 and COX-2 immunoreactivity after 7 days culture under either static or shear stress conditions. LPS treated cells had 0.1µg E.coli LPS added to their medium for the duration of the 7 days.

B. COX-1 and COX-2 immunoreactivity after 24 hours culture under either static or shear stress conditions. LPS treated cells had 0.1µg E.coli LPS added to their medium for the full 24 hours. Data were pooled from 11-12 images obtained from cells of 3 pigs with two images taken of each preparation and 2 preparations per animal.

*Data are presented as mean ±SEM and were analysed by paired 2-tailed t-test. P=<0.05 was deemed significant and is indicated by *.*

A

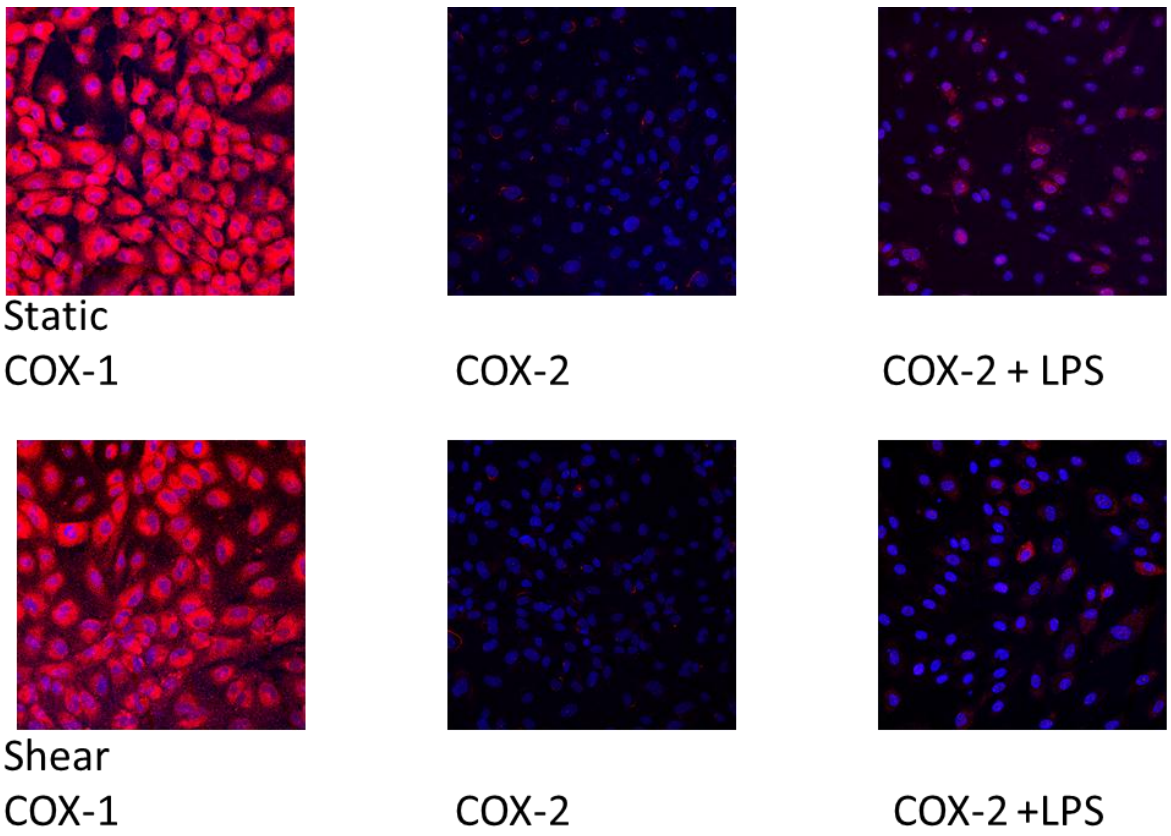

B

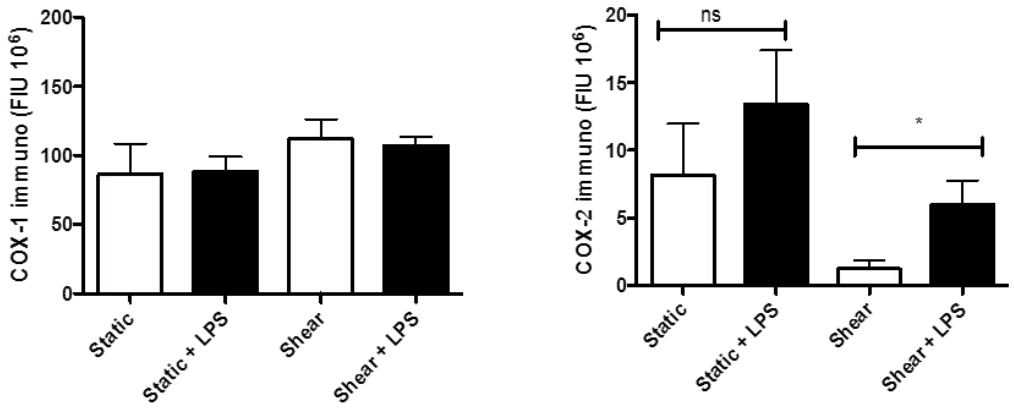

Figure 6.10 COX Immunoreactivity in HAEC in the presence or absence of LPS after 7 days culture under static or shear stress conditions ***(Legend continues on next page)***

HAEC were cultured for 7 days under either static or shear stress conditions. 0.1µg/ml E.coli LPS was added for the final 24 hours of the experiment in some cases to induce COX-2.

Figure 6.10 COX Immunoreactivity in HAEC in the presence or absence of LPS after 7 days culture under static or shear stress conditions (<u>Legend continued from previous page)</u>

A. Representative 385.5 x 385.5µM images of HAEC COX immunoreactivity. Cells were stained with DAPI (blue) to indicate nuclei. COX immunoreactivity is shown in red. Data reproduced from (Kirkby et al., 2012).

*B. Data is presented as mean ±SEM for 12 values obtained from cells of 3 human donors. 2 images were taken on either side of 2 wells of cells per donor. Data were analysed by One-way ANOVA. P=<0.05 was taken as significant and is indicated by *.*

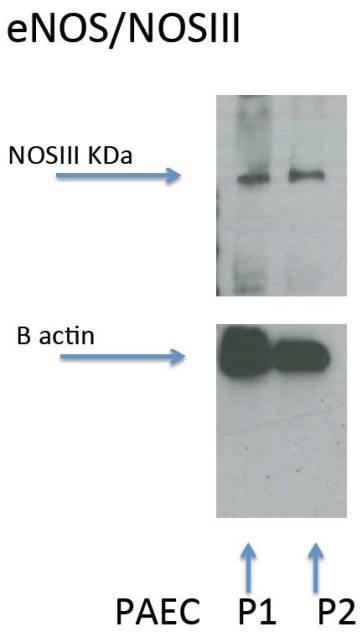

Figure 6.11 NOS III western blot

Western blot of NOSIII (eNOS) (upper panel) and loading control B actin (lower panel) in porcine aortic endothelial cells (PAEC) cultured under static conditions and extracted after two consecutive passages (P1 and P2) NOSIII appears as a band around 135 KDa.

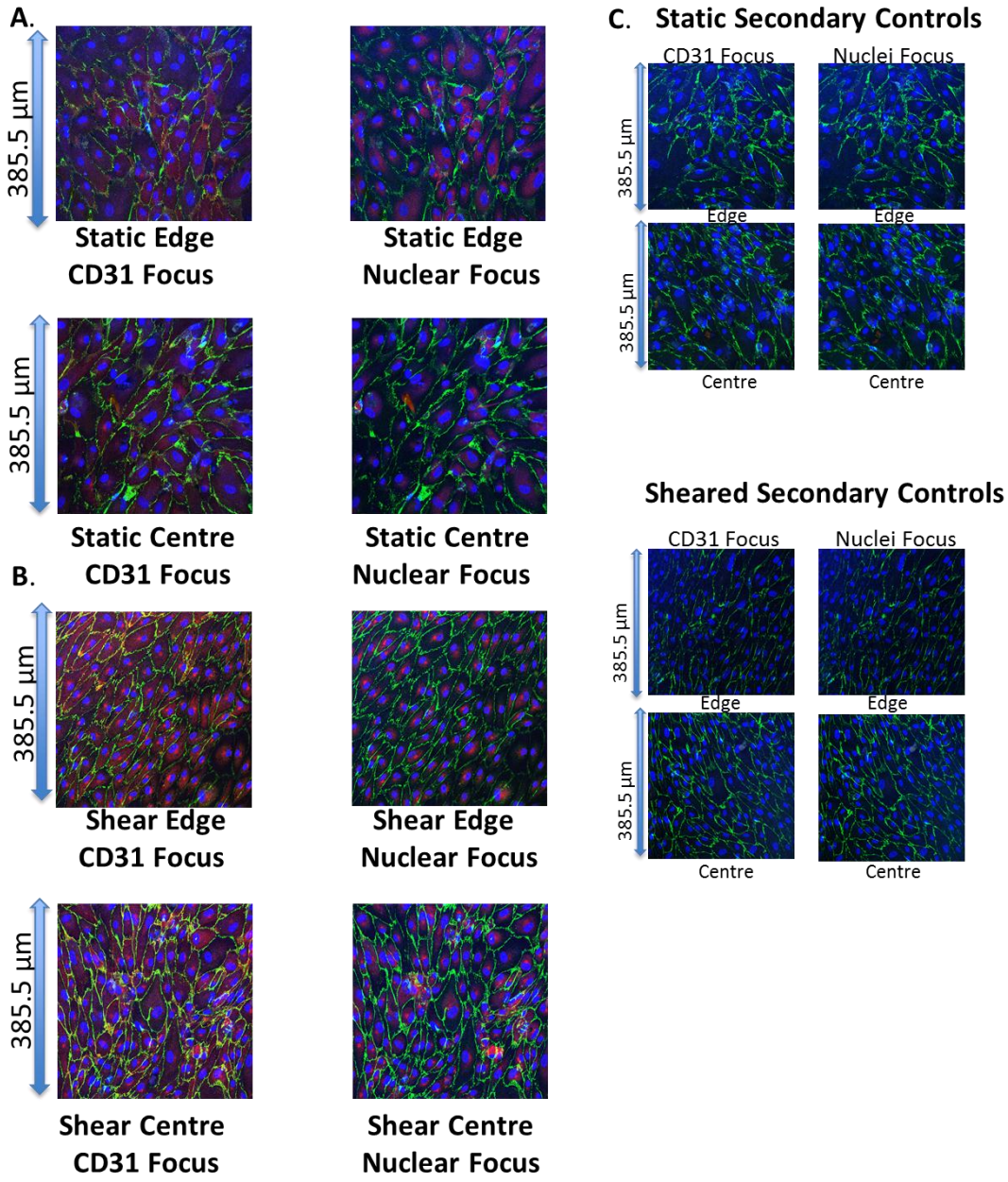

Figure 6.12 NOS III staining in PAEC after 7 days of culture

Representative images of NOSIII expression in static ***(A)*** *and sheared endothelial cells exposed to directional (edge) and non-directional (centre) shear stress* ***(B)*** *for 7 days. Images are representative of n=4 from 2 animals. Images were taken at two focal planes where either nuclei or CD31 were in focus. To highlight localisation of NOS III images shown here are a composite of the NOSIII staining from the plane of focus stated, the CD31 staining from the CD31 plane of focus and the nuclear staining from the nuclear plane of focus.*

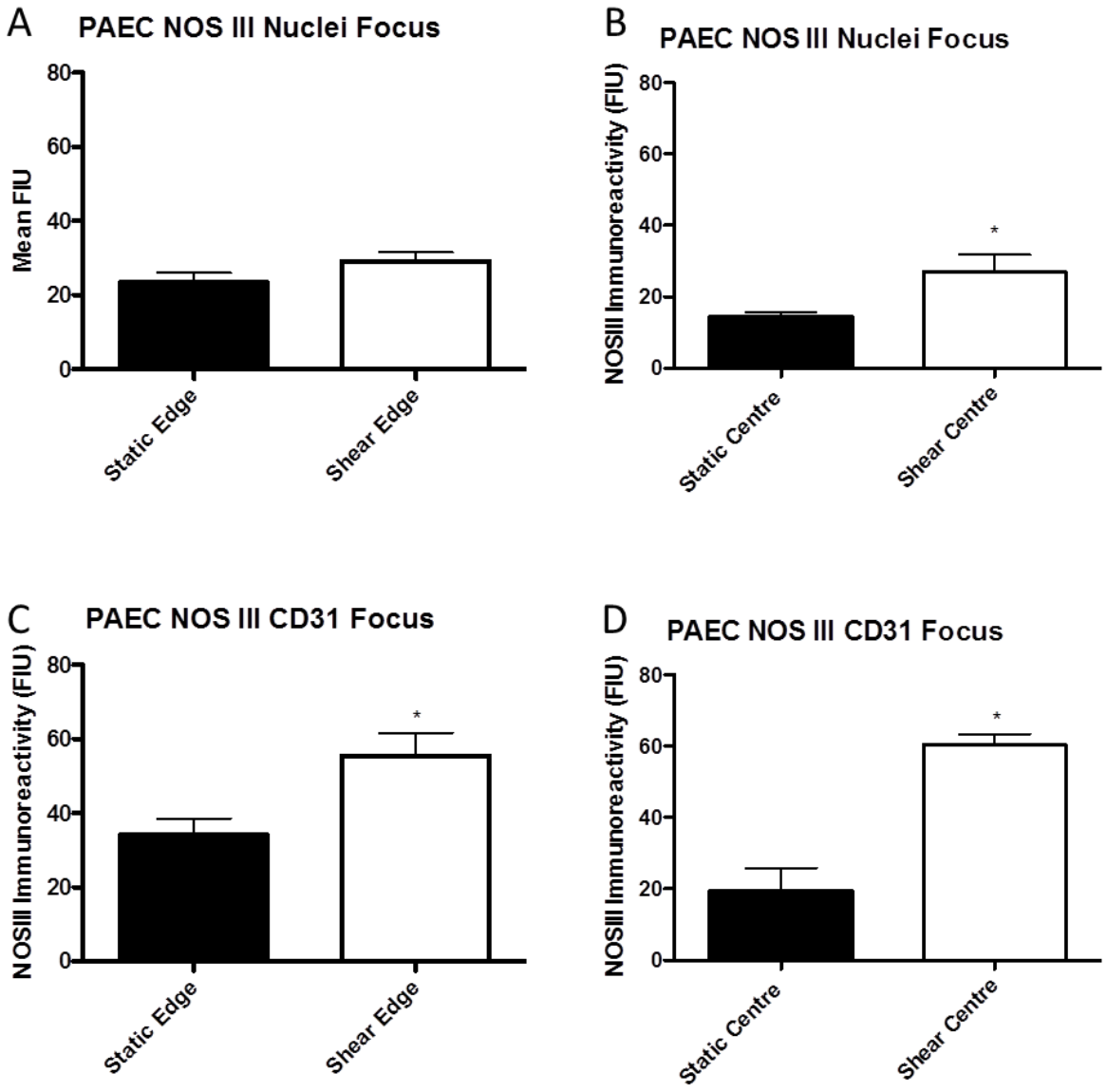

Figure 6.13 Quantification of NOSIII expression in static and sheared PAEC exposed to directional (edge) and non-directional (center) shear stress for <u>7 days</u>.

*Images were taken at two focal planes where either nuclei (A,B) or CD31 were in focus (C,D). Data are representative of n=4 images from cells of 2 animals. Data were analysed by Students T-test. * indicates statistical significance (p=<0.05)*

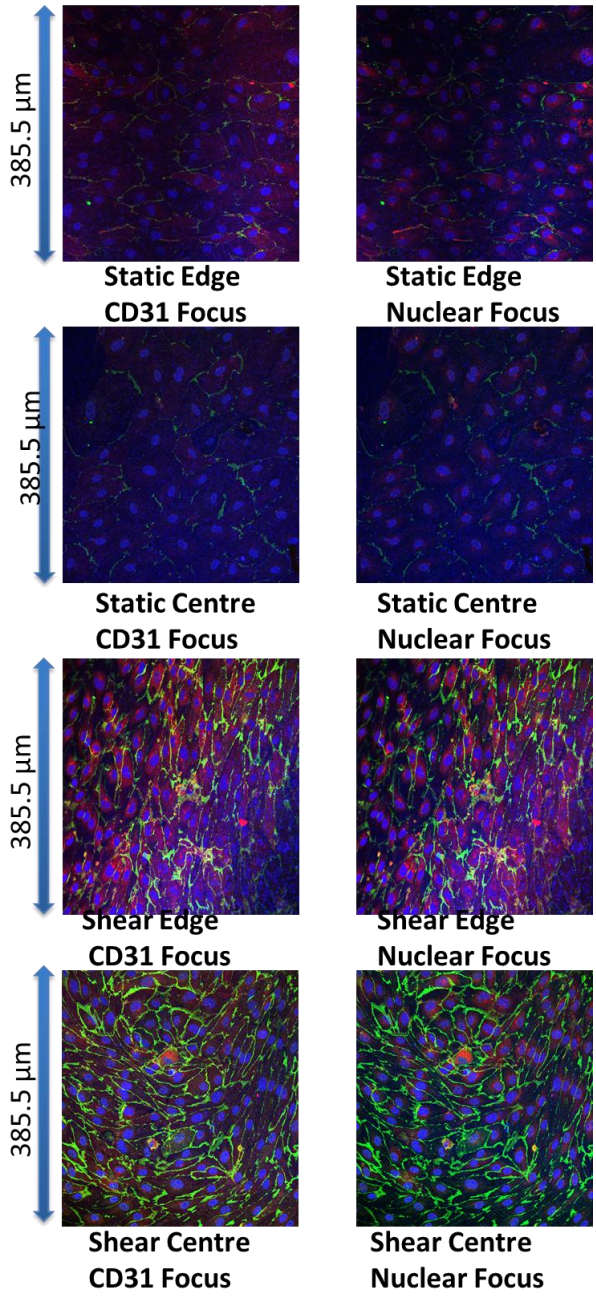

Figure 6.14 NOS III staining in BOEC after 7 days of culture

Representative images of NOSIII expression in static ***(A)*** *and sheared endothelial cells exposed to directional (edge) and non-directional (centre) shear stress* ***(B)*** *for 5 days. Images are representative of n=4 from 2 wells of a single donor sample. Images were taken at two focal planes where either nuclei or CD31 were in focus. To highlight localisation of NOS III images shown here are a composite of the NOSIII staining from the plane of focus stated, the CD31 staining from the CD31 plane of focus and the nuclear staining from the nuclear plane of focus.*

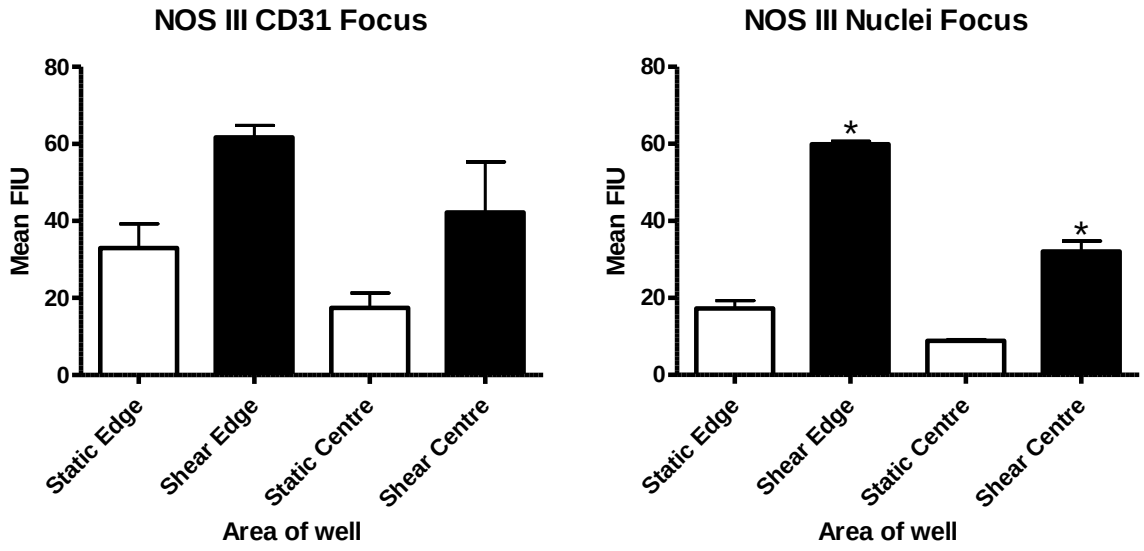

Figure 6.15 Quantification of NOSIII expression in static and sheared BOEC exposed to directional (edge) and non-directional (center) shear stress for 5 days.

*Images were taken at two focal planes where either nuclei (A, B) or CD31 were in focus (C, D). Data are representative of n=4 images from cells of a single donor. Data were analysed by Students T-test. * indicates statistical significance (p=<0.05)*

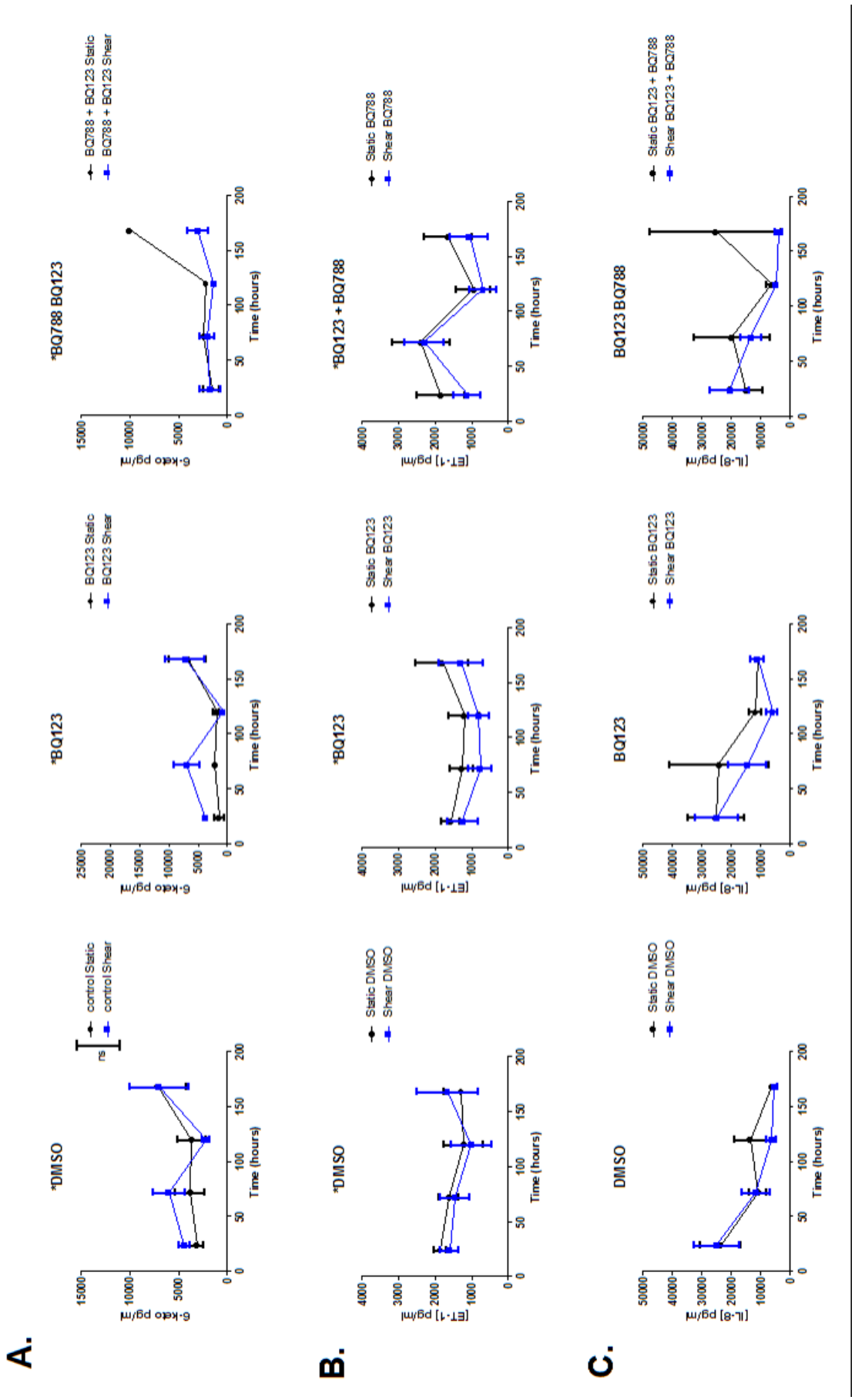

Figure 6.16: Variation in release of vascular mediators in PAEC over a 7 day period in the presence of DMSO soluble drugs (<u>Legend continues on next page</u>)

Figure 6.16: Variation in activity of vascular mediators in PAEC over a 7 day period in the presence of DMSO soluble drugs <u>(Legend continued from previous page)</u>

PAEC were cultured over 7 days with drugs known to influence the production of the hormones/cytokines prostacyclin, ET-1 and IL-8. Media samples were taken upon media changes every second day and analysed by ELISA. Due to the unstable nature of prostacyclin it was measured by the surrogate marker 6-ketoPGF$_{1\alpha}$. Drugs BQ123 an ET-1α receptor antagonist and BQ788 an ET-1β receptor antagonist were reconstituted in DMSO are compared against a DMSO vehicle control. Student's t-test revealed no significant difference in mediator activity regardless of whether cells were grown under static or shear stress conditions. Data are n=3 from 3 animals.

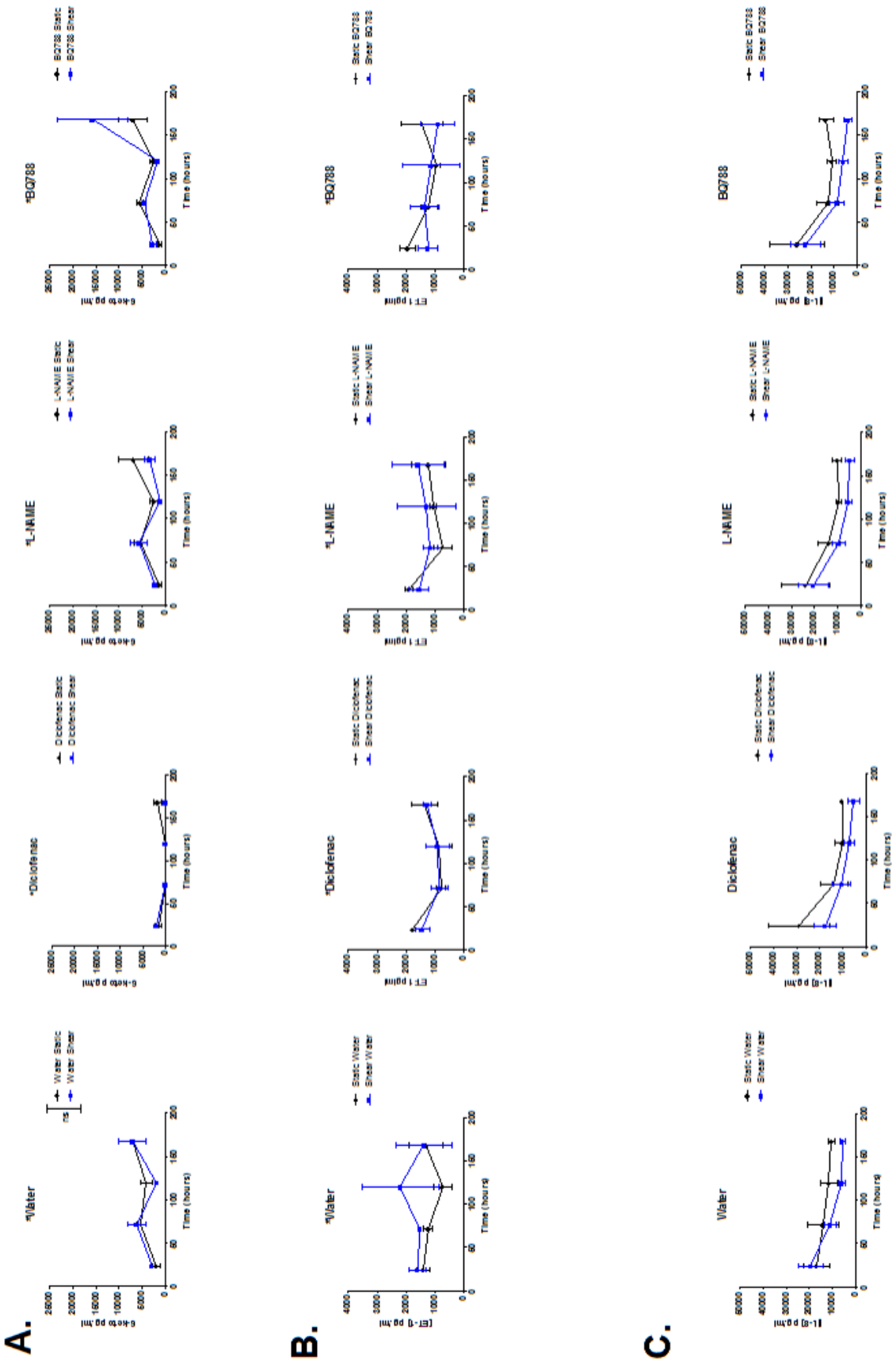

Figure 6.17 Variation in release of vascular mediators in PAEC over a 7 day period in the presence of water soluble drugs ***(Legend continues on next page)***

Figure 6.17 Variation in release of vascular mediators in PAEC over a 7 day period in the presence of water soluble drugs <u>(Legend continued from previous page)</u>

PAEC were cultured over 7 days with drugs known to influence the production of the hormones/cytokines prostacyclin, ET-1 and IL-8. Media samples were taken upon media changes every second day and analysed by ELISA. Due to the unstable nature of prostacyclin it was measured by the surrogate marker 6-ketoPGF$_{1\alpha}$. Drugs diclofenac, an NSAID, L-NAME an NO inhibitor and BQ788 an ET-1ϐ receptor antagonist were reconstituted in water and are compared against a water vehicle control. Data are n=3 from 3 animals. Student's t-test revealed no significant difference in mediator release regardless of whether cells were grown under static or shear stress conditions.

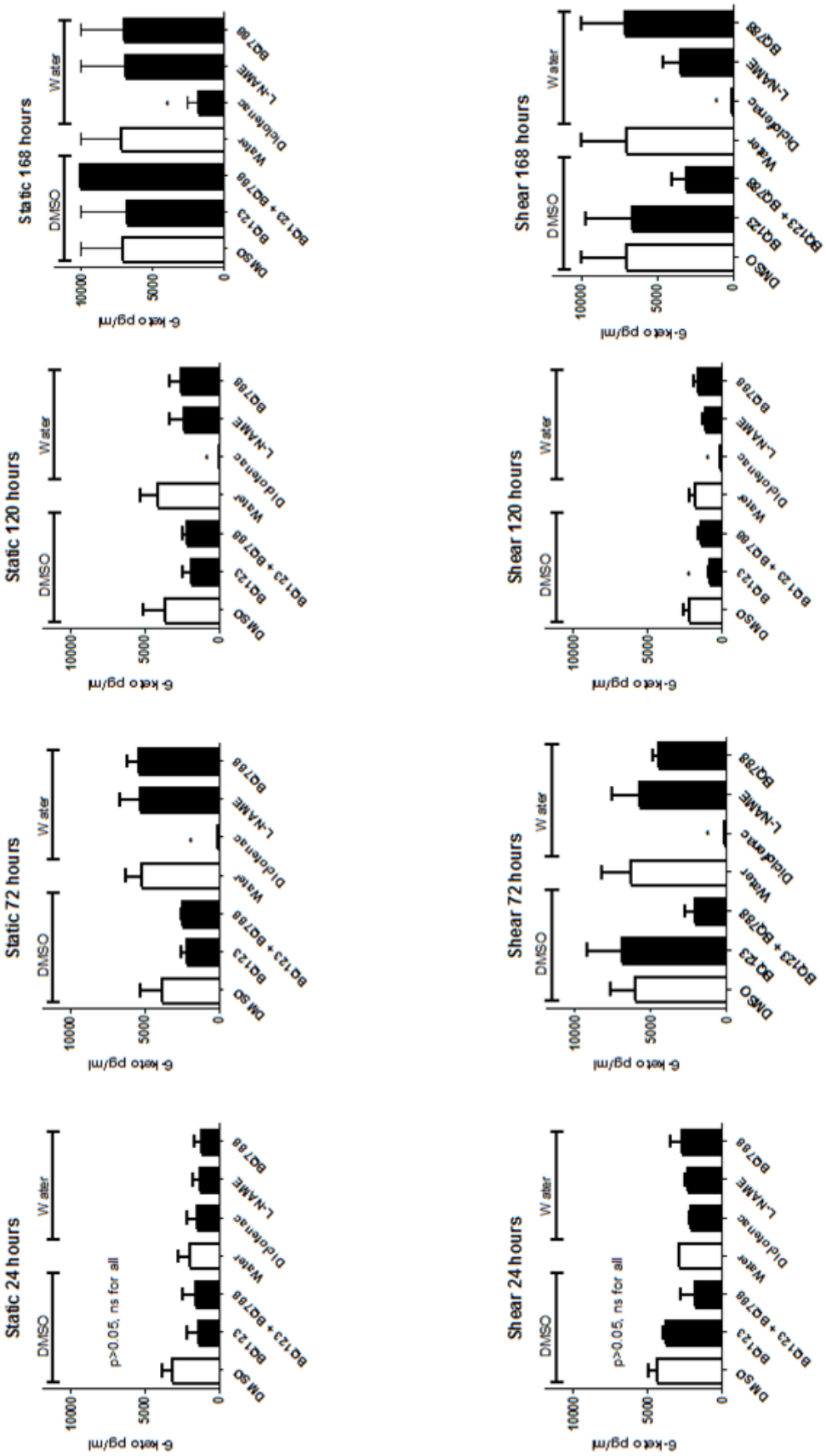

Figure 6.18 PAEC 6-ketoPGF1α release over 7 days in response to multiple drug treatments

Figure 6.18 PAEC 6-ketoPGF1α release over 7 days in response to multiple drug treatments <u>(Legend continued from previous page)</u>

6-ketoPGF1α was measured as a stable surrogate of prostacyclin release in response to multiple DMSO or water soluble drugs over a 7 day time period. ONE-way ANOVA followed by bonferroni post-test showed that only diclofenac significantly reduced prostacyclin release (p=<0.05). Shear stress did not appear to influence prostacyclin release. N=3 from 3 animals.

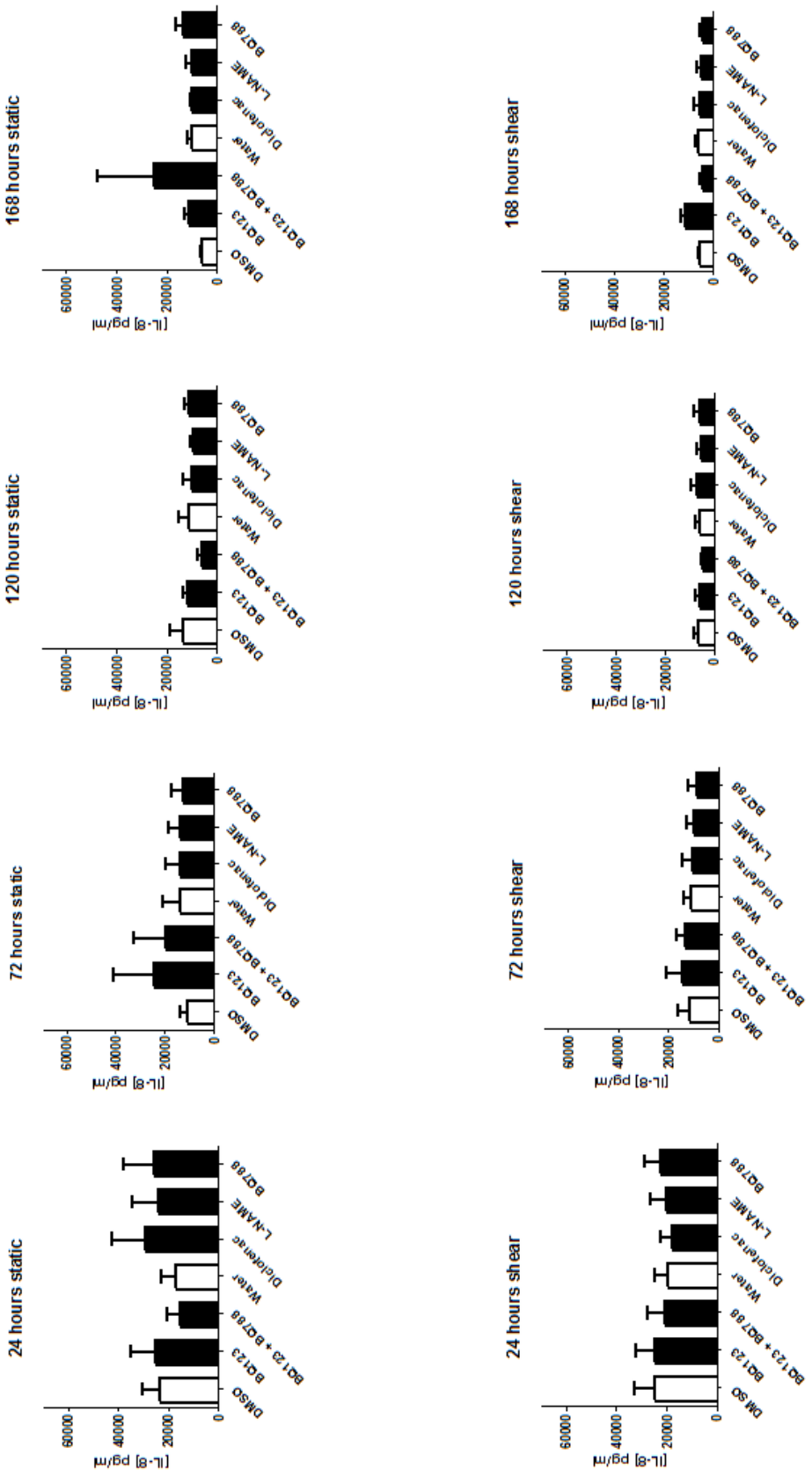

Figure 6.19 PAEC IL-8 release over 7 days in response to multiple drug treatments (<u>Legend continues on next page)</u>

Figure 6.19 PAEC IL-8 release over 7 days in response to multiple drug treatments <u>(Legend continued from previous page)</u>

PAEC release of the inflammatory cytokine IL-8 was measured in response to treatment with multiple drugs known to influence vascular function. None of these drugs was found to have influence on IL-8 release. Shear stress also had no bearing on IL-8 release.

N=3 from 3 animals. Data were analysed by one-way ANOVA followed by Bonferroni post-test.

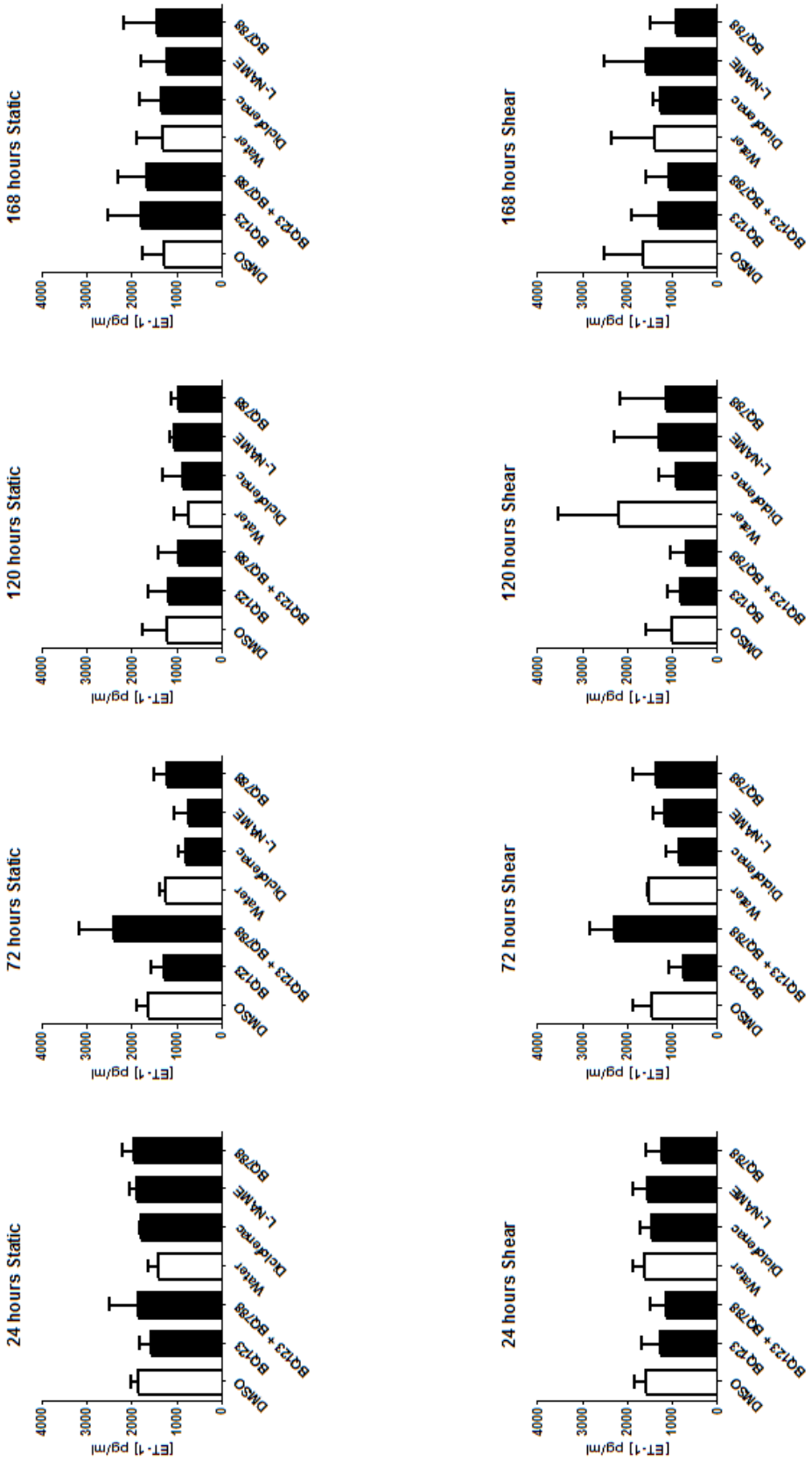

Figure 6.20 PAEC ET-1 release over 7 days in response to multiple drug treatments

(Legend continues on next page)

Figure 6.20 PAEC ET-1 release over 7 days in response to multiple drug treatments <u>(Legend continued from previous page)</u>

PAEC release of the vasoconstrictor ET-1 was measured in response to treatment with multiple drugs known to influence vascular function. None of these drugs was found to have influence on ET-1 release. Shear stress also had no bearing on IL-8 release. N=3 animals. Data were analysed by one-way ANOVA followed by Bonferroni post-test.

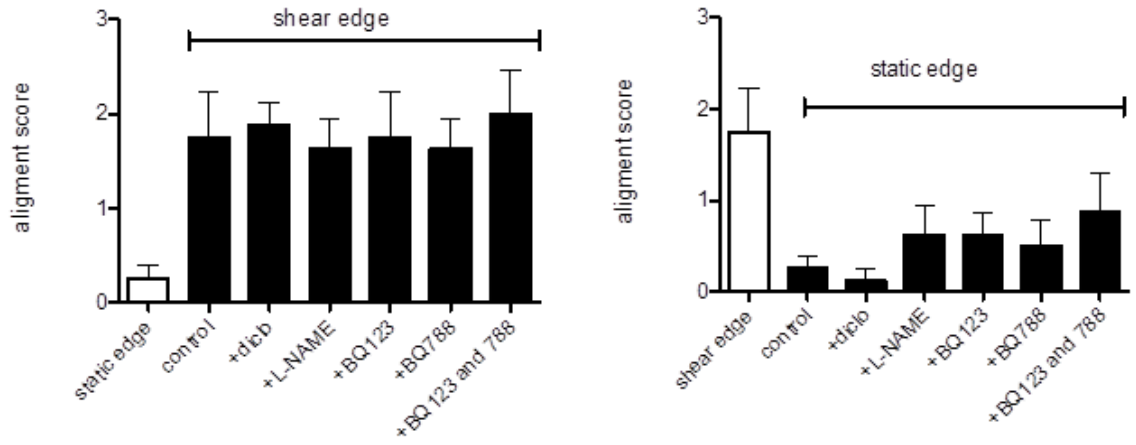

Figure 6.21 PAEC alignment scores in response shear stress in combination with vasoactive drug treatment

PAEC alignment was scored for cells having received a number of treatments on a scale of 0 where all cells were rounded and randomly orientated to 3 where all cells were unidirectionally aligned.

6 images from 3 preparations from 3 donors were individually scored by 2 independent observers. The results for each image from the 2 scorers were averaged. Data is presented as mean ±SEM for the 6 values obtained after this averaging.

A. Shear edge. Alignment scores were similar in response to all treatments and considerably higher than at the edge in static wells

B. Static edge. Alignment scores were similar in all cases and considerably lower than the edge in sheared wells.

Summary

There was no evidence that COX-2 is expressed in either healthy porcine or human endothelial cells under static or shear stress conditions.

Both PAEC and HAEC produce COX-2 in response to the inflammatory stimulus LPS under both static and shear stress conditions.

HAEC and PAEC both express abundant COX-1 but this is not regulated by shear stress.

Though COX-1 and COX-2 are not shear stress responsive proteins vasodilator NOS III appears to show increased expression with application of both directional and non-directional shear stress in pilot data gathered both from both porcine and human cells.

Vasoactive mediators NOSIII, PGI_2 and ET-1 appear to have no influence on endothelial cell alignment in response to application of shear stress.

Chapter 7
Effect of Shear on HAEC Transcriptomic Profile and Mediator Release

Rationale

Results shown in previous chapters demonstrated that clear, time dependent morphological changes in endothelial cells are brought about by chronic exposure to shear stress. 24 hours of shear stress is required for the commencement of morphological changes which eventually result in cell elongation and alignment. In the model of shear stress described in this thesis (an orbital shaker), shear stress is complex, with directional shear stress towards the edge of the well and non-directional shear stress at the centre. These patterns of shear may be representative of the two different shear environments found in discrete regions of the vasculature, laminar flow in straight arterial segments and oscillatory flow at bends.

Shear stress in this orbital shaker model has also been shown to affect cellular function, specifically expression of NOSIII, as well as responsiveness to LPS. This chapter describes how a transcriptomic approach was taken in order to corroborate findings of previous chapters on a genetic level and to explore how a range of other proteins would be influenced. Transcriptomics allows determination of how transcription of all genes in the genome is regulated by a given stimulus. As detailed in the Introduction, few studies in the literature have looked at how a full transcriptional profile is affected by shear stress and fewer still have examined long term shear stress.

In Results Chapters 3-6 a 6-well plate Transwell™ system was used on an orbital shaker. This system was suitable for two key reasons; firstly, because this model had been previously described for use in our group in permeability assays and secondly, because the Transwell™ filter was easy to remove for confocal microscopy. However, it is important to note the limitations of this model. One such limitation is the difficulty scraping and collecting cells from the flexible surface which is easily broken. Another is comparison of magnitude of shear stress which is produced with other published data. The highest level of shear stress reached is ~5 dyn/cm^2 whilst the lowest is ~2 dyn/cm^2 both these values are considered by many to be representative of low physiological shear stress by many though they may be normal levels in resting individuals (Tang *et al.*, 2006) .

In assessment of transcriptional changes it was viewed as important to look at genes over a long time period in a way which would be comparable to existing literature values whilst still physiological.

Shear stress magnitude is in part determined by medium velocity. For this reason increasing the diameter of the well, though not the rotation speed was found to be enough to increase velocity. Conventional 6-well plates with a solid base were chosen as a suitable model. These plates had a diameter of 38mm as opposed to 26mm. Collaborator Eric Berson was once more able to model the degree of shear experienced in this system.

Due to time constraints optimisation of a protocol to allow isolation of RNA from discrete regions of the well was not possible. RNA for transcriptomics analysis had to be pooled from cells cultured across the whole surface of the well. This may mean that more subtle differences in gene transcription between the centre (low level, non-directional shear) and the edge (high level, directional shear) that exist have been obscured. In future it is hoped that the data shown here can be compared to that from individual areas of the well.

Methods

HAEC from 3 donors were cultured on 6 well plates and allowed to grow to 80% confluence over 24 hours before their exposure to shear stress, on the orbital shaker at 150RPM with a fluid height of 3mm. As described (shown in Figure 7.1C) shear was found to range from 0.5 dyn/cm^2 to 10.5 dyn/cm^2, with the non-slip boundary condition being observed at the very edge of the model. It should be noted that peak levels at the edge of the well in this system are considerably higher than in the Transwell™ system used in previous chapters. Mean shear also differs across regions of the well however, preferred directionality at the edge and non-directionality at the centre is still an observed trait.

At the agreed time points of 1 hour, 24 hours, 72 hours and 144 hours RNA was collected. Cells were lysed using lysis buffer and the lysate of cells from 2 wells pooled before RNA purification was carried out using Qiagen spin columns. Purified RNA was assessed for

purity from contamination (Table 7.1) before being snap frozen in liquid nitrogen until hybridised to Illumina chips.

All fluorescence intensity data were analysed in GeneSpring as detailed in Chapter 2.8.2.

Results

Morphology of HAEC exposed to shear stress for 1-144 hours

Previous chapters demonstrate the clear alignment of endothelial cells under directional shear stress and the significant, though less dramatic alignment of cells exposed to non-directional shear stress. As these results were obtained in Transwells™ and the transcriptomics studies were to be carried out in 6-well plates it was important to first validate that these morphological changes would be the same.

As seen in PAEC cultured in Transwells™ HAEC aligned with exposure to shear stress in a time dependent manner. Elongation and alignment can be most clearly seen after 144 hours at the edge of the well and elongation, but limited alignment at the centre of the well (Figure 7.2).

Effect of shear stress on release of endothelial cell vascular mediators

ET-1 is an endothelial hormone, elevated levels of which are associated with cardiovascular disease as it is a potent vasoconstrictor. As expected HAEC release high basal levels of ET-1. There was no discernible difference in ET-1 release between cells cultured under static conditions and cells cultured under shear stress after 24 hours (Figure 7.3A). However at 72 hour and 144 hour time points ET-1 release was significantly reduced in cells cultured under shear stress. (Figure 7.3 B and C). The cytokine CXCL8/IL-8 is, like ET-1 also associated with inflammation. In line with the results for ET-1, CXCL8/IL-8 was also significantly reduced in cells that had been exposed to 72 hours or 144 hours of shear stress (Figure 7.4). These results suggested that shear stress may in some way be a protective stimulus. In light of this the vascular protective hormone PGI_2 was measured through its more stable breakdown product 6-keto$PGF_{1\alpha}$. There was no significant difference in PGI_2release between static and sheared cells at any of the time points studied (Figure 7.5).

To further investigate this perceived protective effect of shear stress cells were treated for 4 hours with bacterial LPS, designed to provide an inflammatory stimulus. ET-1 release was not influenced by LPS treatment in either static or shear stress conditions at the 72 hour time point or the 144 hour time point (Figure 7.6). CXCL8/IL-8 release was significantly increased by LPS treatment at both 72 hours and 144 hours under static conditions (Figure 7.7A). However, at the 72 hour time point under shear stress there was no significant increase in IL-8 production, though there was at the 144 hour time point (Figure 7.7B). The reasons for the differences between the two time points are unclear. LPS had no significant effect on prostacyclin release under static or shear stress conditions (Figure 7.8).

Effect of shear stress on the HAEC transcriptome

Having identified differences in vascular mediator release between static and sheared HAEC samples and a possible protective effect of shear the decision was made to run transcriptomics analysis on 36 samples. The timepoints examined were 1 hour, 24 hours, 72 hours and 144 hours under both static and shear stress conditions. LPS treated static and sheared samples were also run at the 72 hour and 144 hour timepoint. 3 HAEC donors were tested.

Quality Control

Having obtained the raw fluorescence intensity signals for each Illumina chip it was necessary to run normalisation to ensure that readings from each chip were comparable (Figure 7.9). Unfortunately the static 72 hour sample from donor 1 had to be excluded at this point in the analysis as it did not fit the normalisation criteria (Figure 7.10).

Effect of duration of shear stress on HAEC transcriptomic analysis

Gene fluorescence intensity was measured in comparison to the intensity for the average gene and the fold change difference between each gene and the average reported. Genes with a 1.5 fold or greater difference from the average are reported and shown in heat maps, which highlight above average expression in red and below average expression in turquoise. From the genes identified and shown in this heat map up to 10 with the greatest above

average expression and up to 10 with the greatest fall below average expression were selected. Each of these genes was searched in the NCBI gene database to gather a brief description of function, so that some conclusion could be drawn as to the pathways influenced by shear stress and the effect the changes would likely have on the HAEC if they were carried through to protein level.

1 hour of shear stress resulted in an upregulation in expression of a large number of genes and downregulation of expression of a smaller number when compared to static conditions (Figure 7.11). Many of the upregulated genes were members of the TGF-β signalling pathway (Table 7.2). TGFβ is a critical regulator of the cell cycle and has been previously been shown to be upregulated by short durations of shear stress. It has been implicated as a substance preventative of harmful vascular remodelling through inhibition of smooth muscle proliferation. The genes downregulated were predominately those involved in inflammatory signalling.

As at the 1 hour timepoint, 24 hours of shear stress resulted in the upregulation of many genes and the downregulation of a smaller number (Figure 7.12). At this timepoint the majority of the upregulated genes appear to be anti-inflammatory/atheroprotective inhibitors of cytokine signalling. Others appear to regulate cell junction formation and the actin cytoskeleton, which may relate to the morphology changes occurring at this time point. Down regulated genes are largely involved with inflammatory signalling, as at the first time point (Table 7.3).

As at the 1 hour and 24 hour timepoints, many more genes are upregulated by shear than downregulated at the 72 hour timepoint (Figure 7.13). Upregulated genes are again anti-inflammatory and many are associated with the vasodilatory hormone NOSIII (Table 7.4). Roles of the 3 downregulated genes are less clear but at least one of them appears to be associated with inflammation.

At 144 hours a transcriptional event appears to have occurred in the static cells with many inflammatory cytokines greatly upregulated. This degree of upregulation is not seen in the sheared cells; however there is a downregulation of some of the previously expressed

atheroprotective genes (Figure 7.14). Genes upregulated with shear stress seem to be important in cell signalling and boundary maintenance (Table 7.5).

A Venn diagram was prepared to compare common genes influenced by shear stress across the different time points (Figure 7.16). It can be clearly seen that genes upregulated at one time point may be downregulated at the next. This was a reminder that transcription can be a cyclical event and due to its variation it is important to study gene expression changes within the context of time.

Only 1 gene was influenced at all time points and this was transcription factor KLF4. KLF4 was upregulated at 1 hour, 24 hours and 72 hours but downregulated at 144 hours in sheared cells compared to static cells. KLF4 is a transcription factor thought to have a role in atheroprotection. 72 hour and 144 hour timepoints had the most genes commonly influenced, with above average expression at the 24 hour time point and below average expression at the 144 hour time point. A similar situation existed between genes upregulated at the 24 hour time point and downregulation at the 144 hour timepoint (Table 7.6).

Though many protective genes are downregulated at 144 hours compared to earlier timepoints some inflammatory cytokines such as CXCL2/IL-2 are still downregulated after 144hours, so it does not seem that an inflammatory event has occurred. It may be that there has been negative regulation of transcription of these genes due to build-up of translated proteins in the cell, or the lack of signalling from other cellular components due to the absence of smooth muscle and fibroblast layers in culture.

Sub analysis of genes of interest

Though it was interesting to note general changes across the whole transcriptome through research in this thesis a number of genes had come to light that may be of particular importance. Data related to those genes can be seen in Figure 7.15.

CDH5 is the code for the gene expressed as VE-cadherin. As stated in chapter 1 VE-cadherin is an important component of endothelial cell junctions. Protein immunoreactivity levels of VE-cadherin were shown to be unchanged by shear stress in a previous chapter and a similar observation could be made about mRNA here, with relatively constant levels under both static and shear conditions throughout the duration of the experiment.

EDN-1 is the code for the gene expressed as the protein ET-1. Though ET-1 expression appears to be altered with shear stress, based on the results of ELISA, this effect may not be at the transcriptional level, as ET-1 expression appeared to be ~0.3 fold higher than average under static conditions and about ~-0.2 fold below average in the shared samples.

IL-1β is an inflammatory cytokine likely to be expressed if an endothelial cell had encountered an inflammatory stimulus. Expression levels seemed slightly lower than average in both static and sheared cells throughout the duration of the experiment.

CXCL8/Il-8 is another inflammatory cytokine. Expression of this cytokine is elevated in static and shear samples after one hour, perhaps reflecting a lack of confluence in the cells as at later time points in both static and sheared cells expression is significantly below average.

KLF2 is a transcription factor considered to be important in the maintenance of the endothelium as an anti-thrombotic surface and it has been suggested that its expression is regulated by shear stress (Dekker et al 2005). A transcriptomics study carried out on HUVEC over 7 days showed that its expression remained higher than average throughout the duration of shear exposure (Dekker et al 2002). In this study KLF-2 expression was close to or ~1 fold below average through most of the time course under static conditions, reaching ~1 fold higher than average expression at 144 hours. Under shear stress conditions KLF-2 expression was slightly above average to 1 fold higher for the first days of the time course falling to ~1 fold below average at 144 hours into the time course. At no time was expression above or below the 1.5 fold change cut off for significant change.

NFE2L2 is the code for the gene of the transcription factor nrf2. Nrf2 is a transcription factor for numerous anti-oxidant proteins and it has been speculated that its upregulation

through shear stress may be atheroprotective, through prevention of ROS mediate destruction of NO (see Chapter 1) (Hosoya et al 2005). NFE2L2 levels were relatively constant under shear stress but were seen to be slightly above average in static cells at the 144 hour timepoint.

NFκB is an inflammatory transcription factor studied in a previous chapter. No difference was reported in protein immunoreactivity levels between static and sheared cells and no difference can be seen at the genetic level with slightly below average expression throughout the timecourse of the experiment in both static and sheared endothelial cells.

NOSII/iNOS is an inducible form of nitric oxide expressed in response to inflammatory stimuli. No upregulation of expression is seen at any time point in static or sheared cells.

NOSIII/eNOS protein immunoreactivity was measured in Chapter 5 where it was shown to be upregulated by shear, as has been found in many previous studies. Above average expression was reported at 24 hours and 72 hours shear stress as was expected. At 144 hours expression declined in sheared cells but slightly above average expression was seen in static cells.

PECAM-1/CD31 is an important molecule for the recruitment of leukocytes to endothelial cells in inflammation. Levels were close to average fluorescence intensity in both static and sheared endothelial cells though there was a slight increase in static cells after 144 hours which may be related to the increased expression of inflammatory genes at this time point. Absolute levels of CD31/PECAM-1 expression remained unchanged in Chapter 4 however, expression localisation did appear to be different.

In Chapter 5 I showed that neither COX-1 nor COX-2 were altered by shear stress, but that NOSIII appeared to be upregulated. In this chapter the gene induction results corroborate those observations. NOSIII gene expression was increased by shear stress. By contrast COX-1 and COX-2 was not altered by shear. Interestingly, COX-2 was high at initial cell plating and then declined dramatically over the course of the experiment. This effect was not altered by shear.

Effect of shear stress on LPS-induced hormone release and transcriptomic changes

In order to more easily interpret the effect of shear stress on LPS induced transcriptomic changes was measured. In analysis of these data a 2 fold cut off was applied. The key finding was that cells cultured under shear stress showed a more robust response to LPS than genes cultured under static conditions, with increases in genes for inflammatory proteins (Figure 7.17). This seems to be in agreement with NFkB data in Chapter 6 where there was a greater amount of NFkB in the nucleus in sheared cells at the edge of the well. At the 72 hour/3day time point 6 proteins associated with inflammatory signalling and recruitment of inflammatory cell types were activated in both sheared and static cells. At the 144 hour/3day timepoint 78 inflammatory pathways are influenced that are in common with the two cell types. The expression of the majority is above average in sheared cells but in static cells many are below average. These data seem to suggest that cells cultured under static conditions are less able to adapt and respond to inflammatory stimuli than their sheared counterparts and that shear stress exposure may be essential for maintenance of the host defence system. Looking at the heat maps from cells treated with LPS after 72 hours of shear the increased number of changes in sheared cells treated with LPS are readily apparent (Figure 7.18). When comparing the heat maps at the 144 hour time point both static and shear cells have undergone a similarly large degree of changes however, many more of the genes changed are expressed at above average levels in the sheared cells (Figure 7.19).

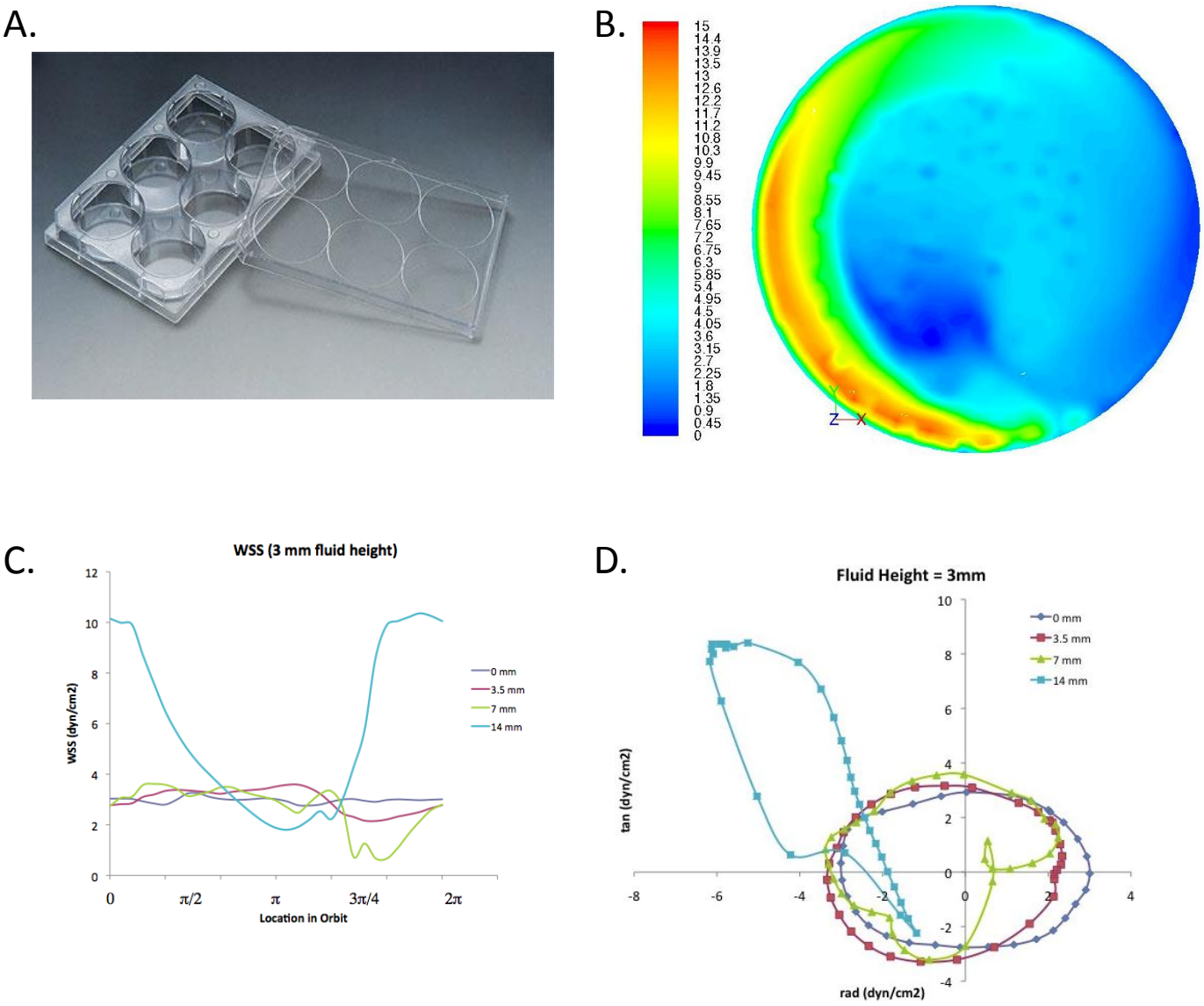

Figure 7.1 Use of a 6-well plate on an orbital shaker to model shear stress

A: A conventional 6-well plate was used as a cell culture surface. Wells were filled with 3ml of medium to provide 3mm of fluid coverage.

B: Computational fluid dynamics solution for time averaged shear stress in a single well of a 6 well plate. There appears to be an increasing temporal gradient of shear stress moving from the centre to the edge of the well.

C: The predicted shear stress (dynes/cm^2) profile experienced by cells 14mm, 7mm and 3.5mm from the centre of 36mm diameter wells of a 6 well plate respectively.

D: Relationship between radial and tangential components of shear at 4 discrete regions of the well (14mm, 7mm, 3.5mm and 0mm from the centre)

Sample	Concentration (ng/µl)	Ratio 260:280nm
1 Static 1 hour	123.2	2.00+/-0.1
2 Static 1 hour	132.4	2.00+/-0.1
3 Static 1 hour	105	2.00+/-0.1
1 Shear 1 hour	149.4	2.00+/-0.1
2 Shear 1 hour	263.6	2.00+/-0.1
3 Shear 1 hour	97.5	2.00+/-0.1
1 Static 24 hours	237.6	2.1
2 Static 24 hours	164.9	2.08
3 Static 24 hours	177.3	2.05
1 Shear 24 hours	81.1	2.14
2 Shear 24 hours	190.3	2.07
3 Shear 24 hours	128	2.03
1 Static 72 hours	202.3	2.09
2 Static 72 hours	387.4	2.07
3 Static 72 hours	210.4	2.08
1 Static + LPS 72 hours	227.3	2.09
2 Static + LPS 72 hours	461.9	2.05
3 Static + LPS 72 hours	266.1	2.09
1 Shear 72 hours	224.1	2.09
2 Shear 72 hours	328.7	2.08
3 Shear 72 hours	228	2.07
1 Shear + LPS 72 hours	126.4	2.12
2 Shear + LPS 72 hours	192.2	2.09
3 Shear + LPS 72 hours	100.4	2.09
1 Static 144 hours	199.4	2.07
2 Static 144 hours	309.8	2.07
3 Static 144 hours	170.6	2.04
1 Static + LPS 144 hours	242.2	2.08
2 Static + LPS 144 hours	526	2.03
3 Static + LPS 144 hours	247.5	2.06
1 Shear 144	164.2	2.07
2 Shear 144 hours	415.9	2.02
3 Shear 144 hours	222.9	2.08
1 Shear + LPS 144 hours	197.8	2.06
2 Shear + LPS 144 hours	279.1	2.05
3 Shear + LPS 144 hours	170.3	2.06

Table 7.1 ***Quantities and purities of RNA extracted from HAEC***

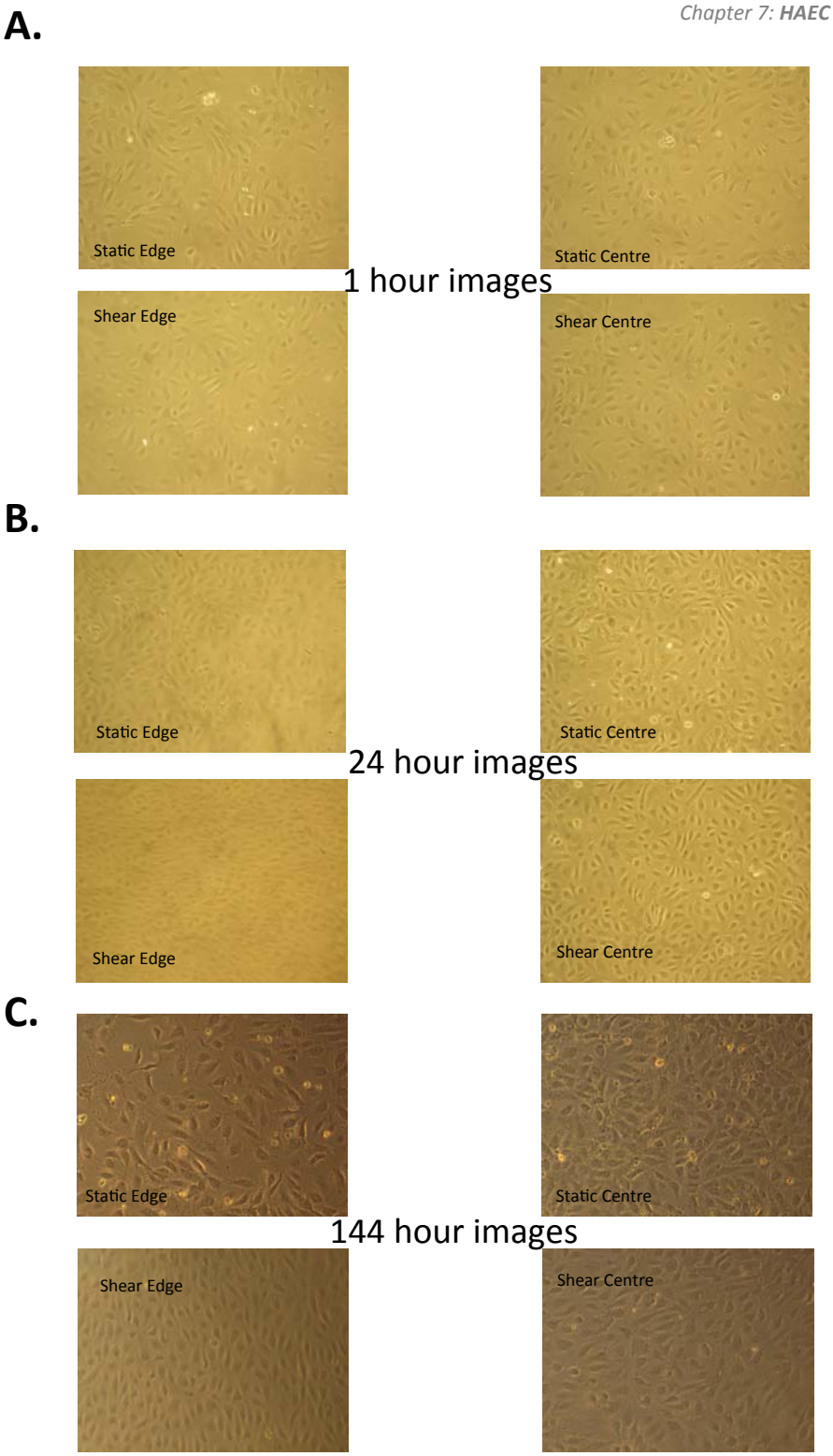

Figure 7.2 Morphology of HAEC cultured on 6 well plates across a timecourse of 6 days

Cells were plated at a density of 150,000 cells per well and left to grow to 80% confluence for 24 hours before beginning experimental conditions.

A: Static and sheared cells after 1 hour of experimental conditions

B: Static and sheared cells after 24 hours of culture under experimental conditions

C: Static and sheared cells after 144 hours of culture under experimental conditions.

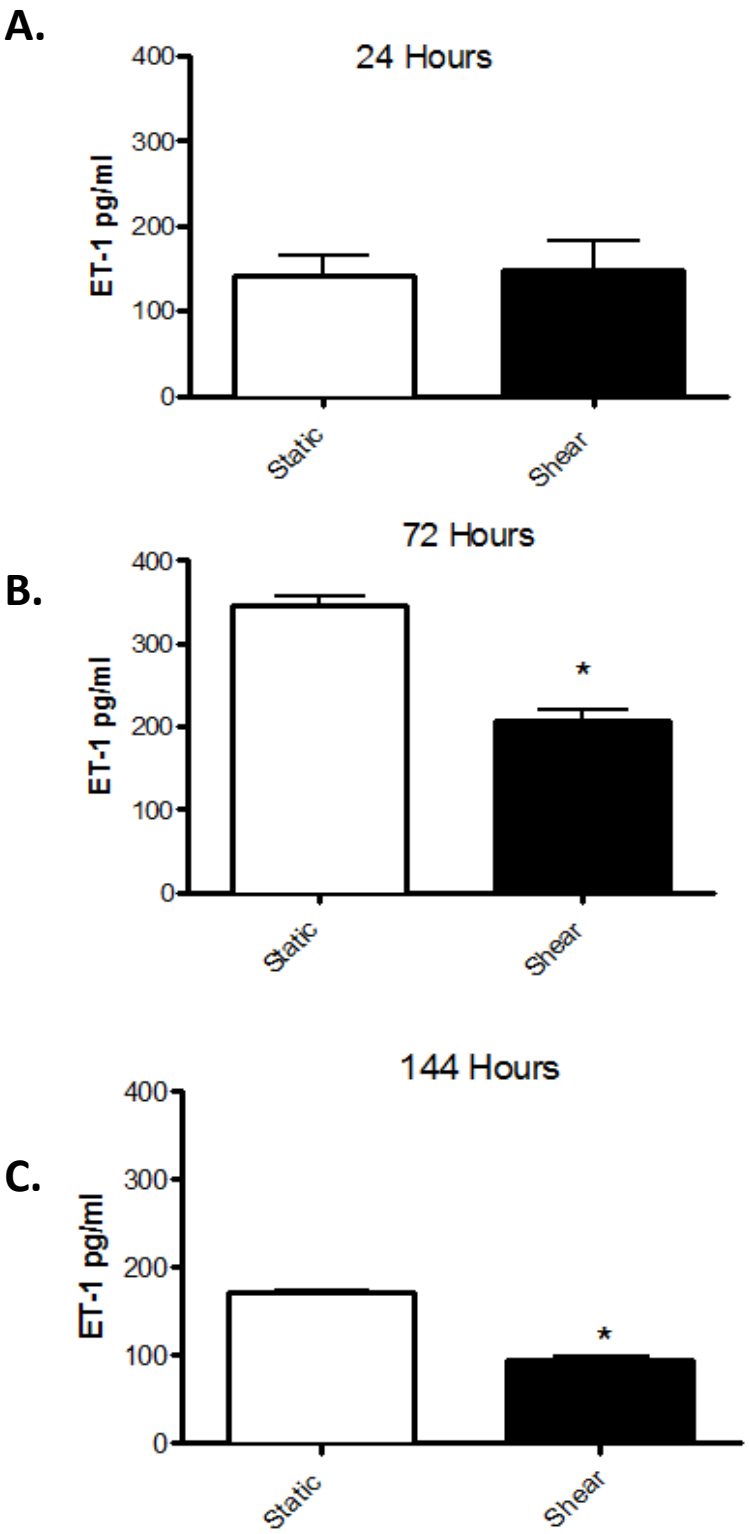

Figure 7.3 ET-1 release from HAEC

*ET-1 release was measured after 24 hours of accumulation at three time points; 24 hours, 72 hours and 144 hours. N=3 from 3 donors. Samples were pooled from medium from 2 wells per donor. Data were analysed using Student's t-test. Results indicated by * were significant ($p<0.05$).*

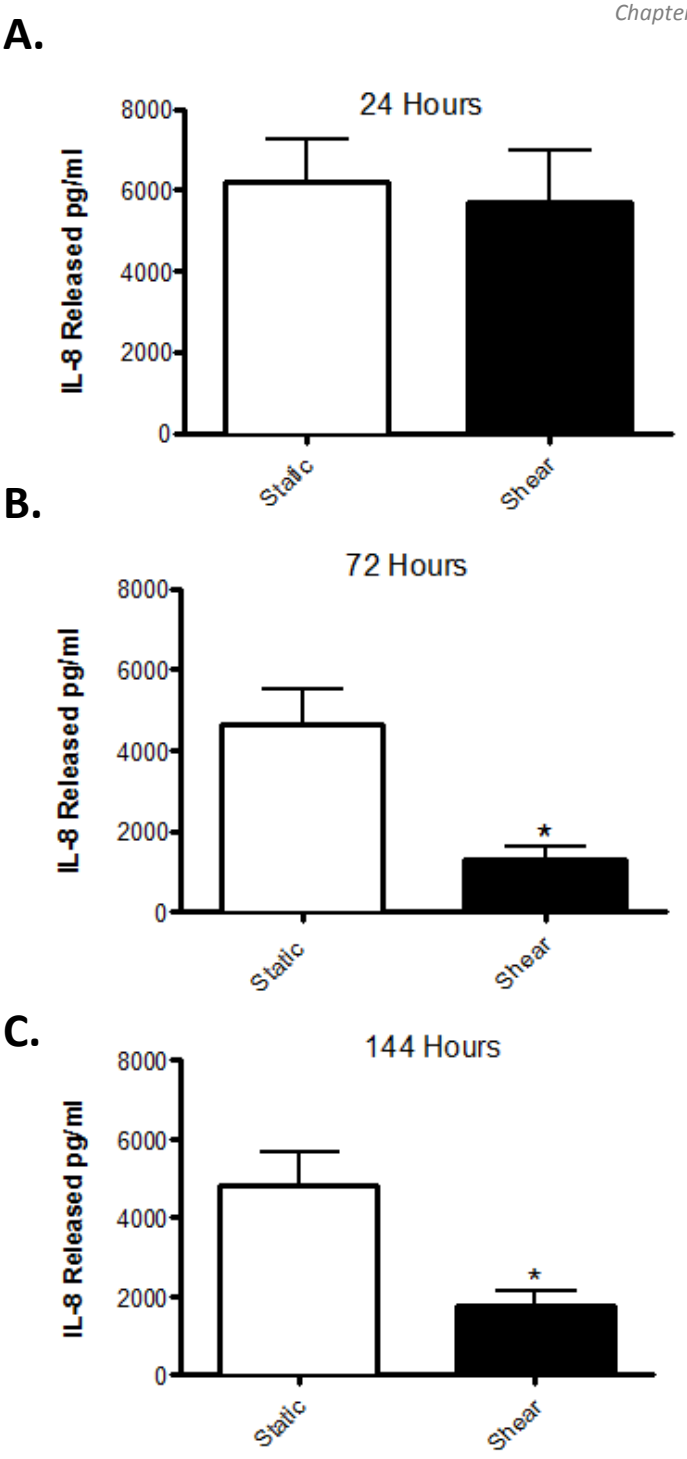

Figure 7.4 CXCL8/IL-8 release from HAEC

*CXCL8 release was measured after 24 hours of accumulation at three time points, 24 hours, 72 hours and 144 hours. N=6 from 3 donors, medium from 2 wells per donor. Data were analysed using Student's t-test. Results indicated by * were significant ($p<0.05$).*

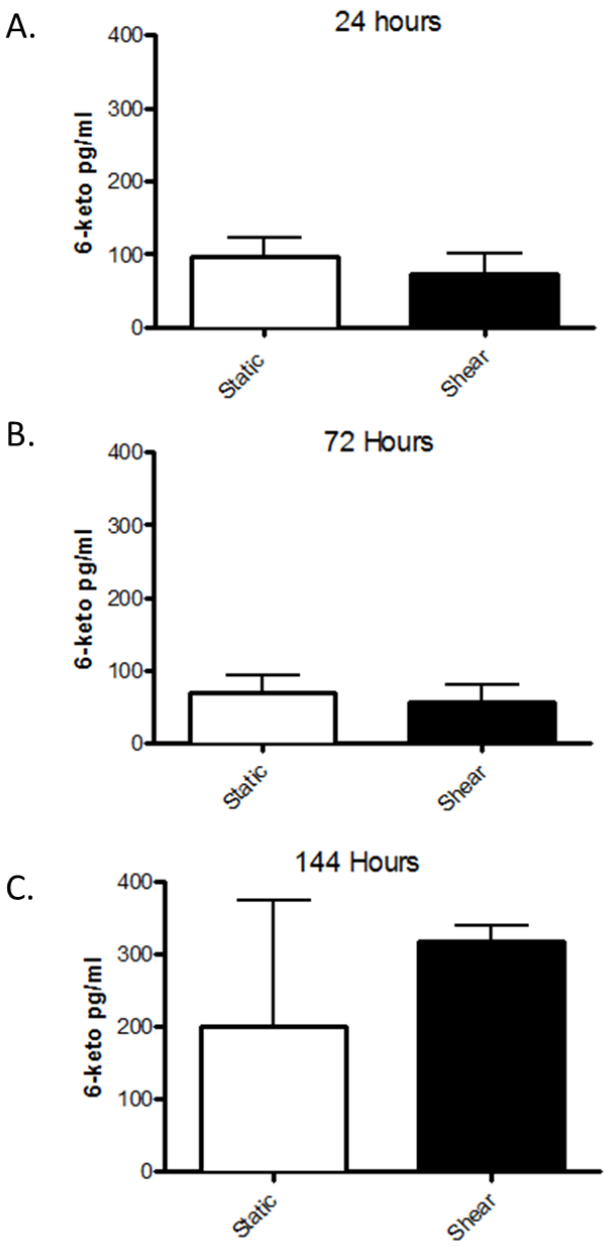

Figure 7.5 6-ketoPGF$_{1\alpha}$ release from HAEC

*6-ketoPGF$_{1\alpha}$ release was measured after 24 hours of accumulation at three time points, 24 hours, 72 hours and 144 hours. N=6 from 3 donors, medium from 2 wells per donor. Data were analysed using Student's t-test. Results indicated by * were significant ($p<0.05$).*

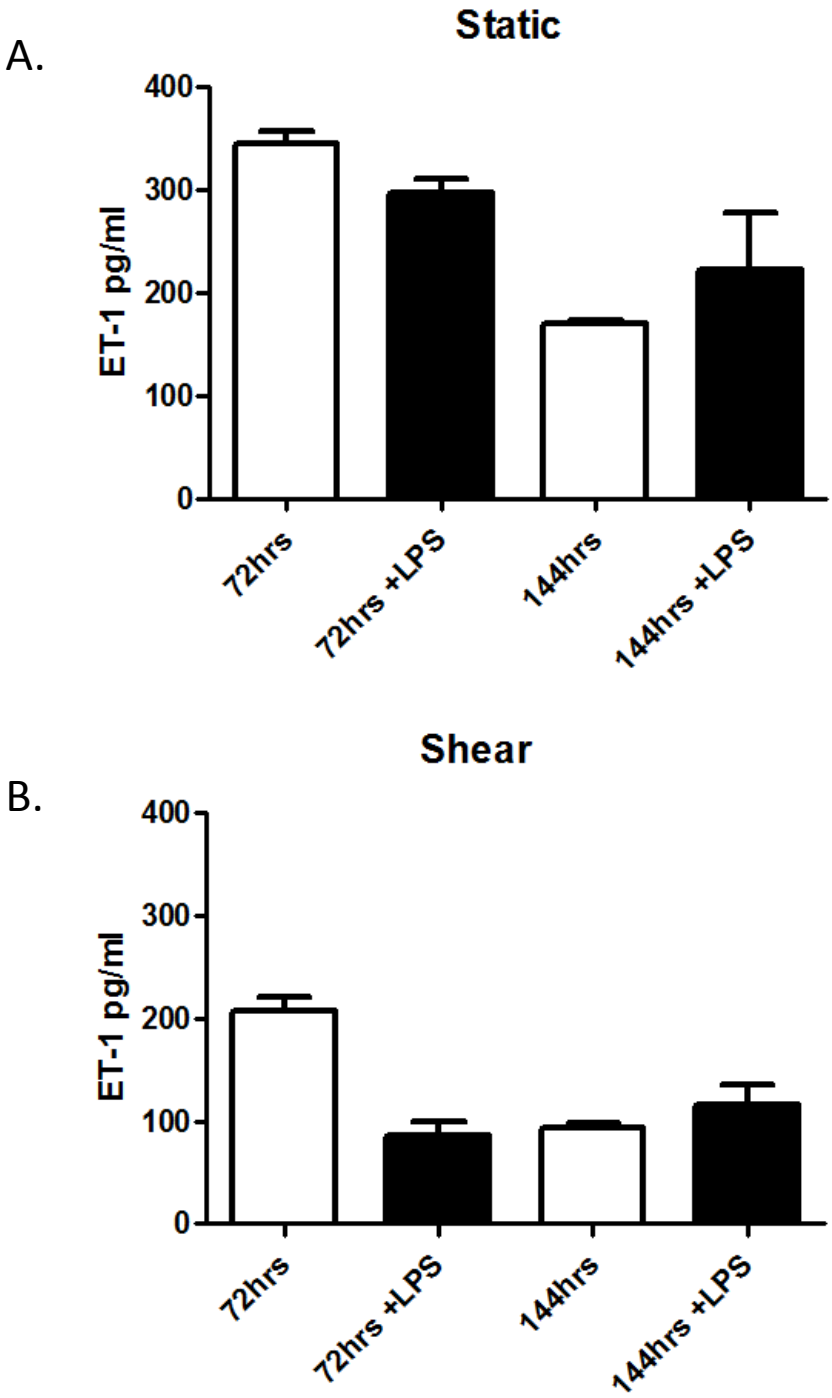

Figure 7.6 ET-1 release from HAEC under static and shear conditions in the presence or absence of LPS

*ET-1 release was measured after 24 hours of accumulation at two time points, 72 hours and 144 hours in control cells or cells that had been treated with 1µg/ml LPS for 4 hours. N=3 from 3 donors pooled from medium from 2 wells per donor. Data were analysed using Student's t-test. Results indicated by * were significant (p<0.05).*

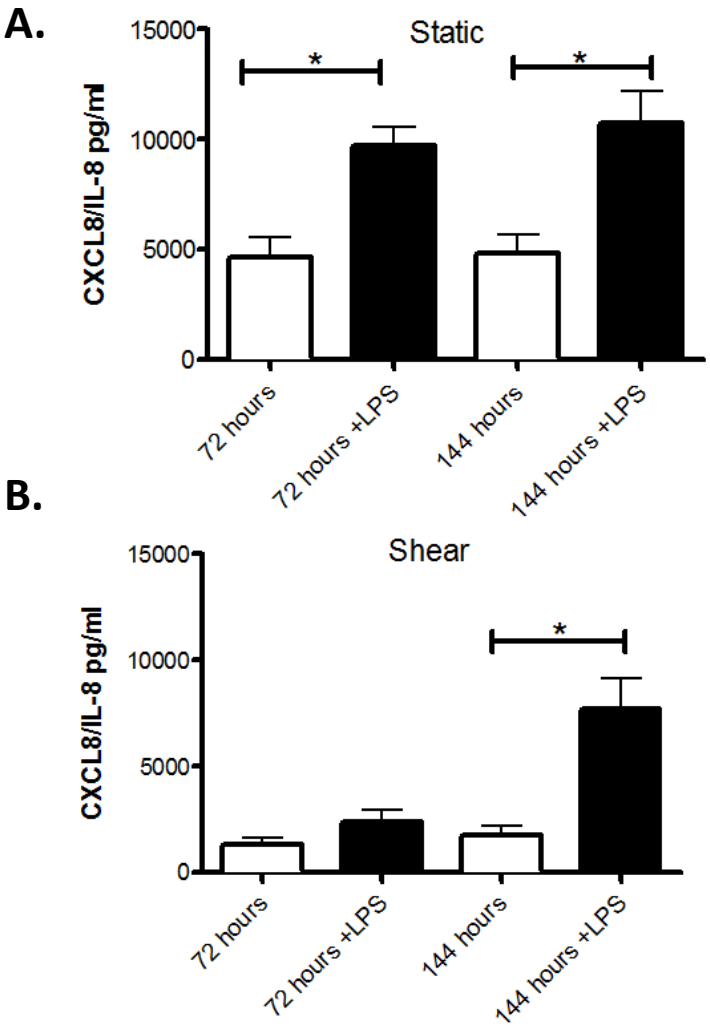

Figure 7.7 CXCL8/IL-8 release from HAEC under static and shear conditions in the presence or absence of LPS

*CXCL8/IL-8 release was measured after 24 hours of accumulation at two time points, 72 hours and 144 hours in control cells or cells that had been treated with 1µg/ml LPS for 4 hours. N=6 from 3 donors, medium from 2 wells per donor. Data were analysed using Student's t-test. Results indicated by * were significant ($p<0.05$).*

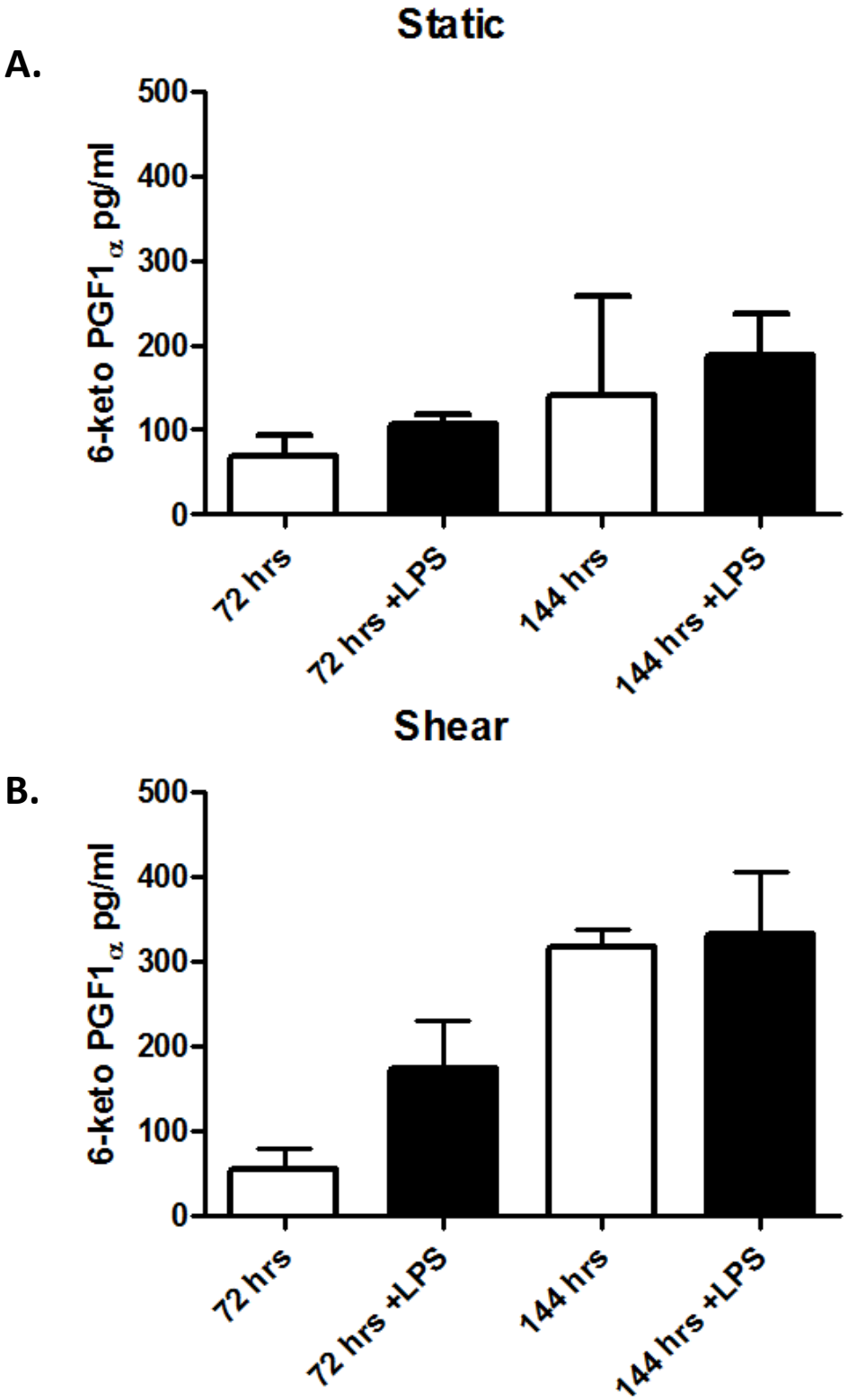

Figure 7.8 6-ketoPGF$_{1\alpha}$ release from HAEC under static and shear conditions in the presence or absence of LPS

*6-ketoPGF$_{1\alpha}$ release was measured after 24 hours of accumulation at two time points, 72 hours and 144 hours in control cells or cells that had been treated with 1µg/ml LPS for 4 hours. N=6 from 3 donors, medium from 2 wells per donor. Data were analysed using Student's t-test. Results indicated by * were significant (p<0.05).*

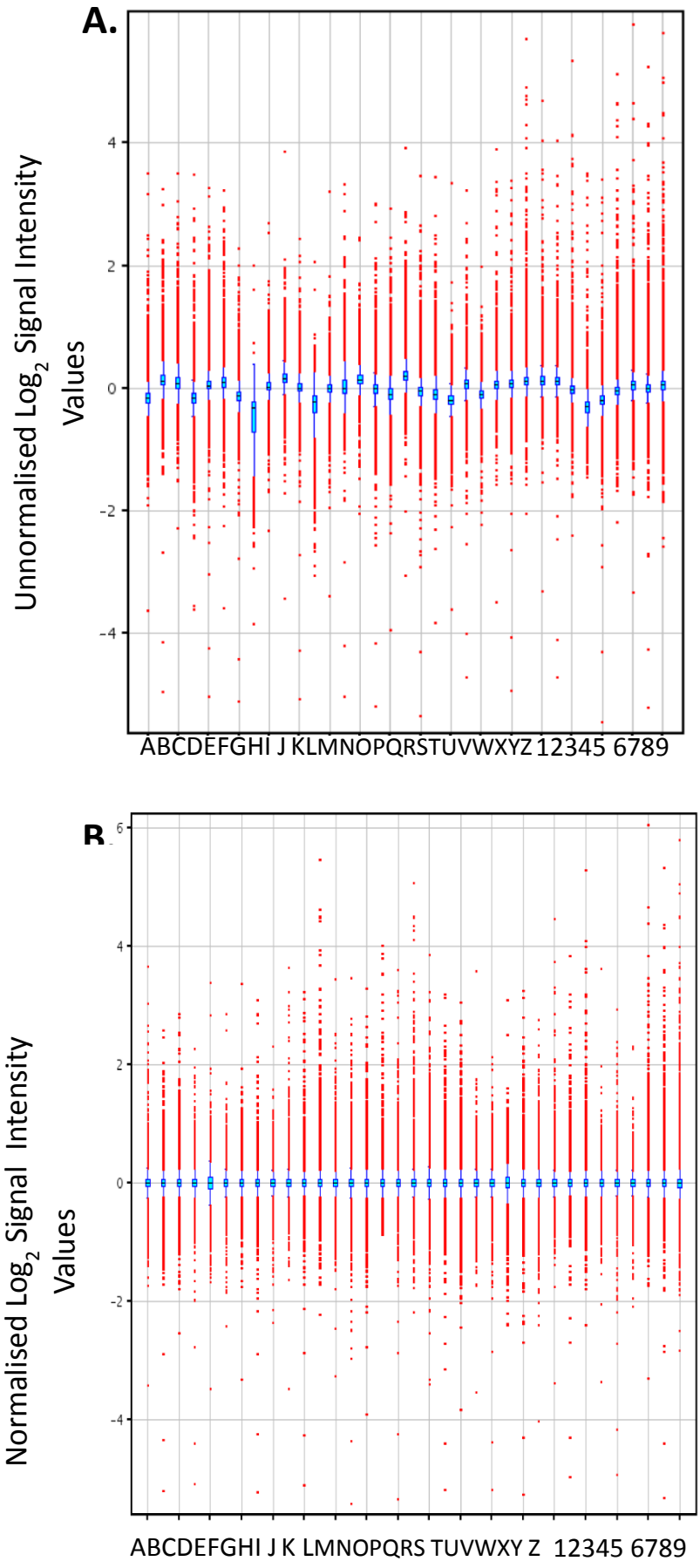

Code	Sample
A	Static 1 1hr
B	Static 2 1 hr
C	Static 3 1 hr
D	Static 1 24 hrs
E	Static 2 24 hrs
F	Static 3 24 hrs
G	Static 1 72 hrs
H	Static 2 72 hrs
I	Static 3 72 hrs
J	Static 1 144 hrs
K	Static 2 144 hrs
L	Static 3 144 hrs
M	Static 1 72 hrs LPS
N	Static 2 72 hrs LPS
O	Static 3 72 hrs LPS
P	Static 1 144 hrs LPS
Q	Static 2 144 hrs LPS
R	Static 3 144 hrs LPS
S	Shear 1 1hr
T	Shear 2 1 hr
U	Shear 3 1 hr
V	Shear 1 24 hrs
W	Shear 2 24 hrs
X	Shear 3 24 hrs
Y	Shear 2 72 hrs
Z	Shear 3 72 hrs
1	Shear 1 144 hrs
2	Shear 2 144 hrs
3	Shear 3 144 hrs
4	Shear 1 72 hrs LPS
5	Shear 2 72 hrs LPS
6	Shear 3 72 hrs LPS
7	Shear 1 144 hrs LPS
8	Shear 2 144 hrs LPS
9	Shear 3 144 hrs LPS

Figure 7.9 Signal intensity values for cDNA fluorescence

Box-whisker plots showing fluorescence signal intensity values of A: unnormalised raw data and B: quantile normalised data averaged. All cDNA was hybridised to Illumina human-8ref v3 chips and data processed using GeneSpring version GX12.01. Samples analysed are indicated in the accompanying table.

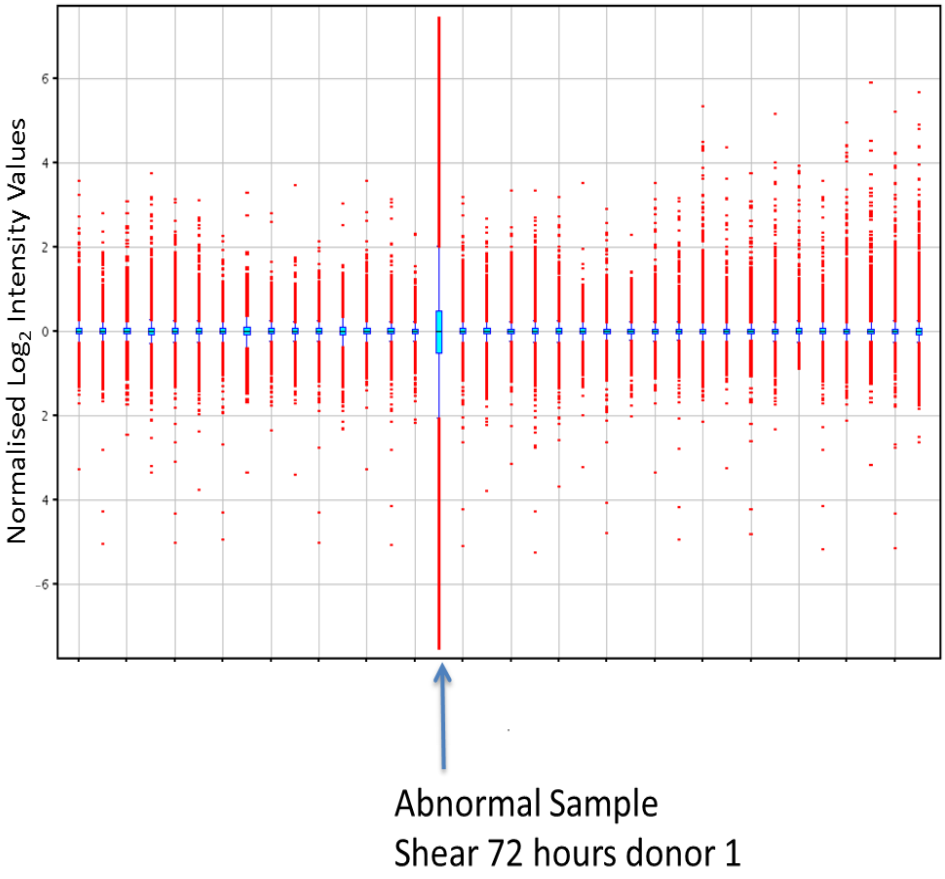

Figure 7.10 Box whisker plot highlighting that the 72 hour sheared sample from donor 1 cannot be normalised alongside the rest of the data set

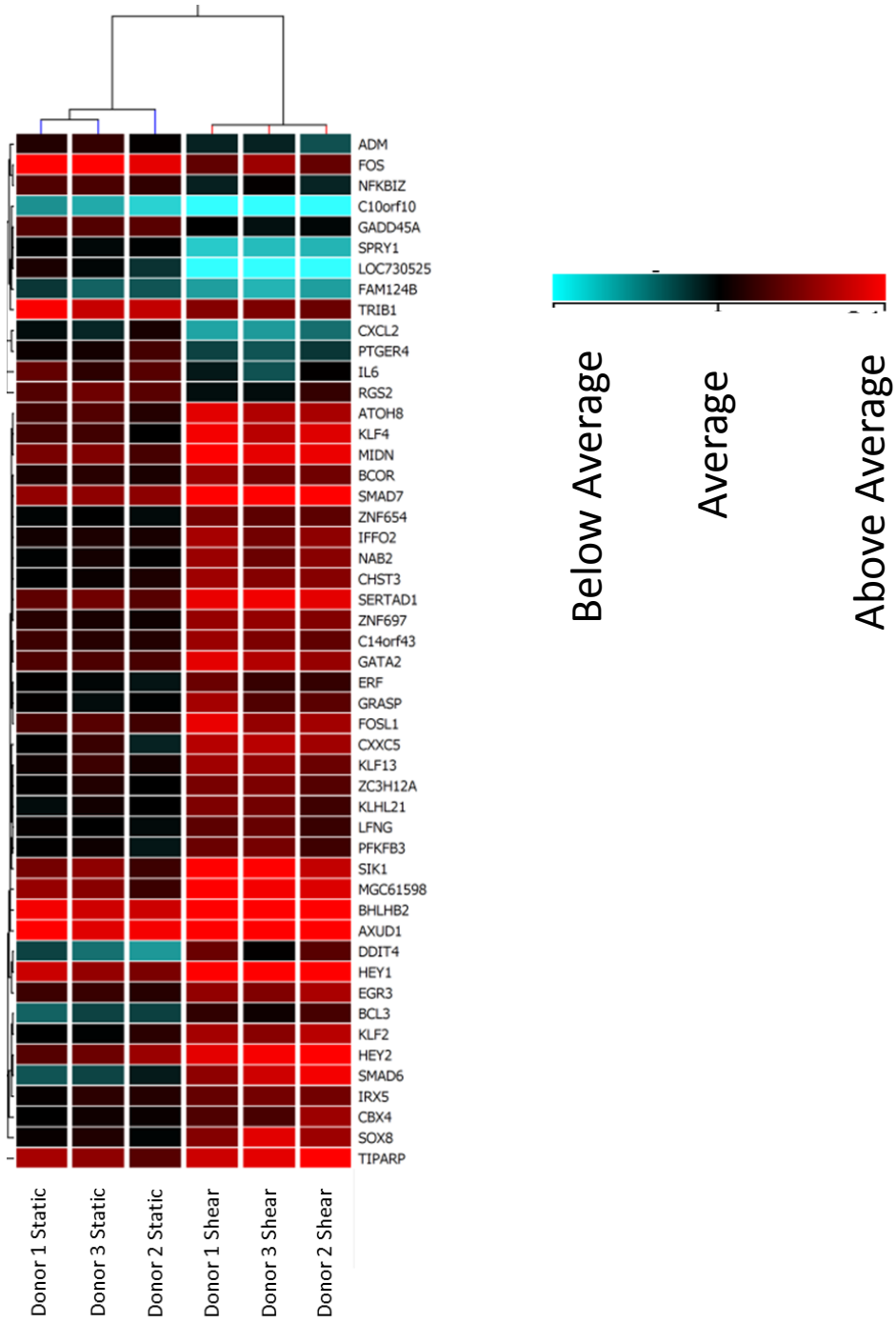

Figure 7.11 Heat map showing gene expression changes in HAEC, above a 1.5 fold cut-off, after 1 hour exposure to shear stress

Normalised intensity values represented as a heat map of HAEC cultured under static conditions versus HAEC cultured under shear stress for 1 hour. Red indicates above average fluorescence intensity for a gene, suggesting higher expression levels. Turquoise indicates below average fluorescence intensity, suggesting reduced levels of expression. Samples were hierarchically clustered using Pearson's centred distance metric and Ward's linkage rule, the shorter the line indicating the clustering the closer the relationship between samples.

Abbreviation	Full Name	Function	Fold Change	P value
SMAD6	SMAD family member 6	Signal Transducer, TGF-β negative regulator	3.844	0.011
HEY1	Hairy/enhancer-of-split related with YRPW motif 1	Induced by notch and c-jun, role in angiogenesis	3.164	0.017
DDIT4	DNA-damage-inducible transcript 4	mTOR signalling, transcription and cell survival	2.497	0.026
KLF4	Kruppel-like factor 4	Negative regulator of NFkB and other inflammatory pathways	2.470	0.015
CXXC5	CXXC finger protein 5	Transcription, Wnt signalling	2.423	0.015
SMAD7	SMAD family member 7	TGF-β Receptor Degradation	2.332	0.009
SOX8	SRY (sex determining region Y)-box 8	Transcriptional Activator	2.297	0.017
SIK1	Salt-inducible kinase 1	TGF-β signalling	2.189	0.036
KLF2	Kruppel-like factor 2	Atheroprotective, negative regulator of IL-1 and IL-6	2.164	0.011
HEY2	Hairy/enhancer-of-split related with YRPW motif 2	Notch signalling, angiogenesis	2.090	0.020
NFKBIZ	Nuclear factor of kappa light chain polypeptide gene enhancer in B-cells inhibitor, zeta	Activator of IL-6	-1.590	0.017
GADD45A	Growth arrest and DNA-damage-inducible 45A	Activates p38/JNK in response to environmental stress	-1.613	0.002
TRIB1	Tribbles homolog 1	Negative regulator of kinase activity	-1.628	0.020
PTGER4	Prostaglandin E receptor 4 (subtype EP4)	Regulator of stability of COX-2 mRNA	-1.698	0.019
IL6	Interleukin 6 (interferon, beta 2)	Inflammation, fever, B-cell activation	-1.780	0.036
CXCL2	Chemokine (C-X-C motif) ligand 2	Inflammatory Mediator	-2.017	0.016
FOS	FBJ murine osteosarcoma viral oncogene homolog	Transcription factor AP-1 complex, implicated with apoptosis	-2.483	0.020
SPRY1	Sprouty homolog 1	Inhibits angiogenesis	-2.649	0.001
LOC730525	Hypothetical protein LOC730525	Unknown	-4.224	0.004
C10orf10	Chromosome 10 open reading frame 10	Elk-1 Phosphorylation and activation	-4.400	0.010

Table 7.2 HAEC genes most influenced by shear stress at a 1 hour timepoint

Fold change in mRNA expression levels compared to the average gene was calculated and the highest and lowest expressed genes reported here. An NCBI search was carried out on each gene to identify pathways it may be involved in.

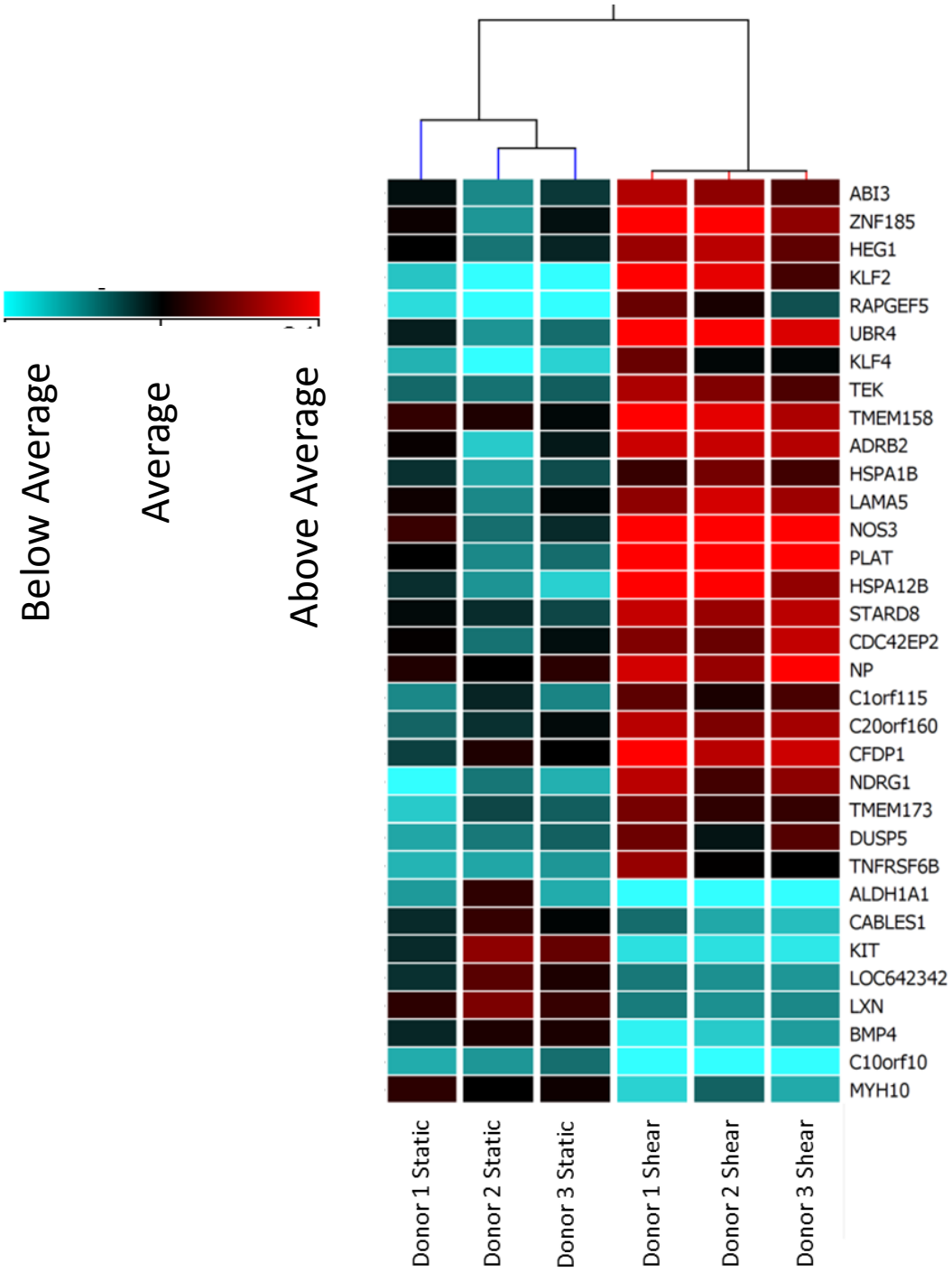

Figure 7.12 Heat map showing gene expression changes in HAEC, above a 1.5 fold cut-off, after 24 hours exposure to shear stress

Normalised intensity values represented as a heat map of HAEC cultured under static conditions versus HAEC cultured under shear stress for 1 hour. Red indicates above average fluorescence intensity for a gene, suggesting higher expression levels. Turquoise indicates below average fluorescence intensity, suggesting reduced levels of expression. Samples were hierarchically clustered using Pearson's centred distance metric and Ward's linkage rule, the shorter the line indicating the clustering the closer the relationship between samples.

Abbreviation	Full Name	Function	Fold Change	P value
KLF2	Kruppel-like factor 2	Atheroprotective, negative regulator of IL-1 and IL-6	3.836	0.038
HSPA12B	Heat shock 70kD protein 12B	May be involved in susceptibility to atherosclerosis	3.005	0.048
PLAT	Plasminogen activator, tissue	Cell migration, tissue remodelling, clot lysis, blood brain barrier	2.783	0.038
UBR4	Ubiquitin protein ligase E3 component n-recognin 4	Cytoskeletal component, chromatin scaffold, calmodulin-linked	2.504	0.032
NOS3	Nitric oxide synthase 3	Vasodilator	2.346	0.038
NDRG1	N-myc downstream regulated 1	Mitosis, cell cycle control	2.272	0.038
RAPGEF5	Rap guanine nucleotide exchange factor (GEF) 5	Signal Transduction	2.227	0.048
ZNF185	Zinc finger protein 185 (LIM domain)	Actin cytoskeleton association, proliferation	2.053	0.048
ADRB2	Adrenoceptor beta 2, surface	Down regulation associated with obesity and type II diabetes	2.006	0.048
KLF4	Kruppel-like factor 4	Negative regulator of NFkB and other inflammatory pathways	1.936	0.038
C1orf115	Chromosome 1 open reading frame 115	Unknown	-1.590	0.017
CABLES1	Cdk5 and Abl enzyme substrate 1	Cell cycle regulation and platelet production	-1.613	0.002
LOC642342	Similar to Contactin-associated protein-like 3 precursor (Cell recognition molecule Caspr3)	Unknown	-1.628	0.020
MYH10	Myosin, heavy chain 10, non-muscle	Cell motility and polarity	-1.698	0.019
BMP4	Bone morphogenetic protein 4	MEK/ERK Signalling	-1.780	0.036
LXN	Latexin	Tissue carboxypeptidase inhibitor	-2.017	0.016
C10orf10	Chromosome 10 open reading frame 10	Elk-1 Phosphorylation and activation	-2.483	0.020
KIT	v-kit Hardy-Zuckerman 4 feline sarcoma viral oncogene homologue	Signalling, actin mobilisation, inflammation	-2.649	0.001
ALDH1A1	Aldehyde dehydrogenase 1 family, member A1	Alcohol and retinol metabolism, Ras GTPase regulation	-4.224	0.004

Table 7.3 HAEC genes most influenced by shear stress at a 24 hour timepoint

Fold change in mRNA expression levels compared to the average gene was calculated and the highest and lowest expressed genes reported here. An NCBI search was carried out on each gene to identify pathways it may be involved in.

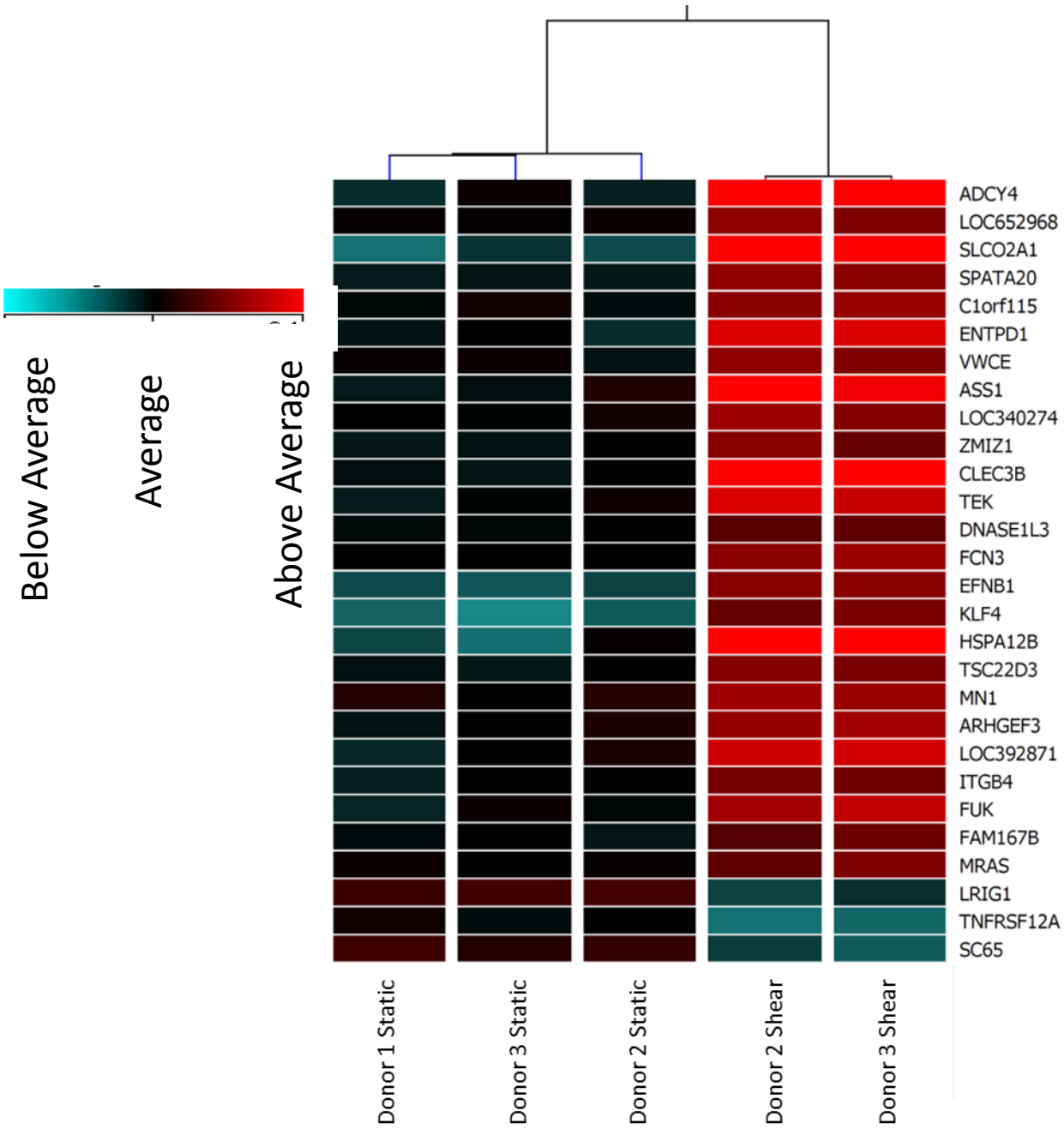

Figure 7.13 Heat map showing gene expression changes in HAEC, above a 1.5 fold cut-off, after 72 hours exposure to shear stress

Normalised intensity values represented as a heat map of HAEC cultured under static conditions versus HAEC cultured under shear stress for 1 hour. Red indicates above average fluorescence intensity for a gene, suggesting higher expression levels. Turquoise indicates below average fluorescence intensity, suggesting reduced levels of expression. Samples were hierarchically clustered using Pearson's centred distance metric and Ward's linkage rule, the shorter the line indicating the clustering the closer the relationship between samples.

Abbreviation	Full Name	Function	Fold Change	P value
SLCO2A1	Solute carrier organic anion transporter family, member 2A1	Prostaglandin transporter, PGE2 and PGH2 across membranes	10.750	0.025
HSPA12B	Heat shock 70kD protein 12B	ATP binding. May be involved in susceptibility to atherosclerosis	4.921	0.048
CLEC3B	C-type lectin domain family 3, member B	Calcium ion binding, cell response to TGF-β	4.141	0.033
ADCY4	Adenylate cyclase 4	Catalyst in the formation of the secondary messenger cyclic adenosine monophosphate (cAMP)	3.318	0.033
ASS1	Argininosuccinate synthetase 1	Catalyses the penultimate step of the arginine biosynthetic pathway, KLF4 may regulate	3.114	0.048
ENTPD1	Ectonucleoside triphosphate diphosphohydrolase 1	ATP metabolism, cell adhesion	2.775	0.033
KLF4	Kruppel-like factor 4	Anti-inflammatory, ASS1 regulator	2.546	0.035
TEK	Tyrosine kinase, endothelial	Angiogenesis, cytoskeletal reorganisation, proliferation, ERK 1/2 cascade	2.485	0.033
LOC392871	Argininosuccinate synthetase 1 pseudogene 11, ASS1P11	ASS-1 transcriptional regulation	2.467	0.048
EFNB1	Ephrin-B1	Cell adhesion, T-cell function	2.446	0.012
TNFRSF12A	Tumour necrosis factor receptor superfamily, member 12A	Elk-1 Phosphorylation and activation	-1.599	0.048
LRIG1	Leucine-rich repeats and immunoglobulin-like domains 1	Signalling, actin mobilisation, inflammation	-1.654	0.028
SC65	LEPREL4-Leprecan-like 4	Component of the interphase nucleus	-1.697	0.049

Table 7.4 HAEC genes most influenced by shear stress at a 72 hour timepoint

Fold change in mRNA expression levels compared to the average gene was calculated and the highest and lowest expressed genes reported here. An NCBI search was carried out on each gene to identify pathways it may be involved in.

Gene	Gene	Gene	Gene	Gene	Gene	Gene	Gene	Gene	Gene	Gene
A2M	C12orf24	CLDN7	DDIT4	FLOT1	ITGA2	LOC392437	NDRG1	PPP1R14A	SERPINB1	TLR4
ABCB1	C15orf54	CLEC3B	DHCR7	FUCA1	ITGB4	LOC392871	NID1	PRICKLE1	SLC24A6	TMEM173
ABHD6	C17orf28	CMAH	DLGAP5	FUK	KANK3	LOC401720	NOS3	PROS1	SLC2A3	TMTC1
ABLIM1	C19orf33	CNKSR3	DNASE1L3	GAS6	KIAA1202	LOC643733	NPM3	PTBP2	SLC35F2	TNFRSF12A
ACP5	C1orf115	CORO6	DOCK10	GBP4	KIAA1522	LOC652968	NT5DC2	PTPRB	SLC44A2	TSC22D3
ADAM15	C1orf198	COTL1	DPYSL4	GFOD1	KIAA1671	LOC653764	NTHL1	PTPRG	SLC7A5	TSPAN7
ADCY4	C20orf100	CPNE8	EFCAB4A	GMFB	KIT	LOC728069	OBFC1	PTPRM	SLCO2A1	TXNIP
AFAP1L2	C20orf160	CPXM1	ENC1	GPD1L	KLF2	LOC731049	ODC1	RAB11A	SOX13	VEGFC
ALS2CR4	C5orf41	CRBN	ENTPD1	GSN	KLF4	LOC88523	PALM	RAB3B	SPHK1	VWCE
ANGPT2	CALCRL	CREG1	EPAS1	GUK1	LAP3	LRP11	PCDH12	RAMP2	SPNS2	ZBTB46
ANKRD47	CARHSP1	CRIP2	EPHA4	HCCA2	LGALS3	LTBP2	PHGDH	RAPGEF4	SPTAN1	ZCCHC24
ANKRD55	CAT	CRTAC1	ERRFI1	HCFC1R1	LIFR	LXN	PI16	RAPGEF5	SPTBN1	ZMIZ1
APOD	CCDC99	CSRP1	ETS1	HEG1	LIMS2	LYN	PIK3C2B	RBMS2P	ST6GALNAC3	ZNF366
ARHGAP22	CCNB1	CTGLF7	ETS2	HLA-E	LIPG	MALL	PLA1A	RENBP	STARD8	ZNF467
ARHGEF3	CCND3	CTHRC1	EXT1	HSPA12B	LMBRD1	METTL7A	PLAT	RILPL2	STC2	
ARMET	CD34	CTSC	FAM107A	HSPA5	LMCD1	MICAL2	PLCD3	RNASE1	STOM	
ARRB1	CD58	CTSF	FAM167B	HSPC111	LMO2	MKNK2	PLCG2	RNF121	STS-1	
ARSJ	CD59	CXADR	FASN	HYOU1	LOC100008589	MN1	PLOD2	S100A10	TAGLN	
ART4	CENPV	CXCL2	FBLN2	IER3	LOC100132394	MRAS	PLVAP	S100A4	TBC1D2	
ASAP3	CHST7	CXorf64	FCN3	IFIT2	LOC100216001	MSMP	PMP22	SCD	TBC1D8	
ASS1	CKS2	CYB5D2	FJX1	IL1R1	LOC286512	MVD	PPAP2A	SDF2L1	TCN2	
AURKB	CLDN11	CYBRD1	FLJ11795	ITGA10	LOC340274	NCRNA00092	PPAP2B	SEC13	TEK	

Figure 7.14 Normalised intensity values represented as a heat map of HAEC cultured under static conditions versus HAEC cultured under shear stress for 144 hours.

Red indicates above average fluorescence intensity for a gene, suggesting higher expression levels. Turquoise indicates below average fluorescence intensity, suggesting reduced levels of expression. Samples were hierarchically clustered using Pearson's centred distance metric and Ward's linkage rule, the shorter the line indicating the clustering the closer the relationship between samples. Gene codes are shown in the accompanying table for clarity

Abbreviation	Full Name	Function	Fold Change	P value
LIPG	Lipase, endothelial	Lipoprotein metabolism	3.638	0.002
CTHRC1	Collagen triple helix repeat containing 1	Wnt signalling	2.792	0.027
CXADR	Coxsackie virus and adenovirus receptor	E-cadherin motility, Adherens junction maintenance,. Immunoregulation	2.296	0.046
ANGPT2	Angiopoietin 2	Signal transduction, angiogenesis	2.276	0.010
PHGDH	Phosphoglycerate dehydrogenase	L-serine biosynthesis, NAD binding	2.245	0.005
TNFRSF12A	Tumor necrosis factor receptor superfamily, member 12A	Angiogenesis, cell attachment to substrate	2.199	0.006
ERRFI1	ERBB receptor feedback inhibitor 1	Angiogenesis, protein kinase activation	2.179	0.007
MSMP	Microseminoprotein, prostate associated	Unknown	2.107	0.014
SCD	Stearoyl-CoA desaturase (delta-9-desaturase)	Enzyme involved in fatty acid biosynthesis	2.065	0.031
TAGLN	Transgelin	Actin crosslinking	2.060	0.005
CRTAC1	Cartilage acidic protein 1	Calcium ion binding	-3.561	0.024
KLF4	Kruppel-like factor 4	Atheroprotective, ASS-1 regulator	-3.591	0.014
KLF2	Kruppel-like factor 2	Atheroprotective	-3.607	0.031
HEG1	HEG homologue 1	Calcium ion binding, cell junction development	-3.675	0.006
RAMP2	Receptor (G protein-coupled) activity modifying protein 2	RAMPs are required to transport calcitonin-receptor-like receptor (CRLR) to the plasma membrane.	-3.892	0.038
ENTPD1	Ectonucleoside triphosphate diphosphohydrolase 1	ATP metabolism, cell adhesion	-4.963	0.005
HSPA12B	Heat shock 70kD protein 12B	ATP binding. Susceptibility to atherosclerosis	-5.684	0.030
TSPAN7	Tetraspanin 7	Plasma membrane cell surface receptor	-5.866	0.021
PPP1R14A	Protein phosphatase 1, regulatory (inhibitor) subunit 14A	Myosin phosphatase inhibitor	-6.019	0.012
SLCO2A1	Solute carrier organic anion transporter family, member 2A1	Prostaglandin transporter, PGE2 and PGH2 across membranes	-10.648	0.016

Table 7.5 HAEC genes most influenced by shear stress at a 144 hour timepoint

Fold change in mRNA expression levels compared to the average gene was calculated and the highest and lowest expressed genes reported here. An NCBI search was carried out on each gene to identify pathways it may be involved in.

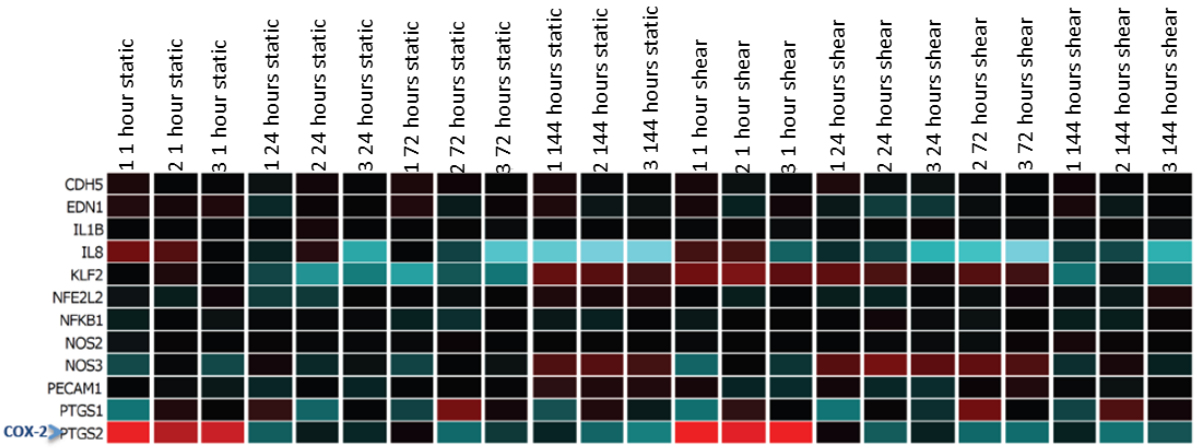

Gene	1h Static 1	1h Static 2	1h Static 3	24h Static 1	24h Static 2	24h Static 3	72h Static 1	72h Static 2	72h Static 3	144h Static 1	144h Static 2	144h Static 3	1h Shear 1	1h Shear 2	1h Shear 3	24h Shear 1	24h Shear 2	24h Shear 3	72h Shear 2	72h Shear 3	144h Shear 1	144h Shear 2	144h Shear 3
CDH5	0.302	0.000	-0.038	-0.178	0.197	-0.025	0.307	0.150	0.036	0.266	-0.094	-0.049	0.238	-0.165	-0.084	0.335	-0.136	-0.169	-0.105	0.019	0.150	-0.025	0.059
EDN1	0.386	0.236	0.349	-0.415	0.119	0.038	0.369	-0.269	0.108	0.325	-0.214	-0.161	0.249	-0.325	0.183	-0.246	-0.630	-0.568	-0.149	0.000	0.266	-0.235	-0.010
IL1β	-0.008	0.018	-0.002	0.011	0.247	-0.013	-0.035	-0.051	-0.115	-0.030	-0.018	-0.055	-0.080	0.078	-0.111	-0.070	0.038	0.108	-0.092	-0.103	-0.079	0.051	-0.115
IL8	1.255	0.941	0.000	-0.300	0.443	-1.841	-0.010	-0.689	-2.357	-2.449	-2.956	-3.893	0.785	0.788	-1.055	-0.451	-0.707	-1.971	-2.225	-4.017	-0.642	-0.738	-1.935
KLF2	0.000	0.328	-0.006	-0.735	-1.583	-1.328	-1.748	-0.911	-1.259	1.112	0.991	0.710	1.246	1.389	1.028	1.045	0.868	0.259	0.937	0.763	-1.213	-0.115	-1.412
NFE2L2	-0.193	-0.296	0.140	-0.577	-0.588	0.046	-0.026	-0.145	0.048	0.332	0.234	0.361	0.000	-0.290	-0.021	-0.280	-0.337	-0.075	-0.137	0.136	-0.125	-0.250	0.309
NFKβ1	-0.291	0.000	-0.189	-0.082	-0.066	-0.103	-0.326	-0.477	-0.034	-0.252	-0.318	-0.041	-0.238	0.037	0.025	-0.028	0.177	-0.113	-0.176	0.048	-0.289	-0.285	0.087
NOS2	-0.191	0.077	0.000	0.076	-0.078	-0.080	-0.101	0.116	-0.001	0.042	-0.050	0.033	-0.096	0.031	0.003	-0.018	-0.090	-0.122	-0.132	0.121	0.247	0.105	0.043
NOS3	-0.766	-0.073	-0.758	0.213	-0.410	-0.158	-0.714	0.000	-0.181	0.913	0.958	0.766	-1.072	0.029	-0.536	0.990	1.310	1.036	1.069	0.897	-0.470	0.259	-0.320
PECAM1	0.000	-0.120	-0.248	-0.378	0.005	-0.358	-0.004	0.043	-0.039	0.497	0.345	0.368	0.239	-0.342	-0.440	0.192	-0.391	-0.463	0.127	0.373	-0.077	-0.188	0.061
PTGS1	-1.239	0.366	0.053	0.585	-1.064	0.017	-0.686	1.306	0.233	-0.867	0.361	-0.268	-1.204	0.547	-0.021	-1.237	0.085	-0.472	1.274	0.000	-0.712	0.911	0.197
PTGS2	2.657	2.032	2.253	-1.000	-0.270	-0.398	0.141	-1.146	-0.581	-0.354	-1.081	-1.360	3.086	2.547	3.057	0.130	-0.966	-0.303	-1.122	-1.174	-0.332	-1.216	-0.887

Figure 7.15 Subanalysis of transcriptomic changes of particular genes of interest over the 144 hour time course

A subset of genes reported to be influenced by shear stress or that were deemed to be particularly interesting were analysed for variation over the 144 hour time course.

These genes were:

CDH5-Gene for VE-cadherin

EDN-1- Gene for ET-1

IL1β-Gene for IL-1β

IL-8-Gene for CXCL8/IL-8

KLF2-Gene for transcription factor KLF2

NFE2L2-Gene for transcription factor Nrf2

NFκB1-Gene for NFκB

NOS2-Gene for NOS II/iNOS

NOS3-Gene for NOS III/eNOS

PECAM1-Gene for PECAM-1/CD31

PTGS1-Gene for COX-1

PTGS2-Gene for COX-2

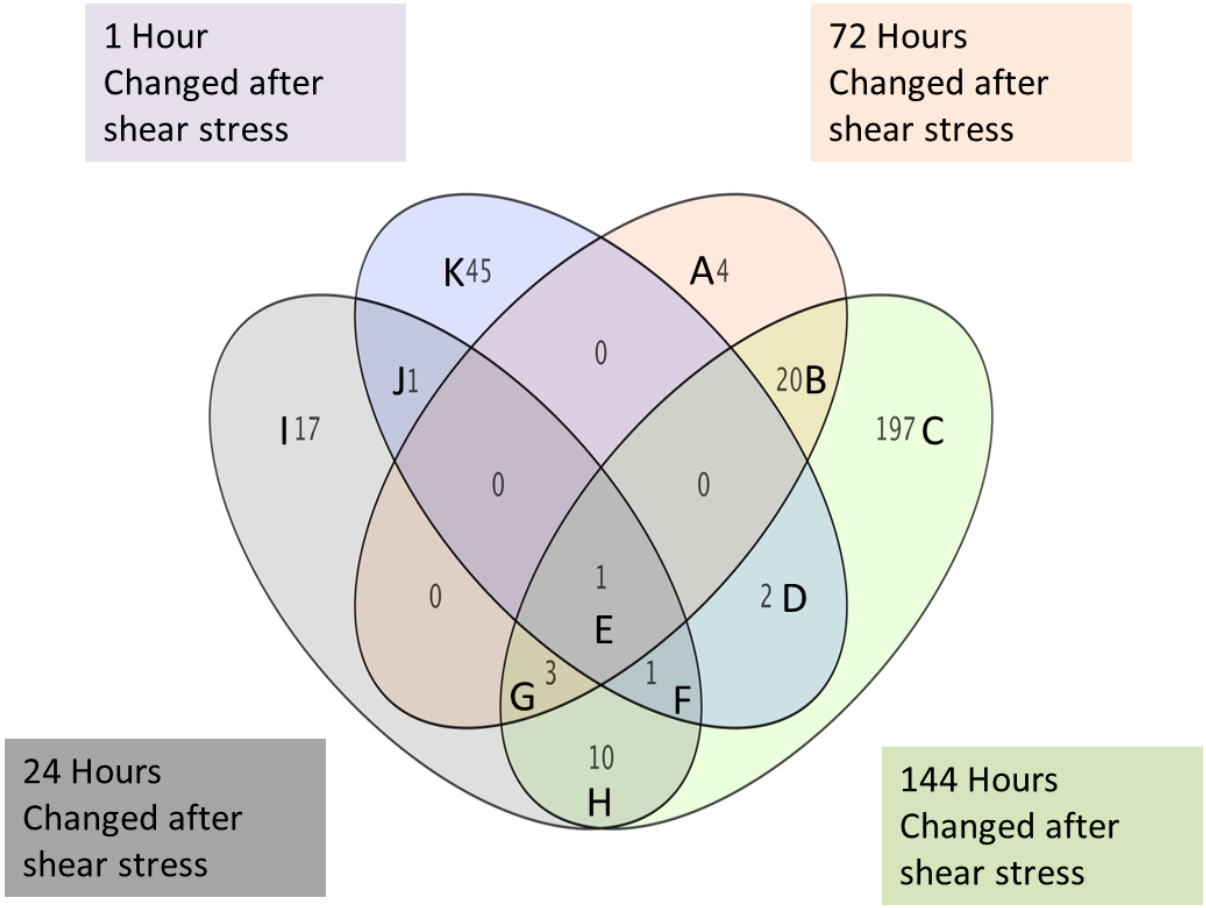

Figure 7.16 Venn diagram showing overlap in genes with altered expression levels due to shear stress at each of the 4 timepoints analysed

Each segment with expressed genes is allocated a unique letter code

A. 72 hours

B. 72 hours and 144 hours

C. 144 hours

D. 1 hour and 144 hours

E. 1 hour, 24 hours, 72 hours, 144 hours

F. 1hour, 24 hours, 144 hours

G. 24 hours, 72 hours, 144 hours

H. 24 hours, 144 hours

I. 24 hours

J. 1 hour, 24 hours

K. 1 hour

B. 72 hours and 144 hours

Abbreviation	Full Name	Function	How changed
ADCY4	Adenylate cyclase 4	Catalyst in the formation of the secondary messenger cyclic adenosine monophosphate (cAMP)	72 hours, 144 hours
ARHGEF3	Rho guanine nucleotide exchange factor (GEF) 3	Signal Transduction	72 hours, 144 hours
ASS1	argininosuccinate synthase 1		72 hours, 144 hours
CLEC3B	C-type lectin domain family 3, member B	Cell response to TGF-B signalling	72 hours, 144 hours
DNASE1L3	Deoxyribonuclease I-like 3	DNA hydrolysis in apoptosis	72 hours, 144 hours
ENTPD1	Ectonucleoside triphosphate diphosphohydrolase 1	Cell adhesion	72 hours, 144 hours
FAM167B	Family with sequence similarity 167, member B	Unknown	72 hours, 144 hours
FCN3	Ficolin (collagen/fibrinogen domain containing) 3 (Hakata antigen)	Activator of the complement pathway	72 hours, 144 hours
FUK	Fucokinase	Utilisation of free fucose, involved in inflammation	72 hours, 144 hours
ITGB4	integrin, beta 4	Cell adhesion, cell junction assembly	72 hours, 144 hours
LOC340274	argininosuccinate synthetase 1 pseudogene 11	ASS-1 transcriptional regulation	72 hours, 144 hours
LOC392871	argininosuccinate synthetase 1 pseudogene 11 variant	ASS-1 transcriptional regulation	72 hours, 144 hours
LOC652968	GATS protein-like 3	Unknown	72 hours, 144 hours
MN1	Meningioma (disrupted in balanced translocation) 1	Unknown	72 hours, 144 hours
MRAS	muscle RAS oncogene homologue	Actin cytoskeleton organisation	72 hours, 144 hours
SLCO2A1	solute carrier organic anion transporter family, member 2A1	Prostaglandin transporter, PGE2 and PGH2 across membranes	72 hours, 144 hours
TNFRSF12A	tumor necrosis factor receptor superfamily, member 12A	Weak inducer of apoptosis and IL-6	72 hours, 144 hours
TSC22D3	TSC22 domain family, member 3	Anti-apoptotic transcriptional regulator	72 hours, 144 hours
VWCE	von Willebrand factor C and EGF domains	B-catenin signalling	72 hours, 144 hours
ZMIZ1	zinc finger, MIZ-type containing 1	Transcriptional regulator	72 hours, 144 hours

Table 7.6 Genes commonly influenced by shear stress across multiple timepoints ***(Continues on next page)***

D. 1 hour and 144 hours

Abbreviation	Full Name	Function	How changed
CXCL2 7	Chemokine (C-X-C motif) ligand 2	Inflammatory mediator, chemotaxis	1 hour, 144 hours
DDIT4	DNA-damage-inducible transcript 4	Apoptosis, negative regulator of mTOR	1 hour, 144 hours

E. 1 hour, 24 hours, 72 hours, 144 hours

Abbreviation	Full Name	Function	How Changed
KLF4	Kruppel-like factor 4	Atheroprotective, ASS-1 regulator	1 hour, 24 hours, 72 hours, 144 hours

F. 1 hour, 24 hours, 72 hours

Abbreviation	Full Name	Function	How changed
KLF2	Kruppel-like factor 2	Atheroprotective, negative regulator of IL-1 and IL-6	1 hour, 24 hours, 72 hours

G. 24 hours, 72 hours, 144 hours

Abbreviation	Full Name	Function	How changed
C1orf115	Chromosome 1 open reading frame 115	Unknown	24 hours, 72 hours, 144 hours
HSPA12B	Heat shock 70kDa protein 12B	Association with susceptibility to atherosclerosis	24 hours, 72 hours, 144 hours
TEK	Tyrosine kinase, endothelial	Positive regulator of endothelial proliferation	24 hours, 72 hours, 144 hours

Table 7.6 Genes commonly influenced by shear stress across multiple timepoints

(Continues on next page)

H. 24 hours and 144 hours

Abbreviation	Full Name	Function	How changed
c20orf160	Chromosome 20 open reading frame 160	Unknown	24 hours, 144 hours
HEG1	HEG homologue 1 (zebrafish)	Cell-Cell junction formation	24 hours, 144 hours
KIT	v-**kit** Hardy-Zuckerman 4 feline sarcoma viral oncogene homologue	Actin cytoskeleton regulation, cytokine signalling	24 hours, 144 hours
LXN	Latexin	Tissue carboxypeptidase inhibitor	24 hours, 144 hours
NDRG1	N-myc downstream regulated 1	Mitosis, cell cycle control	24 hours, 144 hours
NOS3	Nitric oxide synthase 3	Vasodilator	24 hours, 144 hours
PLAT	Plasminogen activator, tissue	Cell migration	24 hours, 144 hours
RAPGEF5	Rap guanine nucleotide exchange factor (GEF) 5	Signal transduction	24 hours, 144 hours
STARD8	StAR-related lipid transfer (START) domain containing 8	Regulator of GTPase mediated signal transduction	24 hours, 144 hours
TMEM173	Transmembrane protein 173	Activation of innate immune response	24 hours, 144 hours

J. 1 hour and 24 hours

Abbreviation	Full Name	Function	How Changed
C10orf10 2	chromosome 10 open reading frame 10	Elk-1 transcriptional activation	1 hour, 24 hours

Table 7.6 Genes commonly influenced by shear stress across multiple timepoints

(Continues on next page)

Table 7.6 Genes commonly influenced by shear stress across multiple timepoints (<u>Continued from previous page</u>)

Where a gene is commonly influenced between 2 or more of the timepoints at which transcriptomic analysis was carried out it is reported in this table. Where expression is above average the timepoint listed has been coloured red. Where expression is below average it has been coloured green.

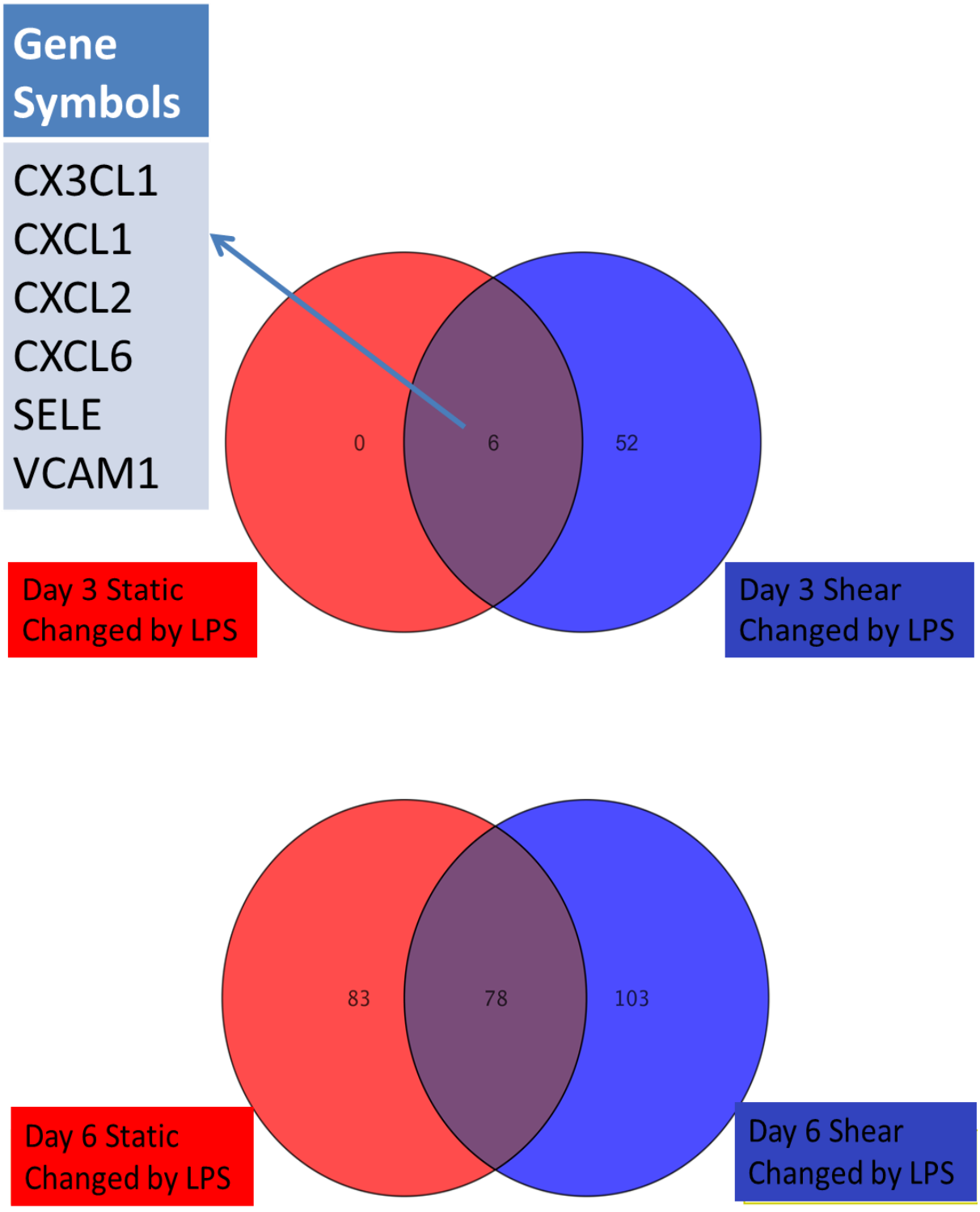

Figure 7.17 Venn Diagrams highlighting the number of common genes changed by 4 hours exposure to 1µg/ml LPS in static vs. sheared HAEC

HAEC were cultured for 72 hours/3 days and 144 hours/6 day. 4 hours before conclusion of the experiment the cells were treated with E.coli LPS. Common genes influenced by LPS treatment in both static and sheared cells are shown in the region of overlap between the red circle (static) and the blue circle (shear).

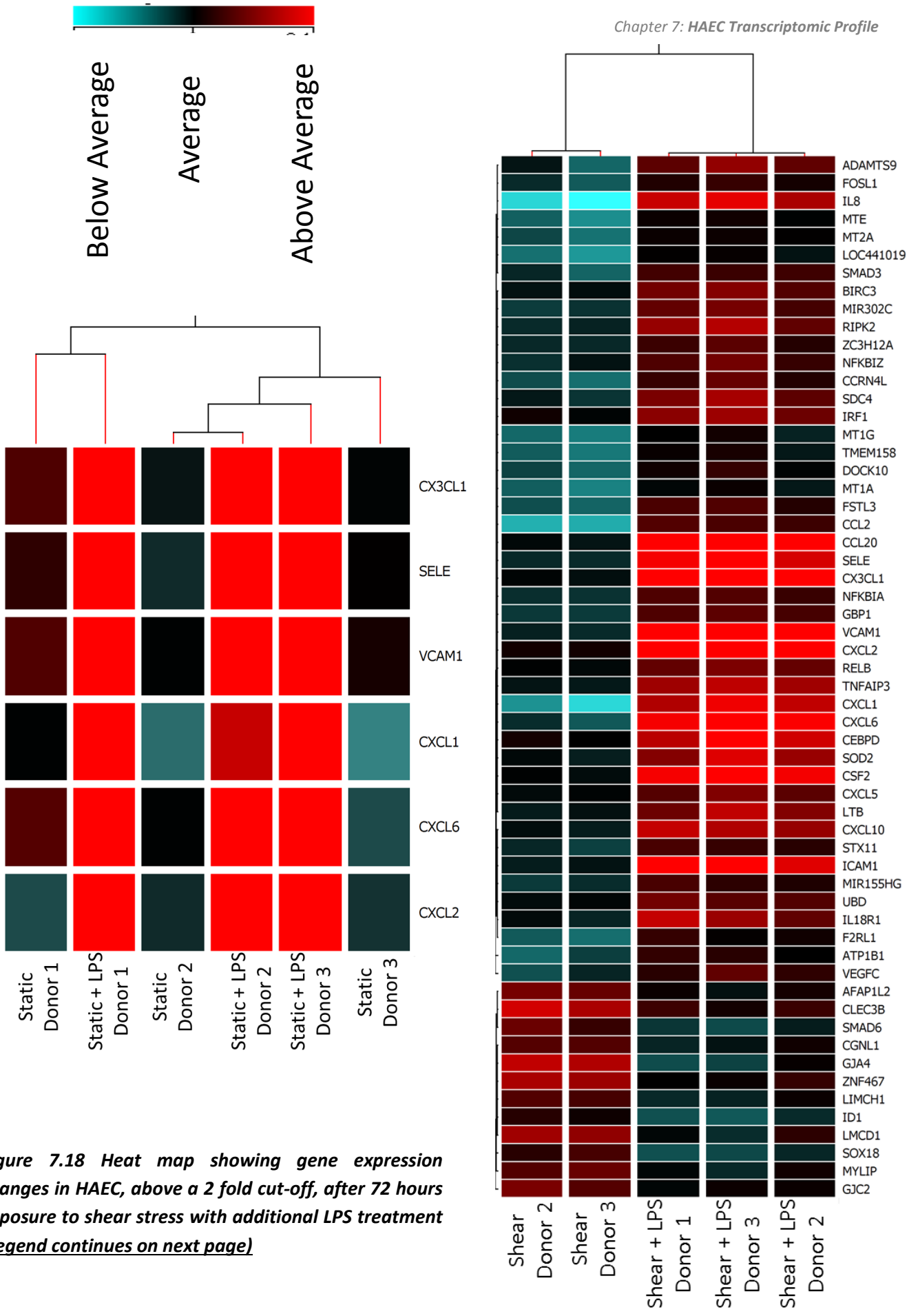

Figure 7.18 Heat map showing gene expression changes in HAEC, above a 2 fold cut-off, after 72 hours exposure to shear stress with additional LPS treatment

(Legend continues on next page)

.

Figure 7.18 Heat map showing gene expression changes in HAEC, above a 2 fold cut-off, after 72 hours exposure to shear after additional LPS treatment (<u>Legend continued from previous page)</u>

Normalised intensity values represented as a heat map of HAEC cultured under static conditions versus HAEC cultured under shear stress for 72 hours ± 1µg LPS for the final 4 hours. Red indicates above average fluorescence intensity for a gene, suggesting higher expression levels. Turquoise indicates below average fluorescence intensity, suggesting reduced levels of expression. Samples were hierarchically clustered using Pearson's centred distance metric and Ward's linkage rule, the shorter the line indicating the clustering the closer the relationship between samples.

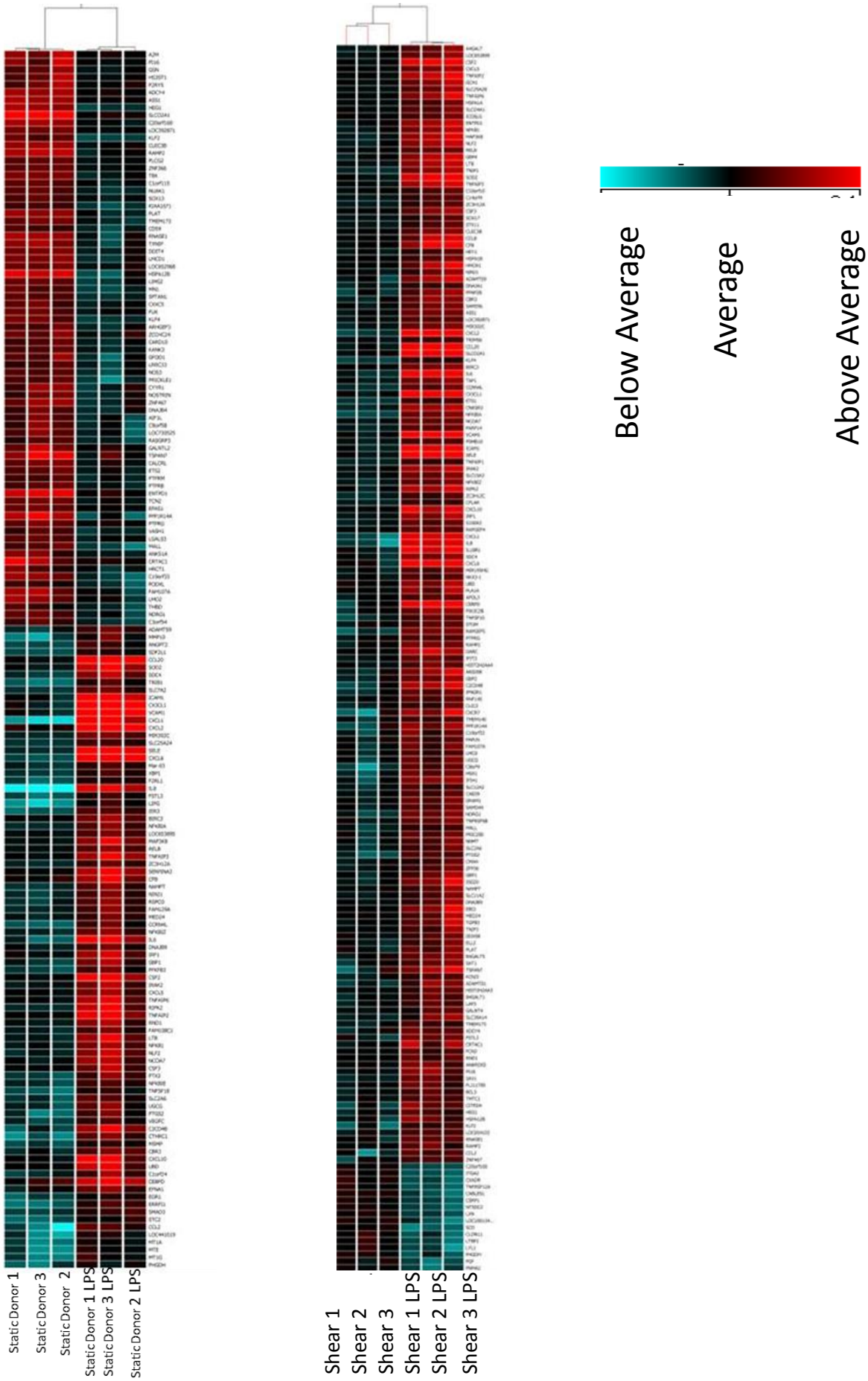

Figure 7.19 Heat map showing gene expression changes in HAEC, above a 2 fold cut-off, after 144 hours exposure to with additional LPS treatment ***(Legend continues on next page)***

Figure 7.19 Heat map showing gene expression changes in HAEC, above a 2 fold cut-off, after 144 hours exposure to shear stress with additional LPS treatment <u>(Legend continued from previous page)</u>

Normalised intensity values represented as a heat map of HAEC cultured under static conditions versus HAEC cultured under shear stress for 144 hours ± 1µg LPS for the final 4 hours. Red indicates above average fluorescence intensity for a gene, suggesting higher expression levels. Turquoise indicates below average fluorescence intensity, suggesting reduced levels of expression. Samples were hierarchically clustered using Pearson's centred distance metric and Ward's linkage rule, the shorter the line indicating the clustering the closer the relationship between samples.

Summary

HAEC align in response to shear stress in a time and shear level dependent manner in a 6-well plate model of orbital stress.

Transcriptomics results have failed to provide evidence that a short term shear stress stimulus is registered as an inflammatory event by endothelial cells. Indeed, at a time point as early as 1 hour there appears to be some negative regulation of inflammatory cytokine RNA transcription. However, the limited overlap between genes influenced by shear stress at different points in the time course suggests that the up and downregulation of RNA expression is a transient event and that the cell cycle may be the key driver of expression. Therefore to study genes only at a single timepoint may not provide the most reliable data.

A major finding of this study was that shear stress seemed to have a protective effect on HAEC under basal conditions and when challenged with an acute inflammatory stimulus. In terms of protein expression a reduced level of the inflammatory mediators ET-1 and CXCL8/IL-8 was seen in HAEC cultured under shear stress. When looking at mRNA expression HAEC cultured under shear stress were much more responsive to inflammatory stimuli than HAEC cultured under static conditions. This increased responsiveness may mean that HAEC under shear are able to mount an increased immune response when required.

Focusing on expression of specific genes corresponding to proteins dealt with in earlier chapters mRNA expression largely reflected what had been seen on a protein level. COX-1 and COX-2 mRNA were unchanged by shear stress. In keeping with ET-1 release data shown in Chapter 6 mRNA for ET-1 was downregulated with shear stress. This was particularly clear at early timepoints.

Discussion

Chapter 8

Since discovery of its role in maintenance of vascular health and homeostasis, study of the endothelium has been of great interest to scientists. Due to its relative inaccessibility, being as it lines the inside of blood vessels, cell culture models have been a preferred means of doing so however, the culture environment, outside of the pulsatility of blood flow, may not provide an accurate representation of physiological conditions. The hypothesis set out in this thesis was, that in its natural environment the endothelium is subject to shear stress and understanding the influence of shear stress is thus critical to our understanding of vascular biology.

A PubMed search with the key word 'endothelium' reveals 135032 papers but when 'endothelium' is searched in conjunction with 'shear stress' numbers are reduced to 2859. Closer study of these papers reveals that in the majority of cases where cell cultures have been used and shear stress has been considered it has been maintained for less than 24 hours, and in most cases less than 3 hours. Part of my hypothesis was that this short duration was not physiological and was possibly even an inflammatory stimulus. The major reason behind the general acceptance of such short lengths of time is the lack of suitable culture methods for exposure of cells to long durations of shear stress. The major aim of this thesis was thus to validate an orbital shaker model of shear stress for long term culture of endothelial cells. This validation took the form of morphological studies and studies at the protein and genetic level.

Cultured cell morphology

In Chapter 3 I showed that shear stress, in the orbital shaker model, influenced PAEC elongation and alignment. Cells were more aligned where they experienced the greatest gradient of shear stress and the highest peak shear, despite the mean shear being the same. Assessment of these physical changes through examination of the cell border, based on visualisation of CD31 and VE-cadherin and scoring by eye, led to the re-evaluation of the model by mathematicians. This resulted in the subsequent discovery that, in this model, shear stress gradient was not the only variable but that direction of medium flow was also altered. Where there was the greatest gradient of shear and where cells were elongated and aligned flow had a preferred direction. Where shear stress magnitude was relatively

low and constant there was no preferred direction in medium flow and cells were less likely to be elongated. These elongation and alignment changes began within 24 hours but were not fully established until later time-points. Once shear stress ceased the changes were fully reversible within 24 hours with cell movement seen in as little as 1 hour. Fixed cells were imaged using confocal microscopy and live cells were imaged using SICM.

These morphological changes were consistent with those reported using other means to model shear stress (Levesque *et al.*, 1985), but less research has focused on the role of directionality as the primary determinant in cell morphology, rather than magnitude of shear stress. Directionality of flow is an important consideration. Low shear stress in the vasculature is often associated with oscillatory flow and particularly regions where there is flow reversal and stagnation. The mechanisms by which cells sense shear stress may also be sensitive to the direction of flow by, for example their positioning on the cell surface. Consideration of direction may be more important than shear stress magnitude in future characterisation of *in vivo* flow profiles. Interruptions and backflow are associated with a number of inflammatory vascular conditions, including deep vein thrombosis and pulmonary hypertension (Bergan *et al.*, 2006), which occur in regions not associated with the development of atherosclerosis.

Elongation and alignment changes were seen in cells of both humans and pigs. This was to be expected in the case of aortic endothelial cells as both species are of a similar size and heart rate and thus would be expected to have been in a similar shear stress environment but it was interesting to note that HUVEC, which as cells resident of a vein would have been likely to experience reduced shear stress, also responded in the same way to the shear stress profile in the model. There was a similar response from cells of the pulmonary artery which experiences a considerably reduced blood pressure and of blood outgrowth endothelial cells. The origins of blood outgrowth endothelial cells are not well understood. It has been suggested that they are released into the circulation from the bone marrow in response to vascular injury or alternatively that they circulate in the blood having detached from the vascular wall, in either case it is difficult to estimate the profile of shear they would experience. The similar response of all these cells suggests that there is a limited influence of a cells environment before culture on its ability to respond to mechanical changes, at

least in terms of an adaptation of morphology. By changing the size of the dish in which cells are grown, the depth of the medium and the rotational speed of the shaker it would be possible to develop a situation where a number of shear profiles could be modelled and each used for the culture of cells in a shear environment most similar to what the cells would see *in vivo*.

PAEC were initially used in the model as their use had previously been validated by our group (Warboys *et al.*, 2010) but as the most relevant model for understanding the human vasculature should be human cells and because more accurate transcriptomics information can be obtained from human cells due to the more complete characterisation of the human genome the decision was made to switch to HAEC. The similar behaviour of HUVEC in the model in terms of alignment and the fact that they are the preferred human endothelial type used in in vitro culture meant that HUVEC could have been a candidate cell type to use. However, there are numerous documented differences between HUVEC and cells of the mature vasculature as HUVEC are a foetal cell type rather than a mature adult one so the decision was made to use HAEC. As donor tissue was not available these had to be purchased commercially which unfortunately meant that we did not have a patient history and it is highly likely that these patients would have suffered from some level of atherosclerosis which would have differed between patients. In spite of this hierarchical clustering in the transcriptomics studies seemed to show that the majority of the variation between treatment groups rather than donor identities.

In vivo cell morphology

Having confirmed the possibility of the usage of the orbital shaker model of shear stress long term, it was important to confirm the similarity in phenotype to cells of the native endothelium. Pilot data in cells of the porcine valve, known to experience low turbulent flow and high directional flow respectively, supported the observation that endothelial cells in the model were of similar morphologies to that of native tissue, as did corresponding images obtained from the mouse aortic arch. However, observations in the porcine aorta were not as anticipated. It was expected that cells of the inner curvature of the arch would

be cobble-stone in nature and cells of the outer curvature would be elongated and aligned. This was not always clearly seen in the tissue sections sampled. Possibly this was due to the difficulty in accurately extracting small regions from a large tissue and ensuring they are from comparable areas when working with tissue from different animals, with different vessel geometry. However, it may also be explained by an absence of variation in shear stress levels between the two regions. Our group has recently published that shear stress levels in the mouse aorta may not be as clear cut as first assumed and that there may be some controversy surrounding reported levels of shear stress in the mouse arch (Van Doormaal *et al.*, 2012). For this reason it would perhaps have been more appropriate to select a region of more clearly defined shear stress profile and a smaller region of tissue such as the coronary artery. Coronary artery was not initially considered as however supply of fresh tissue was more difficult to guarantee. Others sampling the porcine aorta have used a template to try to ensure regions sampled were the same in all cases, however as geometry is not the same in all animals this method is also not without problems. The only way to ensure that shear stress levels in the regions sampled are as expected is to perform CFD analysis for the geometry of the particular vessel being studied. This would only be possible with access to a facility for prior imaging of the animals and would rely on access to the animals prior to their slaughter unlike in the cases of the tissue received from abattoir.

Though clear cell elongation was not demonstrated in porcine aortic arch through confocal imaging it did appear to be present in images obtained using SICM. Measurement of elongation of cells obtained this way showed a trend for elongation in the cells of the outer curvature of the arch. The reasons for such a difference between results of confocal microscopy and results of SICM are not clear but may relate to the condition of the tissue. SICM was used to image live tissue whereas for confocal imaging tissue had to be fixed in formaldehyde and then pressed between glass slide and coverslip, which may have had an impact on cell shape. With SICM only comparatively small regions of tissue were scanned (80 X 80µM as opposed to 385.5 X 385.5µM) and this may have masked a lack of continuity in shape that would have been seen in larger areas. Most encouraging was the similar compliance values obtained from cells of the outer curvature of the arch and elongated cultured cells suggesting a similar change in physical properties. Compliance values of cells of the inner curvature of the aortic arch were also similar to those of cells grown in static

culture. It is likely that compliance is strongly influenced by actin cytoskeletal structure and these rearrangements are the direct result of shear. It would be interesting to directly correlate the two now that the SICM has been adapted to be able to record fluorescence. A fluorescently labelled anti-filamentous actin could be used and areas between and directly on the fibres could be tested. An alternative hypothesis is that compliance values could be directly influenced by cell surface glycocalyx coverage. There has been some debate as to whether the glycocalyx is present on cultured cells but recently obtained imaging data seems to suggest that it is. If glycocalyx surface structure was significantly different between elongated and aligned cells and cobblestone cells the presence of the structure which is highly hydrophobic could impede deformation due to liquid. This was not something that we tested with these cells but others in our group studying leaflets of the aortic valve were able to successfully treat two phenotypes of cells shown on either side of the valve with numerous enzymes which would degrade specific components of the glycocalyx. Treatment with such enzymes seemed to reverse compliance findings with elongated and aligned cells becoming more compliant and cobblestone cells less compliant. Which component of the glycocalyx was the cause behind this change and why these enzymes should be able to make cells less compliant is the subject of on-going investigation.

To ensure correlation of SICM stiffness results between different cells the highest point of the cell was probed each time. This is likely to have been the area of the cell membrane directly over the nucleus. Compliance values may therefore reflect a change in nuclear size and composition. It would be interesting to see how compliance varied between the high point and low points of the cell but limitations in the throughput of the technique made that this was not possible for this thesis.

This was the first time that SICM had been used for imaging a tissue as large and thick as the aorta. In its current state the system is more suitable for analysing individual cells rather than tissues due to the length of time required for the very small and precise movements of the pipette tip and stage. To gather a single 80 x 80µM image of good resolution can take as long as 20 minutes and with no heating chamber means that cells and tissues are left at around 22^{o}C rather than the 37^{o}C temperatures that would normally be used in maintaining live cell experiments. However, with increasing improvements in technology I am optimistic

about the future of the technique for this kind of imaging. The non-contact nature of the technique makes it a very promising means for gathering accurate cell profile data as it appears to be much less damaging than the cantilever involved in alternative technique atomic force microscopy.

Cell production of genes/proteins

Having established that cell mechanical properties were indeed similar between cells cultured in the shear stress model and elongated and aligned cells of the native tissue it was important for me to study how shear stress in the model influenced the regulation of protein expression. Shear stress is thought to be a transcriptional regulator of a number of genes, which lead to protection of cells that experience high shear stress from the build-up of atherosclerotic plaque. I identified vasoactive mediators of particular interest for study using immunohistochemistry. The first was COX, a protein associated with production of the protective protein Prostaglandin. Controversy has surrounded the issue of the dominant isoform of COX in the endothelium since urinary metabolite studies were used to support the idea that the major source of prostacyclin was endothelial COX-2(McAdam *et al.*, 1999). Though little evidence had been seen for the presence of COX-2 in the native endothelium through immunohistochemistry it was suggested that it was not found because of the absence of shear stress. In order to investigate this hypothesis numerous short term studies were carried out by a number of research groups in which cells were exposed to shear stress for less than 24 hours and mRNA measured(Di Francesco *et al.*, 2009; Doroudi *et al.*, 2000; Topper *et al.*, 1996). In Chapter 4 it is shown that COX-2 protein is not detected in porcine cells exposed to shear stress for either 24 hours or 7 days. In Chapter 7 it can be seen that COX-2 mRNA production is transiently increased in both static and sheared cells at the time of plating but is at similar below average levels in both static and sheared cells at all late time-points. As the transient COX-2 increase is seen in both static and sheared cells it is most likely due to be because the cells are not 100% confluent. A general absence of COX-2 in the healthy endothelium is supported by a body of other experiments carried out in our group in static cells and murine tissue from the heart and lungs of wild-type mice as well as mice which have had the genes for COX-1 and COX-2 selectively deleted (Kirkby *et al.*, 2012). These findings are important as they show that inhibition of vascular COX-2 is not

the cause of the adverse cardiovascular side effects associated with the use of COX-2 selective and classic NSAIDs. This finding invites increased research into the true nature of these side effects, which may potentially lead to the development of drugs with an improved safety profile.

Though in the case of COX no evidence of shear induced regulation was found that is not to say that no genes are influenced by shear. I showed that eNOS/NOSIII is significantly upregulated by shear in terms of protein expression, based on immunofluorescence after 5 days of shear and that mRNA expression is higher than in static cells at a number of time-points. It seems protective genes may be activated by shear but further research is required into which are the most active. I would imagine that the most important genes regulated by shear are transcriptional regulators which inhibit transcription of inflammatory genes. A transcriptomics time-course showed that at numerous timepoints over a 144 hour period inflammatory cytokines were reduced in mRNA expression compared to in their static counterparts. This is of course only the beginning of the story and more data will be elucidated from follow up experiments in which it will be possible to differentiate between the two distinct shear profiles in the well for mRNA analysis. In experiments carried out by others, where shear was not determined computationally, an orbital shaker was used and cells cultured only in specific regions, based on the placement of silicon gaskets to inhibit cell attachment(Dardik *et al.*, 2005). Such a system should be possible to use in both the Transwell™ and 6-well plate systems in this model, though some optimisation will be required to ensure a suitable yield of RNA can be gathered. Utilisation of advanced techniques such as Mass-Spectrometry Imaging will also allow even broader analysis of regions in the well, even going as far as to map surface molecules to differentiate between neighbouring cells with subtly different levels of shear.

Response of endothelial cells to inflammatory stimulus

Having established that endothelial cell behaviour in the orbital shaker model had many similarities to that of native tissue I continued with the model noting how cells would behave under conditions of inflammatory stress. LPS was used as an inflammatory stimulant. Bacteria have been associated with atherosclerotic plaques, with Gram negative bacteria known to cause gum disease isolated from a number of autopsy specimens (Koren

et al., 2010; Kozarov *et al.*, 2005). An inappropriate response to an inflammatory stimulus may be a contributing factor to the initiation or exacerbation of plaque development and arterial remodelling.

Initial studies showed that LPS treatment led to the migration of CD31 away from endothelial cell borders and its redistribution throughout the cytoplasm. CD31 is thought to act as a signalling molecule in the sensing of shear stress (Tzima *et al.*, 2005). It is also important in the regulation of lymphocyte binding to the endothelium. This change in localisation of CD31 is important as it is known to be associated with a change in the proteins role from one of control of lymphocyte migration through the cell junctions to one of macrophage attraction for engulfment of dead cells. It has been shown to be activated through the inflammatory cytokine TNFα (Shaw *et al.*, 2001). Though this observation was not quantitatively assessed it supports the theory that shear stress protects cells from LPS-induced apoptosis. This is reinforced by data showing cell number is more greatly reduced with LPS treatment in the absence of shear and that static cells that have been treated with LPS are larger.

Polymorphisms in the human form of CD31 may be associated with increased risk of cardiovascular events and increased risk of atherosclerosis (Andreotti *et al.*, 2002). . Studies have also shown that in mice, where NFkB seems to be activated in response to oscillatory flow no activation is seen where CD31 is knocked out (Chen *et al.*, 2009). These findings together seem to suggest that CD31 has an important role to play in the development and progression of atherosclerosis.

In both static and sheared endothelial cells in both regions of the well 24 hours of LPS treatment triggered production of the inflammatory mediator COX-2. COX-2 immunoreactivity appeared to be at a similar level in both static and sheared cells which suggested a similar response to inflammatory stimulus. In the experiments where cells had been treated with LPS for 7 days there was no significant upregulation of COX-2 immunofluorescence, it is possible that this may be because the cells had become refractory to the LPS. This is a phenomenon that has been described by others (Ogawa *et al.*, 2003) and for this reason the decision was made that in future experiments with LPS the

treatment period would only be for a period of hours rather than days. It would be interesting to look at the time-scale in which this LPS desensitisation occurred. Transcriptomics data suggested that sheared cells showed a reduced expression of inflammatory cytokines compared to static cells so it may be that they would take longer to reach tis refractory stage.

COX-2, along with a number of other LPS inducible genes, is known to be partially under the regulation of the transcription factor NFkB (Appleby, 1994; Crofford *et al.*, 1997) and so it was of interest to investigate how the appearance of this was influenced by shear. NFkB is normally held inactive in the cytoplasm but translocates to the nucleus when active. Looking at the distribution of NFkB between the nucleus and the cytoplasm in unstimulated conditions, between static and sheared cells there was no difference in immunoreactivity. LPS treatment leads to NFkB activation and it was interesting to see that NFkB was more nuclear at the shear edge than elsewhere. This was contrary to expectations when thinking of directional shear stress as a protective force. However, it may simply be that shear stress effects the time period in which NFkB is active. It is also important to remember that NFkB also activates the transcription of protective genes as well as inflammatory genes. To further investigate the time dependent changes in LPS that may be occurring when performing the RNA assay two timepoints were also assayed after 4 hours of LPS treatment. These were the 72 hour and 144hour timepoints. As anticipated there was a considerable difference in response between static and sheared cells. At the 72 hour timepoint many more differences were identified in sheared cells in response to LPS than in static cells. The majority of altered genes were for inflammatory cytokines. This suggested an increased sensitivity of the sheared cells to inflammatory stimulus. This increased response may mean that in cells under shear inflammation is resolved faster than in static cells. Interestingly at the 144 hour timepoint many more genes were influenced by LPS treatment. This may be due to some form of global transcriptional event occurring in the 72 hours between sampling. Many genes changed in both static and shear LPS challenged situations are those for inflammatory cytokines.

More work is necessary in order to establish the full changes in pathway regulation that come about due to the presence of shear stress.

Suitability of the Model

The orbital shaker model offers the opportunity to study cells exposed to different shear profiles and different directions of flow over chronic time periods which would certainly seem to be more accurate in terms of physiological modelling but it is difficult to arbitrarily make a cut-off as to which duration of shear would provide the conclusive physiological environment. As seen in the transcriptomics chapter regulation of gene expression is continually changing and is under the influence of many factors. It is also important to note that endothelial cells *in vivo* are subject to additional forces such as cyclic stretch as the vessel contracts and relaxes as well as negative feedback from other cell types including vascular smooth muscle, platelets and leukocytes.

Cyclic stretch can be modelled using a cell stretching device (Moore *et al.*, 1994) but such a device is difficult to operate in conjunction with shear stress and long term culture is difficult to sustain. Cyclic stretch is often seen as a force of lesser importance than the regulation of atherosclerosis however it has been shown to have a role in the regulation of reactive oxygen species (Birukov, 2009).

The utilisation of a Transwell™ system means that co-culture of smooth muscle cells would be possible in the model and it would be interesting to see how their presence would affect vascular mediator release and gene expression, however the nature of separation between the two layers by a flexible membrane would be substantially different from the in vivo situation as the same junctional proteins would not be present. Because of the nature of the Transwell™ requiring medium in both compartments it is also likely that the smooth muscle cells would directly experience shear stress through the movement of the shaker and this would also not be physiological. How smooth muscle cells respond to shear stress is a subject of interest though. Unpublished data from our group looking at mouse tissue samples suggests that smooth muscle is arranged parallel to the endothelial cell layer above and it would be interesting to see how this is influenced by shear stress. It would also be interesting to see how shear stress affects the adhesion of platelets and monocytes through co-incubation of them in the model.

The overall complexities of the vascular system make it very difficult to develop a model that is fully physiological and to still be able to take away meaningful outcomes from the results. The orbital shaker model is at least useful for assessing the impact of shear stress alone and with better understanding of this other areas of importance will likely emerge.

In order to fully optimise the model it would be preferential that a greater number of research groups study shear stress magnitude in human subjects with state of the art technology rather than relying on historical measurements which may have inaccuracies.

Future use of the model

The orbital shaker offers the advantage of being able to expose large numbers of cells to shear stress simultaneously through stacking multiple 6-well plates atop one another. This advantage is likely to be beneficial in cases where shear stress exposure needs to be scaled up as would be necessary as would be necessary in conducting future experiments for pharmacological testing. Recent years have seen the emergence of stem cell technology, allowing the development of replacement organs and vessels. This kind of technology currently relies on the *in vitro* culture of cells before their injection (Parikh *et al.*, 2000) or transfer onto a scaffold (Gulbins *et al.*, 2004) before being transplanted into a patient. Results in this thesis showed that endothelial cells that were exposed to shear stress overall had a less inflamed phenotype compared to cells cultured under static conditions. It may be that performance of such cells for vascular benefit could be improved by exposure to shear stress though as alignment changes are rapid after shear ceases it is not yet known how long this anti-inflammatory phenotype may persist.

Concluding Statement

In this thesis I have demonstrated that an orbital shaker is a viable model for long term culture of endothelial cells under shear stress conditions. I have used a number of techniques to characterise endothelial cells in this model and have shown that in both conventional 6-well plates and 6 well plates with Transwell™ inserts two distinct profiles of shear stress are present directional high shear stress and non-directional low shear stress which can be used to represent atheroprotected and atheroprone environments of shear respectively.

My hypothesis was that short term exposure to shear stress may act as an inflammatory stimulus and was not truly representative of the environment in the vasculature. Though I have seen no evidence of inflammation due to shear stress I have shown that shear stress changes cell morphology, structural properties and proteomic and transcriptomic properties in a time dependent manner and that changes are still occurring well beyond the 24 hour time-point, by which most shear stress experiments previously conducted had concluded.

Evidence in this thesis suggests that shear stress is a protective force leading to reduced production of inflammatory cytokines under conditions of immune system challenge as well as control systems and further investigation is warranted into the mechanisms behind this.

Aird WC (2012). Endothelial Cell Heterogeneity. *Cold Spring Harbor Perspectives in Medicine* **2**(1).

Aird WC (2007). Phenotypic Heterogeneity of the Endothelium. *Circulation Research* **100**(2)**:** 158-173.

Ando J, Nomura H, Kamiya A (1987). The effect of fluid shear stress on the migration and proliferation of cultured endothelial cells. *Microvascular Research* **33**(1)**:** 62-70.

Andreotti F, Porto I, Crea F, Maseri A (2002). Inflammatory gene polymorphisms and ischaemic heart disease: review of population association studies. *Heart* **87**(2)**:** 107-112.

Appleby SBR, A; Neilson, K; Narko, K; Hla, T (1994). Structure of the human cyclo-oxygenase-2 gene. *Biochem. J.* **302**(3)**:** 723-727.

Bagi Z, Frangos JA, Yeh J-C, White CR, Kaley G, Koller A (2005). PECAM-1 Mediates NO-Dependent Dilation of Arterioles to High Temporal Gradients of Shear Stress. *Arteriosclerosis, Thrombosis, and Vascular Biology* **25**(8)**:** 1590-1595.

Barakat A, Lieu D (2003). Differential responsiveness of vascular endothelial cells to different types of fluid mechanical shear stress. *Cell Biochem Biophys* **38**(3)**:** 323-343.

Barakat AI, Karino T, Colton CK (1997). Microcinematographic studies of flow patterns in the excised rabbit aorta and its major branches. *Biorheology* **34**(3)**:** 195-221.

Bazzoni G (2006). Endothelial Tight Junctions: Permeable Barriers of the Vessel Wall. *Thrombosis and Haemostasis* **95**(1)**:** 1-204.

Bazzoni G, Dejana E (2004). Endothelial Cell-to-Cell Junctions: Molecular Organization and Role in Vascular Homeostasis. *Physiological Reviews* **84**(3)**:** 869-901.

Bergan JJ, Schmid-Schönbein GW, Smith PDC, Nicolaides AN, Boisseau MR, Eklof B (2006). Chronic Venous Disease. *New England Journal of Medicine* **355**(5)**:** 488-498.

Bidarra SJ, Barrias CC, Barbosa MA, Soares R, Amédée J, Granja PL (2011). Phenotypic and proliferative modulation of human mesenchymal stem cells via crosstalk with endothelial cells. *Stem Cell Research* **7**(3)**:** 186-197.

Birukov KG (2009). Cyclic Stretch, Reactive Oxygen Species, and Vascular Remodeling. *Antioxidants & Redox Signaling* **11**(7)**:** 1651-1667.

Bogle RG, Baydoun AR, Pearson JD, Mann GE (1996). Regulation of L-arginine transport and nitric oxide release in superfused porcine aortic endothelial cells. *The Journal of Physiology* **490**(Pt 1)**:** 229-241.

Bombardier C, Laine L, Reicin A, Shapiro D, Burgos-Vargas R, Davis B*, et al.* (2000). Comparison of upper gastrointestinal toxicity of rofecoxib and naproxen in patients with rheumatoid arthritis. *New England Journal of Medicine* **343**(21)**:** 1520-1528.

Boulanger C, Lüscher TF (1990). Release of endothelin from the porcine aorta. Inhibition by endothelium-derived nitric oxide. *The Journal of Clinical Investigation* **85**(2)**:** 587-590.

Brooks AR, Lelkes PI, Rubanyi GM (2002). Gene expression profiling of human aortic endothelial cells exposed to disturbed flow and steady laminar flow. *Physiol. Genomics* **9**(1)**:** 27-41.

Buga GM, Gold ME, Fukuto JM, Ignarro LJ (1991). Shear stress-induced release of nitric oxide from endothelial cells grown on beads. *Hypertension* **17**(2)**:** 187-193.

Bussolari SR, Dewey CF, Gimbrone MA (1982). Apparatus for subjecting living cells to fluid shear stress. *Review of Scientific Instruments* **53**(12)**:** 1851-1854.

C. F. Dewey J, Bussolari SR, M. A. Gimbrone J, Davies PF (1981). The Dynamic Response of Vascular Endothelial Cells to Fluid Shear Stress. *Journal of Biomechanical Engineering* **103**(3)**:** 177-185.

Caro CG (2009). Discovery of the Role of Wall Shear in Atherosclerosis. *Arteriosclerosis Thrombosis and Vascular Biology* **29**(2)**:** 158-161.

Caro CG, Fitz-Gerald JM, Schroter RC (1971). Atheroma and Arterial Wall Shear Observation, Correlation and Proposal of a Shear Dependent Mass Transfer Mechanism for Atherogenesis. *Proceedings of the Royal Society of London. Series B. Biological Sciences* **177**(1046)**:** 109-133.

Caro CGF-G, J. M.; Schroter, R.C. (1969). Arterial Wall Shear and Distribution of Early Atheroma in Man. *Nature* **223:** 1159.

Caughey GE, Cleland LG, Penglis PS, Gamble JR, James MJ (2001). Roles of cyclooxygenase (COX)-1 and COX-2 in prostanoid production by human endothelial cells: Selective up-regulation of prostacyclin synthesis by COX-2. *Journal of Immunology* **167**(5)**:** 2831-2838.

Chaytor AT, Edwards DH, Bakker LM, Griffith TM (2003). Distinct hyperpolarizing and relaxant roles for gap junctions and endothelium-derived H2O2 in NO-independent relaxations of rabbit arteries. *Proceedings of the National Academy of Sciences* **100**(25)**:** 15212-15217.

Chen BPC, Li Y-S, Zhao Y, Chen K-D, Li S, Lao J*, et al.* (2001). DNA microarray analysis of gene expression in endothelial cells in response to 24-h shear stress. *Physiological Genomics* **7**(1)**:** 55-63.

Chen Z, Tzima E (2009). PECAM-1 Is Necessary for Flow-Induced Vascular Remodeling. *Arteriosclerosis, Thrombosis, and Vascular Biology* **29**(7)**:** 1067-1073.

Cheng C, Tempel D, van Haperen R, van der Baan A, Grosveld F, Daemen MJAP*, et al.* (2006). Atherosclerotic Lesion Size and Vulnerability Are Determined by Patterns of Fluid Shear Stress. *Circulation* **113**(23)**:** 2744-2753.

Cheng CP, Herfkens RJ, Taylor CA (2003). Abdominal aortic hemodynamic conditions in healthy subjects aged 50–70 at rest and during lower limb exercise: in vivo quantification using MRI. *Atherosclerosis* **168**(2)**:** 323-331.

Chu TJ, Peters DG (2008). Serial analysis of the vascular endothelial transcriptome under static and shear stress conditions. *Physiological Genomics* **34**(2)**:** 185-192.

Cines DB, Pollak ES, Buck CA, Loscalzo J, Zimmerman GA, McEver RP*, et al.* (1998). Endothelial Cells in Physiology and in the Pathophysiology of Vascular Disorders. *Blood* **91**(10)**:** 3527-3561.

Collins NT, Cummins PM, Colgan OC, Ferguson G, Birney YA, Murphy RP*, et al.* (2006). Cyclic Strain–Mediated Regulation of Vascular Endothelial Occludin and ZO-1. *Arteriosclerosis, Thrombosis, and Vascular Biology* **26**(1)**:** 62-68.

Collins T, Cybulsky MI (2001). NF-κB: pivotal mediator or innocent bystander in atherogenesis? *The Journal of Clinical Investigation* **107**(3)**:** 255-264.

Conway DE, Williams MR, Eskin SG, McIntire LV (2010). Endothelial cell responses to atheroprone flow are driven by two separate flow components: low time-average shear stress and fluid flow reversal. *American Journal of Physiology - Heart and Circulatory Physiology* **298**(2)**:** H367-H374.

Cosentino F, Katusic ZS (1995). Tetrahydrobiopterin and Dysfunction of Endothelial Nitric Oxide Synthase in Coronary Arteries. *Circulation* **91**(1)**:** 139-144.

Crofford LJ, Tan B, McCarthy CJ, Hla T (1997). Involvement of nuclear factor kB in the regulation of cyclooxygenase-2 expression by interleukin-1 in rheumatoid synoviocytes. *Arthritis & Rheumatism* **40**(2)**:** 226-236.

Cuhlmann S, Van der Heiden K, Saliba D, Tremoleda JL, Khalil M, Zakkar M*, et al.* (2011). Disturbed Blood Flow Induces RelA Expression via c-Jun N-Terminal Kinase 1 / Novelty and Significance. *Circulation Research* **108**(8)**:** 950-959.

Cybulsky MI, Iiyama K, Li H, Zhu S, Chen M, Iiyama M*, et al.* (2001). A major role for VCAM-1, but not ICAM-1, in early atherosclerosis. *The Journal of Clinical Investigation* **107**(10)**:** 1255-1262.

Dardik A, Chen L, Frattini J, Asada H, Aziz F, Kudo FA*, et al.* (2005). Differential effects of orbital and laminar shear stress on endothelial cells. *Journal of Vascular Surgery* **41**(5)**:** 869-880.

de Waard V, van den Berg BMM, Veken J, Schultz-Heienbrok R, Pannekoek H, van Zonneveld A-J (1999). Serial analysis of gene expression to assess the endothelial cell response to an atherogenic stimulus. *Gene* **226**(1)**:** 1-8.

Deanfield Ja, Donald Aa, Ferri Cb, Giannattasio Cc, Halcox Ja, Halligan Sd*, et al.* (2005). Endothelial function and dysfunction. Part I: Methodological issues for assessment in the different vascular beds: A statement by the Working Group on Endothelin and Endothelial Factors of the European Society of Hypertension. *Journal of Hypertension* **23**(1)**:** 7-17.

Dewey CF, Bussolari SR, Gimbrone MA, Davies PF (1981). The dynamic response of vascular endothelial cells to fluid shear stress. *Journal of Biomechanical Engineering* **103**(3)**:** 177-185.

Di Francesco L, Totani L, Dovizio M, Piccoli A, Di Francesco A, Salvatore T*, et al.* (2009). Induction of Prostacyclin by Steady Laminar Shear Stress Suppresses Tumor Necrosis Factor-{alpha} Biosynthesis via Heme Oxygenase-1 in Human Endothelial Cells. *Circ Res* **104**(4)**:** 506-513.

Doroudi R, Gan L-m, Selin Sjögren L, Jern S (2000). Effects of Shear Stress on Eicosanoid Gene Expression and Metabolite Production in Vascular Endothelium as Studied in a Novel Biomechanical Perfusion Model. *Biochemical and Biophysical Research Communications* **269**(1)**:** 257-264.

Dumitru CD, Ceci JD, Tsatsanis C, Kontoyiannis D, Stamatakis K, Lin J-H*, et al.* (2000). TNF-α Induction by LPS Is Regulated Posttranscriptionally via a Tpl2/ERK-Dependent Pathway. *Cell* **103**(7)**:** 1071-1083.

Erez A, Nagamani SCS, Shchelochkov OA, Premkumar MH, Campeau PM, Chen Y*, et al.* (2011). Requirement of argininosuccinate lyase for systemic nitric oxide production. *Nat Med* **17**(12)**:** 1619-1626.

Eskin SG, Ives CL, McIntire LV, Navarro LT (1984). Response of cultured endothelial cells to steady flow. *Microvascular Research* **28**(1)**:** 87-94.

Evans WH, Martin PEM (2002). Gap junctions: structure and function (Review). *Molecular Membrane Biology* **19**(2)**:** 121-136.

Feng L, Sun WQ, Xia YY, Tang WW, Chanmugam P, Soyoola E*, et al.* (1993). Cloning Two Isoforms of Rat Cyclooxygenase: Differential Regulation of Their Expression. *Archives of Biochemistry and Biophysics* **307**(2)**:** 361-368.

FitzGerald GA (2002). Cardiovascular pharmacology of nonselective nonsteroidal anti-inflammatory drugs and coxibs: clinical considerations. *The American Journal of Cardiology* **89**(6, Supplement 1)**:** 26-32.

Fitzgerald KA, Palsson-McDermott EM, Bowie AG, Jefferies CA, Mansell AS, Brady G*, et al.* (2001). Mal (MyD88-adapter-like) is required for Toll-like receptor-4 signal transduction. *Nature* **413**(6851)**:** 78-83.

Fleming I, Busse R (1999). Signal transduction of eNOS activation. *Cardiovascular Research* **43**(3)**:** 532-541.

Fleming I, Fisslthaler B, Dixit M, Busse R (2005). Role of PECAM-1 in the shear-stress-induced activation of Akt and the endothelial nitric oxide synthase (eNOS) in endothelial cells. *J. Cell Sci.* **118**(18)**:** 4103-4111.

Florey L (1966). The Endothelial Cell. *The British Medical Journal* **2**(5512)**:** 487-490.

Flower RJ (2003). The development of COX2 inhibitors. *Nat Rev Drug Discov* **2**(3)**:** 179-191.

Flower RJB, G.J. (1976). The importance of phospholipase-A2 in prostaglandin biosynthesis. *Biochemical Pharmacology* **3**(25)**:** 285-291.

Folkman J, Haudenschild CC, Zetter BR (1979). Long-term culture of capillary endothelial cells. *Proceedings of the National Academy of Sciences of the United States of America* **76**(10)**:** 5217-5221.

Fry DL (1969). Certain Histological and Chemical Responses of the Vascular Interface to Acutely Induced Mechanical Stress in the Aorta of the Dog. *Circ Res* **24**(1)**:** 93-108.

Fryer DG, Birnbaum G, Luttrell CN (1966). Human endothelium in cell culture. *Journal of atherosclerosis research* **6**(2)**:** 151-163.

Funk CD, FitzGerald GA (2007). COX-2 inhibitors and cardiovascular risk. *Journal of Cardiovascular Pharmacology* **50**(5)**:** 470-479.

Furchgott RF, Zawadzki JV (1980). The obligatory role of endothelial cells in the relaxation of arterial smooth muscle by acetylcholine. *Nature* **288**(5789)**:** 373-376.

Garita B, Jenkins MW, Han M, Zhou C, Vanauker M, Rollins AM*, et al.* (2011). Blood flow dynamics of one cardiac cycle and relationship to mechanotransduction and trabeculation during heart looping. *American journal of physiology. Heart and circulatory physiology* **300**(3)**:** H879-891.

Garlanda C, Dejana E (1997). Heterogeneity of Endothelial Cells. *Arteriosclerosis, Thrombosis, and Vascular Biology* **17**(7)**:** 1193-1202.

Gerrity RR, M; Somer, JB; Bell, FP; Schwartz, CJ (1977). Endothelial Cell Morphology in Areas of In Vivo Evans Blue Uptake in the Aorta of Young Pigs. *Am J Pathol* **89**(2)**:** 313-334.

Giaid A, Yanagisawa M, Langleben D, Michel RP, Levy R, Shennib H*, et al.* (1993). Expression of Endothelin-1 in the Lungs of Patients with Pulmonary Hypertension. *New England Journal of Medicine* **328**(24)**:** 1732-1739.

Gimbrone MA, Cotran RS, Folkman J (1974). Human Vascular Endothelial Cells in Culture. *The Journal of Cell Biology* **60**(3)**:** 673-684.

Grosvenor S (2012). A New Era in Cell Culture Medium Development. *BioPharm International* **25**(7).

Gulbins H, Dauner M, Petzold R, Goldemund A, Anderson I, Doser M*, et al.* (2004). Development of an artificial vessel lined with human vascular cells. *The Journal of Thoracic and Cardiovascular Surgery* **128**(3)**:** 372-377.

Hajra L, Evans AI, Chen M, Hyduk SJ, Collins T, Cybulsky MI (2000). The NF-kappa B signal transduction pathway in aortic endothelial cells is primed for activation in regions predisposed to atherosclerotic lesion formation. *Proceedings of the National Academy of Sciences of the United States of America* **97**(16)**:** 9052-9057.

Hammarström S, Falardeau P (1977). Resolution of prostaglandin endoperoxide synthase and thromboxane synthase of human platelets. *Proceedings of the National Academy of Sciences* **74**(9)**:** 3691-3695.

Hansma PK, Drake B, Marti O, Gould SAC, Prater CB (1989). The Scanning Ion-Conductance Microscope. *Science* **243**(4891)**:** 641-643.

Hayden MS, Ghosh S (2004). Signaling to NF-κB. *Genes & Development* **18**(18)**:** 2195-2224.

Hennig B, Shasby DM, Spector AA (1985). Exposure to fatty acid increases human low density lipoprotein transfer across cultured endothelial monolayers. *Circulation Research* **57**(5)**:** 776-780.

Hexum TD, Hoeger C, Rivier JE, Baird A, Brown MR (1990). Characterization of endothelin secretion by vascular endothelial cells. *Biochemical and Biophysical Research Communications* **167**(1)**:** 294-300.

Heydarkhan-Hagvall S, Chien S, Nelander S, Li Y-C, Yuan S, Lao J*, et al.* (2006). DNA microarray study on gene expression profiles in co-cultured endothelial and smooth muscle cells in response to 4- and 24-h shear stress. *Molecular and Cellular Biochemistry* **281**(1)**:** 1-15.

Hoareau LB, Karima; Rondeau, Philippe; Murumalla, Ravi; Ravanan, Palaniyandi; Tallet, Frank; Delarue, Pierre; Cesari, Maya; Roche, Regis; Festy, Franck (2010). Signaling pathways involved in LPS induced TNFalpha production in human adipocytes. *Journal of Inflammation* **7**(1).

Holman RMJ, HC; Strong, JP; Geer JC (1958). The Natural History of Atherosclerosis: The Early Aortic Lesions as Seen in New Orleans at the Middle of the 20th Century. *The American Journal of Pathology* **34**(2)**:** 209-235.

Hoyer LW, de los Santos RP, Hoyer JR (1973). Antihemophilic Factor Antigen. Localization in Endothelial Cells by Immunofluorescent Microscopy. *The Journal of Clinical Investigation* **52**(11)**:** 2737-2744.

Ignarro LJ, Buga GM, Wood KS, Byrns RE, Chaudhuri G (1987). Endothelium-derived relaxing factor produced and released from artery and vein is nitric oxide. *Proceedings of the National Academy of Sciences* **84**(24)**:** 9265-9269.

Ingber DE (2003). Tensegrity I. Cell structure and hierarchical systems biology. *Journal of Cell Science* **116**(7)**:** 1157-1173.

Ingram DA, Mead LE, Tanaka H, Meade V, Fenoglio A, Mortell K*, et al.* (2004). Identification of a novel hierarchy of endothelial progenitor cells using human peripheral and umbilical cord blood. *Blood* **104**(9)**:** 2752-2760.

Jaffe EA, Hoyer LW, Nachman RL (1973a). Synthesis of Antihemophilic Factor Antigen by Cultured Human Endothelial Cells. *The Journal of Clinical Investigation* **52**(11)**:** 2757-2764.

Jaffe EA, Nachman RL, Becker CG, Minick CR (1973b). Culture of Human Endothelial Cells Derived from Umbilical Veins - Identification by Moprphologic and Immunological Criteria. *Journal of Clinical Investigation* **52**(11)**:** 2745-2756.

Janeway CA, Medzhitov R (2002). Innate Immune Recognition. *Annual Review of Immunology* **20**(1)**:** 197-216.

Jeremy JY, Rowe D, Emsley AM, Newby AC (1999). Nitric oxide and the proliferation of vascular smooth muscle cells. *Cardiovascular Research* **43**(3)**:** 580-594.

Johnson CM, Hanson MN, Helgeson SC (1987). Porcine cardiac valvular subendothelial cells in culture: Cell isolation and growth characteristics. *Journal of Molecular and Cellular Cardiology* **19**(12)**:** 1185-1193.

Jongstra-Bilen J, Haidari M, Zhu SN, Chen M, Guha D, Cybulsky MI (2006). Low-grade chronic inflammation in regions of the normal mouse arterial intima predisposed to atherosclerosis. *Journal of Experimental Medicine* **203**(9)**:** 2073-2083.

Katritsis D, Kaiktsis L, Chaniotis A, Pantos J, Efstathopoulos EP, Marmarelis V (2007). Wall Shear Stress: Theoretical Considerations and Methods of Measurement. *Progress in Cardiovascular Diseases* **49**(5)**:** 307-329.

Kawai T, Takeuchi O, Fujita T, Inoue J-i, Mühlradt PF, Sato S*, et al.* (2001). Lipopolysaccharide Stimulates the MyD88-Independent Pathway and Results in Activation of IFN-Regulatory Factor 3 and the Expression of a Subset of Lipopolysaccharide-Inducible Genes. *The Journal of Immunology* **167**(10)**:** 5887-5894.

Kawka DW, Ouellet M, Hetu PO, Singer, II, Riendeau D (2007). Double-label expression studies of prostacyclin synthase, thromboxane synthase and COX isoforms in normal aortic endothelium. *Biochimica Et Biophysica Acta-Molecular and Cell Biology of Lipids* **1771**(1)**:** 45-54.

Kempe S, Kestler H, Lasar A, Wirth T NF-κB controls the global pro-inflammatory response in endothelial cells: evidence for the regulation of a pro-atherogenic program. *Nucleic Acids Research* **33**(16)**:** 5308-5319.

Khachigian LM, Resnick N, Gimbrone MA, Collins T (1995). Nuclear factor-kappa B interacts functionally with the platelet-derived growth factor B-chain shear-stress response element in vascular endothelial cells exposed to fluid shear stress. *The Journal of Clinical Investigation* **96**(2)**:** 1169-1175.

Kirkby NS, Lundberg MH, Harrington LS, Leadbeater PDM, Milne GL, Potter CMF*, et al.* (2012). Cyclooxygenase-1, not cyclooxygenase-2, is responsible for physiological production of prostacyclin in the cardiovascular system. *Proceedings of the National Academy of Sciences*.

Korchev YE, Gorelik J, Lab MJ, Sviderskaya EV, Johnston CL, Coombes CR*, et al.* (2000). Cell Volume Measurement Using Scanning Ion Conductance Microscopy. *Biophysical Journal* **78**(1)**:** 451-457.

Korchev YE, Milovanovic M, Bashford CL, Bennett DC, Sviderskaya EV, Vodyanoy I*, et al.* (1997). Specialized scanning ion-conductance microscope for imaging of living cells. *Journal of Microscopy* **188**(1)**:** 17-23.

Koren O, Spor A, Felin J, Fåk F, Stombaugh J, Tremaroli V*, et al.* (2010). Human oral, gut, and plaque microbiota in patients with atherosclerosis. *Proceedings of the National Academy of Sciences*.

Kozarov EV, Dorn BR, Shelburne CE, Dunn WA, Progulske-Fox A (2005). Human Atherosclerotic Plaque Contains Viable Invasive Actinobacillus actinomycetemcomitans and Porphyromonas gingivalis. *Arteriosclerosis, Thrombosis, and Vascular Biology* **25**(3)**:** e17-e18.

Ku DN, Giddens DP, Zarins CK, Glagov S (1985). Pulsatile flow and atherosclerosis in the human carotid bifurcation. Positive correlation between plaque location and low oscillating shear stress. *Arteriosclerosis, Thrombosis, and Vascular Biology* **5**(3)**:** 293-302.

Kucharczak J, Simmons MJ, Fan Y, Gelinas C (2003). To be, or not to be: NF-[kappa]B is the answer - role of Rel//NF-[kappa]B in the regulation of apoptosis. *Oncogene* **22**(56)**:** 8961-8982.

Lampugnani MG, Dejana E (2007). Adherens junctions in endothelial cells regulate vessel maintenance and angiogenesis. *Thrombosis Research* **120, Supplement 2**(0)**:** S1-S6.

Landmesser U, Merten R, Spiekermann S, Büttner K, Drexler H, Hornig B (2000). Vascular Extracellular Superoxide Dismutase Activity in Patients With Coronary Artery Disease. *Circulation* **101**(19)**:** 2264-2270.

Laubichler MDA, William C; Maienschein, Jane (2007). The Endothelium in History. In: Aird WC (ed)^(eds). *Endothelial Biomedicine*, edn: Cambridge University Press. p^pp 5-19.

Leeper NJ, Hunter AL, Cooke JP (2010). Stem Cell Therapy for Vascular Regeneration. *Circulation* **122**(5)**:** 517-526.

Levesque MJ, Nerem RM (1985). The Elongation and Orientation of Cultured Endothelial Cells in Response to Shear Stress. *Journal of Biomechanical Engineering* **107**(4)**:** 341-347.

Lush CW, Cepinskas G, Kvietys PR (2000). LPS tolerance in human endothelial cells: reduced PMN adhesion, E-selectin expression, and NF-κB mobilization. *American Journal of Physiology - Heart and Circulatory Physiology* **278**(3)**:** H853-H861.

Malek AM, Alper SL, Izumo S (1999). Hemodynamic Shear Stress and Its Role in Atherosclerosis. *JAMA* **282**(21)**:** 2035-2042.

McAdam BF, Catella-Lawson F, Mardini IA, Kapoor S, Lawson JA, FitzGerald GA (1999). Systemic biosynthesis of prostacyclin by cyclooxygenase (COX)-2: The human pharmacology of a selective inhibitor of COX-2. *Proceedings of the National Academy of Sciences of the United States of America* **96**(1)**:** 272-277.

McCormick SM, Eskin SG, McIntire LV, Teng CL, Lu C-M, Russell CG*, et al.* (2001). DNA microarray reveals changes in gene expression of shear stressed human umbilical vein endothelial cells. *Proceedings of the National Academy of Sciences of the United States of America* **98**(16)**:** 8955-8960.

Megens RTA, Reitsma S, Schiffers PHM, Hilgers RHP, De Mey JGR, Slaaf DW*, et al.* (2007). Two-Photon Microscopy of Vital Murine Elastic and Muscular Arteries. *Journal of Vascular Research* **44**(2)**:** 87-98.

Mitchell JA, Ali F, Bailey L, Moreno L, Harrington LS (2008). Role of nitric oxide and prostacyclin as vasoactive hormones released by the endothelium. *Experimental Physiology* **93**(1)**:** 141-147.

Mitchell JA, Lucas R, Vojnovic I, Hasan K, Pepper JR, Warner TD (2006). Stronger inhibition by nonsteroid anti-inflammatory drugs of cyclooxygenase-1 in endothelial cells than platelets offers an explanation for increased risk of thrombotic events. *The FASEB Journal* **20**(14)**:** 2468-2475.

Moncada S, Gryglewski R, Bunting S, Vane JR (1976). An enzyme isolated from arteries transforms prostaglandin endoperoxides to an unstable substance that inhibits platelet aggregation. *Nature* **263**(5579)**:** 663-665.

Moore J, Bürki E, Suciu A, Zhao S, Burnier M, Brunner H*, et al.* (1994). A device for subjecting vascular endothelial cells to both fluid shear stress and circumferential cyclic stretch. *Annals of Biomedical Engineering* **22**(4)**:** 416-422.

Moore Jr JE, Xu C, Glagov S, Zarins CK, Ku DN (1994). Fluid wall shear stress measurements in a model of the human abdominal aorta: oscillatory behavior and relationship to atherosclerosis. *Atherosclerosis* **110**(2)**:** 225-240.

Morgan JF, Morton HJ, Parker RC (1950). Nutrition of Animal Cells in Tissue Culture. I. Initial Studies on a Synthetic Medium. *Proceedings of the Society for Experimental Biology and Medicine. Society for Experimental Biology and Medicine (New York, N.Y.)* **73**(1)**:** 1-8.

Morré SA, Stooker W, Lagrand WK, van den Brule AJC, Niessen HWM (2000). Microorganisms in the aetiology of atherosclerosis. *Journal of Clinical Pathology* **53**(9)**:** 647-654.

Mott RE, Helmke BP (2007). Mapping the dynamics of shear stress-induced structural changes in endothelial cells. *American Journal of Physiology - Cell Physiology* **293**(5)**:** C1616-C1626.

Murase T, Kume N, Korenaga R, Ando J, Sawamura T, Masaki T*, et al.* (1998). Fluid Shear Stress Transcriptionally Induces Lectin-like Oxidized LDL Receptor-1 in Vascular Endothelial Cells. *Circulation Research* **83**(3)**:** 328-333.

Nachman RL, Jaffe EA (2004). Endothelial cell culture: beginnings of modern vascular biology. *The Journal of Clinical Investigation* **114**(8)**:** 1037-1040.

Needleman P, Raz A, Minkes MS, Ferrendelli JA, Sprecher H (1979). Triene prostaglandins: Prostacyclin and thromboxane biosynthesis and unique biological properties. *Proceedings of the National Academy of Sciences* **76**(2)**:** 944-948.

Novak P, Li C, Shevchuk AI, Stepanyan R, Caldwell M, Hughes S*, et al.* (2009). Nanoscale live-cell imaging using hopping probe ion conductance microscopy. *Nat Meth* **6**(4)**:** 279-281.

Ogawa H, Rafiee P, Heidemann J, Fisher PJ, Johnson NA, Otterson MF*, et al.* (2003). Mechanisms of Endotoxin Tolerance in Human Intestinal Microvascular Endothelial Cells. *The Journal of Immunology* **170**(12)**:** 5956-5964.

Ohno M, Gibbons GH, Dzau VJ, Cooke JP (1993). Shear stress elevates endothelial cGMP. Role of a potassium channel and G protein coupling. *Circulation* **88**(1)**:** 193-197.

Ohta K, Hirata Y, Imai T, Kanno K, Emori T, Shichiri M*, et al.* (1990). Cytokine-induced release of endothelin-1 from porcine renal epithelial cell line. *Biochemical and Biophysical Research Communications* **169**(2)**:** 578-584.

Ohura N, Yamamoto K, Ichioka S, Sokabe T, Nakatsuka H, Baba A*, et al.* (2003). Global Analysis of Shear Stress-Responsive Genes in Vascular Endothelial Cells. *Journal of Atherosclerosis and Thrombosis* **10**(5)**:** 304-313.

Okahara K, Sun B, Kambayashi J-i (1998). Upregulation of Prostacyclin Synthesis–Related Gene Expression by Shear Stress in Vascular Endothelial Cells. *Arterioscler Thromb Vasc Biol* **18**(12)**:** 1922-1926.

Opitz CF, Ewert R, Kirch W, Pittrow D (2008). Inhibition of endothelin receptors in the treatment of pulmonary arterial hypertension: does selectivity matter? *European Heart Journal* **29**(16)**:** 1936-1948.

Osawa M, Masuda M, Kusano K-i, Fujiwara K (2002). Evidence for a role of platelet endothelial cell adhesion molecule-1 in endothelial cell mechanosignal transduction. *The Journal of Cell Biology* **158**(4)**:** 773-785.

Ott MJ, Olson JL, Ballermann BJ (1995). Chronic In Vitro Flow Promotes Ultrastructural Differentiation of Endothelial Cells. *Endothelium* **3**(1)**:** 21-30.

Ott SJ, El Mokhtari NE, Musfeldt M, Hellmig S, Freitag S, Rehman A*, et al.* (2006). Detection of Diverse Bacterial Signatures in Atherosclerotic Lesions of Patients With Coronary Heart Disease. *Circulation* **113**(7)**:** 929-937.

Pahakis MY, Kosky JR, Dull RO, Tarbell JM (2007). The role of endothelial glycocalyx components in mechanotransduction of fluid shear stress. *Biochemical and Biophysical Research Communications* **355**(1)**:** 228-233.

Palmer RMJ, Ashton DS, Moncada S (1988). Vascular endothelial cells synthesize nitric oxide from L-arginine. *Nature* **333**(6174)**:** 664-666.

Palmer RMJ, Ferrige AG, Moncada S (1987). Nitric oxide release accounts for the biological activity of endothelium-derived relaxing factor. *Nature* **327**(6122)**:** 524-526.

Pardridge WM, Boado RJ, Farrell CR (1990). Brain-type glucose transporter (GLUT-1) is selectively localized to the blood-brain barrier. Studies with quantitative western blotting and in situ hybridization. *J. Biol. Chem.* **265**(29)**:** 18035-18040.

Parfenova H, Parfenov VN, Shlopov BV, Levine V, Falkos S, Pourcyrous M*, et al.* (2001). Dynamics of nuclear localization sites for COX-2 in vascular endothelial cells. *American Journal of Physiology-Cell Physiology* **281**(1)**:** C166-C178.

Parikh SA, Edelman ER (2000). Endothelial cell delivery for cardiovascular therapy. *Advanced Drug Delivery Reviews* **42**(1–2)**:** 139-161.

Passerini AG, Polacek DC, Shi C, Francesco NM, Manduchi E, Grant GR*, et al.* (2004). Coexisting proinflammatory and antioxidative endothelial transcription profiles in a disturbed flow region of the adult porcine aorta. *Proceedings of the National Academy of Sciences of the United States of America* **101**(8)**:** 2482-2487.

Peng X, Recchia FA, Byrne BJ, Wittstein IS, Ziegelstein RC, Kass DA (2000). In vitro system to study realistic pulsatile flow and stretch signaling in cultured vascular cells. *American Journal of Physiology - Cell Physiology* **279**(3)**:** C797-C805.

Pomerat CM, Slick WC (1963). Isolation and Growth of Endothelial Cells in Tissue Culture. *Nature* **198**(4883)**:** 859-861.

Potter CMF, Lundberg MH, Harrington LS, Warboys CM, Warner TD, Berson RE*, et al.* (2011). Role of Shear Stress in Endothelial Cell Morphology and Expression of Cyclooxygenase Isoforms. *Arterioscler Thromb Vasc Biol* **31**(2)**:** 384-391.

Potter CMF, Schobesberger S, Lundberg MH, Weinberg PD, Mitchell JA, Gorelik J (2012). Shape and Compliance of Endothelial Cells after Shear Stress In Vitro or from Different Aortic Regions: Scanning Ion Conductance Microscopy Study. *PLoS ONE* **7**(2)**:** e31228.

Pourati J, Maniotis A, Spiegel D, Schaffer JL, Butler JP, Fredberg JJ*, et al.* (1998). Is cytoskeletal tension a major determinant of cell deformability in adherent endothelial cells? *American Journal of Physiology - Cell Physiology* **274**(5)**:** C1283-C1289.

Prins BA, Hu RM, Nazario B, Pedram A, Frank HJ, Weber MA*, et al.* (1994). Prostaglandin E2 and prostacyclin inhibit the production and secretion of endothelin from cultured endothelial cells. *J. Biol. Chem.* **269**(16)**:** 11938-11944.

Qin X, Tian J, Zhang P, Fan Y, Chen L, Guan Y*, et al.* (2007). Laminar shear stress up-regulates the expression of stearoyl-CoA desaturase-1 in vascular endothelial cells. *Cardiovascular Research* **74**(3)**:** 506-514.

Radomski MW, Palmer RM, Moncada S (1990). An L-arginine/nitric oxide pathway present in human platelets regulates aggregation. *Proceedings of the National Academy of Sciences* **87**(13)**:** 5193-5197.

Radomski MW, Palmer RMJ, Moncada S (1987). Endogenous Nitric Oxide Inhibits Human Platelet Adhesion to Vascular Endothelium. *The Lancet* **330**(8567)**:** 1057-1058.

Rahme E, Nedjar H (2007). Risks and benefits of COX-2 inhibitors vs non-selective NSAIDs: does their cardiovascular risk exceed their gastrointestinal benefit? A retrospective cohort study. *Rheumatology* **46**(3)**:** 435-438.

Resnick N, Collins T, Atkinson W, Bonthron DT, Dewey CF, Gimbrone MA (1993). Platelet-derived growth factor B chain promoter contains a cis-acting fluid shear-stress-responsive element. *Proceedings of the National Academy of Sciences of the United States of America* **90**(10)**:** 4591-4595.

Roberts JC, Moses C, Wilkins RH (1959). Autopsy Studies in Atherosclerosis. *Circulation* **20**(4)**:** 511-519.

Samuelsson B, Goldyne M, Granstrom E, Hamberg M, Hammarstrom S, Malmsten C (1978). Prostaglandins and Thromboxanes. *Annual Review of Biochemistry* **47**(1)**:** 997-1029.

Sánchez D, Johnson N, Li C, Novak P, Rheinlaender J, Zhang Y*, et al.* (2008). Noncontact Measurement of the Local Mechanical Properties of Living Cells Using Pressure Applied via a Pipette. *Biophysical Journal* **95**(6)**:** 3017-3027.

Shaw SK, Perkins BN, Lim Y-C, Liu Y, Nusrat A, Schnell FJ*, et al.* (2001). Reduced Expression of Junctional Adhesion Molecule and Platelet/Endothelial Cell Adhesion Molecule-1 (CD31) at Human Vascular Endothelial Junctions by Cytokines Tumor Necrosis Factor-α Plus Interferon-γ Does Not Reduce Leukocyte Transmigration Under Flow. *The American Journal of Pathology* **159**(6)**:** 2281-2291.

Simionescu M, Gafencu A, Antohe F (2002). Transcytosis of plasma macromolecules in endothelial cells: A cell biological survey. *Microscopy Research and Technique* **57**(5)**:** 269-288.

Slager CJ, Wentzel JJ, Gijsen FJH, Schuurbiers JCH, van der Wal AC, van der Steen AFW*, et al.* (2005). The role of shear stress in the generation of rupture-prone vulnerable plaques. *Nat Clin Pract Cardiovasc Med* **2**(8)**:** 401-407.

Somer JB, Evans G, Schwartz CJ (1972). Influence of experimental aortic coarctation on the pattern of aortic Evans Blue uptake in vivo. *Atherosclerosis* **16**(1)**:** 127-133.

Stamatovic SM, Keep RF, Andjelkovic AV (2008). Brain Endothelial Cell-Cell Junctions: How to Open the Blood Brain Barrier. *Current Neuropharmacology* **6**(3)**:** 179-192.

Stolpen AHG, E.C; Fiers, W; Pober, J.S (1986). Recombinant tumor necrosis factor and immune interferon act singly and in combination to reorganize human vascular endothelial cell monolayers. *Am J Pathol* **123**(1)**:** 16-24.

Sun N, Wood NB, Hughes AD, Thom SAM, Yun Xu X (2007). Effects of transmural pressure and wall shear stress on LDL accumulation in the arterial wall: a numerical study using a multilayered model. *American Journal of Physiology - Heart and Circulatory Physiology* **292**(6)**:** H3148-H3157.

Sung H-J, Yee A, Eskin SG, McIntire LV (2007). Cyclic strain and motion control produce opposite oxidative responses in two human endothelial cell types. *American Journal of Physiology - Cell Physiology* **293**(1)**:** C87-C94.

Suo J, Ferrara DE, Sorescu D, Guldberg RE, Taylor WR, Giddens DP (2007). Hemodynamic Shear Stresses in Mouse Aortas: Implications for Atherogenesis. *Arterioscler Thromb Vasc Biol* **27**(2)**:** 346-351.

Takeda K, Akira S (2005). Toll-like receptors in innate immunity. *International Immunology* **17**(1)**:** 1-14.

Tang BT, Cheng CP, Draney MT, Wilson NM, Tsao PS, Herfkens RJ*, et al.* (2006). Abdominal aortic hemodynamics in young healthy adults at rest and during lower limb exercise: quantification using image-based computer modeling. *American Journal of Physiology - Heart and Circulatory Physiology* **291**(2)**:** H668-H676.

Topol EJ (2004). Failing the Public Health — Rofecoxib, Merck, and the FDA. *New England Journal of Medicine* **351**(17)**:** 1707-1709.

Topper JN, Cai J, Falb D, Gimbrone MA (1996). Identification of vascular endothelial genes differentially responsive to fluid mechanical stimuli: cyclooxygenase-2, manganese superoxide dismutase, and endothelial cell nitric oxide synthase are selectively up-regulated by steady laminar shear stress. *Proceedings of the National Academy of Sciences of the United States of America* **93**(19)**:** 10417-10422.

Truskey GA, Barber KM, Robey TC, Olivier LA, Combs MP (1995). Characterization of a sudden expansion flow chamber to study the response of endothelium to flow recirculation. *Journal of Biomechanical Engineering* **117**(2)**:** 203-210.

Tzima E, Irani-Tehrani M, Kiosses WB, Dejana E, Schultz DA, Engelhardt B*, et al.* (2005). A mechanosensory complex that mediates the endothelial cell response to fluid shear stress. *Nature* **437**(7057)**:** 426-431.

Valiron O, Chevrier V, Usson Y, Breviario F, Job D, Dejana E (1996). Desmoplakin expression and organization at human umbilical vein endothelial cell-to-cell junctions. *Journal of Cell Science* **109**(8)**:** 2141-2149.

Van Doormaal MA, Kazakidi A, Wylezinska M, Hunt A, Tremoleda JL, Protti A*, et al.* (2012). Haemodynamics in the mouse aortic arch computed from MRI-derived velocities at the aortic root. *Journal of The Royal Society Interface* **9**(76)**:** 2834-2844.

Vane JR, Warner TD (2000). Nomenclature for COX-2 Inhibitors. *The Lancet* **356**(9239)**:** 1373-1374.

Vincent PE, Plata AM, Hunt AAE, Weinberg PD, Sherwin SJ (2011). Blood flow in the rabbit aortic arch and descending thoracic aorta. *Journal of The Royal Society Interface* **8**(65)**:** 1708-1719.

von Offenberg Sweeney N, Cummins PM, Birney YA, Cullen JP, Redmond EM, Cahill PA (2004). Cyclic strain-mediated regulation of endothelial matrix metalloproteinase-2 expression and activity. *Cardiovascular Research* **63**(4)**:** 625-634.

Waldman SM, F (1988). Biochemical Mechanisms Underlying Vascular Smooth Muscle Relaxation: The Guanylate Cyclase-Cyclic GMP System. *Journal of Cardiovascular Pharmacology*(12)**:** S115-S118.

Warboys CM, Berson RE, Mann GE, Pearson JD, Weinberg PD (2010). Acute and chronic exposure to shear stress have opposite effects on endothelial permeability to macromolecules. *Am J Physiol Heart Circ Physiol***:** ajpheart.00114.02010.

Weibel ER, Palade GE (1964). New Cytoplasmic Components In Arterial Endothelia. *The Journal of Cell Biology* **23**(1)**:** 101-112.

Weinberg PD, Ethier CR (2007). Twenty-fold difference in hemodynamic wall shear stress between murine and human aortas. *Journal of Biomechanics* **40**(7)**:** 1594-1598.

Willecke K, Eiberger J, Degen J, Eckardt D, Romualdi A, Güldenagel M*, et al.* (2002). Structural and Functional Diversity of Connexin Genes in the Mouse and Human Genome. In: *Biological Chemistry* Vol. 383, p 725.

Wolfe MM, Lichtenstein DR, Singh G (1999). Gastrointestinal Toxicity of Nonsteroidal Antiinflammatory Drugs. *New England Journal of Medicine* **340**(24)**:** 1888-1899.

Yanagisawa M, Kurihara H, Kimura S, Tomobe Y, Kobayashi M, Mitsui Y*, et al.* (1988). A novel potent vasoconstrictor peptide produced by vascular endothelial cells. *Nature* **332**(6163)**:** 411-415.

Yang HYT, Erdos EG (1967). Second Kininase in Human Blood Plasma. *Nature* **215**(5108)**:** 1402-1403.

Yang HYT, Erdos EO, Levin Y (1971). Characterisation of a Dipeptide Hydrolase (Kinninase II: Angiotensin I Converting Enzyme). *Journal of Pharmacology and Experimental Therapeutics* **177**(1)**:** 291-300.

Yee A, Sakurai Y, Eskin S, McIntire L (2006). A Validated System for Simulating Common Carotid Arterial Flow <i>In Vitro : Alteration of Endothelial Cell Response. *Annals of Biomedical Engineering* **34**(4)**:** 593-604.

Yeh H-I, Rothery S, Dupont E, Coppen SR, Severs NJ (1998). Individual Gap Junction Plaques Contain Multiple Connexins in Arterial Endothelium. *Circulation Research* **83**(12)**:** 1248-1263.

Yoon HJ, Cho SW, Ahn BW, Yang SY (2010). Alterations in the activity and expression of endothelial NO synthase in aged human endothelial cells. *Mechanisms of Ageing and Development* **131**(2)**:** 119-123.

Yu Y, Ricciotti E, Scalia R, Tang SY, Grant G, Yu Z*, et al.* (2012). Vascular COX-2 Modulates Blood Pressure and Thrombosis in Mice. *Science Translational Medicine* **4**(132)**:** 132ra154.

Zakkar M, Luong LA, Chaudhury H, Ruud O, Punjabi PP, Anderson JR*, et al.* (2011). Dexamethasone Arterializes Venous Endothelial Cells by Inducing Mitogen-Activated Protein Kinase Phosphatase-1 / Clinical Perspective. *Circulation* **123**(5)**:** 524-532.

Zhang C, Xie S, Li S, Pu F, Deng X, Fan Y*, et al.* (2012). Flow patterns and wall shear stress distribution in human internal carotid arteries: The geometric effect on the risk for stenoses. *Journal of Biomechanics* **45**(1)**:** 83-89.